



<https://theses.gla.ac.uk/>

Theses Digitisation:

<https://www.gla.ac.uk/myglasgow/research/enlighten/theses/digitisation/>

This is a digitised version of the original print thesis.

Copyright and moral rights for this work are retained by the author

A copy can be downloaded for personal non-commercial research or study, without prior permission or charge

This work cannot be reproduced or quoted extensively from without first obtaining permission in writing from the author

The content must not be changed in any way or sold commercially in any format or medium without the formal permission of the author

When referring to this work, full bibliographic details including the author, title, awarding institution and date of the thesis must be given

Enlighten: Theses

<https://theses.gla.ac.uk/>
research-enlighten@glasgow.ac.uk

**A study of the SNARE protein Syntaxin 16 and
its role in the intracellular trafficking of glucose
transporter GLUT4 in 3T3-L1 adipocytes**

A thesis submitted to the
FACULTY OF BIOMEDICAL AND LIFE SCIENCES

For the degree of
DOCTOR OF PHILOSOPHY

By
Kirsty M. Proctor M.Sci. M.Res.

Department of Biochemistry and Molecular Biology
University of Glasgow

July 2006

© K.M. Proctor 2006

ProQuest Number: 10390993

All rights reserved

INFORMATION TO ALL USERS

The quality of this reproduction is dependent upon the quality of the copy submitted.

In the unlikely event that the author did not send a complete manuscript and there are missing pages, these will be noted. Also, if material had to be removed, a note will indicate the deletion.



ProQuest 10390993

Published by ProQuest LLC (2017). Copyright of the Dissertation is held by the Author.

All rights reserved.

This work is protected against unauthorized copying under Title 17, United States Code
Microform Edition © ProQuest LLC.

ProQuest LLC.
789 East Eisenhower Parkway
P.O. Box 1346
Ann Arbor, MI 48106 – 1346

GLASGOW
UNIVERSITY
LIBRARY:

*This thesis is dedicated to my Mum and Dad, Catherine and Duncan
Proctor, and my dog, Lucky,
who fill my life with so much happiness*

Abstract

In muscle and adipose tissue insulin promotes glucose uptake by stimulating the translocation of the glucose transporter GLUT4 from an intracellular location to the plasma membrane. This exocytic delivery of GLUT4 to the plasma membrane is fundamental for the maintenance of blood glucose homeostasis. Individuals with insulin resistance or type II diabetes exhibit a blunted ability of insulin to stimulate GLUT4 translocation, and, as a result, a decreased rate of insulin stimulated glucose transport. To design effective therapies we require a clear understanding of the molecular basis of intracellular GLUT4 trafficking.

Recent studies support a model in which the intracellular GLUT4 itinerary involves two intracellular cycles. In the basal state, GLUT4 recycles between the PM and endosomes in the fast recycling endosomal system. However, unique sequences within GLUT4 cause a large population to be sorted away from the endosomal system, into a slowly recycling intracellular pathway between endosomes and the TGN. This pathway involves the sorting of GLUT4 into unique storage vesicles, (GLUT4 storage vesicles, GSVs) which are mobilised in response to insulin, and are responsible for the majority of GLUT4 that is delivered to the cell surface in response to insulin. The intracellular sorting of GLUT4 is therefore essential to direct GLUT4 into the insulin-responsive compartment and to effectively sequester GLUT4 from the cell surface in the basal state. However, the molecules responsible for regulating this intracellular sorting pathway remain largely unknown.

Previous studies have implicated the TGN localised t-SNARE, STX16, in GLUT4 trafficking in 3T3-L1 adipocytes. STX16 is a phosphoprotein in these cells and phosphorylation is decreased in response to acute insulin stimulation. This study aimed to elucidate the role, if any, of STX16 in GLUT4 trafficking, and to determine whether phosphorylation was responsible for the regulation of this process.

In this study, experiments to identify the exact site of insulin-regulated phosphorylation were carried out in HEK 293 cells and suggest that STX16 phosphorylation may be specific to adipocytes. Immunoprecipitation studies revealed the existence of a STX16 containing SNARE complex in 3T3-L1 adipocytes with the t-SNAREs STX6 and Vtila; however, this SNARE complex does not appear to be regulated by insulin. These studies also suggest that STX16 does not bind to its cognate SM protein, mVps45, when part of this SNARE complex, either in the presence or absence of insulin.

Recombinant adenoviruses were generated to express wild-type STX16 and STX16 mutants in 3T3-L1 adipocytes to assess their effects on glucose transport. Expression of these STX16 mutants proved problematic due to a property inherent in STX16, which requires stabilisation by its cognate SM protein, mVps45. It appears that STX16 expressed in excess of mVps45 is subject to proteasomal degradation, since expression could be dramatically increased when proteasome function was inhibited.

One mutant, STX16_{cyt}, constituted the dominant negative cytosolic domain of STX16 and was expressed in adipocytes to perturb endogenous STX16 function. Expression of STX16_{cyt} significantly slowed the endocytic retrieval of GLUT4 following insulin-withdrawal. In contrast, expression of STX16_{cyt} had no effect on the secretion of an adipocyte-derived adipokine, ACRP30. In a complementary approach, endogenous STX16 was knocked down by > 90 % using a specific Morpholino Antisense Oligonucleotide. 3T3-L1 adipocytes depleted of STX16 in this way showed a significant decrease in insulin-stimulated glucose transport. This corresponded with ~ 30 % decrease in cellular GLUT4 levels. These data were rationalised within a model in which STX16 functions to sequester GLUT4 from the PM in the basal state in a step which involves the intracellular sorting of GLUT4 from the fast cycling endosomal system into the slowly recycling intracellular pool of which GSVs are part. In cells depleted of STX16, this pathway is blocked and GLUT4 appears to be directed into a degradative pathway.

Contents

	Page
Abstract	2
Table of contents	5
List of figures	11
Acknowledgements	13
Authors's declaration	14
Abbreviations	15
Appendix	228
References	231

Table of Contents

Chapter 1

1.	INTRODUCTION	17
1.1.	Type II Diabetes	17
1.2.	Facilitative glucose transporters	18
1.2.1.	GLUT4	18
1.3.	Insulin	21
1.3.1.	Function of insulin	21
1.3.2.	Insulin signalling	21
1.3.3.	Insulin resistance	22
1.3.4.	The importance of adipose tissue	22
1.3.5.	Secretion from adipocytes	22
1.4.	Intracellular protein trafficking	23
1.4.1.	Introduction	23
1.4.2.	The endocytic pathway	23
1.4.3.	The secretory pathway	25
1.4.4.	Membrane fusion	27
1.5.	SNAREs	31
1.5.1.	Introduction	31
1.5.2.	The Synaptic SNAREs as a model for other systems	34
1.5.3.	Classification of SNAREs	37
1.5.4.	The SNARE core-complex	37
1.5.5.	Syntaxins	40
1.5.6.	SNAP-25	41
1.5.7.	SM proteins	41
1.5.8.	Regulation of SNARE complex formation	42
1.6.	Syntaxin 16 (STX16)	44
1.6.1.	STX16	44
1.6.2.	Syntaxin 6 (STX6)	46
1.6.3.	STX16 and STX6 binding	48
1.6.4.	Yeast homolog - Tlg2p	48
1.6.5.	mVps45	49
1.7.	Intracellular trafficking of GLUT4	51
1.7.1.	Intracellular locations of GLUT4	51
1.7.2.	Endosomes	51
1.7.3.	The role of the TGN	52
1.7.4.	GSVs	52
1.7.5.	Biogenesis of GSVs	53
1.7.6.	Targeting signals on GLUT4	53
1.7.7.	SNAREs involved in GLUT4 vesicle fusion with the PM	54
1.7.8.	GLUT4 Trafficking Model	54
1.8.	STX16 in GLUT4 trafficking	57
1.8.1.	Evidence implicating STX6 and STX16 in trafficking of GLUT4	57
1.8.2.	Phosphorylation of STX16	58

1.9. Hypothesis	59
1.10. Aims	59
Chapter 2	
2. MATERIALS AND METHODS	64
2.1. Materials	64
2.1.1. General reagents	64
2.1.2. Cell culture materials	66
2.1.3. Plasmids	67
2.1.4. Primary antibodies	67
2.1.5. Escherichia coli (<i>E. coli</i>) strains	68
2.1.6. Cell Culture Media	68
2.1.7. General Solutions	68
2.1.8. Primers	70
2.2. Molecular Biology Methods / Procedures	70
2.2.1. Amplification of target DNA by PCR	70
2.2.2. Purification of PCR products	71
2.2.3. Agarose gel electrophoresis	72
2.2.4. Gel extraction of DNA	72
2.2.5. A-tail reaction (Taq treatment)	73
2.2.6. TA cloning	73
2.2.7. Restriction digest	73
2.2.8. Ligation	74
2.2.9. Transformation of <i>E. coli</i>	74
2.2.10. Mini-cultures	75
2.2.11. Small-scale DNA preparations (Mini-preps)	75
2.2.12. Large-scale DNA preparations (Maxi-preps)	75
2.2.13. Site-directed mutagenesis	76
2.2.14. DNA concentration determination	77
2.2.15. Ethanol Precipitation	78
2.2.16. Sequencing	78
2.2.17. Preparation of glycerol stocks of transformed bacteria	78
2.3. Mammalian Cell Culture Methods / Procedures	79
2.3.1. General conditions	79
2.3.2. Trypsinisation and passage of cells	79
2.3.3. Freezing down and resurrection of cells	79
2.3.4. 3T3-L1	80
2.3.5. HeLa	81
2.3.6. HEK 293	82
2.4. Biochemical Methods / Procedures	83
2.4.1. Immunoprecipitation	83
2.4.2. Trichloroacetic acid (TCA) precipitation	85
2.4.3. SDS gel electrophoresis / SDS-PAGE	85
2.4.4. Transfer to nitrocellulose	86
2.4.5. Immunoblotting (Western blotting)	86
2.4.6. Stripping nitrocellulose	87

2.4.7.	Protein concentration determination (Bradford Assay)	87
--------	--	----

Chapter 3

3.	PHOSPHORYLATION OF STX16	88
3.1.	Introduction	88
3.1.1.	Phosphorylation	88
3.1.1.1.	Regulation by phosphorylation	88
3.1.1.2.	Phosphorylation of SNAREs	89
3.1.1.3.	Tlg2p is phosphorylated in yeast	90
3.1.1.4.	STX16 is a phosphoprotein in 3T3-L1 adipocytes	90
3.1.2.	Is STX16 phosphorylated by PKA?	91
3.1.2.1.	PKA	91
3.1.2.2.	Insulin-stimulated GLUT4 trafficking and regulation of PKA	91
3.2.	Hypothesis	94
3.3.	Aims	94
3.4.	Methods	96
3.4.1.	PhosphoProtein Purification Kit	96
3.4.2.	Immunoprecipitation of STX6 from 3T3-L1 adipocytes +/- insulin +/- NEM	97
3.4.2.1.	Cell treatment and preparation of lysates	97
3.5.	Results	98
3.5.1.	Identification of phosphorylation site in STX16	98
3.5.1.1.	Overview	98
3.5.1.2.	<i>in silico</i> analysis of possible phosphorylation sites	98
3.5.1.3.	Construction of STX16 pCR3.1	105
3.5.1.4.	Transfection of HeLa cells with STX16 pCR3.1	105
3.5.1.5.	Immunoprecipitation of myc-tagged STX16 expressed in HeLa cells	106
3.5.1.6.	Mutagenesis of potential phosphorylation sites in STX16: T90, S94 & S94 to A	110
3.5.1.7.	Expression of STX16 and T90 in HEK 293 cells	111
3.5.1.8.	PhosphoProtein purification kit	113
3.5.1.9.	Analysis of STX16, T90 and S94&95 with ³² P	116
3.5.1.10.	Expression of mutants	116
3.5.1.11.	Analysis of mutants with ³² P	116
3.5.1.12.	Labelling with ³² Pi and immunoprecipitation	116
3.5.2.	Identification of STX16 SNARE binding partners in 3T3-L1 adipocytes	120
3.5.2.1.	Overview	120
3.5.2.2.	Immunoprecipitation of STX6 from 3T3-L1 adipocytes	120
3.5.2.3.	STX6 co-immunoprecipitates STX16	121
3.5.2.4.	STX6 co-immunoprecipitates Vti1a	121
3.5.2.5.	STX6 does not co-immunoprecipitate mVps45	121
3.6.	Discussion	125

Chapter 4

4. GENERATION OF RECOMBINANT ADENOVIRUSES AND OPTIMISATION OF ADENOVIRUS-MEDIATED EXPRESSION OF STX16 MUTANTS IN 3T3-L1 ADIPOCYTES	131
4.1. Introduction	131
4.1.1. Introduction to adenovirus	131
4.1.1.1. General properties of the adenovirus	131
4.1.1.2. Structure and genome	131
4.1.1.3. Infectious cycle of the adenovirus	134
4.1.1.4. Cell receptors for the adenovirus	134
4.1.1.5. Use of adenoviral vectors to confer gene transfer into mammalian cells	136
4.1.1.6. HEK 293 cells	136
4.1.1.7. Construction recombinant adenoviruses	137
4.1.1.8. Receptor availability may affect protein expression	137
4.1.1.9. Why use adenovirus in this study?	138
4.2. Aims	138
4.3. Materials and Methods	139
4.3.1. Generation of recombinant adenoviruses	139
4.3.1.1. ViraQuest	139
4.3.1.2. Amplification of pShuttle-CMV virus in HEK 293 cells	141
4.3.1.3. Purification of viral particles from HEK 293 cells	141
4.3.1.4. Calculation of virus titre for accurate infections	142
4.3.1.5. Multiplicity of infection (MOI)	143
4.3.2. Infection of 3T3-L1 adipocytes with adenovirus	143
4.3.3. Infection of HeLa cells with adenovirus	144
4.3.4. Treatment of infected 3T3-L1 adipocytes with MG132	144
4.3.5. Adenovirus use and safety considerations	144
4.4. Results	145
4.4.1. Design of STX16 mutants	145
4.4.1.1. The cytosolic domain (STX16 _{cyt})	145
4.4.1.2. N-terminal deletion mutant (STX16 _T)	145
4.4.1.3. Full-length STX16 (STX16 _F)	147
4.4.2. Construction of recombinant adenoviruses to express STX16 _{cyt} , STX16 _T and STX16 _F in 3T3-L1 adipocytes	152
4.4.2.1. Cloning of STX16 _{cyt} , STX16 _T and STX16 _F into pShuttle-CMV	152
4.4.2.2. ViraQuest	154
4.4.3. Control virus	154
4.4.4. Optimisation of infection of STX16 _{cyt} in 3T3-L1 adipocytes	157
4.4.4.1. Trial infection of HeLas	157
4.4.4.2. Infection of 3T3-L1 adipocytes	157
4.4.4.3. Infection in 3T3-L1 adipocytes +/- 0.5 % BSA	157
4.4.4.4. $\alpha v\beta 5$ integrins	158
4.4.4.5. Why such low expression?	163
4.4.4.6. Expression of STX16 _{cyt} is increased by infection of 3T3-L1 adipocytes on days 4 and 6 post-differentiation	163
4.4.4.7. Expression of STX16 _{cyt} is increased when 3T3-L1 adipocytes are treated with Proteasome Inhibitors (MG132) following infection on day 6 post-differentiation	164

4.4.4.8.	Levels of IRAP, mVps45, STX4, Vti1a, VAMP2 and endogenous STX16 remain constant with MG132 treatment	165
4.4.4.9.	Optimisation of STX16F in 3T3-L1 adipocytes	170
4.4.4.10.	Optimisation of STX16T in 3T3-L1 adipocytes	171
4.5.	Discussion	175
 Chapter 5		
5.	THE ROLE OF STX16 IN THE INTRACELLULAR TRAFFICKING OF GLUT4	182
5.1.	Introduction	182
5.1.1.	Morpholino Antisense Oligonucleotides (MAOs)	182
5.1.2.	GLUT4 trafficking	184
5.1.3.	Secretion of ACRP30 from adipocytes	184
5.2.	Aims	185
5.3.	Materials and Methods	185
5.3.1.	Assays	185
5.3.1.1.	ACRP30 Secretion Assay	186
5.3.1.2.	Glucose Transport Assay	186
5.3.1.3.	Reversal of GLUT4 translocation after insulin withdrawal	186
5.3.1.4.	Statistical analysis	187
5.3.2.	Electroporation of 3T3-L1 adipocytes with MAO	187
5.4.	Results	188
5.4.1.	Effect of STX16cyt, STX16T and STX16F on GLUT4 trafficking	188
5.4.1.1.	Overview	188
5.4.1.2.	Effect of MG132 Proteasome Inhibitors on basal and insulin-stimulated deGlc transport	188
5.4.1.3.	Effect of STX16cyt on deGlc transport in basal and insulin-stimulated cells and following insulin withdrawal	189
5.4.1.4.	Effect of STX16T and STX16F on basal and insulin-stimulated glucose transport	195
5.4.2.	Effect of STX16cyt on the secretion of ACRP30	198
5.4.2.1.	Overview	198
5.4.2.2.	Effect of MG132 on ACRP30 secretion	198
5.4.2.3.	Effect of STX16cyt on ACRP30 secretion	198
5.5.	Knockdown of STX16 in 3T3-L1 adipocytes	202
5.5.1.	Overview	202
5.5.2.	STX16 specific MAO	202
5.5.2.1.	Blast search and design of STX16 MAO	202
5.5.3.	Internalisation of fluoresceinated MAO using Endo-Porter reagent	202
5.5.4.	Electroporation of 3T3-L1 adipocytes to achieve delivery of MAO	203
5.5.4.1.	STX16 is knocked down by > 90 % in 3T3-L1 adipocytes using STX16 MAO	203
5.5.4.2.	Knockdown of STX16 expression reduces insulin-stimulated deGlc transport	204
5.5.4.3.	Knockdown of STX16 expression reduces total cell GLUT4 levels	204

5.6. Discussion	210
Chapter 6	
6. CONCLUSIONS AND FUTURE DIRECTIONS	218
6.1. Phosphorylation of STX16	218
6.2. Effect of STX16 on GLUT4 trafficking in 3T3-L1 adipocytes	220
6.3. Model of STX16 in GLUT4 trafficking	223

Table of Figures

Chapter 1

	Page	
1.1	GLUT4 in 3T3-L1 adipocytes	20
1.2	Schematic representation of the endocytic pathway	29
1.3	Schematic representation of the secretory pathway	30
1.4	Intracellular localisation of SNARE proteins in a typical mammalian cell	33
1.5	Cycle of assembly and disassembly of the SNARE complex in synaptic vesicle exocytosis	36
1.6	SNARE proteins form a four-helical bundle complex that drives membrane fusion	39
1.7	Two different modes of coupling between Syntaxins and SM proteins	43
1.8	Naturally occurring STX16 splice variants	50
1.9	A model depicting the transport of GLUT4 in insulin responsive cells	56
1.10	A model depicting the potential involvement of STX16 in GLUT4 trafficking in adipocytes	60
1.11	Model depicting a possible role for STX16 phosphorylation in regulation of GLUT4 trafficking	61

Chapter 3

3.0	Insulin regulation of GLUT4 translocation and PKA activity in adipocytes	93
3.1	Model for the regulation of a SNARE complex involving STX16 and STX6 by phosphorylation	95
3.2	Sequence alignment of STX16 with Tlg2p	100
3.3	Analysis of STX16 sequence for potential phosphorylation sites	101
3.4	STX16 sequence analysed for consensus motifs pertaining to a particular kinase	104
3.5	Construction of STX16 pCR3.1 plasmid	107
3.6	Western Blot of myc-tagged STX16 expressed in HeLa cells	108
3.7	Immunoprecipitation of myc-tagged STX16 expressed in HeLa cells	109
3.8	Expression of STX16 and STX16 T90 in HEK 293 cells	112
3.9	Fractions collected before and after the purification on the Phosphoprotein Binding Column	115
3.10	Expression and immunoprecipitation of myc-tagged STX16, T90 and S94&95 in HEK 293 cells	118
3.11	³² P analysis of STX16 in HEK 293 cells	119
3.12	STX6 and STX16 co-immunoprecipitate in 3T3-L1 adipocytes	123
3.13	STX6 co-immunoprecipitates Vti1a but not mVps45 in 3T3-L1 adipocytes	124

Chapter 4

4.1	Structure of adenovirus	133
4.2	Binding and internalisation of the adenovirus	135
4.3	Generation of recombinant adenovirus using the RAPAd.1 system	140
4.4	Comparison of domain structures of STX16F, STX16cyt and STX16T	148
4.5	STX16 Kyte-Doolittle Plot, indicating the position of the transmembrane domain	149
4.6	Comparative models of wild-type STX16 and STX16T	150
4.7	Sequence alignment of STX16 with Tlg2p	151
4.8	Construction of STX16cyt pShuttle-CMV	155

4.9	Construction of STX16T and STX16F pShuttle-CMV plasmids	156
4.10	Expression of STX16cyt in HeLa cells	160
4.11	Infection of 3T3-L1 adipocytes with STX16cyt in the presence and absence of 0.5 % BSA	161
4.12	Expression of α v and β 5 subunits in 3T3-L1 adipocytes from day 2 to day 10 post differentiation	162
4.13	Expression of STX16cyt in 3T3-L1 adipocytes is increased when cells are infected of days 4 and 6 post differentiation	167
4.14		168
4.15	Levels of IRAP, mVps45, STX4, Vtila, VAMP2 and endogenous STX16 remain constant following treatment with MG132 proteasome inhibitors	169
4.16	Optimisation of STX16F expression in 3T3-L1 adipocytes	173
4.17	Optimisation of STX16T expression in 3T3-L1 adipocytes	174

Chapter 5

5.1	Structure of a Morpholino subunit	183
5.2	Effect of MG132 on basal and insulin-stimulated deGlc transport	191
5.3	Effect of STX16cyt on deGlc transport in basal and insulin-stimulated cells and following insulin withdrawal	193
5.4	Quantification of STX16cyt produced by cells infected days 4 and 6	194
5.5	Quantification of STX16T and STX16F produced by cells infected days 4 and 6	196
5.6	Effect of STX16T and STX16F on deGlc transport in 3T3-L1 adipocytes	197
5.7	Effect of MG132 treatment on ACRP30 secretion in 3T3-L1 adipocytes	200
5.8	Effect of STX16cyt on ACRP30 secretion in 3T3-L1 adipocytes	201
5.9	Delivery of a fluoresceinated MAO at various concentrations into 3T3-L1 adipocytes	206
5.10	MAO-depletion of STX16 expression in 3T3-L1 adipocytes	207
5.11	Insulin-stimulated deGlc transport is inhibited by MAO-depletion of STX16 in 3T3-L1 adipocytes	208
5.12	GLUT4 levels are decreased in 3T3-L1 adipocytes depleted of STX16 in 3T3-L1 adipocytes	209
5.13	A model depicting the involvement of STX16 in GLUT4 trafficking in adipocytes	216

Chapter 6

6.1	A possible model depicting the involvement of STX16 in GLUT4 trafficking in adipocytes	226
6.2	Model depicting the possible role of STX16 phosphorylation in regulation of GLUT4 trafficking	227

Acknowledgements

First and foremost, I would like to thank my supervisor, Prof. Gwyn W. Gould, for his invaluable help and support with all aspects of my PhD work, for helpful conversations, encouragement, help with experiments, for not laughing too much at my spectacular fall over his laptop and generally for being an excellent supervisor! I thoroughly enjoyed my time in Gwyn's lab and it was a privilege to be able to work there for three years. I would also like to thank Dr. Nia Bryant for her interest in my project and for many helpful suggestions, discussions and encouragement, without forgetting an extremely memorable conference trip to Austria! Of course, I would like to thank the Wellcome Trust for awarding me this studentship and for funding my research.

I would also like to thank all the members of Lab 241, past and present, not only for help in the lab, but for making my three years in the lab so enjoyable and for organising so many great nights out! I would especially like to thank Dr. Scott Shanks for his help with phosphorylation experiments, Dr. Marie Anne Ewart for her help with adenoviral work and Excel analysis, Dr. Steven Miller for help with electroporation, and Drs. Ian Salt and Luke Chamberlain for providing answers to my many questions. I would also like to thank all my friends for encouraging me throughout my PhD.

My deepest thanks go to my Mum and Dad, Catherine and Duncan Proctor, for their never-ending support, encouragement and love over the years, and for their patience, help and support during my PhD and the writing of this thesis. Thanks also to my Gran and Papa, Margaret and Thomas Proctor, and my Grandma and my late Papa, Margaret and Walter Proctor, for their encouragement and love over the years. My acknowledgments would not be complete without a special thank you to my dog, Lucky (Proctor!), for being the best companion I could have hoped for during the writing of this thesis.

Author's declaration

I declare that the work described in this thesis has been carried out by myself unless otherwise cited or acknowledged. It is entirely of my own composition and has not, in whole or in part, been submitted for any other degree.

...Kirsty...Proctor

Kirsty M. Proctor

July 2006

Abbreviations

ACRP30	Adipocyte complement-related protein of 30 kDa
CMV	Cytomegalovirus
<i>E. coli</i>	<i>Escherichia coli</i>
EE	Early Endosome
ER	Endoplasmic Reticulum
GLUT	Glucose transporter
GLUT4	Glucose transporter 4
GSV	GLUT4 Storage Vesicle
LE	Late Endosome
MPR (CD and CI)	Mannose 6 phosphate receptor (cation-dependent / independent)
NSF	N-ethyl-maleimide-sensitive fusion protein
PM	Plasma Membrane
RE	Recycling Endosome
<i>S. cerevisiae</i>	<i>Saccharomyces Cerevisiae</i>
SM protein	Sec1/Munc18 protein
SNAP-25	Synaptosome-associated protein of 25 kDa
SNARE	Soluble NSF attachment protein receptor
STX	Syntaxin
STX16	Syntaxin 16
STX16 _{cyt}	Syntaxin 16 (cytosolic domain)
STX16F	Syntaxin 16 (full-length)
STX16T	Syntaxin 16 (N-terminal truncation)
STX6	Syntaxin 6
TfR	Transferrin receptor
TGN	Trans-Golgi network
VAMP	Vesicle Associated Membrane Protein

Chapter 1

Introduction

1. Introduction

1.1. Type II Diabetes

Type II diabetes is now one of the main threats to human health in the 21st century, with an explosive increase in the worldwide occurrence of this heterogeneous disorder in the past two decades (reviewed in Zimmet et al., 2001). An estimated 6 % of the adult population in the Western world is affected and the number of people affected worldwide is anticipated to increase by 6 % per annum, potentially reaching a total of 200–300 million cases in 2010 (Amos et al., 1997; Kopelman and Hitman, 1998).

The type II diabetes epidemic is taking place both in developed and developing nations and is particularly pronounced in certain ethnic groups, for example in Pacific and Indian Ocean island populations, groups in India and Australian Aboriginal communities (Zimmet et al., 2001). Originally a disease associated with onset in later life, type II diabetes has now been reported in children and adolescents in various countries, including the UK (Zimmet et al., 2001). The main reasons for the epidemic proportions of the disorder are believed to be the prevalence of a sedentary lifestyle, and in particular, obesity (Zimmet et al., 2001).

Type II diabetes is characterised by insulin resistance and / or abnormal insulin secretion, either of which may predominate. Insulin resistance is characterised by dysfunctional glucose uptake into muscle and adipose tissue, in conjunction with an oversupply of glucose from the liver, which results in high circulating plasma glucose levels. This leads to many of the complications associated with type II diabetes including blindness, renal failure, nerve damage and limb amputation (Brownlee, 2001), with atherosclerotic cardiovascular disease being responsible for 80 % of diabetic mortality (Moller, 2001).

Glucose uptake into muscle and adipose tissues is facilitated by the glucose transporter, GLUT4 (Section 1.2.1) (Bryant et al., 2002; Watson et al., 2004). As dysfunctional glucose uptake into these tissues contributes to insulin resistance and the onset of type II diabetes, a clear understanding of the molecular basis of intracellular GLUT4 trafficking is required to design effective therapies (Bryant et al., 2002; Watson et al., 2004).

1.2. Facilitative glucose transporters

Glucose is a primary source of energy for eukaryotic cells. Glucose is distributed throughout the various tissues of the body in mammals by a family of glucose transporters, called GLUTs, of which there are 12 known members (reviewed in Gould and Bell, 1990; Mueckler, 1994; Olson and Pessin, 1996). These members differ in their tissue distribution and kinetic properties, as well as in their intracellular localisation.

GLUTs are integral membrane proteins, and when present at the cell surface, act as shuttles to allow glucose to cross the plasma membrane (PM). GLUT proteins share a similar topology with 12 transmembrane helices, which form an aqueous pore that allows glucose to diffuse down its concentration gradient in a non-energy dependent process (Gould and Bell, 1990; Mueckler, 1994). Thus the rate of glucose entry into a cell is dependent of the quantity of glucose transporters present at the cell surface.

Many mammalian tissues, such as the brain, have a constitutively high glucose requirement and as such possess transporters that are constitutively targeted to the cell surface, for example GLUTs 1-3 (Olson and Pessin, 1996). By contrast, certain tissues require a regulated glucose transport system, as in the case of GLUT4 facilitated glucose uptake into muscle and fat cells (Bryant et al., 2002; Watson et al., 2004).

1.2.1. GLUT4

Muscle and adipose tissues have evolved a highly regulated glucose transport system, which allows the rate of glucose uptake to increase in these tissues by 10-40 fold within minutes of exposure to a particular stimulus (reviewed in Shepherd and Kahn, 1999). This system is essential for the maintenance of blood glucose homeostasis during exercise, when the metabolic demands of the skeletal muscle can increase more than 100-fold, and during the absorptive period (after a meal), when insulin stimulation increases the uptake of glucose into muscle and adipose tissue for subsequent storage as glycogen and triglycerides.

The glucose transporter responsible for the insulin-stimulated transport of glucose into muscle and fat cells is GLUT4, which is expressed in high levels in only white and brown adipocytes and in cardiac and skeletal myocytes (Bryant et al., 2002; Olson and Pessin, 1996; Watson et al., 2004). Unlike other members of the facilitative glucose transporter family, GLUT4 is almost completely intracellularly localised in the basal state. In response

to insulin, GLUT4 is mobilised (translocated) to the PM, allowing an increase in the rate of glucose entry (Bryant et al., 2002; Watson et al., 2004). Dysfunctional glucose uptake into muscle and fat cells contributes to the onset of type II diabetes.

Figure 1.1 shows adipocytes immuno-stained for GLUT4, indicating its intracellular location in basal cells and its subsequent movement to the cell surface in response to insulin. The mechanism by which this translocation occurs will be described in detail in Section 1.7.

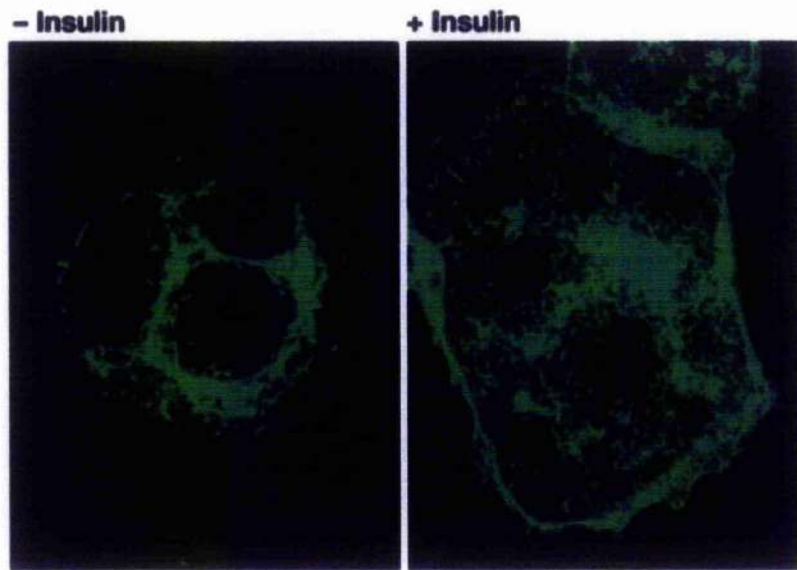


Figure 1.1 GLUT4 in 3T3-L1 adipocytes (taken from Bryant et al., 2002)

Confocal image of 3T3-L1 adipocytes incubated either with (right panel) or without (left panel) 100 nM insulin for 15 mins. The location of GLUT4 in these cells is shown using an antibody that specifically recognises GLUT4 and a secondary antibody conjugated to Alexa-488 (green). In the basal state, GLUT4 is localised mainly to intracellular vesicles, whereas upon insulin stimulation it is delivered to the PM.

1.3. Insulin

1.3.1. *Function of insulin*

In normal individuals, plasma glucose is maintained in a narrow range between 4 and 7 mM during periods of feeding and fasting by a balance between glucose absorption from the intestine, production by the liver, and uptake and metabolism by peripheral tissues. As well as increasing glucose uptake in muscle and adipose tissue, insulin inhibits hepatic glucose production, thus acting as the primary regulator of blood glucose homeostasis (reviewed in Saltiel and Kahn, 2001). In addition, insulin stimulates cell growth and differentiation, and promotes the storage of substrates in fat, liver and muscle by stimulating lipogenesis, glycogen and protein synthesis, and inhibiting lipolysis, glycogenolysis and protein breakdown. Insulin resistance or deficiency results in profound dysregulation of these processes, and produces elevations in fasting and postprandial glucose and lipid levels (Saltiel and Kahn, 2001).

1.3.2. *Insulin signalling*

Insulin responsive cells, such as muscle and fat cells, express a cell-surface receptor to which the hormone can bind. Upon insulin binding, a conformational change is induced in the receptor, leading to activation of its tyrosine-kinase domain and the phosphorylation of several proximal substrates, translating the signal into an intracellular cascade responsible for the many cellular effects of insulin (reviewed in Saltiel and Kahn).

Activation of the insulin receptor results in the tyrosine phosphorylation of members of the insulin-receptor-substrate (IRS) family (IRS-1 and IRS-2 in muscle and fat cells), which recruit effector molecules, such as the lipid kinase phosphatidylinositol 3-kinase (PI3K), to the PM. A signalling pathway involving PI3K has been implicated in GLUT4 trafficking (Bryant et al., 2002; Saltiel and Kahn, 2001; Tengholm and Meyer, 2002). There is considerable evidence to suggest that the Class 1a PI3K might have an important role in insulin-stimulated GLUT4 translocation (Bryant et al., 2002; Saltiel and Kahn, 2001). Insulin signalling will be discussed further in Section 3.1.2.2 (Chapter 3).

1.3.3. *Insulin resistance*

As mentioned previously, one of the main pathophysiological defects in type II diabetes is insulin resistance, a decrease in cellular responses to insulin. This insulin resistance is characterised by defects at many levels, for example, decreases in receptor concentration and kinase activity, the concentration and phosphorylation of IRS-1 and -2, PI(3)K activity, GLUT4 and the activity of intracellular enzymes (Pessin and Saltiel, 2000). This decreased insulin sensitivity includes a reduction in insulin-stimulated glucose uptake into fat and muscle cells, due to a defect in the ability of insulin to stimulate GLUT4 translocation to the PM in these cells. In adipocytes, decreased insulin sensitivity is caused additionally by decreased GLUT4 expression (Minokoshi et al., 2003; Shepherd and Kahn, 1999), an effect that is not observed in muscle. Indeed, GLUT4 protein and mRNA levels are decreased in adipocytes in most cases of insulin resistance, including that present in human obesity and type II diabetes (Shepherd and Kahn, 1999).

1.3.4. *The importance of adipose tissue*

Adipose tissue accounts for only a small fraction of glucose disposal after a meal, with the majority of glucose taken up by muscle (Minokoshi et al., 2003). On this basis, it would not be expected that diminished glucose uptake into adipocytes would have a significant impact on glucose homeostasis. However, whereas mice with a knockout of the insulin receptor in muscle have normal glucose tolerance (Bruning et al., 1998), those with adipose specific ablation of GLUT4 have impaired glucose tolerance, which appears to be due to insulin resistance being induced in muscle and liver (Abel et al., 2001). Further experimental evidence has now demonstrated conclusively that decreased GLUT4 expression in adipocytes decreases insulin sensitivity in muscle and liver, resulting in a change in glucose homeostasis (Minokoshi et al., 2003).

1.3.5. *Secretion from adipocytes*

Excess adipose tissue in obesity and lack of adipose tissue in lipodystrophic states are associated with insulin resistance and type II diabetes mellitus in human and animal studies (Ganda, 2000; Kahn and Flier, 2000), demonstrating that adipose tissue is crucial in regulating metabolism beyond its ability to take up glucose. Until recently, adipose tissue was commonly viewed exclusively as a depot for lipids. However, adipocytes are now viewed as highly active cells with potent autocrine, paracrine and endocrine functions,

which play active roles in normal metabolic homeostasis and in the development of disease (Mora and Pessin, 2002).

Adipose tissue controls energy expenditure through the secretion of several physiologically active polypeptide hormones, collectively called adipocytokines or adipokines, which may profoundly influence metabolism (reviewed in Ritchie et al., 2004). The best studied of these is leptin, which acts on receptors in the central nervous system and other sites to inhibit food intake and promote energy expenditure. However, a number of other significant adipokines have been discovered in recent years (Ritchie et al., 2004), including ACRP30 (described in Section 5.1.2), adiponectin, IL (interleukin)-6, TNF- α and resistin. Secretion of the adipokines is altered in obese individuals and many are thought to play an important role in insulin resistance.

1.4. Intracellular protein trafficking

1.4.1. Introduction

Eukaryotic cells have been endowed with extensive internal membranes that enclose specific compartments, or organelles, each of which plays a unique role in the growth and metabolism of the cell. As such, each organelle contains a collection of specific enzymes that catalyse necessary chemical reactions and house an intracellular environment, which differs from that of the cytosol and other organelles, specific to its function. Membrane impermeable substances, such as proteins and lipids are transported between these organelles and to and from the cell surface in membrane bound vesicles which bud from the donor compartment membrane and fuse with the acceptor compartment membrane, releasing their contents. Two distinct intracellular trafficking pathways are known to exist in eukaryotic cells: the endocytic and the secretory / biosynthetic pathways. Communication between these pathways occurs by vesicle trafficking between the Golgi complex and endosomes.

1.4.2. The endocytic pathway

Endocytosis is the collective term given to the various mechanisms by which eukaryotic cells take up extracellular or cell surface material (reviewed in Mellman, 1996). This

process is essential to maintain cellular homeostasis and cellular communication by the uptake of nutrients, extracellular fluid, ligands and receptors.

The most common type of endocytosis is known as receptor mediated endocytosis, and involves the selective uptake of ligands, such as proteins, glycoproteins, or carbohydrates, that bind with high affinity to PM receptors and are then internalised. The cell utilises this method to obtain nutrients, such as iron (see below) or cholesterol, and to remove potentially harmful molecules (such as hormones, which are needed acutely but briefly) from the extracellular environment. In addition, cells take up extracellular fluid in small vesicles, in a process known as pinocytosis, however, this will not be discussed further here.

Newly synthesised molecules travel along the secretory pathway (Section 1.4.3) and many join the endocytic pathway at the *trans*-Golgi network (TGN) on route to their correct intracellular location, sometimes travelling via the PM, and as such endocytosis is a necessary part of the itinerary. In addition, endocytosis is required for the removal of molecules such as GLUT4 (Section 1.2.1), which are required at the PM for a limited time in response to certain stimuli, from the extracellular environment. The pathway can also be used to retrieve molecules that have been incorrectly targeted to the PM by secretory activity.

Endosomes are the major sorting stations / compartments along the endocytic pathway, and consist of, mainly, the early or sorting endosome (EE), recycling endosome (RE) and late endosome (LE) (reviewed in Clague, 1998; Mellman, 1996). The organisation of the endocytic pathway is depicted in Figure 1.2. Endosomes are distinguished based on, among other criteria, the presence of specific biochemical markers (Figure 1.2) for example proteins of the Rab GTPase family (Clague, 1998; Mellman, 1996). The extent to which these endosomes represent distinct stable compartments remains controversial, with the possibility that they exist transiently as intermediates in a process of endosomal maturation. An important element controlling sorting along the endocytic pathway is the pH gradient that extends through the sequential endosomal compartments (Figure 1.2).

Cargo enters the endocytic pathway in vesicles budding from specialised regions of the PM to the EE where it is sorted and directed into various destinations (Mellman, 1996) (Figure 1.2). Cargo to be recycled may return to the cell surface directly or via the RE, whereas material intended for degradation can be transferred from LEs to lysosomes, the comprehensive digestive centres of the cell. In cells that undergo regulated trafficking,

cargo may be directed to specialised endosomal derived recycling vesicles or secretory vesicles. The TGN represents the link between the endosomal and the secretory / biosynthetic pathways, and as such, cargo may either be recycled back to this compartment through endosomes or join the endosomal system following synthesis in the ER (Section 1.4.3). In the case of receptor-mediated endocytosis, most ligands are dissociated from their receptors in the acidic environment of the EE or RE and the receptors are recycled to the PM.

The biogenesis of transport vesicles is initiated by the recruitment of large multi-subunit proteins called coats. The assembly of coat proteins is important in the selection of cargo and deforming the lipid bilayer into a budding vesicle. The coat protein centrally involved in endocytosis is clathrin (reviewed in Kirchhausen, 2000), which forms clathrin coated vesicles in conjunction with adaptor proteins (AP-1 to AP-4) at in addition to the PM, the TGN and endosomes. Clathrin dependent endocytosis occurs at specialised patches on the PM, called clathrin-coated pits. The GTPase, dynamin has been implicated as being important in “pinching” these vesicles from the membrane (Schmid et al., 1998). The majority of receptor mediated endocytosis events occur via clathrin dependent endocytosis. So-called clathrin independent mechanisms of endocytosis exist (Mellman, 1996), including pinocytosis (above) and caveolae/raft dependent endocytosis (Nabi and Le, 2003). Intracellular trafficking vesicles also utilise coat proteins, known as COPs, (Salama and Schekman, 1995). COP1 is associated with EEs and in retrograde transport from the Golgi to the ER (Barlow, 2000), whereas COPII is associated with vesicles targeted to the Golgi from the ER (Barlow, 2000; Kuehn and Schekman, 1997).

The transferrin receptor (TfR), which mediates cellular iron uptake by binding to the iron-carrying protein transferrin is considered a prototype resident of the early/recycling endosomal pathway. TfR binds to its ligand before being internalised via clathrin-coated pits to the EEs, where iron is released in the acidic environment of the compartment. The TfR, carrying iron-free transferrin, is then returned directly from the EE to the PM with a half time of about two to three minutes (Mayor et al., 1993), however, a proportion of TfR is returned to the PM via the RE, with a longer half time of about five to ten minutes (Daro et al., 1996).

1.4.3. The secretory pathway

The biosynthetic or secretory pathway represents the pathway by which newly synthesised proteins in the ER are transported to the cell surface for secretion into the extracellular

space or to their correct intracellular destination (Ellgaard et al., 1999). Traffic in the early secretory pathway between the ER and the Golgi is bidirectional, ensuring that proteins required to form and fuse vesicles with organelles are recycled as secretory cargo advances (Barlow, 2000). From the ER, newly synthesised proteins are directed, via a compartment commonly referred to as the intermediate compartment, to the Golgi stack (Gruenberg and Kreis, 1995). However, it has also been suggested that this transport process may proceed via a compartment maturation process (Allan and Balch, 1999). A network of tubular-cisternal structures, the *cis*-Golgi network, is the point of entry for material destined to reach and transit through the cisternae of the Golgi complex. Cargo proceeds through the medial to *trans*-Golgi (Allan and Balch, 1999), where it enters the exit site of the Golgi complex, the TGN. The classical marker of the TGN is TGN38, a resident protein of the TGN, which actually recycles continuously between the TGN and the PM, presumably via EEs and / or LEs (Miesenbock and Rothman, 1995).

In the TGN, proteins are sorted into different vesicular carriers and delivered to their final destination (reviewed in Traub and Kornfeld, 1997). Depending on the cell type, the cargo that arrives in the TGN can be distributed, via distinct transport carriers, to several different intracellular locations. The intracellular itinerary taken by each protein depends on sorting signals encoded in the polypeptide chain. The three possibilities are summarised in Figure 1.3.

The first represents the constitutive or default pathway, which delivers proteins directly to the cell surface (Traub and Kornfeld, 1997). Secretion is a constitutive activity of most cells, as is the biosynthesis and turnover of resident PM proteins and lipids. These activities result in a steady stream of both proteins and lipids from the TGN to the cell surface.

The second selective pathway sorts protein traffic from the TGN into the intracellular endosomal membrane system (Traub and Kornfeld, 1997) (described above, Section 1.4.2). Once in the endosomal system, proteins can be delivered to the PM or to their intracellular location along the secretory pathway. A classic example of this pathway is the transport of hydrolytic enzymes and glycoproteins from the TGN to the lysosome where they are required carry out the degradative functions of the organelle. Coated vesicles transport hydrolytic enzymes and integral membrane glycoproteins to the lysosome via early or late endosomes or both. Some lysosomal membrane glycoproteins travel via the PM before delivery to lysosomes along the endocytic pathway. Mannose 6-phosphate receptors (MPRs) are responsible for binding to individual prohydrolase molecules in the TGN

before being packaged into carrier vesicles and are delivered to lysosomes via the endosomal system (Ghosh et al., 2003). After MPRs discharge their cargo, other vesicles carry the unoccupied MPRs back from the endosomes to the TGN.

The third fate of proteins emerging from the TGN occurs in cells that specialise in regulated secretion, such as endocrine, neuroendocrine and exocrine cells. These proteins are secreted via the so-called regulated secretory pathway (reviewed in Tooze et al., 2001). This pathway is required for the regulated secretion of bioactive molecules such as hormones and peptides in response to hormonal or neuronal stimulation. Most of the body's polypeptide hormones, enzymes used in the digestive tract, and many other products that are needed intermittently rather than continuously, utilise this pathway for secretion. Regulated secretory cells package secretory proteins into large, dense core granules that accumulate in the cytosol and fuse with the PM only upon stimulation.

The formation of a mature secretory granule occurs in four stages (described in Tooze et al., 2001). First the regulated secretory proteins are accumulated and sorted to the membrane in the TGN and secretory granules initially classified as immature secretory granules, bud from these regions of the TGN. During maturation, the immature secretory granules undergo homotypic fusion to build the mature secretory granule. This fusion is followed by remodelling and removal of excess membrane through the formation of clathrin coated vesicles. This process involves the sorting away of molecules that are not required in mature secretory granules, such as MPR-ligand complexes (Klumpperman et al., 1998) and proteins involved in the homotypic fusion events (Wendler et al., 2001). Finally, the mature secretory granules accumulate, poised for the exocytotic release of their contents into the extracellular milieu in response to an external stimulus.

1.4.4. Membrane fusion

The final stage of intracellular protein trafficking involves the fusion of the cargo vesicles derived from the donor compartment with membrane of the correct target compartment. It is energetically unfavourable to fuse two membranes (phospholipid bilayers) in an aqueous environment, because the electrostatic repulsive and hydration forces between the two membranes have to be overcome. All types of membrane fusion are believed to share common protein machinery (Bennett and Scheller, 1993; Ferro-Novick and Jahn, 1994). Fusion occurs via a highly ordered mechanism that has multiple co-ordinated steps including vesicle docking/tethering, priming and finally fusion. As such, this process is thought to involve the concerted action of a number of protein families, including the

Sec1/Munc18 homologs (SM proteins) (Jahn and Sudhof, 1999; Lin and Scheller, 2000), Rab GTPases, AAA ATPases and various membrane tethering proteins, the discussion of which is beyond the scope of this thesis. The molecules suggested to be centrally involved in this membrane fusion process are soluble N-ethylmaleimide-sensitive factor attachment protein receptor or SNARE proteins (Jahn and Sudhof, 1999; Lin and Scheller, 2000), which have been proposed to mediate all intracellular membrane fusion events (Section 1.5).

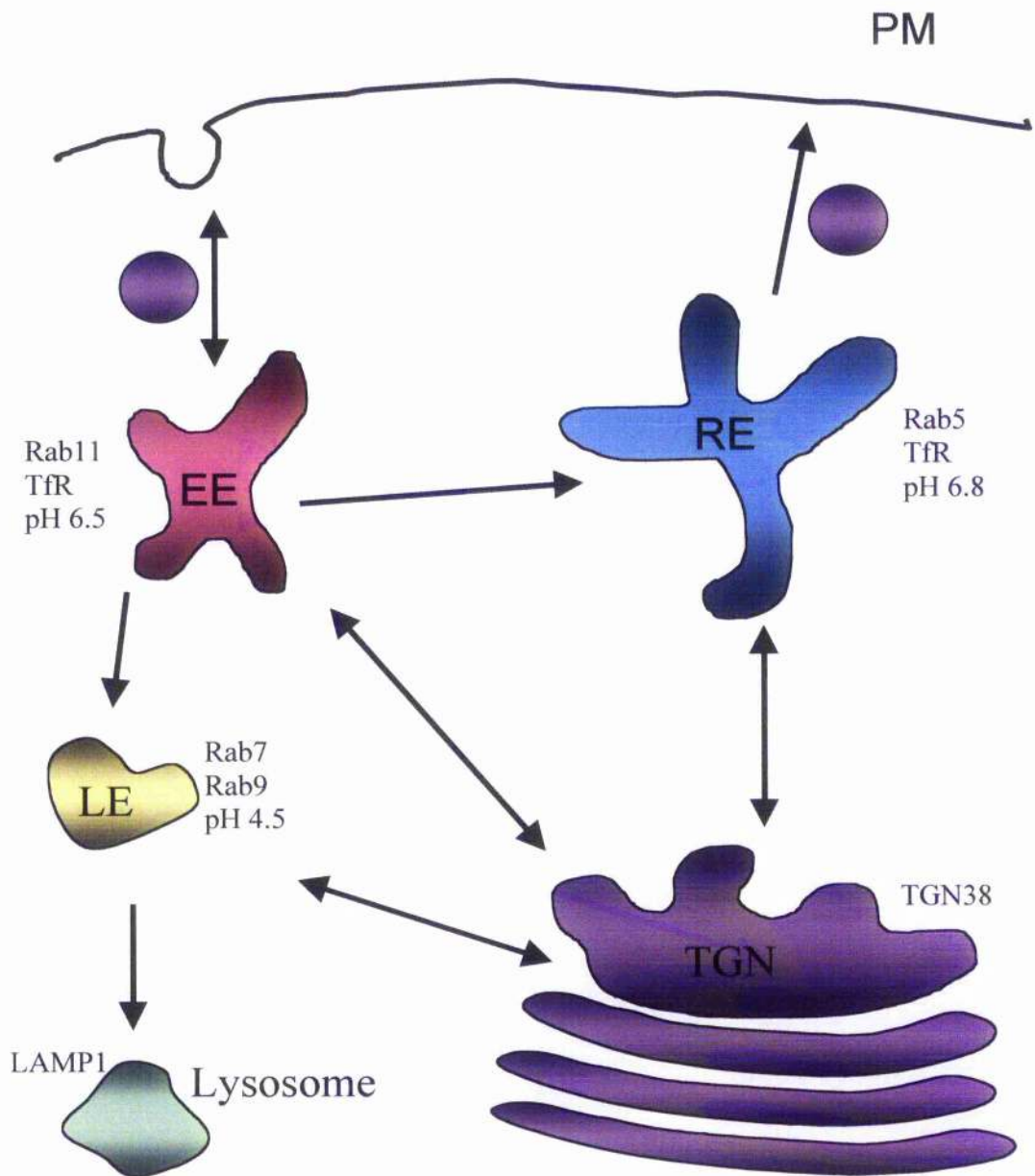


Figure 1.2 Schematic representation of the endocytic pathway

The endocytic pathway along with typical marker proteins (of the Rab GTPase family) for each compartment (Clague, 1998) and the characteristic pH associated with each compartment. Cargo enters the pathway in vesicles that bud from specialised regions of the PM. Recycling cargo, such as the TfR, may return to the PM directly or via REs. Cargo intended for degradation may be directed to the lysosome via LEs. The TGN represents the point of exchange between the endocytic and secretory / biosynthetic pathway. TGN38 and LAMP1 are markers of the TGN and lysosomes respectively.

PM, plasma membrane; EE, early endosome; RE, recycling endosome; LE, late endosome; TGN, *trans*-Golgi network; TfR, transferrin receptor

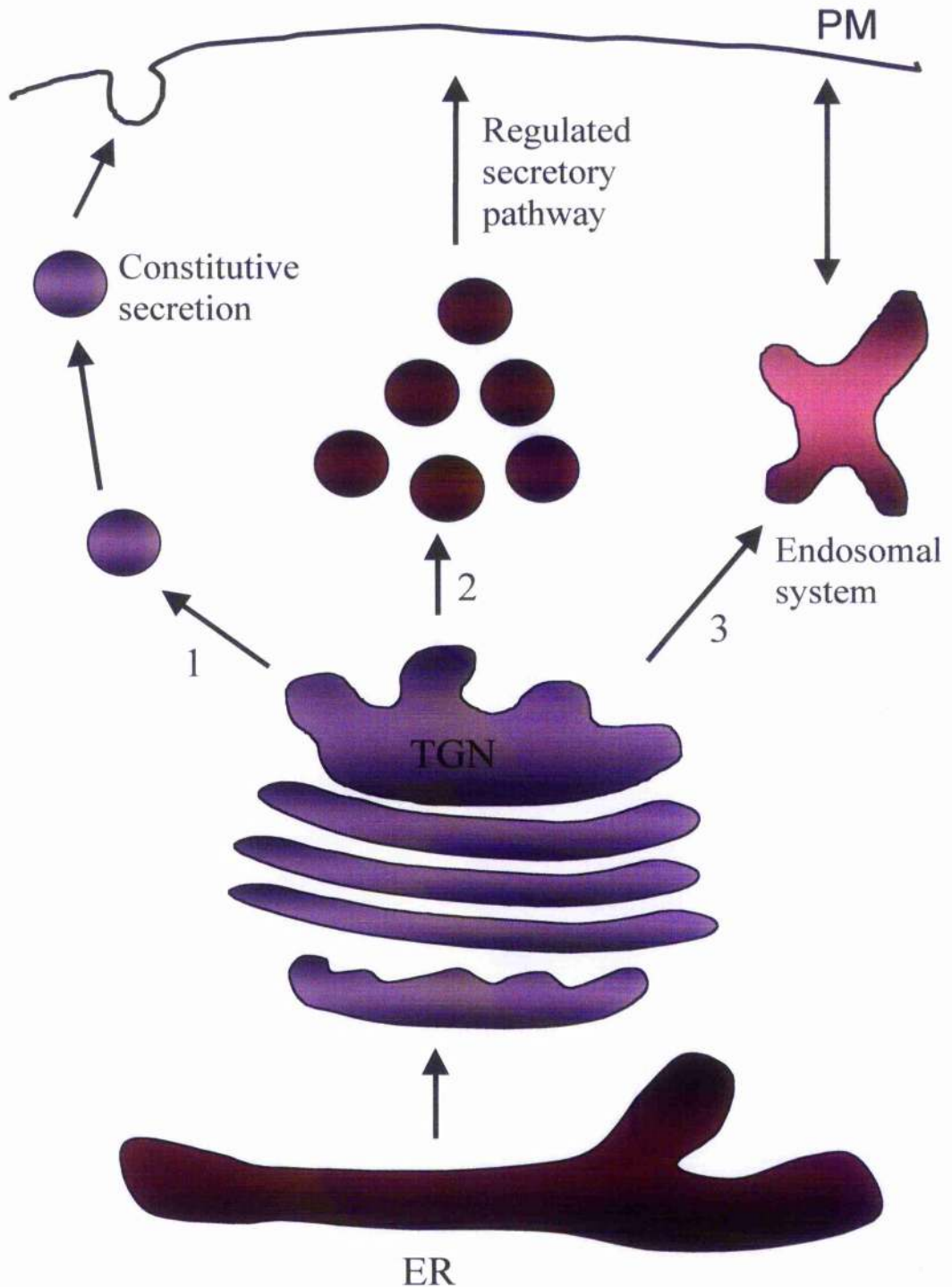


Figure 1.3 Schematic representation of the secretory pathway

Newly synthesised proteins exit the ER and progress through the Golgi stack to the TGN where the fate of the protein is decided.

(1) The constitutive secretory pathway, where cargo is directed directly to the PM for secretion into the extracellular milieu. (2) The regulated secretory pathway. Cargo is packaged into dense-core secretory granules, which accumulate in the cytosol, poised for exocytotic release in response to external stimuli. (3) Cargo may be directed to the endosomal system (Section 1.4.2 and Figure 1.2) from where it can be directed into a recycling pathway or to lysosomes.

ER, endoplasmic reticulum; TGN, *trans*-Golgi network; PM, plasma membrane

1.5. SNAREs

1.5.1. Introduction

The SNARE (soluble NSF attachment protein receptor where NSF stands for N-ethylmaleimide-sensitive fusion protein) proteins form a multi-gene superfamily involved in catalysing membrane fusion (reviewed in Chen and Scheller, 2001; Jahn and Sudhof, 1999; Lin and Scheller, 2000; Pelham, 2001). All SNAREs share a homologous membrane proximal domain of approximately 60 amino acids, known as the SNARE motif, which has a high propensity to form coiled coils (Fasshauer et al., 1998b; Hay, 2001; Jahn and Sudhof, 1999). The SNARE motif is the defining feature of all SNAREs.

The majority of SNAREs are type II integral membrane proteins, anchored to the membrane via a C-terminal transmembrane domain with a short extracytoplasmic domain and the N-terminus in the cytosol; however, some SNAREs do not contain a transmembrane domain but instead are tethered to the membrane via palmitoylation or prenylation (reviewed in Hay, 2001). The cytosolic N-terminal regions contain both hydrophobic and hydrophilic regions and are able to adopt cytoplasmic amphipathic helices.

In 1993, Rothman and colleagues suggested the concept of the SNARE hypothesis to explain the specificity of membrane fusion events (Sollner et al., 1993). It supposed that for all vesicle trafficking events, there exists a unique vesicle-associated SNARE (v-SNARE), which specifically recognises and interacts with a cognate SNARE localised to the target membrane (t-SNARE) (Rothman, 1994; Sollner et al., 1993). These v- and t-SNAREs were thought to bind in a specific manner to form complexes that were capable of bridging the two membranes, ultimately resulting in fusion.

Functional studies have provided insights into how SNARE proteins interact with each other to generate the driving force needed to fuse lipid bilayers (Chen and Scheller, 2001; Jahn and Sudhof, 1999). Reconstitution experiments have suggested that SNAREs alone can indeed cause bilayer merger but at a slow rate (Weber et al., 1998), suggesting that additional factors are required for physiological membrane fusion.

To date, 36 SNARE proteins have been identified in the human genome and 21 in the yeast genome (Bock et al., 2001). Figure 1.4 shows the distribution of known mammalian SNAREs throughout the secretory pathway. Most SNAREs are specifically localised to distinct membrane compartments throughout the cell (Chen and Scheller, 2001; Scales et al., 2000), perhaps suggesting a role in controlling the specificity of membrane fusion events. This notion was partly responsible for the development of the SNARE hypothesis (Sollner et al., 1993).

In recent years, the SNARE hypothesis has been challenged by studies which suggest SNARE pairing may be more promiscuous than previously thought (Yang et al., 1999), however, it nonetheless remains the basis of our understanding of SNARE function.

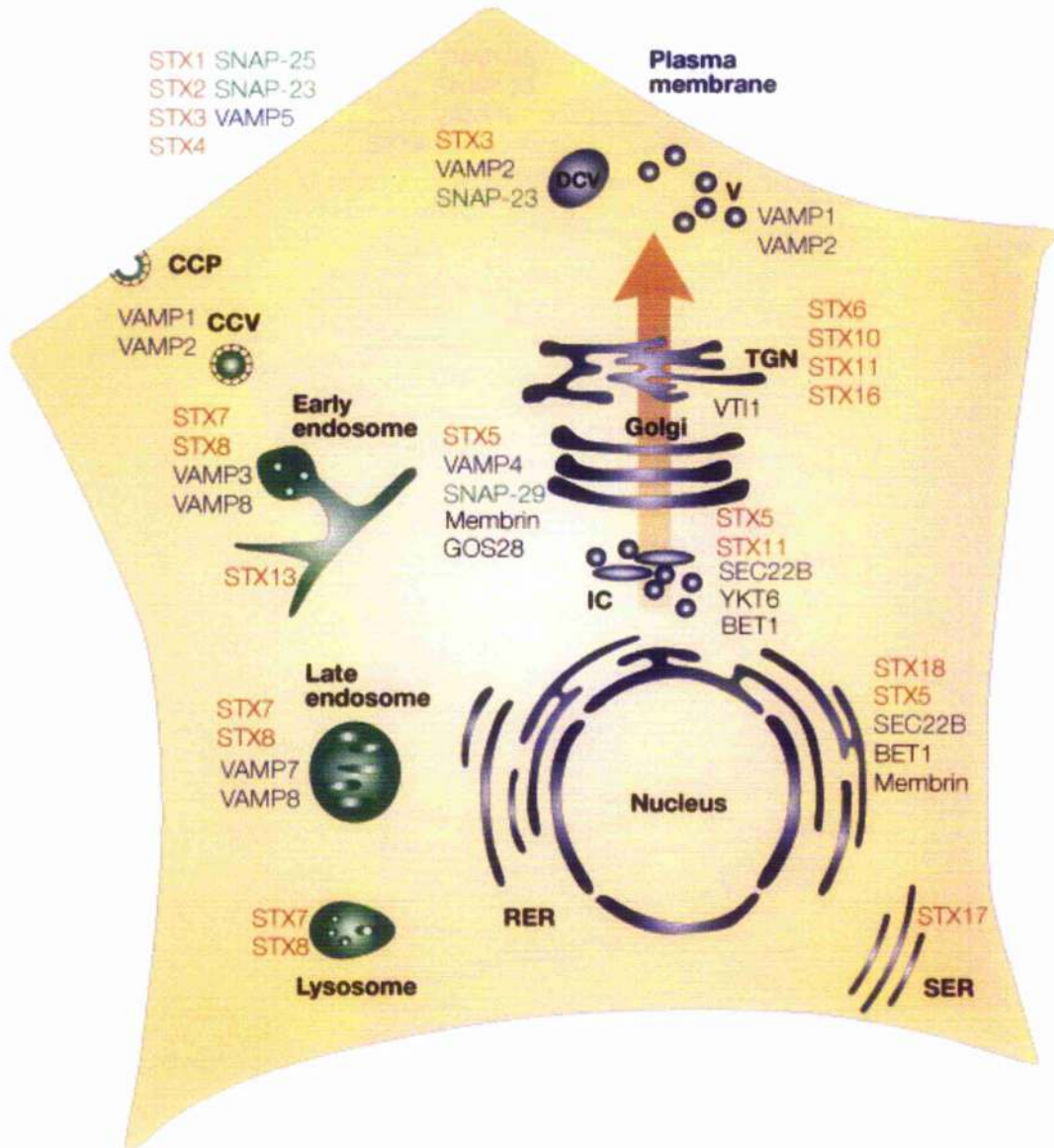


Figure 1.4 Intracellular localisation of SNARE proteins in a typical mammalian cell (taken from Chen and Scheller, 2001)

The mammalian SNAREs that have been studied so far localise to distinct subcellular compartments throughout the secretory pathway, indicating a possible role in controlling the specificity of membrane trafficking/fusion events.

Red, Syntaxin (STX) family; blue, VAMP family; green, SNAP-25 family; black, others; CCP, clathrin coated pit; CCV, clathrin coated vesicles; DCV, dense core vesicles; IC, intermediate compartment; RER, rough endoplasmic reticulum; SER, smooth endoplasmic reticulum; TGN, *trans*-Golgi network; V, vesicles.

1.5.2. *The Synaptic SNAREs as a model for other systems*

In the nervous system, membrane fusion is an essential step in chemical synaptic transmission because neurotransmitter-filled presynaptic vesicles fuse in a calcium-dependent manner with the plasma membrane to release their content into the synaptic cleft. The first SNAREs to be discovered were those functioning in synaptic vesicle exocytosis in neurons (reviewed in Lin and Scheller, 2000). Much of our current knowledge regarding SNARE function is derived from numerous detailed studies of the synaptic SNAREs. Studies involving homologs of these and other SNARE proteins in yeast, suggest that parallels can be drawn from this system to all known fusion events. Therefore, synaptic vesicle fusion will be used here to explain the basis of SNARE complex formation and membrane fusion.

The fusion of synaptic vesicles involves the concerted action of three SNARE proteins: the PM associated t-SNAREs STX1a (Syntaxin1a) (Bennett et al., 1992) and SNAP-25 (25 kDa synaptosome-associated protein) (Oyler et al., 1989), and the vesicular protein VAMP (vesicle-associated membrane protein, also called synaptobrevin) (Baumert et al., 1989; Trimble et al., 1988). STX1a and VAMP are anchored to their respective membranes via a transmembrane domain, and each contains one SNARE motif at the membrane proximal end of the molecule. SNAP-25, on the other hand, possesses two SNARE motifs, connected by a cysteine-rich linker region. SNAP-25 is devoid of a transmembrane domain and palmitoylation confers membrane attachment. The proteins interact via their SNARE motifs to form the SNARE complex (Section 1.6.5.1), an extremely stable four-helix bundle containing the four α -helical SNARE motifs at its core (two from SNAP-25 and one each from VAMP and STX1a) (Fasshauer et al., 1998a; Poirier et al., 1998a; Poirier et al., 1998b; Sutton et al., 1998). Figure 1.5 shows the cycle of assembly and disassembly of the SNARE complex in synaptic vesicle exocytosis.

STX1a contains an N-terminal region that precedes the SNARE motif and includes an autonomously folded three helical domain termed the H_{abc} domain (Fernandez et al., 1998). The presence of this domain confers to STX1a the ability to adopt two distinct conformations: a "closed conformation" in which the H_{abc} domain folds back onto the SNARE motif, and a more "open" conformation in which the SNARE motif is exposed (Dulubova et al., 1999). In this way, the three helices of the H_{abc} domain compete with the SNARE motifs of VAMP and SNAP-25 for binding to the STX1a SNARE motif (Misura

et al., 2001). The SM protein (Section 1.5.7) Munc18a binds to the “closed” conformation of STX1a (Dulubova et al., 1999; Misura et al., 2000). These features perhaps impose some regulation on SNARE complex formation.

It has been suggested that when not present in a complex, SNAREs are relatively unstructured (Fasshauer et al., 1998a). The “zipper” model of SNARE function postulates that the pairing begins at the membrane distal end and “zips-up” towards the membrane proximal end, with the SNAREs becoming more α -helical in character as zipping proceeds (Lin and Scheller, 1997). This “zipping” of the SNAREs brings the vesicle and plasma membranes into close contact and the formation of the stable SNARE complex is hypothesised to overcome the energy barrier to drive fusion of the lipid bilayers (Lin and Scheller, 1997). Partially assembled / “zipped” complexes have been isolated, suggesting that complexes exist in various stages of completion (Zhang et al., 2005). To account for this, SNAREs are often referred to being in either *cis* - (on the same membrane) (Weber et al., 1998) or *trans* - (on opposing membranes) conformations (Chen and Scheller, 2001). A SNARE complex in the *cis* conformation probably resembles the fully assembled complex, whereas SNAREs in a *trans*-complex might only loosely or partially interact because of the resistance posed by the membranes.

After fusion, and the release of the vesicle contents, *cis*-SNARE complexes can be disassembled and SNAREs recycled for another round of fusion. Due to the extremely stable nature of the complex, energy in the form of ATP is required to dissociate it into monomeric components (Chen and Scheller, 2001). Disassembly is carried out by two proteins, the ATPase NSF (N-ethyl-maleimide-sensitive fusion protein) and an adaptor protein, α -SNAP (soluble NSF attachment protein). Several structural studies of α -SNAP, NSF and a SNARE-SNAP-NSF complex formed prior to dissociation (Hanson et al., 1997; Hohl et al., 1998; Lenzen et al., 1998; May et al., 1999; Yu et al., 1998; Yu et al., 1999) suggest NSF may act as a “rotational shear” to dissociate the complex.

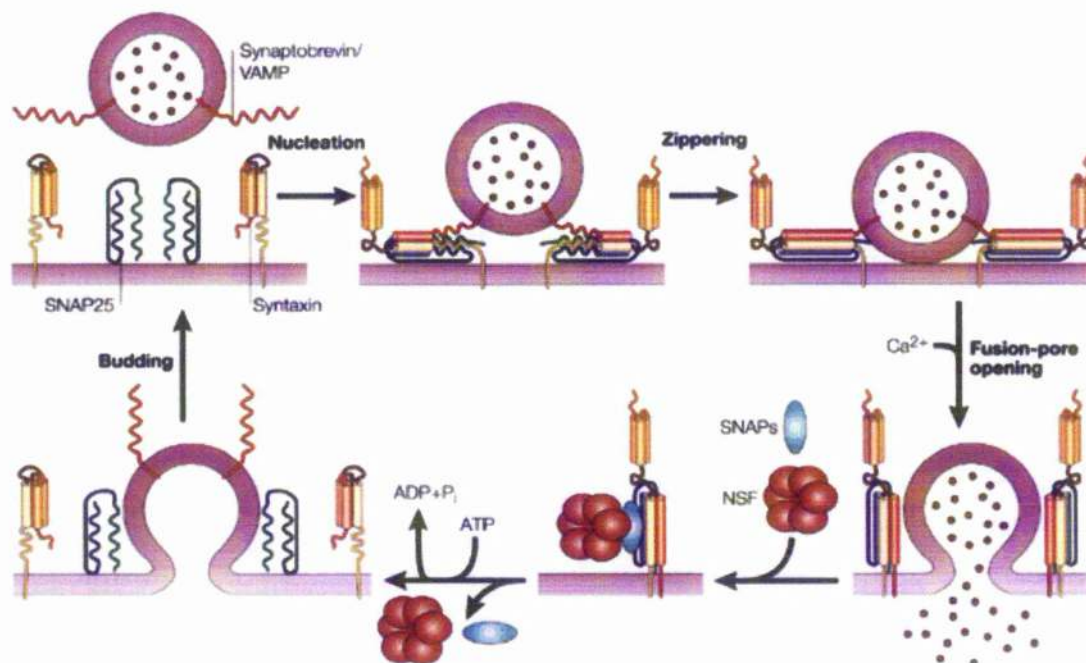


Figure 1.5 Cycle of assembly and disassembly of the SNARE complex in synaptic vesicle exocytosis (taken from Rizo and Sudhof, 2002)

STX1a (Syntaxin in this figure) exists in a closed conformation, which may inhibit SNARE complex assembly with its SNARE partners, SNAP-25 and VAMP2. After conversion to the open conformation, SNARE complex assembly (nucleation) can proceed. “Zippering” of the *trans*-SNARE complex in the direction of the carboxyl terminus brings the vesicle and PM into close contact, which may ultimately result in fusion. After fusion and release of the vesicle contents, the *cis*-SNARE complexes are disassembled by NSF in conjunction with SNAP proteins. Thus the SNAREs are recycled to take part in another round of membrane fusion.

Orange, STX1a H_{abc} domain; yellow, STX1a SNARE motif; red, VAMP2 SNARE motif; blue, SNAP-25 N-terminus SNARE motif; green, SNAP-25 C-terminus SNARE motif.

1.5.3. Classification of SNAREs

As mentioned previously, on the basis of their localisation to target or vesicle membranes, SNAREs were initially classified as t-SNAREs and v-SNAREs (Sollner et al., 1993). However, due to promiscuous binding and the ability of SNAREs to interact in a number of various trafficking steps, this classification was considered to be a huge oversimplification. With the additional benefit of preventing ambiguity in homotypic fusion events, SNAREs were grouped according to their homology with the synaptic SNAREs into the Syntaxin, SNAP-25 (described in detail in Sections 1.5.4 and 1.5.5) and VAMP families, on the basis of their sequence homology and domain structure. SNAREs were then further categorised according to the identity of a highly conserved ionic residue located in the SNARE motif (Fasshauer et al., 1998b), as R-SNAREs (arginine-containing SNAREs) or Q-SNAREs (glutamine containing SNAREs). Using the coiled-coil SNARE domain of the 35 known SNAREs in the human genome and all known yeast, *D. melanogaster* and *C. elegans* SNAREs, Bock et al. (Bock et al., 2001) classified Q- and R-SNAREs into four groups. Qa-SNAREs are homologous to Syntaxins, R-SNAREs to VAMPs, and Qb- and Qc-SNAREs are homologous to the N and C-terminus of SNAP-25 respectively. This classification has prompted a revision of the SNARE hypothesis and postulates that one member of each group contributes one chain to the four-helix bundle SNARE complex.

1.5.4. The SNARE core-complex

Biochemical studies with the soluble coiled-coil-forming domains of recombinant STX1a, SNAP-25 and VAMP have indicated that the neuronal SNARE complex is extremely stable (Fasshauer et al., 1998a; Poirier et al., 1998a). For example, it is resistant to SDS denaturation (Hayashi et al., 1994), protease digestion (Fasshauer et al., 1998a; Hayashi et al., 1994; Poirier et al., 1998a) and clostridial neurotoxin cleavage (Hayashi et al., 1994) and is heat stable up to 90 °C (Yang et al., 1999).

The crystal structure of the neuronal SNARE core complex has been solved revealing a four-helical bundle comprising one Syntaxin, one VAMP and two SNAP-25 coils (Sutton et al., 1998) (Figure 1.6). The four α -helical SNARE motifs are arranged in a parallel fashion with all amino termini at one end of the bundle. The crystal structure revealed that the helix bundle is highly twisted and contains several salt bridges on the surface, as well

as layers of interior hydrophobic residues (Sutton et al., 1998). Like other coiled-coil structures, the residues residing at “a” or “d” positions on a heptad helical wheel contribute to the hydrophobic core interactions that are important in stabilising the structure. These residues are the most conserved in the SNARE family (Fasshauer et al., 1998b). The interactions between the SNAREs occur on 16 levels with the so-called zero-layer at the core (Figure 1.6). This layer is characterised by the presence of the ionic residues mentioned above (an R residue from VAMP and three Q residues, one from STX1a and two from SNAP-25). The purpose of this zero layer is not totally known although it has been suggested that it may support the correct “register” during SNARE complex formation. This polar layer is present throughout the SNARE family (Fasshauer et al., 1998b; Sutton et al., 1998).

These observations have led to the proposal that all core complexes consist of four-helix bundles that are formed by three Q-SNAREs and one R-SNARE. Indeed, the crystal structure of a mammalian endosomal SNARE complex is remarkably similar to that of the neuronal complex, despite the low level of sequence conservation (Antonin et al., 2002). However, whereas SNAP-25 provides both the Q_b- and Q_c-SNAREs in SNARE complexes involved in exocytosis, it is thought that in intracellular membrane fusion events, the Q_b- and Q_c- chains are provided by separate SNAREs (Fasshauer et al., 1998b) and therefore requires the concerted action of four independent SNARE motifs/ proteins. This proposal has been supported by biophysical and reconstitution experiments (Antonin et al., 2002; McNew et al., 2000; Nicholson et al., 1998; Parlati et al., 2002; Paumet et al., 2001).

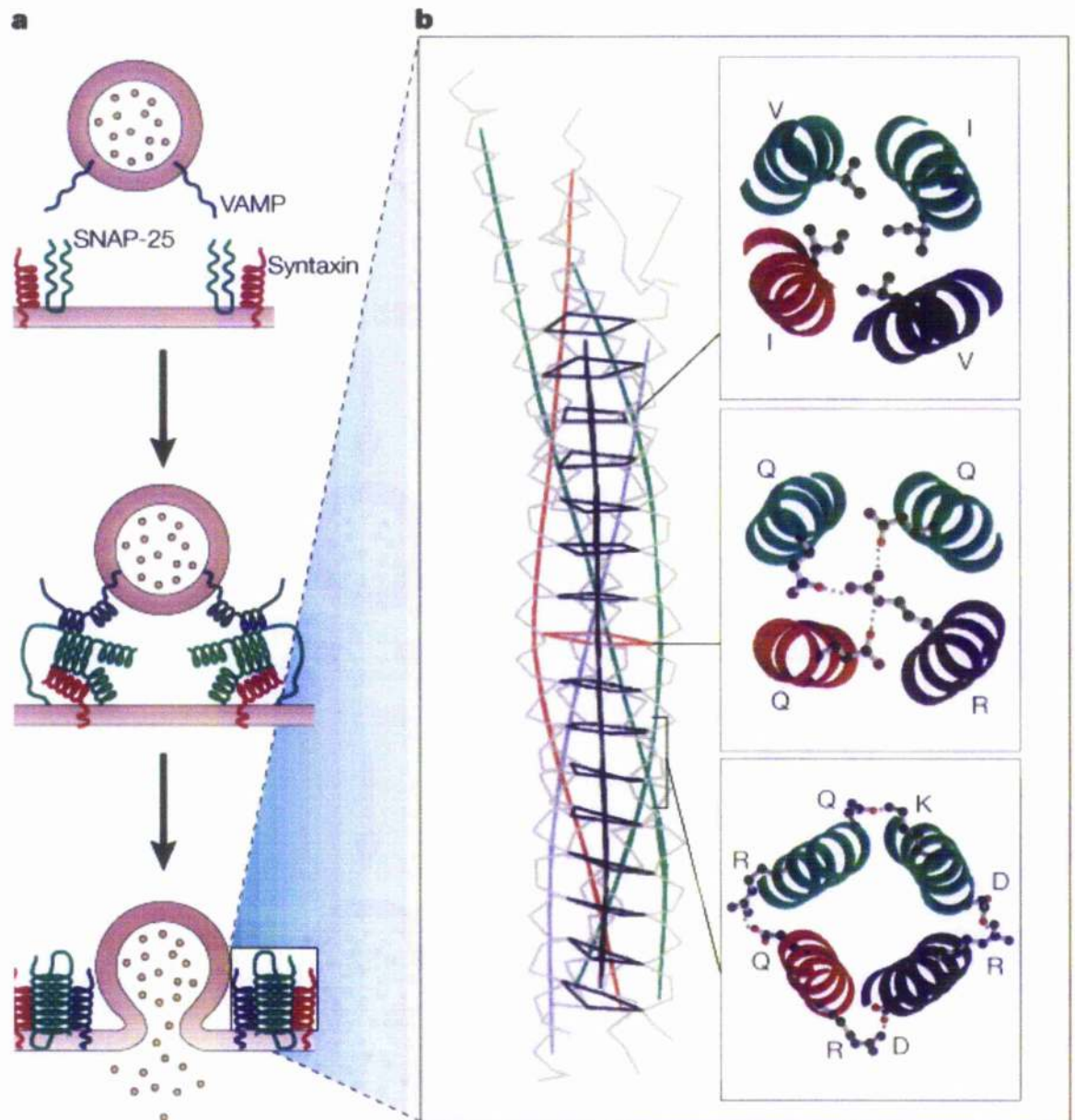


Figure 1.6 SNARE proteins form a four-helical bundle complex that drives membrane fusion (taken from Chen and Scheller, 2001)

- VAMP (blue) on the vesicle interacts with STX1a (Syntaxin in this figure, red) and SNAP-25 (green) on the PM to form a four-helix bundle that zips-up concomitant with bilayer fusion.
- The backbone of the SNARE complex is shown on the left (Sutton et al., 1998), with the central ionic layer (red) and 15 hydrophobic layers (black) that mediate the core interactions highlighted. Top-down views of side-chain interactions are shown on the right, with the four SNARE helices shown as ribbons. The ball and stick structures represent the indicated amino acids; the dotted lines represent hydrogen bonds or salt bridges that stabilise interactions between SNAREs. Q-SNAREs and R-SNAREs are characterised by a glutamine (Q) or arginine (R) residue, respectively, in the central layer of the SNARE complex

1.5.5. Syntaxins

Syntaxins comprise the largest SNARE family identified to date (reviewed in Teng et al., 2001) with 15 genes in mammals and 7 in yeast (Gerst, 1999). Their importance is emphasised by the presence of Syntaxin-like sequences in all eukaryotes examined to date (Teng et al., 2001). Syntaxins were originally described as two 35 kDa proteins (now known as STX1a and STX1b) that interact with the synaptic-vesicle protein synaptotagmin (Bennett et al., 1992). Typically, Syntaxins are proteins of about 300 amino acids. Subsequently, a number of the members of Syntaxin family were identified in a variety of membrane compartments of the exocytic and endocytic pathways of eukaryotic cells (Figure 1.4).

STXs 1,2,3 and 4 are predominantly localised to the PM where they take part in constitutive and regulated vesicle transport to the PM (Bennett et al., 1993; Inoue et al., 1992). STX5 is localised to the Golgi (Dascher et al., 1994). The majority of STX6 (Bock et al., 1997), STX10 (Tang et al., 1998b), STX11 (Valdez et al., 1999) and STX16 (Simonsen et al., 1998; Tang et al., 1998a) are localised to the TGN. Recently, STXs 6, 8 and 10 have been classified as Qc-SNAREs, rather than Qa-SNAREs based on the genome scale comparison of SNARE-motif sequences described above (Bock et al., 2001). STX7 (Wong et al., 1998), STX8 (Subramaniam et al., 2000) and STX12 (Tang et al., 1998c) which is considered to be identical to STX13, are localised in post-Golgi endosomal membranes. STX17 is distributed in smooth endoplasmic reticulum (Steegmaier et al., 2000) and STX18 in the endoplasmic reticulum (Hatsuzawa et al., 2000).

Syntaxins share similar structural features like those described above for STX1a (Section 1.5.2) (reviewed in Teng et al., 2001). All mammalian Syntaxins except STX11 are type II integral membrane proteins anchored to the membrane by their C-terminal tail. The TM tail anchor is essential for Syntaxin membrane localisation, but in most cases it is not sufficient for targeting to specific membranes. Compartmental targeting signals, which are ill defined, reside in the targeting domains. The cytosolic N-terminus contains several hydrophobic regions with the potential to form coiled-coil α -helical structures. Four such domains have been recognised from the majority of Qa-SNAREs. One of these comprises the characteristic membrane proximal SNARE motif of approximately 60 residues. The remaining three domains may constitute the existence of H_{abc} domains, similar to that proposed for STX1a. N-terminal domains of Syntaxin are conserved between Syntaxins

that function in the same trafficking pathway. These domains were found to be different between Syntaxins that function at different trafficking steps (Weimbs et al., 1997).

1.5.6. SNAP-25

SNAP-25 was first identified as a 206 amino acid synaptosomal protein expressed in neuronal tissues (Oyler et al., 1989). As described above, SNAP-25 contributes two SNARE motifs, separated by a cysteine rich linker region, to the neuronal SNARE complex and as such has been categorised as a Qbc-SNARE. Subsequently, two ubiquitously expressed homologs SNAP-23 and SNAP-29 were described (Hodel, 1998; Steegmaier et al., 1998) with highly conserved N- and C- terminal domains also predicted to form coiled-coil structures. Like SNAP-25, SNAP-23 is primarily localised to the PM and confers membrane attachment through palmitoyl residues that are thioester linked to four adjacent cysteine residues located in the middle of the protein (Hodel, 1998). While SNAP-25 is involved in synaptic vesicle exocytosis (Section 1.5.2), SNAP-23 has been implicated in the exocytosis of GLUT4 containing vesicles with the PM in conjunction with STX4 in muscle and fat cells (Section 1.7.7). SNAP-29 is predominantly found in intracellular membranes and lacks this cysteine rich palmitoylation site and is thought to be associated with membranes by interaction with other membrane proteins such as Syntaxins (Steedmaier et al., 1998).

1.5.7. SM proteins

SM (Sec1/Munc18) proteins are a family of hydrophilic 60-70 kDa polypeptides that share homology evenly throughout their sequence (reviewed in Rizo and Sudhof, 2002). Sec1 was discovered in screens for genes involved in the yeast secretory pathway (Steedmaier et al., 1998), whereas its mammalian homolog Munc18a was isolated due to its ability to bind to STX1a (Hata et al., 1993). Members of the family are now referred to as SM (Sec1/Munc18) proteins. Various studies indicate that SM proteins are essential for fusion. For example, neurotransmitter release and /or general secretion can be completely blocked by mutations in SM proteins (Harrison et al., 1994; Hosono et al., 1992; Ossig et al., 1991; Schekman, 1992; Verhage et al., 2000), and further studies have indicated that all types of intracellular membrane traffic require an SM protein, similar to the requirement for SNAREs (reviewed in Rizo and Sudhof, 2002).

As mentioned previously, the SM protein involved in neuronal exocytosis, Munc18a, binds tightly to the closed conformation of STX1a (Hata et al., 1993) and this binding is not

compatible with SNARE complex formation. This appears to be the general trend, with each SM protein associated with a cognate Qa-SNARE or Syntaxin molecule. However, the mode of binding to the cognate Syntaxin remains controversial. Studies involving STX1a and Munc18a led to the general belief that all SM proteins function by binding to the closed conformation of the corresponding Syntaxin. However, where the yeast plasma membrane Syntaxin Sso1p adopts a closed conformation (Munson et al., 2000), the corresponding SM protein Sec1p binds to core complexes containing Sso1p rather than to isolated Sso1p (Carr et al., 1999). In addition, the yeast vacuolar Syntaxin Vam3p does not adopt a closed conformation and its SNARE motif is sufficient to capture the SM protein Vps33p from yeast extracts (Dulubova et al., 2001). More recently, it was shown that the yeast ER and Golgi Syntaxins, Ufe1p and Sed5p, bind to the SM proteins through a novel, evolutionarily conserved mode that involves a short peptide motif at the very N-terminus of Ufe1p and Sed5p (Yamaguchi et al., 2002). Figure 1.7 shows the two hypothesised modes of binding between SNAREs and SM proteins, with the general belief that complexes involved in exocytosis may follow the STX1a/Munc18a mode of binding, whereas those involved in intracellular complexes the SM protein binding is compatible with SNARE complex formation (Rizo and Sudhof, 2002).

Since Munc18a is essential for exocytosis (Verhage et al., 2000), it was suggested that SM proteins may somehow assist in core complex assembly (Misura et al., 2000; Munson et al., 2000). However, the exact function of SM proteins remains ambiguous, with studies suggesting that they may exert both positive and negative regulatory effects on SNARE complex formation. It has also been suggested that they may play a role in stabilising the associated syntaxin (Bryant and James, 2001).

1.5.8. Regulation of SNARE complex formation

A plethora of molecules are known to bind to SNAREs, either directly or indirectly, and in doing so to exert regulatory effects on them. These molecules include synaptotagmin, GATE-16, LMA1, Munc13/UNC13, synaptophysin, tomosyn, and Vsm1. A detailed discussion of all of these potential regulatory molecules is beyond the scope of this thesis. For more information refer to the excellent review by J.E. Gerst (Gerst, 2003). Most relevant to this study is the possible regulation provided by SM proteins, the presence of a Syntaxin autoinhibitory domain (both of which will be considered in Chapter 4) and phosphorylation (Chapter 3).

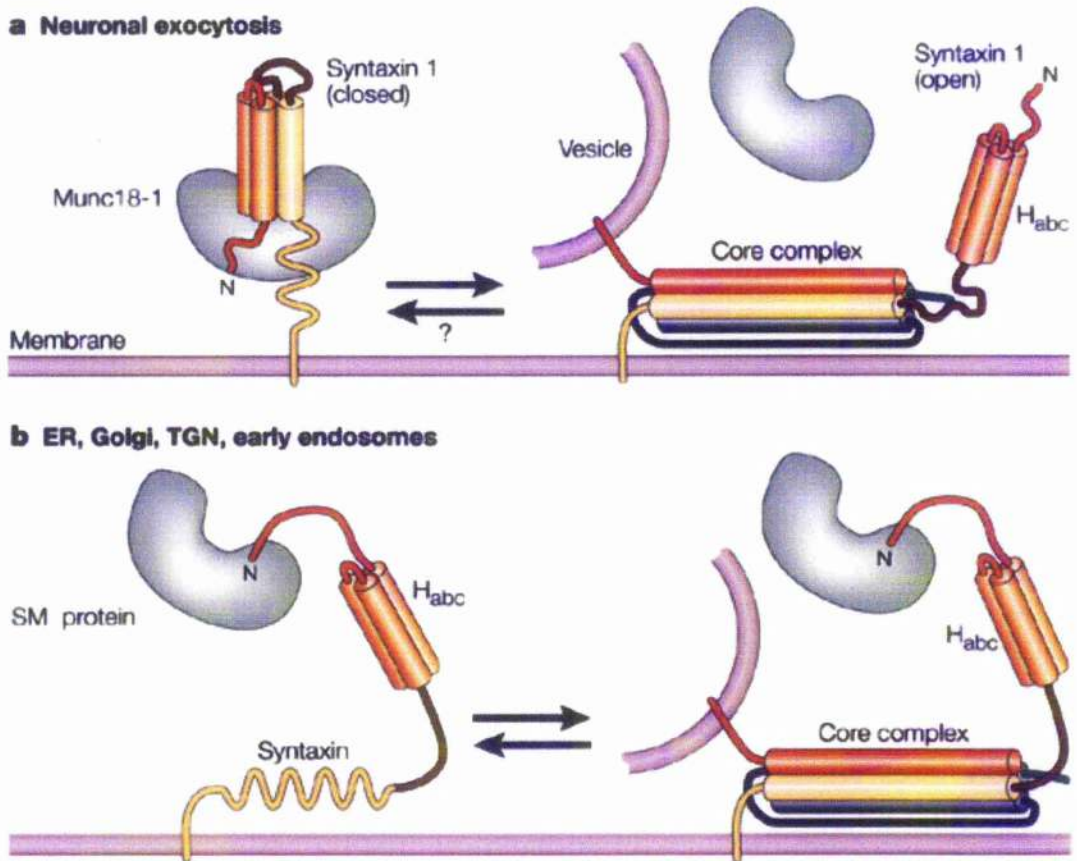


Figure 1.7 Two different modes of coupling between Syntaxins and SM proteins (taken from Rizo and Sudhof, 2002)

a) In neuronal exocytosis (Section 1.5.2), the interaction between Munc18a (Munc18-1 in this figure, grey) and the closed conformation of STX1a (Syntaxin 1 in this figure, yellow and orange) (Dulubova et al., 1999; Misura et al., 2000) is incompatible with formation of the core complex by the SNARE motifs of STX1a, SNAP-25 and VAMP2.

b) The interaction of Syntaxin amino-terminal peptide motifs with Sec1/Munc18 homologs (SM proteins) that occurs in the ER, the Golgi apparatus, TGN and the EE is fully compatible with core-complex formation (Dulubova et al., 2002).

Orange, STX1a H_{abc} domain; yellow, STX1a SNARE motif; red, VAMP2 SNARE motif; blue, SNAP-25 N-terminus SNARE motif; green, SNAP-25 C-terminus SNARE motif.

1.6. Syntaxin 16 (STX16)

1.6.1. STX16

STX16, the key protein in this study, has been implicated as playing a role in GLUT4 trafficking (Perera et al., 2003; Shewan et al., 2003). STX16 belongs to the superfamily of SNARE proteins. As a member of the Syntaxin family, STX16 is a t-SNARE and more specifically, has been categorised as a Qa-SNARE (Bock et al., 2001) (Section 1.5.3).

STX16 was first cloned and sequenced by Simonsen *et al.*, who demonstrated that the protein exists in three spliced forms, STX16A, STX16B and STX16C (Simonsen et al., 1998). The investigators searched the expressed sequence tag (EST) database of randomly sequenced cDNAs for sequences similar to the C-termini of Syntaxins. After identifying a Syntaxin-like EST from human colon (Genbank accession no. AA100145), which contained a 246 bp region with Syntaxin homology, they designed PCR primers to amplify the full-length cDNA from HeLa and brain plasmid cDNA libraries. The two longest HeLa cDNAs obtained (STX16A and STX16C) were identical, except for a 161 bp insertion and a 12 bp deletion in STX16A compared to STX16C. The STX16C cDNA contained an in-frame stop codon instead of the STX16A insert, giving rise to a C-terminally truncated translation product. The longest cDNA obtained from brain (STX16B) was identical to STX16A, but it contained in addition a 63 bp insertion. The three forms were supposed to originate from alternative splicing of the same transcript. STX16A, STX16B and STX16C cDNAs encode proteins of 303, 324 and 115 residues respectively and respective molecular masses of 34621 Da, 36840 Da and 13018 Da. The relative tissue distribution of each individual STX16 form could not be determined due to the similarity in size of the mRNAs in a Northern Blotting experiment, however, the distribution of the combined signal was enriched particularly in the pancreas, followed by skeletal muscle, heart, and brain. Epitope-tagged STX16A and STX16B were found to colocalise with the Golgi marker β -COP, while STX16C was found in the cytosol. STX16A associated posttranslationally with microsomes, and appeared to be transported to the Golgi via the endoplasmic reticulum. The authors concluded that the three STX16 forms might have different roles in intracellular trafficking. Sequence comparisons with other Syntaxins suggested that STX16A and STX16B contained the hydrophobic C-terminus characteristic for Syntaxins, as well as a conserved coiled-coil region, potentially the SNARE domain,

close to the C-terminus. STX16C, on the other hand, a truncated version of STX16A, lacked these C-terminal coiled-coil and hydrophobic regions characteristic of Syntaxins.

In a similar study to identify and clone potential members of the Syntaxin family, the same human EST (Genbank accession no. AA100145) was identified and used as a probe to isolate cDNAs from a human pancreas cDNA library (Tang et al., 1998a). Sequencing revealed an open reading frame encoding a polypeptide of 307 amino acids bearing sequence homology to other Syntaxin molecules, with potential coiled-coil domains and a 21 amino acid carboxy-terminal hydrophobic tail, characteristic of other members of the Syntaxin family. The cDNA was highly homologous, but not identical to, both STX16A and STX16B (Simonsen et al., 1998) and the N-terminal 115 amino acids were identical to STX16C. However, it remained unclear how the sequences were related and so the sequence was denoted human Syntaxin 16 or STX16H (Tang et al., 1998a).

The tissue distribution of STX16H was shown to be fairly ubiquitous, being slightly more enriched in the heart and the pancreas (Tang et al., 1998a). The Golgi localisation described by Simonsen *et al.* (Simonsen et al., 1998), was verified when a myc-tagged STX16H was localised to the Golgi apparatus by immunofluorescence, showing colocalisation with lens culinaris agglutinin, an established Golgi marker (Tang et al., 1998a).

A more recent study attempted to characterise the STX16 splice variants (Dulubova et al., 2002). The study showed that STX16C is truncated in the middle of the H_{abc} domain, with a stop codon in the middle of the predicted H_b helix. NMR analysis indicated that STX16C is largely unfolded and that the only intact functional domain is an N-terminal peptide region predicted to bind to its cognate SM protein, mVps45 (Section 1.6.5). STX16 A, B and H differ in an alternatively spliced region located between the N-terminal peptide that binds to mVps45 and the H_{abc} domain, and NMR analysis of the predicted H_{abc} domain STX16H indicated that it does indeed form a three-helix bundle. The investigators also highlighted the presence of another STX16 splice variant, STX16D, which contains a stop codon after the H_{abc} domain but before the SNARE domain (Dulubova et al., 2002). The sequences of the known STX16 splice variants are compared in Figure 1.8. Although northern blot analysis indicated that the STX16 splice variants are uniformly expressed in all tissues (Simonsen et al., 1998; Tang et al., 1998a), only one immunoreactive band, corresponding to the full length protein, was expressed in all tissues tested with the highest abundance in brain (Dulubova et al., 2002), suggesting that the truncated variants were not normally present at detectable steady-state levels, especially in brain.

Despite the discrepancies in nomenclature and sequences described above, recent studies refer to the full-length protein in various cell types, such as HcLa cells and 3T3-L1 adipocytes, simply as STX16 (Dulubova et al., 2002; Mallard et al., 2002; Perera et al., 2003; Shewan et al., 2003). In this study, I investigated the function of overexpressed STX16A (Simonsen et al., 1998) and endogenous murine STX16 expressed in 3T3-L1 adipocytes. For simplicity, these full-length molecules will be referred to henceforth as STX16.

STX16 has been shown to interact with STX6 (Mallard et al., 2002; Perera et al., 2003; Shewan et al., 2003), another SNARE protein previously implicated in GLUT4 trafficking, and the SM protein mVps45 (Dulubova et al., 2002). Each of these important molecules, including the yeast homolog of STX16, Tlg2p (Abeliovich et al., 1998), will be considered below.

1.6.2. Syntaxin 6 (STX6)

STX6 is perhaps one of the most distant members of the Syntaxin family, due to its ability to exhibit both Qa- and Qc-SNARE behaviour (reviewed in Wendler and Tooze, 2001). STX6 was originally identified through its homology to the yeast Qa-SNARE Pep12p, however, it was also shown to share significant homology with the C-terminus of SNAP-25 (Bock et al., 1996). As such, despite its classification as a Syntaxin, STX6 has been categorised as a Qc-SNARE (Section 1.5.3) (Bock et al., 2001). Interestingly, the crystal structure of the N-terminal domain of STX6 was recently solved and revealed strong structural similarity to the Syntaxin family members STX1a and Sso1p, despite a very low level of sequence similarity (Misura et al., 2002). However, the STX6 SNARE motif was able to substitute for the C-terminal SNARE motif of SNAP-25, supporting its classification as a Qc-SNARE. The closest yeast homolog of STX6 is therefore considered to be Tlg1p (Bock et al., 2001), which is known to form a SNARE complex with the STX16 homolog Tlg2p (Section 1.6.4)

STX6 is a 255- amino acid protein, expressed in a variety of cell types with higher expression levels in brain, lung and kidney (Bock et al., 1996). STX6 contains a C-terminal transmembrane anchor, and two N-terminal regions, denoted H1 and H2, which mediate interactions with other proteins, each with a high probability of forming coiled-coils (Bock et al., 1996). The membrane proximal H2 domain, showed similarity to the STX1a SNARE motif, and was therefore predicted to represent the SNARE motif, whereas the more amino terminal H1 domain was suggested to be involved in α -SNAP binding (Bock

et al., 1996). Another function was suggested for the H2 domain in conferring TGN localisation (Watson and Pessin, 2000). This domain was also predicted to function in concert with a PM retrieval signal (YGRL), located between the H1 and H2 domains, to maintain STX6 in the TGN (Watson and Pessin, 2000).

The high SNARE-pairing specificity observed between SNAREs involved in exocytosis, such as the neuronal SNARE complex (Section 1.5.2), appears to be less important for SNAREs that take part in intracellular membrane fusion. STX6 is a classic example of this scenario, as studies show it is found in many intracellular compartments and can associate with multiple SNARE partners, in addition to STX16, suggesting it is involved in multiple membrane-trafficking events (Wendler and Tooze, 2001). In addition, recent studies suggest that STX6 may exhibit cell-type specific function and SNARE-binding specificity (Wendler and Tooze, 2001).

As anticipated for a Qc-SNARE, STX6 has been found associated with a number of R-, Qa and Qb-SNAREs. The R-SNAREs include cellubrevin and / or VAMP2, VAMP4, VAMP7 and VAMP8 (Bock et al., 1997; Steegmaier et al., 1999; Wade et al., 2001). Along with VAMP7 and VAMP8, STX6 was shown to form a SNARE complex with the Qa-SNARE STX7 and the Qb-SNARE Vti1b (Wade et al., 2001). Curiously, STX6 was also shown to interact with SNAP-25-like Qbc- SNARE proteins, including SNAP-23, during exocytosis in human neutrophils, and SNAP-25 and SNAP-29 in PC12 cells (Martin-Martin et al., 2000; Wendler et al., 2001). The interaction of STX6 with SNAP-25-like SNAREs, is a further indication that the molecule possesses properties of both Qa- and Qc-SNAREs.

STX6 is mainly localised to the TGN in fibroblast cell lines (Bock et al., 1996; Bock et al., 1997; Klumperman et al., 1998), suggesting a role for STX6 in *trans*-Golgi or post Golgi membrane fusion events. However, a role for STX6 in maturation of immature secretory granules (Section 1.4.3) in neuroendocrine cells has also been suggested. STX6 has been localised to post-Golgi immature secretory granules in the neuroendocrine PC12 cell line and this study suggested that STX6 is sorted away from these granules during maturation, along with MPR-ligand complexes, by AP-1/clathrin coated vesicles, which may then fuse with endosomes (Klumperman et al., 1998). These findings were supported by a more recent study, in which STX6 was shown to be absent from mature secretory granules in PC12 cells (Wendler et al., 2001). In the same study STX6 was shown to be required for the homotypic fusion of immature secretory granules and that its presence was required on both the donor and acceptor membranes (Wendler et al., 2001).

1.6.3. STX16 and STX6 binding

STX16 and STX6 have been shown to interact in a number of systems, for example in 3T3-L1 adipocytes and synaptosomes (Kreykenbohm et al., 2002; Perera et al., 2003). Mallard *et al.* demonstrated that STX6 and STX16 form part of a SNARE complex with the t-SNARE Vti1a, and the v-SNAREs VAMP3 and VAMP4 in HeLa cells (Mallard et al., 2002). This SNARE complex was shown to control trafficking of cargo between endosomes and the TGN.

The interaction between the Qa-SNARE, STX16 and the Qc-SNARE STX6 has been proposed to be similar to that between SNAP-25 and STX1a in the formation of the neuronal SNARE complex described in Section 1.5.2.

1.6.4. Yeast homolog - Tlg2p

Tlg2p, the yeast homolog of STX16, is localised to the TGN and early endosomes in yeast, and plays a critical role in membrane traffic in these compartments. Recent work in our laboratory demonstrated that STX16 was able to compliment Tlg2p in yeast lacking Tlg2p (Marion Symington Struthers, unpublished data).

Tlg2p is a 396 amino acid protein with a putative SNARE motif (based on the sequence homology among the SNARE motifs from the Syntaxin family) followed by a transmembrane region and a 63 residue C-terminal sequence that is unusual in the Syntaxin family and is not essential for Tlg2p function (Abeliovich et al., 1998; Dulubova et al., 2002).

Cells lacking Tlg2p exhibit defects in endocytosis, in sorting of vacuolar proteins such as carboxypeptidase Y, and in retrieval of TGN-resident proteins such as Kex2p (Abeliovich et al., 1998; Holthuis et al., 1998b). In addition, Tlg2p carries out a number of other functions, which are beyond the scope of this thesis but are described elsewhere (Abeliovich et al., 1999; Brickner et al., 2001; Lewis et al., 2000; Panek et al., 2000; Seron et al., 1998). The SNARE Vti1p and the STX6 homolog, Tlg1p are required for some of these trafficking events, and both co-immunoprecipitate with Tlg2p, suggesting that they participate in a common SNARE complex (Coe et al., 1999; Holthuis et al., 1998a). As mentioned previously STX16, STX6 and Vti1a, the putative mammalian homologs of Tlg2p, Tlg1p and Vti1p, have been implicated in EE to TGN transport (Mallard et al., 2002). The yeast Tlg SNAREs also co-immunoprecipitate with the v-SNARE Snc1p or the

closely related Snc2p (Abeliovich et al., 1998; Holthuis et al., 1998a). While these v-SNAREs mediate exocytosis, they also function in endocytosis (Gurunathan et al., 2000). The notion that Snc1p or Snc2p can form a functional core complex with Tlg2p/Tlg1p/Vti1p acting as the t-SNAREs was recently supported by experiments with recombinant proteins reconstituted into liposomes (Paumet et al., 2001).

Tlg2p interacts physically and functionally with Vps45p, the SM protein involved in TGN/early endosomal transport (Abeliovich et al., 1999; Brickner et al., 2001; Bryant and James, 2001).

1.6.5. *mVps45*

The mammalian homolog of Vps45p, *mVps45* (Tellam et al., 1997), was recently shown to bind directly to STX16 (Dulubova et al., 2002; Yamaguchi et al., 2002). *mVps45* is a ubiquitously expressed SM protein with a predicted molecular mass of 65 kDa, which localises to perinuclear Golgi-like and TGN compartments in CHO cells. The tissue distribution was found to match that of STX6 and correspondingly, it was shown to interact weakly with STX6 (Bock et al., 1996; Bock et al., 1997; Tellam et al., 1997) although the interaction was quantitatively less than that observed between other SM protein / Syntaxin isoforms. This weak interaction could be explained by indirect binding to STX6, as more recently, *mVps45* was shown to bind directly to STX16, which also binds to STX6 (Dulubova et al., 2002; Perera et al., 2003; Yamaguchi et al., 2002). Like other SM proteins, *mVps45* is a cytosolic protein, but confers membrane association presumably through its interaction with STX6 (Bock et al., 1997) or STX16.

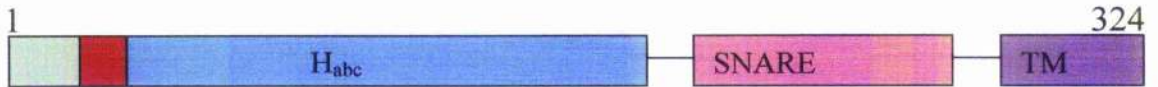
Dulubova *et al.* demonstrated that *mVps45* binds directly to STX16 through an evolutionarily conserved peptide motif in the N-terminal 55 residues of the protein in a mode of interaction identical to Tlg2p binding to Vps45p (Dulubova et al., 2002). Sequence alignments suggested that STX16 has a similar domain structure to Tlg2p, with the well-conserved N-terminal peptide motif responsible for binding to *mVps45*, and an H_{abc} domain characteristic of Syntaxins (Dulubova et al., 2002). A matter of current debate is whether all Syntaxins can adopt a closed conformation similar to STX1a, required for binding to the associated SM protein (Section 1.5.7). Although Dulubova *et al.* demonstrated that Tlg2p does not adopt a closed conformation (Dulubova et al., 2002), STX16 was not tested in this regard. This possibility will be considered elsewhere in this thesis.

A)

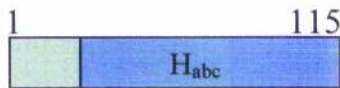
STX16A



STX16B



STX16C



B)

<i>Synt16H</i>	MATRRLLTDAFLLLRNNSIQNRQLLAEQ-----ELDELADDRMALVSGI	43
<i>Synt16A</i>	MATRRLLTDAFLLLRNNSIQNRQLLAEQ-----LADDRMALVSGI	39
<i>Synt16B</i>	MATRRLLTDAFLLLRNNSIQNRQLLAEQVSSHITSSPLHSRSIAAELDELADDRMALVSGI	60
<i>Synt16C</i>	MATRRLLTDAFLLLRNNSIQNRQLLAEQ-----ELDELADDRMALVSGI	43
<i>Synt16D</i>	<u>MATRRLLTDAFLLLRNNSIQNRQLLAEQ-----ELDELADDRMALVSGI</u>	43
<i>Synt16H/A/B</i>	SLDPEAAIGVTKRPPPKWVDGVDEIQYDVGRIKQKQKELASLHDKHLNRPTLDDSSKEEH	103
<i>Synt16C</i>	SLDPEAAIGVTKRPPPKWVDGVDEIQYDVGRIKQKQKESASLHDKHLNRPTLDDSSKEEH	103
<i>Synt16D</i>	SLDPEAAIGVTKRPPPKWVDGVDEIQYDVGRIKQKQKELASLHDKHLNRPTLDDSSKEEH	103
<i>Synt16H/A/B</i>	AIEITTQEITQLFHRCQRAVQALPSRARACSEGEGRLLGNVVASLAQALQELSTSFRAHQ	163
<i>Synt16C</i>	AIEITTQEITQA*	115
<i>Synt16D</i>	AIEITTQEITQLFHRCQRAVQALPSRARACSEGEGRLLGNVVASLAQALQELSTSFRAHQ	163
<i>Synt16H/A/B</i>	SGYLKRMKNREERSQHFFDTSVPLMDDGDDNTLYHRGFTEQDLVLVEQNTLMVEEREREI	223
<i>Synt16D</i>	SGYLKRMKNREERSQHFFDTSVPLMDDGDDNTLYHRRTS*	202
<i>Synt16H/A/B</i>	ROMVQSISDLNEIFRDLGAMIVEQGTVLDRIDYNVEQSCIKTEDGLKQLHKAEQYQKKNR	283
<i>Synt16H/A/B</i>	<u>KMLVILILFVIIIVLIVLVGV</u> KSR*	308

Figure 1.8 Naturally occurring STX16 splice variants (adapted from Simonsen et al., 1998 and Dulubova et al., 2002)

A) Domain structures of STX16A, B and C. STX16A consists of an N-terminal motif predicted to facilitate binding of mVps45 (green), followed by the H_{abc} domain (blue), the SNARE motif (pink) and a C-terminal transmembrane domain (purple). STX16B is identical, except for a 21 amino acid insertion (red), predicted to occur between the mVps45 binding motif and the H_{abc} domain. STX16C is truncated in the middle of the predicted H_b helix. B) Sequence comparisons of STX16 (Synt16 in this figure) A, B, C, D and H. Asterisks, positions of stop codons; dashes, gaps; double underlined sequence, N-terminal peptide sequence that binds to mVps45; sequences in bold, predicted α -helices of the H_{abc} domain (based on sequence comparison with Tlg2p); italicised sequence underlined with a dotted line, SNARE motif; boxed sequence, transmembrane domain. Numbers on the right correspond to STX16H splice variant.

1.7. Intracellular trafficking of GLUT4

As described in Section 1.2.1, insulin stimulates glucose uptake in muscle and fat cells by triggering the translocation of the glucose transporter, GLUT4, from an intracellular compartment to the cell surface (Bryant et al., 2002; Pessin et al., 1999; Watson et al., 2004). Section 1.7 will detail the current knowledge involving the intracellular trafficking of GLUT4, concluding with the current accepted model for insulin-stimulated GLUT4 translocation.

1.7.1. Intracellular locations of GLUT4

In contrast to the other members of the facilitative glucose transporter family (Section 1.2), GLUT4 is almost completely intracellularly localised under basal conditions and exhibits a complex intracellular itinerary. In the absence of insulin, > 90 % of cellular GLUT4 is intracellularly sequestered and has been localised to the endosomal system, the TGN and a tubulo-vesicular compartment present throughout the cell (Martin et al., 1994; Martin et al., 2000a; Ploug et al., 1998; Ramm et al., 2000; Slot et al., 1991b; Slot et al., 1997). In response to insulin, GLUT4 levels in each of these regions are decreased in parallel with the movement of GLUT4 to the cell surface (Martin et al., 1994; Ploug et al., 1998; Ramm et al., 2000; Slot et al., 1991b; Slot et al., 1991a).

1.7.2. Endosomes

Previous studies have indicated a role for endosomes in GLUT4 trafficking (Livingstone et al., 1996; Slot et al., 1991b) but suggest that they may not represent a major storage compartment in adipocytes. GLUT4 shows co-localisation with known endosomal recycling proteins, for example the TfR (one of the most well studied constitutive recycling proteins in mammalian cells (Section 1.4.2)) (Livingstone et al., 1996). However, detailed analysis of GLUT4 traffic to and from the cell surface revealed that in non-insulin-stimulated adipocytes, the exocytosis of GLUT4 is approximately 10-fold slower than that of TfR (Holman et al., 1994; Tanner and Lienhard, 1987). This finding points to the intracellular retention of GLUT4 in a more static compartment or futile cycle distinct from endosomes. This assumption was verified when chemical ablation of endosomes containing the TfR using a transferrin (Tf)-horseradish peroxidase (HRP) conjugate

demonstrated that only ~ 30-40 % of intracellular GLUT4 (Livingstone et al., 1996; Martin et al., 1996) was subject to ablation. Furthermore, it has been shown that following endocytosis of GLUT4 from the cell surface, GLUT4 is segregated from the TfR in the endosomal system into a separate population of transport vesicles (Lampson et al., 2001; Lim et al., 2001; Martin et al., 1996; Sandoval et al., 2000). The possible nature of these vesicles will be considered in Section 1.7.4.

1.7.3. The role of the TGN

Several observations suggest an important role for the TGN in GLUT4 trafficking, however, the precise role of this organelle is at present unclear. There is a significant amount of GLUT4 in the TGN area in insulin responsive cells (Martin et al., 2000a; Ploug et al., 1998; Ralston and Ploug, 1996; Slot et al., 1991b; Slot et al., 1991a; Slot et al., 1997; Wang et al., 1996) a proportion of which does not represent newly synthesised protein (Slot et al., 1991b; Slot et al., 1991a). In addition, there is significant overlap between GLUT4 and proteins known to traffic between the TGN and endosomes, including the cation-dependent mannose 6-phosphate receptor (CD-MPR) (Martin et al., 2000a), the cation independent mannose 6-phosphate receptor (CI-MPR) (Kandror and Pilch, 1996b) and AP-1 (Gillingham et al., 1999; Martin et al., 2000a). By following the internalisation of GLUT4 from the cell surface of adipocytes, it has been shown that the transporter is transported through endosomes into a perinuclear compartment that is distinct from recycling endosomes (Palacios et al., 2001). More recently, it was shown that this perinuclear compartment represents a subdomain of the TGN enriched in STX6 and STX16 (Shewan et al., 2003). Furthermore, in atrial cardiomyocytes, approximately 60 % of the entire GLUT4 pool is localised to atrial natriuretic factor (ANF)-containing secretory granules and this appears to be due to recycling of GLUT4 through the TGN area (Slot et al., 1997).

1.7.4. GSVs

Various studies suggest that much of the remainder of non-endosomal GLUT4 is localised to a population of ill-defined vesicles, commonly called GLUT4 storage vesicles (GSVs) (reviewed in Bryant et al., 2002; Pessin et al., 1999; Rea and James, 1997) and that the majority of GLUT4 that is delivered to the plasma membrane in response to insulin comes from these unique vesicles. GLUT4 does not colocalise with other adipocyte secretory proteins, such as ACRP30, leptin or adiponectin (Barr et al., 1997; Bogan and Lodish, 1999; Millar et al., 2000), suggesting that GSVs may be specialised vesicles for the translocation

of GLUT4. However, the nature of these vesicles is largely unknown, with regard to whether they represent a static or dynamic recycling pool of GLUT4 in the absence of insulin.

Some studies suggest the existence of a more static secretory pool of insulin-responsive GLUT4, that is analogous to small secretory vesicles present in neuroendocrine tissues and that these can move directly to the cell surface in response to insulin. For example, a discrete population of small (50 nm diameter) vesicles, devoid of other recycling proteins, such as the TfR and the CD-MPR were identified in insulin-responsive cells (Hashiramoto and James, 2000; Kandror and Pilch, 1996a; Ramm et al., 2000). These vesicles were highly responsive to insulin and were enriched in the v-SNARE VAMP2 (the same v-SNARE that is involved in the exocytosis of synaptic vesicles with the PM (Section 1.5.2)) suggesting that they may move directly to the cell surface in response to insulin.

On the other hand, some evidence points to the dynamic recycling of GLUT4 between intracellular compartments, perhaps in some futile cycle. For example, the presence of GLUT4 in AP-1/clathrin coated intracellular transport vesicles suggests that GLUT4 is not restricted to a stable storage compartment within the cell (Gillingham et al., 1999; Martin et al., 2000b).

1.7.5. Biogenesis of GSVs

Little is known about the biogenesis of the GSV compartment. Because GLUT4 is present in both the endosomes and the TGN, it has been speculated that GSVs may arise from either or both of these compartments (Rea and James, 1997). However, it seems plausible that transit through the TGN precedes the packaging of GLUT4 into its insulin-responsive compartment because prolonged incubation of adipocytes at 19 °C, a temperature that blocks exit from the TGN, inhibits insulin action (Robinson and James, 1992).

1.7.6. Targeting signals on GLUT4

The existence of such a complex intracellular itinerary suggests that GLUT4 trafficking must be controlled at various cellular locations by the presence of a number of targeting signals. Indeed, two such signals have been identified which mediate GLUT4 endocytosis. GLUT4 is localised to AP-2 / clathrin coated pits at the cell surface and is endocytosed via a clathrin-mediated process (Kao et al., 1998; Robinson et al., 1992). This is regulated by two endocytosis motifs in GLUT4; a dileucine motif in the C-terminus and an aromatic

amino acid-based motif in the N-terminus (Garippa et al., 1994; Garippa et al., 1996; Kao et al., 1998; Verhey et al., 1995). Furthermore, recent studies identified the presence of a targeting domain in the C-terminus of GLUT4 distal to the di-leucine motif (Shewan et al., 2000), which is responsible for the targeting of GLUT4 to the TGN subdomain enriched in STX6 and STX16 mentioned above.

1.7.7. SNAREs involved in GLUT4 vesicle fusion with the PM

In order to increase the concentration of GLUT4 at the PM in response to insulin, it is necessary for GSVs to fuse with the PM, following translocation from their intracellular location. This event is mediated, at least in part, by a specific set of SNARE proteins (Chen and Scheller, 2001; Jahn and Sudhof, 1999) that are essential in the fusion step (Foster and Klip, 2000). As mentioned previously, GSVs were shown to be enriched in the v- SNARE VAMP2 (Martin et al., 1996). VAMP2 has been shown to form a complex with the t-SNAREs STX4 and SNAP-23, which are highly enriched in the PM of muscle and fat cells (Foster and Klip, 2000). The importance of these proteins was evidenced by the use of clostridial toxins that selectively cleaved both VAMP2 and VAMP3, blocking the insulin - dependent translocation (Cheatham et al., 1996; Chen et al., 1997; Foran et al., 1999; Randhawa et al., 2000; Tamori et al., 1996), and recombinant forms of these SNAREs, which also interfered with the insulin-dependent GLUT4 translocation (Cheatham et al., 1996; Martin et al., 1998; Olson et al., 1997). Munc18c has been identified as the SM protein that controls the formation of this ternary complex (Foster and Klip, 2000). Figure 1.9 (insert) depicts this SNARE complex.

1.7.8. GLUT4 Trafficking Model

To account for the findings described above, several models of GLUT4 traffic have been proposed which can be summarised as follows: GLUT4 could be selectively retained in a sub-domain of the endosomal system or another of its intracellular locations; packaged into specialised secretory vesicles that are mobilised only in response to insulin; or 'trapped' in a futile trafficking cycle within the cell which diverts the molecule away from recycling endosomes and thus away from the cell surface. There is evidence in the literature in support of each of these models (reviewed in Bryant et al., 2002), however, in reality, the situation is likely to possess features of each of these three extreme models.

Bryant *et al.* (Bryant et al., 2002) suggested a model to accommodate the conflicting evidence on GLUT4 trafficking (Figure 1.9). In this model, GLUT4 is engaged in two

intracellular cycles: a fast trafficking event between the PM and endosomes and a more slowly recycling pool between endosomes and the TGN. In this model, insulin-responsive GSVs arise from the TGN and may represent a more static pool of vesicles that are only mobilised in response to insulin, however, it is suggested that they may slowly fuse with endosomes to prevent depletion of GLUT4 in the other locations.

This model therefore supposes that GLUT4 is intracellularly sequestered in the absence of insulin by a mechanism that excludes it from the endosomal system and involves the packaging of GLUT4 into an insulin-responsive vesicular compartment. The molecular mechanisms that control these intracellular steps remain largely unknown.

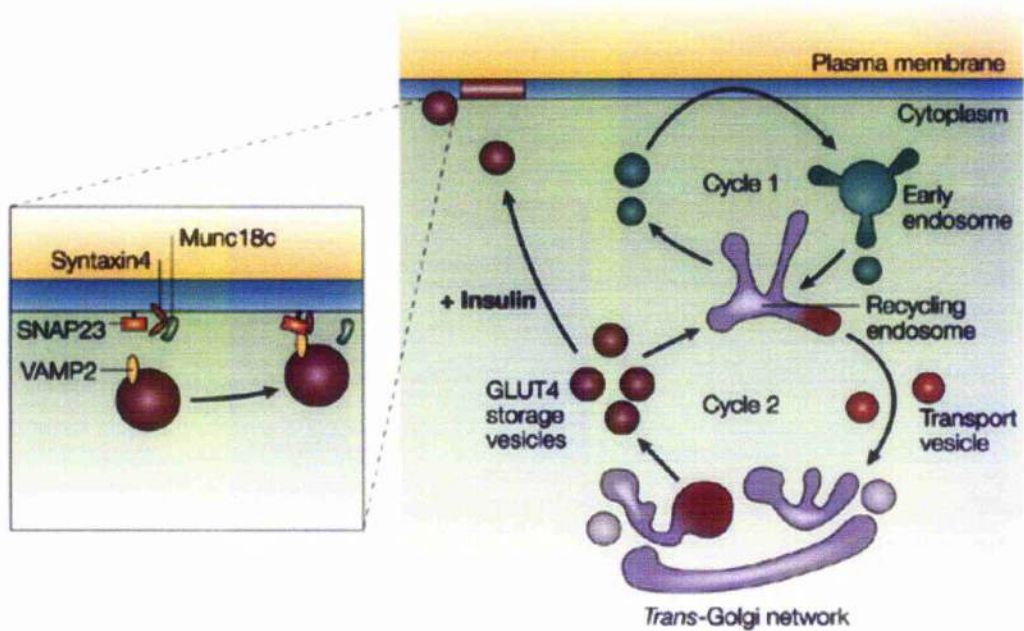


Figure 1.9 A model depicting the transport of GLUT4 in insulin responsive cells (from Bryant et al., 2002)

In this model, GLUT4 occupies two intracellular recycling pathways: cycle 1, between the cell surface and endosomes and cycle 2, between endosomes and the TGN. GLUT4 is sorted into a secretory pathway in the TGN, which may involve the biogenesis of the GSVs. This insulin-responsive compartment may contain the majority of the non-endosomal GLUT4. In the absence of insulin, GSVs might slowly fuse with endosomes to prevent depletion of GLUT4 in other locations. In response to insulin, the GSVs would translocate to and fuse with the PM.

The insert shows the SNARE proteins that are thought to regulate docking and fusion of GSVs with the cell surface (Foster and Klip, 2000). The t-SNAREs STX4 and SNAP-23 in the PM of fat and muscle cells form a ternary complex with the v-SNARE VAMP2, which is present on GSVs. Munc18c has been identified as the SM protein that controls the formation of this ternary complex.

1.8. STX16 in GLUT4 trafficking

1.8.1. Evidence implicating STX6 and STX16 in trafficking of GLUT4

There is much evidence to suggest a role for STX6 and STX16 in GLUT4 trafficking in adipocytes. As mentioned previously, a STX6/STX16 interaction was demonstrated in 3T3-L1 adipocytes (Perera et al., 2003; Shewan et al., 2003) and so it is anticipated that they will act in the same SNARE complex to influence GLUT4 trafficking.

The characteristic ability of 3T3-L1 adipocytes to form an insulin-responsive GLUT4 compartment is markedly upregulated soon after adipocyte differentiation (El Jack et al., 1999), suggesting that the machinery required for the biogenesis of this compartment might be specifically upregulated in these cells. Interestingly, the expression of STX6 and STX16 is upregulated during adipocyte differentiation (Shewan et al., 2003). In addition, both STX6 and STX16 display insulin-stimulated translocation to the PM in 3T3-L1 adipocytes (Perera et al., 2003; Shewan et al., 2003). It has previously been shown that not all TGN proteins undergo insulin-responsive movement to the cell surface (Martin et al., 1994). Insulin caused a slight increase in surface levels of STX13, an endosomal t-SNARE involved in the recycling of the Tfr, but quantitatively less than for STX6 or STX16 (Perera et al., 2003). Also the kinetics of STX6 translocation to the cell surface were identical to those of GLUT4, suggesting that GLUT4 and STX6 are transported in the same vesicle to the plasma membrane upon insulin stimulation. In support of this finding, STX6 and STX16 were shown to co-localise extensively with GLUT4 (Perera et al., 2003). While STX7, STX8 and STX12 are present in GSVs to some extent, only STX6 and STX16 exhibited extensive overlap with GLUT4. Immuno-isolation of GLUT4 containing vesicles showed that ~ 85 % of the cellular STX6 and STX16 was present in GLUT4-containing vesicles (Perera et al., 2003). As mentioned previously, GLUT4 was shown to traffic from the cell surface to a TGN subdomain enriched in STX16 and STX6 via early endosomes and an acidic targeting motif in the C-terminal tail of GLUT4 was shown to play an important role in this process (Shewan et al., 2003).

Previous work in our laboratory tested STX6 for its involvement in GLUT4 trafficking. The dominant negative cytosolic domain of this protein was expressed in 3T3-L1

adipocytes and was shown to perturb GLUT4 trafficking (Perera et al., 2003). Cells overexpressing STX6 cytosolic domain exhibited increased levels of basal transport, but the ability of insulin to stimulate glucose transport and GLUT4 translocation was not impaired. In addition, the ability of GLUT4 to be reinternalised from the cell surface was significantly slowed. This data was rationalised within a model that suggested STX6 was involved in the intracellular sequestration of GLUT4 in 3T3-L1 adipocytes. The role of STX16 was not addressed in this regard. As such, Chapters 4 and 5 of this thesis directly investigate the role of STX16 in GLUT4 trafficking.

1.8.2. Phosphorylation of STX16

Perhaps one of the most compelling pieces of evidence that suggests a role for STX16 in the regulation of GLUT4 trafficking comes from previous work in our laboratory (Perera et al., 2003). STX16 was shown to be a phosphoprotein in 3T3-L1 adipocytes and interestingly, acute insulin stimulation causes approximately a 50 % decrease in phosphorylation. Studies of other SNAREs have suggested that dephosphorylation of t-SNAREs could regulate the formation of a functional SNARE complex (Gerst, 2003). It was therefore speculated that STX16 may be involved in regulating the formation of a SNARE complex, perhaps involving STX6, which may be involved in GLUT4 trafficking. This will be considered further in Chapter 3 of this thesis.

1.9. Hypothesis

STX16 is upregulated upon differentiation of 3T3-L1 fibroblasts into adipocytes (Shewan et al., 2003), suggesting that it may be part of the machinery required for GLUT4 trafficking in these highly differentiated cells. The presence of STX16 in multiple GLUT4 containing compartments, such as the TGN and GSVs (Perera et al., 2003; Shewan et al., 2003), combined with its intriguing translocation to the cell surface in response to insulin, suggests a role for STX16 in the intracellular sorting or the translocation of GLUT4 to the cell surface. Combined with this is the curious dephosphorylation of STX16 following insulin stimulation (Perera et al., 2003), suggesting a role for STX16 in the regulation of this process. With these thoughts in mind I offer the following hypotheses for this thesis:

- STX16 plays a key role in the sorting / translocation of GLUT4
- The phosphorylation status of STX16 regulates SNARE complex assembly (perhaps with STX6), which ultimately controls GLUT4 sorting / translocation

These hypotheses are depicted in Figures 1.10 and 1.11 and were tested experimentally in this thesis.

1.10. Aims

The ultimate aim of this thesis was to determine the role, if any, that STX16 plays in GLUT4 trafficking in 3T3-L1 adipocytes, and additionally, to determine if the phosphorylation status of STX16 was responsible for the regulation of this process. The main aims of each Chapter are summarised as follows:

Chapter 3: identification of the site of insulin-regulated phosphorylation and SNARE binding partners of STX16 in basal and insulin-stimulated 3T3-L1 adipocytes

Chapter 4: optimisation of adenovirus-mediated expression of STX16 mutants and full-length STX16 in 3T3-L1 adipocytes

Chapter 5: the effects of expression of these proteins, as well as knockdown of endogenous STX16, on GLUT4 trafficking in 3T3-L1 adipocytes

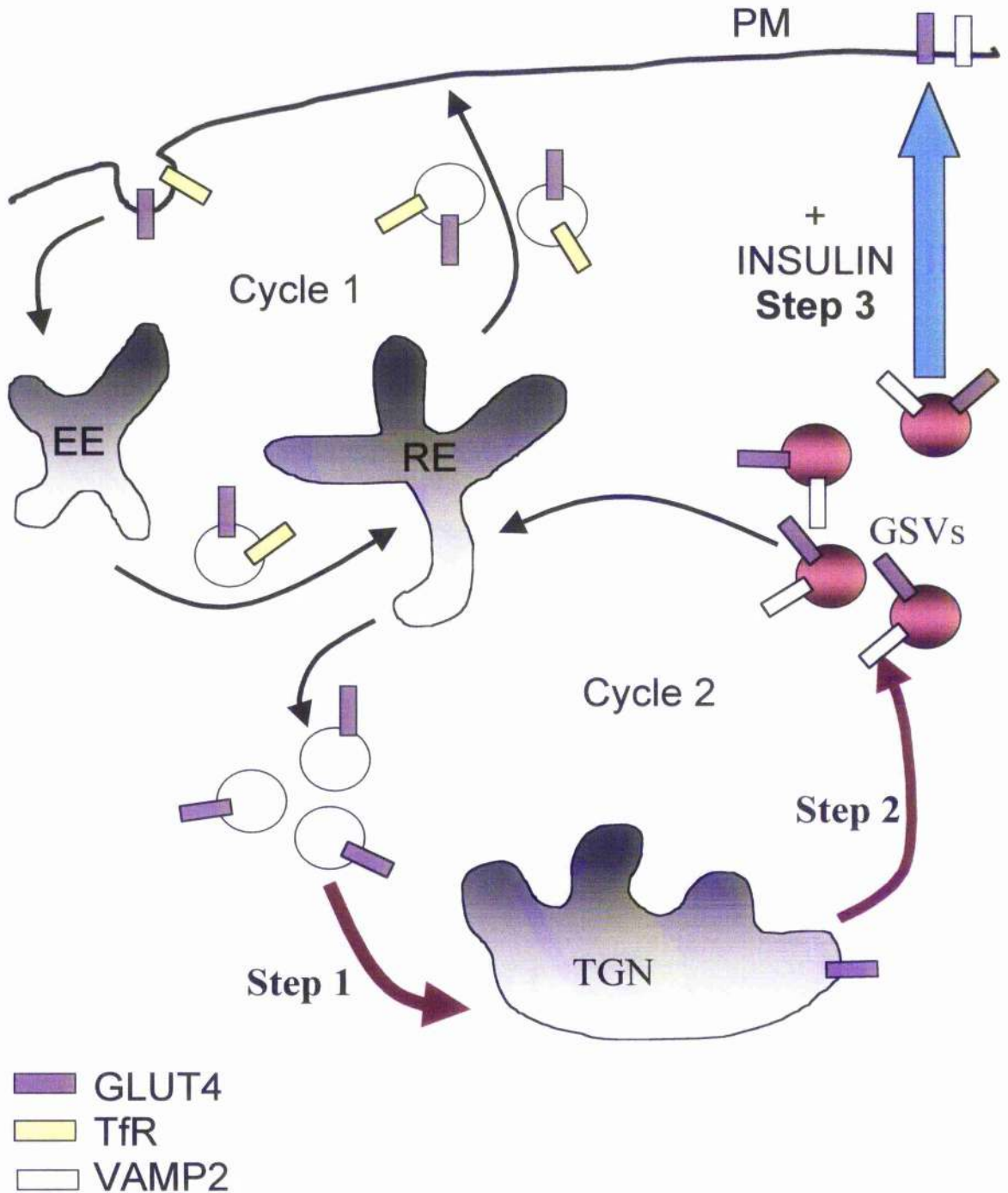


Figure 1.10 A model depicting the potential involvement of STX16 in GLUT4 trafficking in adipocytes (adapted from Bryant et al., 2002)

In this model, GLUT4 occupies two main intracellular recycling pathways. **Cycle 1:** GLUT4 recycles between the cell surface and endosomes, showing co-localisation with molecules such as the TfR. **Cycle 2:** GLUT4 is sequestered away from the endosomal system and recycles more slowly between the TGN and endosomes. Insulin-responsive GSVs, enriched with VAMP2 may bud from the TGN.

I hypothesise that STX16 is involved in the intracellular sorting (steps 1 or 2, mauve arrows) and / or the translocation (step 3, blue arrow) of GLUT4.

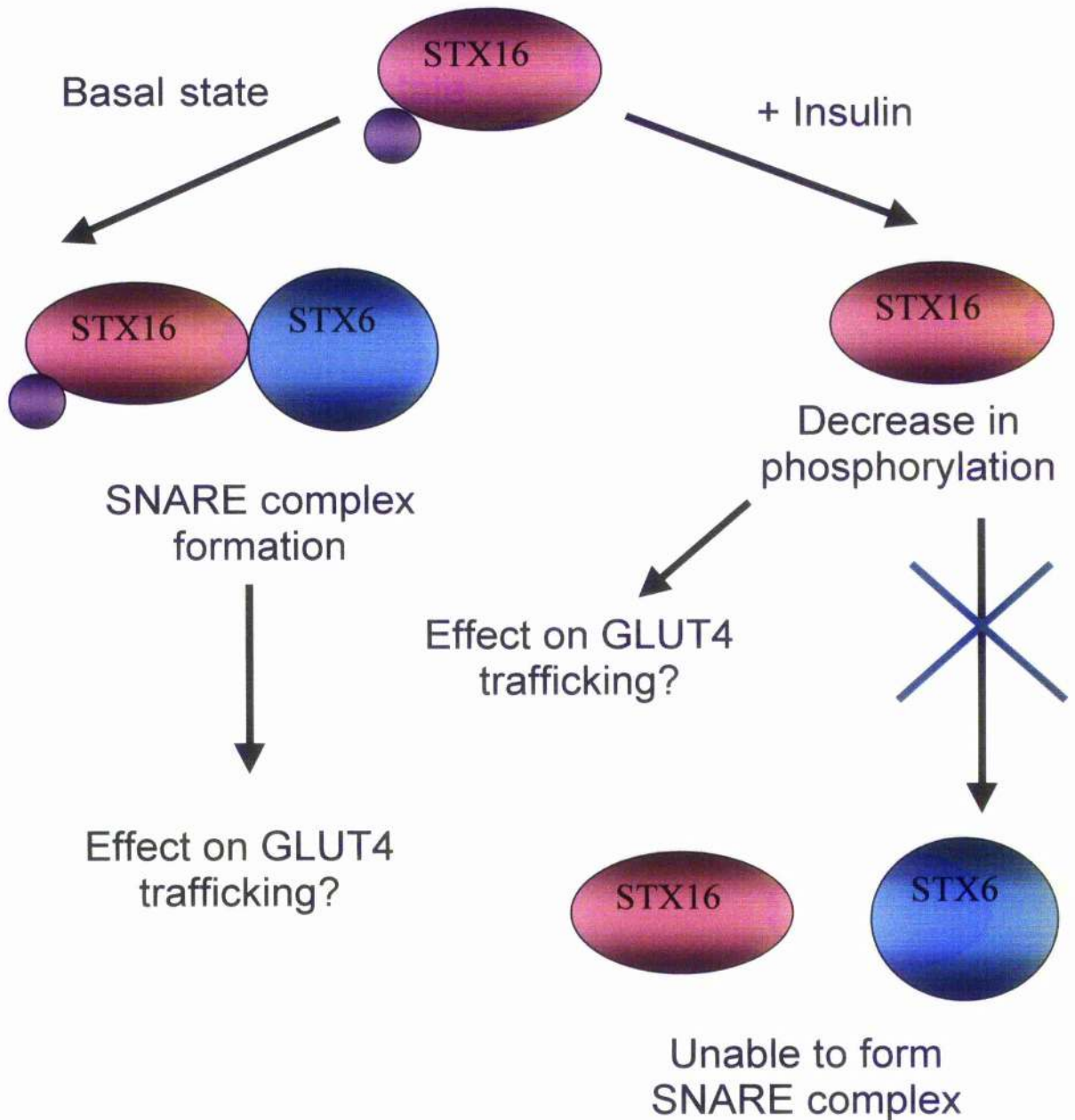


Figure 1.11 Model depicting a possible role of STX16 phosphorylation in regulation of a SNARE complex involved in GLUT4 trafficking

In this model, phosphorylated (purple circle) STX16 (pink oval) can enter into a SNARE complex, perhaps involving STX6 (blue circle), whereas dephosphorylation in response to insulin inhibits formation of this SNARE complex. I hypothesise that each scenario would exert a different regulatory effect on GLUT4 trafficking.

Previous work has suggested that (de)phosphorylation of t-SNAREs could regulate the formation of functional SNARE complexes (Gerst, 2003). This model is based on the assumption that phosphorylation of STX16 will promote SNARE assembly. However, the opposite may also be true, a possibility which will be considered in Chapter 3 of this thesis. The precise role of STX16 in GLUT4 trafficking will also be explored.

Chapter 2

Materials and Methods

2. Materials and Methods

2.1. Materials

Materials used in this study were obtained from the following suppliers:

2.1.1. General reagents

Amersham Pharmacia Biotech, Little Chalfont, Buckinghamshire, UK

ECL Western Blotting Detection Reagents
Horseradish peroxidase (HRP)-conjugated IgG antibodies
Horseradish peroxidase (HRP)-conjugated protein A
Protein G Sepharose
Phosphorus-32 ($H_3^{32}PO_4$ -Orthophosphate in dilute HCl solution)

Anachem Ltd., Luton, Bedfordshire, UK

30 % acrylamide/bisacrylamide

BIOMOL International, LP, Exeter, Devon, UK

MG-132 (Z-Leu-Leu-Leu-CHO), proteasome inhibitor

Bio-Rad Laboratories Ltd, Hemel Hempstead, Hertfordshire, UK

Bradford protein assay reagent
N,N,N',N'-tetramethylethylenediamine (TEMED)

Boehringer Mannheim, Germany

Protease inhibitor cocktail tablets: completeTM and complete miniTM
Thesit (C12E8: Octaethylene glycol dodecyl ether)

Fischer Scientific Ltd, Loughborough, Leicestershire, UK

Ammonium persulphate
Calcium chloride ($CaCl_2$)
Diaminoethanetetra-acetic acid, disodium salt (EDTA)
Disodium hydrogen orthophosphate (Na_2HPO_4)
D-Glucose
Glycerol
Glycine
N-2-hydroxyethylpiperazine-N'-2-ethanesulphonic acid (HEPES)
Hydrochloric acid (HCl)
Isopropanol
Magnesium sulphate ($MgSO_4$)
Methanol
Potassium chloride (KCl)
Potassium dihydrogen orthophosphate (KH_2PO_4)
Sodium chloride (NaCl)

Sodium dihydrogen orthophosphate dihydrate (NaH_2PO_4)
Sodium dodecyl sulphate (SDS)
Sodium hydrogen carbonate (NaHCO_3)
Sucrose
Tetra-sodium citrate ($\text{Na}_4\text{C}_6\text{H}_5\text{O}_7$)
Trichloroacetic acid (TCA)

Invitrogen, Groningen, The Netherlands

Electroporation cuvettes
TA Cloning® Kit (pCR2.1)

Kodak Ltd, Hemel Hempstead, Hertfordshire, UK

X-Omat S film

Life Technologies, Paisley, Scotland, UK

Agarose
1 kb DNA ladder

Merck Ltd (BDH), Lutterworth, Leicestershire, UK

Magnesium chloride (MgCl_2)
Tween 20
Zinc chloride (ZnCl_2)

MWG-Biotech, Germany

Some oligonucleotide primers

New England Biolabs (UK) Ltd, Hitchin, Hertfordshire, UK

Pre-stained protein marker, broad range (6-175 kDa)

Novo Nordisk, Denmark

Insulin (Porcine, monocomponent)

Oxoid Ltd, Hampshire, UK

Bacteriological agar
Tryptone
Yeast Extract

Perkinelmer LAS, Boston, USA

Deoxy-D-Glucose ($\text{C}_6\text{H}_{12}\text{O}_5$) (deGlc) 2-[1,2- ^3H (G)]-

Pierce, Rockford, Illinois, USA

Slide-a-lyser™ dialysis cassettes

Premier Brands UK, Knighton, Adbaston, Staffordshire, UK

Marvel powdered milk

Promega, Southampton, UK

All restriction enzymes
Deoxynucleotide triphosphates (dNTPs)
1 kb DNA Ladder
Nuclease-free water
Pfu polymerase
Taq polymerase

Blue/Orange 6 × DNA loading dye

Qiagen, Crawley, West Sussex, UK

PhosphoProtein Purification Kit

QIAprep™ spin maxiprep kit

QIAprep™ spin miniprep kit

Qiagen gel purification kit

Sigma-Aldrich Company Ltd., Dorset, UK

Cytochalasin B (CB)

Brij

IBMX (3-Isobutyl-1-methylxanthine)

Dexamethasone (9 α -fluoro-16 α -methyl-prednisolone)

Protein A Sepharosc

Schleicher & Schell, Dassel, Germany

Nitrocellulose membrane (pore size: 0.45 μ M)

Stratagene, La Jolla, CA, USA

Dpn1 restriction enzyme (for QuickChange mutagenesis)

TAGN, Gateshead, UK

Some oligonucleotide primers

Whatman International Ltd, Maidstone, UK

Whatman 3 mm filter paper

All other chemicals used were supplied from Sigma Chemical Company Ltd, Poole, Dorset, UK.

2.1.2. Cell culture materials

American Type Culture Collection, Rockville, USA

3T3-L1 fibroblasts

HEK 293 cells

HeLa cells were a kind gift from Pam Scott, University of Glasgow

AS Nunc, DK Roskilde, Denmark CHECK

50 ml centrifuge tubes

13.5 ml centrifuge tubes

Bibby-Sterlin, Staffordshire, UK

Iwaki tissue culture plasticware:

-6-well plates

-75 cm² flasks

-150 cm² flasks

Graduated disposable pipettes

Gibco BRL, Paisley, Lanarkshire, UK

Dulbecco's modified Eagle's medium (DMEM) (with 4500 mg/L glucose, without sodium pyruvate)
Dulbecco's phosphate buffered saline (D-PBS)
FBS (USA)
FBS (EU)
L-Glutamine
Lipofectamine 2000 reagent
Modified Eagles medium (MEM)
NCS
Non-essential amino acids
Opti-MEM
Penicillin (10000 U/ml)/ Streptomycin (10000 U/ml) (P/S)
Trypsin / EDTA solution

Falcon tissue culture plastic ware, Fred Baker, UK

10 cm² dishes
6-well plates
12-well plates

Roche Diagnostics Ltd., East Sussex, UK

Collagenase D

Sigma-Aldrich Inc., Dorset, UK

Phosphate- free Dulbecco's modified Eagle's medium (DMEM) (with 4500 mg/L glucose and L-glutamine, without sodium phosphate and sodium bicarbonate)

2.1.3. Plasmids

The pGEM plasmid housing myc-tagged STX16A was a kind gift from H. Stenmark, The Norwegian Radium Hospital, Montebello, Oslo, Norway.
pCR3.1 and pCR2.1 were from Invitrogen Ltd., Paisley, UK.
pShuttle-CMV was from Stratagene, La Jolla, CA, USA

2.1.4. Primary antibodies

Anti-ACRP30 (polyclonal) was made for this laboratory by Zymed Laboratories, South San Francisco, CA (Ewart et al., 2005)
Anti-Glut4 (polyclonal) was prepared previously in this laboratory (Ewart et al., 2005)
Anti-IRAP (monoclonal) was a kind gift from Prof. Morris J Birnbaum, University of Pennsylvania (Garza and Birnbaum, 2000)
Anti-IRS-1 (polyclonal) was from Ken Siddle, Cambridge, UK
Anti-mVps45 (polyclonal) was from R. Piper, University of Iowa
Anti-myc (monoclonal) was from Sigma-Aldrich Inc., Dorset, UK
Anti-myc (polyclonal) was from Santa-Cruz Biotechnology Inc., California, USA
Anti-PKB was from New England Biolabs (UK) Ltd., Herts, UK
Anti-STX16 (polyclonal) was from B.L. Tang and Wanjin Hong, Membrane Biology Laboratory, Institute of Molecular and Cell Biology, Singapore
Anti-STX4 (polyclonal) was from Prof. David James, University of Queensland, Australia
Anti-STX6 (polyclonal) was generated previously in this laboratory (Perera et al., 2003)

Anti-STX6, Vti1a and Vti1b (all monoclonal) were from BD Transduction Laboratories, Lexington, KY

Anti-VAMP2 (monoclonal) was from Synaptic Systems, Goettingen, Germany

Anti-VAMP3 / cellubrevin (polyclonal) and Arf6 (monoclonal) were from Abcam Plc., Cambridge, UK

Anti- β 5 (80 kDa), anti- α v (125 kDa), anti- α v (25 kDa) and anti- β 3 (90-110 kDa) (all polyclonal) were from W. Cushley, University of Glasgow

Random IgGs (polyclonal and monoclonal) were from Sigma-Aldrich Inc, Dorset, UK

All primary antibodies were diluted to 1:1000 in PBS-T + 1 % Marvel (except anti-VAMP2, 1:10,000) prior to use.

2.1.5. *Escherichia coli* (*E. coli*) strains

Supercompetent XL1-blue were from Stratagene, La Jolla, CA, USA

(Genotype: *recA1 endA1 gyrA96 thi-1 hsdR17 supE44 relA1 lac* [F *proAB lacI*^qZAM15 Tn10 (Tet^r)])

Competent TOP10 were from Invitrogen Ltd, Paisley, UK

(Genotype: F *mcrA* Δ (*mrr-hsdRMS-mcrBC*) ϕ 80*lacZ*AM15 *MacX74 recA1 ara* Δ 139 Δ (*aru-leu*)7697 *galU galK rpsL* (Str^r) *endA1 nupG*)

2.1.6. Cell Culture Media

HeLa growth medium

MEM (minimum essential medium), 10 % (v/v) FCS (EU origin), 1 % non-essential amino acids, 2 mM L-glutamine, 100 U/ml penicillin, 100 μ g/ml streptomycin

HEK 293 growth medium

DMEM, 10 % (v/v) FBS (EU origin), 2 mM L-glutamine, 100 U/ml penicillin, 100 μ g/ml streptomycin

3T3-L1 fibroblast growth medium

DMEM, 10 % (v/v) NCS, 100 U/ml penicillin, 100 μ g/ml streptomycin

3T3-L1 adipocyte growth medium

DMEM, 10 % (v/v) FBS (USA origin), 100 U/ml penicillin, 100 μ g/ml streptomycin

2.1.7. General Solutions

CsCl₂ gradient:

60 % (w/v) CsCl₂ in 10 mM Tris-HCl pH 7.9

30 % (w/v) CsCl₂ in 10 mM Tris-HCl pH 7.9

These solutions were filtered in a fume hood with a 2 μ m filter before use.

Lysis buffer

20 mM Tris-HCl, 150 mM NaCl, 1 % (w/v) C₁₂E₈ (Thesit), pH 7.4, protease inhibitors

Krebs Ringer Phosphate (KRP)

128 mM NaCl, 4.7 mM KCl, 5 mM NaH₂PO₄, 1.25 mM MgSO₄, 1.25 mM CaCl₂, pH7.4

Krebs Ringer MES buffer (KRM)

128 mM NaCl, 4.7 mM KCl, 5 mM MES, 1.25 mM MgSO₄, 1.25 mM CaCl₂, pH6

HES buffer

255 mM sucrose, 20 mM HEPES, 1 mM EDTA, pH7.4

HPFEV buffer

50 mM HEPES, 10 mM sodium pyrophosphate, 100 mM sodium fluoride, 2 mM EDTA, 2 mM sodium orthovanadate (activated) pH 7.4

HU buffer

8 M urea, 5 % (w/v) SDS, 200 mM Tris pH 6.8, 0.1 mM EDTA, bromophenol blue

Phosphate Buffered Saline (PBS)

136 mM NaCl, 10 mM NaH₂PO₄, 2.5 mM KCl, 1.8 mM KH₂PO₄, pH 7.4

Resolving gel buffer (2×)

0.2 % SDS, 4 mM EDTA, 750 mM Tris base, pII 8.9

Resolving gel

10, 12 or 15 % acrylamide, 1 × resolving gel buffer, 0.2 % (w/v) APS, 0.08 % (v/v) TEMED

SDS-PAGE electrode buffer

25 mM Tris, 190 mM, 0.1 % (w/v) SDS

4 × SDS-PAGE sample buffer

250 mM Tris-HCl pH 6.8, 40 % (v/v) glycerol, 12 % (w/v) SDS, 0.05 % (w/v) bromophenol blue, 80 mM dithiothreitol (DTT)

Stacking gel buffer (2×)

0.2 % SDS, 4 mM EDTA, 250 mM Tris base, pH 6.8

Stacking gel

4.5 % acrylamide, 1 × stacking gel buffer, 0.125 % (w/v) APS, 0.125 % (v/v) TEMED

TAE

40 mM Tris acetate, 1 mM EDTA, pH 7.8

TE buffer pH 8.0

10 mM Tris-HCl (pH 8.0), 1 mM EDTA (pH 8.0)

Transfer buffer

25 mM Tris base, 192 mM glycine, 20 % (v/v) methanol

Wash buffer

20 mM Tris-HCl, 150 mM NaCl

2 × YT

1.6 % (w/v) tryptone, 1 % (w/v) yeast extract, 0.5 % (w/v) NaCl

2.1.8. Primers

PCR primers

STX16 pCR3.1

Fwd: 5'-CCGGTACCATGGCCCATATGGAAC-3'

Rev: 5'-CCTCTAGATTATCGAGACTTCAC-3'

STX16_{cyt}

Fwd: 5'-AAAGATCTATGGCCCATATGGAACAAAAA-3'

Rev: 5'-GGAAGCTTTTACCGATTCTTCTTTTGA-3'

STX16T

Fwd:

5'-AGATCTATGTACCCTTACGATGTGCCTGATTACGCAACAGAGGACCAGTTA-3'

Rev: 5'-GGAAGCTTTTATCGAGACTTCACGCCAAC-3'

STX16F

Fwd: 5'-AAAGATCTATGGCCCATATGGAACAAAAA-3'

Rev: 5'-GGAAGCTTTTATCGAGACTTCACGCCAAC-3'

Mutagenesis primers

STX16 T90 →A

Fwd: 5'-AAACAGACCCGCCCTGGATGACGC-3'

Rev: 5'-GCGTCATCCAGGGCGGGTCTGTTT-3'

STX16 S94 & S95 →A

Fwd: 5'-CCCTGGATGACGCCGCCGAAGAGGAAC-3'

Rev: 5'-GTTCTCTTCGGCGGCGTCATCCAGGG-3'

2.2. Molecular Biology Methods / Procedures

2.2.1. Amplification of target DNA by PCR

The polymerase chain reaction (PCR) was used to amplify specific target DNA sequences from plasmid DNA for subsequent molecular biology procedures. Primers were designed to the flanking sequences of the target DNA sequence, adding tags and restriction sites if required. Primers were synthesised at TAGN or MWG-Biotech and supplied in a lyophilised form. These were resuspended in dH₂O to an initial concentration of 1 mg/ml. A 1:10 stock (0.1 mg/ml) was then prepared in dH₂O, which was used directly for the PCR. Pfu DNA polymerase was used to avoid the point-mutations potentially introduced

by Taq polymerase. The following 50 μl reaction mixture was prepared in thin walled tubes:

Reaction cocktail:

5 μl 10 \times Pfu buffer
2.5 μl forward primer (from 0.1 $\mu\text{g}/\mu\text{l}$ stock)
2.5 μl reverse primer (from 0.1 $\mu\text{g}/\mu\text{l}$ stock)
1 μl dNTPs
2 μl template DNA (\sim 0.5 $\mu\text{g}/\mu\text{l}$)
37 μl dH₂O

The above was pulsed in a microfuge before adding:

1 μl Pfu DNA polymerase

The tubes were then added directly to the PCR machine programmed as follows:

Cycling parameters:

94 $^{\circ}\text{C}$ for 2 min

94 $^{\circ}\text{C}$ for 15 sec	}	\times 30 cycles
55 $^{\circ}\text{C}$ for 30 sec		
72 $^{\circ}\text{C}$ for 4 min		

72 $^{\circ}\text{C}$ for 5 min

Soak at 4 $^{\circ}\text{C}$

If the yield of amplified target DNA was low, 5 μl of PCR product was substituted for the template DNA and subjected to a second round of PCR as above (the volume of dH₂O added was adjusted to 35 μl to maintain the 50 μl solution).

2.2.2. Purification of PCR products

Following PCR, and prior to TA cloning, the PCR product was either purified by gel electrophoresis followed by gel extraction (Section 2.2.3 and 2.2.4) or directly using the QIAquick PCR Purification Kit, using the buffers provided and according to the manufacturers protocol. In summary, 5 volumes of Buffer PB were added to one volume of PCR sample and mixed, then applied to the QIAquick column in a 2 ml collection tube and centrifuged for 1 min at 14,000 rpm in a microfuge. The flow-through was discarded and the column was washed by adding 0.75 ml Buffer PE and centrifuging as above. Once

again, the flow through was discarded and the column was centrifuged for a further 1 min to allow removal of residual buffer. The column was then placed into a clean 1.5 ml eppendorf and the purified PCR product was eluted in 30-50 μl (depending on the concentration required) Buffer EB or dH_2O . After adding the Buffer EB or dH_2O to the centre of the column, it was allowed to stand for 1 min prior to centrifugation for 1 min.

2.2.3. Agarose gel electrophoresis

DNA fragments were resolved by gel electrophoresis on 1 % agarose gel, owing to differences in their electrophoretic mobility. A 1 % (w/v) agarose solution was prepared by adding the agarose to 1 \times TAE buffer and heating in a microwave oven to aid dissolving. 0.5 g agarose was added to 50 ml TAE buffer for a small gel and 1.5 g agarose to 150 ml TAE for a large gel. The agarose solution was allowed to cool until no more steam appeared, before the addition of 0.1 % (v/v) (0.5 μl) ethidium bromide (fluoresces an intense orange when bound to double helical DNA) with gentle mixing. DNA fragments were prepared for loading by diluting 10 μl DNA solution with an appropriate volume of 6 \times loading dye (Section 2.1.1). A 1 kb ladder (Section 2.1.1) was run on all gels to facilitate size analysis. Gels were run in TAE buffer at 80 V and DNA bands were observed under ultraviolet light. Bands were identified by comparison with the migration of molecules of known length in the DNA ladder.

2.2.4. Gel extraction of DNA

Following agarose gel electrophoresis (Section 2.2.3 above), the required DNA fragment was excised from the gel with a clean, sharp, scalpel blade and weighed in an eppendorf tube. The QIAquick PCR Purification Kit was used to extract the DNA from the agarose gel slice, following the protocol and using the buffers provided. In summary, three volumes of Buffer QG were added to one volume of gel (100mg \sim 100 μl) and incubated at 37 $^\circ\text{C}$, with vortexing every 2-3 min, for 10 min or until the gel slice had completely dissolved. After the addition of one gel volume of isopropanol, the sample was mixed and applied to a QIAquick column in a 2 ml collection tube. This was centrifuged for 1 min and the flow-through was discarded. Adding 0.5 ml Buffer QG and centrifuging for 1 min removed all traces of agarose. The column was then washed with 0.75 μl Buffer PE, the flow through was discarded and the column was centrifuged for a further 1 min to allow removal of residual buffer. The column was then placed into a clean 1.5 ml eppendorf tube and 30-50 μl Buffer EB or dH_2O were added to the centre of the column. This was allowed to stand for 1 min, before the purified DNA was eluted by centrifugation for 1 min.

2.2.5. A-tail reaction (Taq treatment)

As Pfu polymerase was used for the PCR, it was necessary to treat the PCR product with Taq polymerase before TA cloning to add the overhanging A bases onto the blunt-ended PCR product.

The procedure was carried out by incubating the following mixture at 72 °C for 20 min in a PCR machine:

50 µl	Gel purified PCR product
1 µl	dNTPs
5 µl	Multi-core buffer
1 µl	Taq polymerase

2.2.6. TA cloning

The purified Taq-treated PCR product was cloned into the vector pCR2.1 using the TA Cloning® Kit according to the manufacturers instructions. Briefly, 2 µl purified PCR product was mixed with 0.5 µl pCR2.1 and incubated for 5 min at room temperature. After this incubation, 0.5 µl salt solution (provided) was added and the mixture was transformed into 50 µl TOP10 cells as described in 2.9.9. The transformed cells were selected on 2 × YT agar plates containing 0.025 µg/µl Kanamycin, pre-treated with 40 µl X-Gal, to allow for the selection of white colonies positive for insertion of the gene of interest. The following day, positive white colonies were selected and propagated overnight as in 2.9.9.

2.2.7. Restriction digest

DNA was digested at specific positions using specific restriction endonucleases. The DNA was incubated with the appropriate restriction enzyme(s) in a suitable enzyme buffer at 37 °C for 3 hours. The general reaction mixtures were as follows:

Single digest	Double digest
3 µl DNA (~ 0.5 mg/ml)	3 µl DNA (~ 0.5 mg/ml)
2 µl 10 × enzyme buffer	2 µl 10 × enzyme buffer
14 µl dH ₂ O	13 µl dH ₂ O
1 µl restriction enzyme	1 µl restriction enzyme
	1 µl restriction enzyme

The volumes of DNA and dH₂O could be adjusted, according to the concentration of DNA solution used.

2.2.8. Ligation

PCR products were digested directly or from the TA cloning vector by enzymatic digestion (Section 2.2.7), resolved and purified by gel electrophoresis (Section 2.2.3 and 2.2.4) and ligated into the required vectors, also digested at the same restriction sites in the multiple cloning region. The concentration of DNA was determined as in Section 2.2.14.

Each ligation reaction was optimised individually. As a general rule, an excess of insert to vector of 3: 1 to 10: 1 was required. The vector and insert were incubated with 1.5 µl T4 ligase in 1 × ligase buffer (diluted from 10 × stock) under various conditions (ice / slush overnight, 16 °C for 4 hours or room temperature for 1-4 hours) until optimal conditions were found.

3 µl ligation mixture was then transformed into TOP-10 cells as described in Section 2.2.9.

2.2.9. Transformation of *E. coli*

Transformation of plasmid DNA into competent *E. coli* cells was carried out as follows:

Competent *E. coli* strains (Section 2.1.5) were stored in 50 µl aliquots at – 80 °C in 1.8 ml polypropylene cryo-vials. Prior to transformation, a vial was thawed gently on ice. Plasmid DNA to be transformed was added to the thawed *E. coli* and gently mixed with a pipette tip, before incubation on ice for 30 min. Heat-shock was then induced by incubation of the mixture in a water bath, pre-heated to 42 °C, for 90 sec, before returning to ice for 2 min. The cells were recovered by adding 250 µl 2 × YT media and incubating at 37 °C for 45 min with shaking. During this incubation, 2 × YT agar plates containing 0.025 µg/µl Kanamycin were warmed from 4 °C by incubation at 37 °C. After recovery, the entire culture was pipetted onto the agar plate and spread thoroughly using a sterile glass bacterial spreader. The plates were then allowed to dry, sealed with nescofilm, inverted and incubated at 37 °C overnight for 16 hours. The following day, single colonies could be picked using a sterile pipette-tip for propagation in 2 × YT media (Section 2.2.10 below).

2.2.10. Mini-cultures

A single colony was picked following transformation (Section 2.2.9) or from a freshly streaked selective plate and used to inoculate a starter culture of 5 ml 2 × Y1 containing 0.025 µg/µl Kanamycin in a universal tube. This was incubated at 37 °C with shaking for 16 h. Small scale DNA preparations (Section 2.2.11) were carried out to extract the plasmid DNA or this 5 ml culture could be used to inoculate a larger culture volume.

2.2.11. Small-scale DNA preparations (Mini-preps)

Small-scale DNA preparations were carried out using the QIAprep Spin Mini-prep Kit according to the protocol provided. Mini-preps are designed for purification of up to 20 µg of high-copy plasmid DNA from 1- 5 ml overnight cultures of *E. coli* in LB medium. All buffers used were supplied in the kit.

A 5 ml overnight *E. coli* culture (Section 2.2.10) was harvested by centrifugation at 14,000 rpm for 10 min in a bench-top centrifuge with subsequent removal of the supernatant. The pelleted bacterial cells were then resuspended in 250 µl Buffer P1 (containing RNase A) and transferred to an eppendorf tube. Cells were lysed in 250 µl Buffer P2 with gentle inversion of the tube and incubation for 5 min at room temperature. To neutralise the sample, 350 µl Buffer N3 was added with gentle mixing before centrifugation for 10 min at 14,000 rpm. The supernatant was carefully decanted into the QIAprep spin column, centrifuged for 1 min (to bind the plasmid DNA to the column) and the flow-through was discarded. The column was then washed with 0.5 ml Buffer PB, followed by 0.75 ml Buffer PE by centrifugation for 1 min following the addition of each buffer. The flow-through was discarded and the sample was centrifuged for a further 1 min to remove residual wash buffer. The column was then placed in a clean 1.5 ml eppendorf tube. Finally, 30 – 50 µl (depending on the final concentration required) Buffer EB, TE buffer (Section 2.1.7) or dH₂O were added to the centre of the column, allowed to stand for 1 min and then centrifuged for 1 min to collect the plasmid DNA.

2.2.12. Large-scale DNA preparations (Maxi-preps)

Large-scale plasmid DNA preparations were carried out using the QIAfilter Plasmid Maxi Kit in accordance with the manufacturers instructions and using the buffers supplied in the kit.

Briefly, a 5 ml mini-culture (Section 2.2.10) grown for 8-16 h was used to inoculate 250 ml $2 \times$ YT media containing the appropriate antibiotic. This culture was incubated with vigorous shaking at 37 °C for 16 hours overnight. After this time, the bacterial cells were harvested by centrifugation at $6000 \times g$ for 15 min at 4 °C in a bench-top centrifuge. The supernatant was carefully decanted and the cell pellet was resuspended in 10 ml Buffer P1 by pipetting up and down until no cell clumps were visible. 10 ml Buffer P2 was then added to the cell suspension and mixed thoroughly by inverting the tube 4-6 times, followed by incubation at room temperature for 5 min. Next, to neutralise the lysates, 10 ml chilled Buffer P3 was added and mixed immediately but gently by inverting 4-6 times. The lysates were then immediately poured into the barrel of the QIAfilter Maxi Cartridge (with screw-cap on outlet nozzle and suspended from a clamp stand) and incubated at room temperature for 10 min. A precipitate containing proteins, genomic DNA, and detergent formed at the surface. Meanwhile, the QIAGEN-tip 500 was equilibrated by applying 10 ml Buffer QBT to the column and allowing it to empty by gravity flow. After the 10 min incubation the cap was removed from the QIAfilter Maxi Cartridge and the plunger was inserted into the barrel. The cleared cell lysates were filtered into the previously equilibrated QIAGEN-tip and allowed to enter the resin by gravity flow. The column was washed with 2×30 ml Buffer QC before the DNA was eluted, in 15 ml Buffer QF, into a clean 50 ml falcon tube. The DNA was then precipitated by the addition of 10.5 ml (0.7 volumes) room-temperature isopropanol with mixing. The sample was immediately centrifuged at 4,300 rpm in a bench-top centrifuge for 1 h at 4 °C. The supernatant was carefully decanted the precipitated DNA pellet was washed with 5 ml of room-temperature 70 % ethanol and centrifuged for a further 1 h in a bench-top centrifuge at 4,300 rpm and 4 °C. The supernatant was carefully decanted to avoid disturbing the DNA pellet, which was subsequently allowed to air dry for 5- 10 min. The DNA was then re-dissolved in a suitable volume (generally 200 μ l) of TE buffer, pH 8.0 (Section 2.1.7).

2.2.13. Site-directed mutagenesis

Mutagenesis was carried out using the QuickChangeTM Site-Directed Mutagenesis Kit according to the manufacturers instructions, with some variations, as detailed here. Mutagenesis primers were designed and used in PCR at a concentration of 0.1 μ g/ μ l.

The following reaction was set up in thin walled tubes:

Reaction cocktail:

5 μ l 10 \times Pfu buffer
 1.25 μ l forward primer
 1.25 μ l reverse primer
 1 μ l dNTPs
 3 μ l template DNA (\sim 0.5 μ g/ μ l)
 38.5 μ l dH₂O

The above was pulsed in a microfuge before adding:

1 μ l Pfu DNA polymerase

The tubes were then added directly to the PCR machine programmed as follows:

Cycling parameters:

95 °C for 30sec

95 °C for 30 sec 55 °C for 1 min 68 °C for 12 min	}	× 16 cycles
---	---	-------------

 Soak at 4 °C

If further amplification was required, 5 μ l of the PCR product was put through a second round of PCR as described in 2.2.1.

When the PCR was complete, parental DNA was digested by the restriction enzyme, *DpnI*. 1 μ l of *DpnI* was added directly to the PCR tube, which was then incubated on a hot-block at 37 °C for 1 hour. 1 μ l of the *DpnI* treated product was subsequently transformed into 50 μ l XL1-Blue supercompetent cells as described in 2.2.9.

Finally, the DNA was sequenced (Section 2.2.16) to verify that the correct mutations had been introduced and to verify that the integrity of the remaining DNA was intact.

2.2.14. DNA concentration determination

The concentrations of DNA samples were determined by measuring the optical densities at 260 nm and 280 nm (OD₂₆₀ and OD₂₈₀) using a UV-1201 UV-VIS Spectrophotometer. The

DNA concentration was calculated from OD₂₆₀. One optical density unit at 260 nm in a 1 cm path length is approximately equal to 50 mg/ml of double stranded DNA. Therefore:

$$[\text{DNA}](\text{mg/ml}) = \text{OD}_{260} \times 100 (1 / \text{Dilution Factor}) \times 50$$

The ratio of OD₂₆₀:OD₂₈₀ was calculated as an indication of sample purity. OD₂₆₀:OD₂₈₀ < 1.8 indicated possible protein contamination and OD₂₆₀:OD₂₈₀ > 1.8 indicated possible contamination by RNA.

2.2.15. Ethanol Precipitation

Plasmid DNA could be ethanol precipitated for storage / posting or resuspended in a more suitable volume of appropriate buffer. For sequencing at MWG, the plasmid DNA was ethanol precipitated and sent dried down in an eppendorf tube. When 1 µg DNA was to be precipitated, 1.5 µg (to allow for loss) DNA in dH₂O or Buffer EB was added to a clean eppendorf tube, followed by 2.5 × volume (of DNA) 100 % ethanol and 0.1 × volume (DNA + ethanol) 3.2 M NaOAc, pH 5.2. This mixture was stored at -80 °C for 30 min to overnight to aid precipitation. The samples were then centrifuged at 14,000 rpm for 15 min at 4 °C in a microfuge. After careful removal of the supernatant, 500 µl 70 % ethanol was added with care to the precipitated DNA and the samples were spun again at 14,000 rpm for 15 min at 4 °C. The supernatant was gently decanted and the tubes were stored open and inverted at room temperature and allowed to air-dry overnight.

2.2.16. Sequencing

DNA sequencing reactions were carried out at MWG Biotech, Germany or The Sequencing Service, University of Dundee, Dundee, UK.

2.2.17. Preparation of glycerol stocks of transformed bacteria

Glycerol stocks were made from each transformed *E. coli* sample (Section 2.2.9). 850 µl of an overnight 5 ml culture (Section 2.2.10) was added to 150 µl sterile 100 % glycerol in a 1.8 ml polypropylene cryo-vial. The vial was inverted several times to mix the contents, snap-frozen in liquid nitrogen and transferred for storage at -80 °C.

A small amount of cells could then be streaked out onto agar plates using a sterile tip and selected using the appropriate antibiotic prior to inoculating a culture (Section 2.2.10).

2.3. Mammalian Cell Culture Methods / Procedures

2.3.1. General conditions

All cells were grown in Iwaki plasticware, with the exception of 3T3-L1 cells for differentiation, which were grown in Falcon plasticware for improved adhesion. All cells were grown in Galaxy S incubators (Wolf Laboratories) at 37 °C and 5 % or 10 % CO₂ as indicated. All cell culture procedures were carried out in a UniMat² Class II microbiological safety cabinet (flow-hood).

2.3.2. Trypsinisation and passage of cells

Cells were passaged when they were 70-80 % confluent. The medium was aspirated from the sub-confluent fibroblasts and 2-5 ml of trypsin/EDTA, pre-warmed to 37 °C, was added to cover the base of the flask. After incubation at 37 °C and 10 % CO₂ (for 3T3-L1) or 5 % CO₂ (for HeLa and HEK 293) for 2 to 5 min, the cells were detached by gentle tapping of the flask (verified by viewing under a 20 × objective lens). The trypsinised cells were then resuspended in the required volume of appropriate growth medium and distributed into 75 cm² flasks, 12-well plates or 6-well plates, depending on requirements.

2.3.3. Freezing down and resurrection of cells

Cells were trypsinised as described in section 2.3.2 and resuspended in approximately 8 ml of appropriate growth medium. The cells were then pelleted by centrifugation at 2000 ×g for 5 min before being resuspended in 1 ml growth medium containing 10 % (v/v) DMSO in a 1.8 ml polypropylene cryo-vial. This was stored at -80 °C overnight before being transferred to a liquid nitrogen vat for long-term storage.

Prior to use, cells were thawed rapidly at 37 °C and transferred to a 75 cm² flask containing 15 ml appropriate growth medium, pre-warmed to 37 °C and incubated overnight at 37 °C at 10 % CO₂. The following day, media containing DMSO were removed and replaced with fresh growth media.

2.3.4.3T3-L1

2.3.4.1. Culture of 3T3-L1 murine fibroblasts

3T3-L1 fibroblasts were cultured in 3T3-L1 fibroblast growth medium (Section 2.1.5.), and maintained at 37 °C and 10 % CO₂. Cells for passaging were grown in 75 cm² flasks and fed every two to three days, until approximately 80 % confluent, when they were trypsinised and passaged as described in section 2.3.2. Cells were used between passage 2 and 12 and typically frozen down (Section 2.3.3) between passage 2 and 4. Cells for differentiation and subsequent experiments were split into 12-well or 6-well falcon plates (for better adhesion), and fed every two to three days, until 2-4 days post confluence, and then differentiated into adipocytes.

2.3.4.2. Differentiation of 3T3-L1 fibroblasts

3T3-L1 adipocytes were grown to confluency on falcon plastic-ware as described above (Section 2.3.4.1). At confluency, the cells were fed with 3T3-L1 fibroblast growth medium (Section 2.1.6) and then allowed to grow for a further 2 to 4 days. Differentiation was carried out by treating the cells with 0.25 µM dexamethasone, 0.5 mM isobutyl methyl xanthine (IBMX), and 1 µg/ml insulin in 3T3-L1 adipocyte growth medium.

This was considered to be day 1 post-differentiation. This feed was carefully aspirated on day 3 or 4 (depending on requirements of the cells) and gently replaced with 3T3-L1 adipocyte growth medium containing 1 µg/ml insulin only. The cells were fed again thereafter with 3T3-L1 adipocyte growth medium as required. In this study, the cells were assayed on day 8 post-differentiation.

2.3.4.3. Preparation of 3T3-L1 adipocyte lysates

Lysates were generally prepared from 3T3-L1 adipocytes on day 8 post-differentiation following experimental treatment. Cells were washed three times in ice-cold Wash Buffer (Section 2.1.7), and then an appropriate volume of Lysis buffer (Section 2.1.7) ± 1 % (v/v) thesitol (supplemented with Complete Protease inhibitor tablets) was added (~ 100 µl / well of a 12-well plate). The cells were detached by scraping with a plastic cell scraper and transferred to a clean eppendorf using a pipette. The cells were lysed by passage through a 26G needle six times, then incubated on ice for 30 min, before being spun at 14,000 rpm for 20 min at 4 °C in a bench-top centrifuge. This centrifugation step resulted in the

separation of the lysates into a heavy insoluble pellet, soluble lysate and a buoyant layer of fat. The soluble lysate and fat layer were carefully removed and added separately to clean eppendorf tubes. All fractions of the lysates were stored at $-20\text{ }^{\circ}\text{C}$ prior to analysis.

2.3.5. HeLa

2.3.5.1. Culture of HeLa cells

Human cervical carcinoma (HeLa) cells were cultured in 75 cm^2 flasks in HeLa growth medium (Section 2.1.6) and maintained at 5 % CO_2 and at $37\text{ }^{\circ}\text{C}$. Cells were fed every two to three days, until approximately 80 % confluent, when they were trypsinised and passaged as described in section 2.3.2.

2.3.5.2. Transfection with LipofectamineTM 2000

Transfection of HeLa cells was carried out using Lipofectamine 2000 according to the manufacturers instructions. Briefly, cells were grown in 6 or 12 well plates to 90-95 % confluence in HeLa growth medium. DNA-Lipofectamine 2000 complexes were prepared (per well of a 12-well plate) as follows: 4 μl Lipofectamine 2000 was diluted in 100 μl Opti-MEM, mixed gently and incubated for 5 min at room temperature. Meanwhile, 1.6 μg DNA was also diluted in 100 μl Opti-MEM. The diluted Lipofectamine 2000 was added drop-wise to the diluted DNA, mixed gently and incubated for 20 min at room temperature to allow the DNA- Lipofectamine 2000 complexes to form. During this incubation, the HeLa growth medium was aspirated and the HeLa cells were washed twice in warm Opti-MEM, pre-heated to $37\text{ }^{\circ}\text{C}$. The volume of the DNA- Lipofectamine 2000 complexes was made up to 1 ml (per well of a 12-well plate) with Opti-MEM before adding to the cells. The cells were then incubated at $37\text{ }^{\circ}\text{C}$ and 5 % CO_2 for 24 to 48 hours. After 5 hours, 1 ml HeLa growth medium (containing 20 % FCS) was added to each well (without removal of the DNA-Lipofectamine 2000 complexes). If the cells were to be incubated for 48 hours, the transfection medium was removed and replaced with normal HeLa growth medium for the remaining 24 hours.

2.3.5.3. Preparation of HeLa lysates

Following experimental treatment, cells were washed three times in ice-cold HES buffer (Section 2.1.7). An appropriate volume of HES buffer containing protease inhibitors $\pm 1\%$ thesist (typically 100 μl / well of a 12-well plate) was added to the cells and a plastic cell

scraper was used to detach the cells from the plastic-ware. They were then transferred to a clean eppendorf using a pipette and lysed by passage through a 26G needle six times. This was followed by incubation on ice for 30 min, before centrifugation at 14,000 rpm for 20 min at 4 °C in a microfuge to pellet insoluble material. The supernatant was transferred to a clean eppendorf tube for analysis and stored at – 80 °C, along with the insoluble pellets, for analysis at a later date.

2.3.6. HEK 293

2.3.6.1. Culture of HEK 293 cells

Human embryonic kidney (HEK) 293 cells were cultured in 75 cm² flasks in HEK 293 growth medium (Section 2.1.6) and maintained at 5 % CO₂ and 37 °C. Cells were fed every two to three days, until approximately 80 % confluent, when they were trypsinised and passaged as described in Section 2.3.2.

2.3.6.2. Transfection with Lipofectamine 2000

Transfection of HEK 293 cells with Lipofectamine 2000 was carried out as for transfection of HeLa cells above (Section 2.3.5.2)

2.3.6.3. Calcium phosphate transfection

HEK 293 cells were plated out appropriately into plates or dishes at least one day before the experiment and incubated at 37 °C and 5 % CO₂ until approximately 50 % confluent. Fresh media was added 4 h prior to the experiment. The following mixture was prepared per 10 cm² dish:

30 µg DNA
125 µl 1 M CaCl₂
500 µl dH₂O
500 µl 2 × HBS (HEPES buffered saline, Section 2.1.7)

These quantities were divided by a factor of 8 if transfection was to be carried out in a 12 well plate.

This mixture was then incubated in the flow-hood at room temperature for 20 min before being added drop-wise to the cells and swirled gently to mix. This was then incubated

overnight at 37 °C. The next morning, the cells were washed three times in HEK 293 growth medium and then incubated for a further 24 h in HEK 293 growth medium prior to the assay.

2.3.6.4. Preparation of HEK 293 lysates

HEK 293 lysates were prepared as for HeLa lysates in Section 2.3.5.3.

2.4. Biochemical Methods / Procedures

2.4.1. Immunoprecipitation

2.4.1.1. Immunoprecipitation from 3T3-L1 adipocytes

Lysates were prepared as in Section 2.3.4.3 using 500 µl Lysis Buffer (Section 2.1.7) containing 1 % thesit. The required amount of the appropriate antibody (generally 2 µg) or a random IgG were added to each, mixed by inversion of the tube several times, then incubated on ice for at least one 1 hour. During this incubation, the adsorbent was prepared using either Protein A or Protein G Sepharose as follows: The beads were washed three times by adding 1 ml Lysis Buffer (containing 1 % thesit) (Section 2.1.7), mixing gently, and then spinning at 14,000 rpm for 1 min at 4 °C in a bench-top centrifuge. The supernatant was aspirated carefully each time, taking care not to disturb the beads. The beads were then resuspended in roughly an equal volume of Lysis Buffer. 40 µl of this suspension was added to each of the cell lysates in screw cap tubes. These were then mixed by end over end rotation for at least 2-4 hours at 4 °C.

The samples were then centrifuged at 14, 000 rpm for 1 min at 4 °C. The supernatants were removed and snap-frozen at -80 °C for later analysis by SDS-PAGE (Section 2.4.3.). The pellet was then washed twice by adding 1 ml Lysis Buffer (1 % thesit) (Section 2.1.7), centrifuging and removing the supernatant by careful aspiration. All traces of buffer were removed using a 26G needle to ensure no beads were lost. A final wash into Lysis Buffer (Section 2.1.7) with a lower concentration (0.1 %) of thesit was performed to minimise the detergent in the final sample. The samples were centrifuged and again, all the supernatant was carefully removed using a 26G needle. 40 µl 2 × SDS-PAGE sample buffer (Section

2.1.7) was then added and the samples were boiled for 5 min in a water bath to remove the immunoprecipitated protein and antibody from the beads. Finally, the samples were centrifuged at 14,000 rpm and 4 °C for 1 min to pellet the beads and the immunoprecipitated material was carefully removed and transferred to a clean eppendorf for storage at -20 °C and subsequent analysis by SDS-PAGE (Section 2.4.3).

2.4.1.2. ^{32}P i labelling of HEK 293 cells

HEK 293 cells were transfected in 6-well plates as described in Section 2.3.6.3. The remainder of this procedure was carried out in a controlled radioisotope laboratory. On the morning of the assay, the cells were washed twice in serum-free, phosphate-free DMEM (Section 2.1.2), pre-warmed to 37 °C, before incubation in 0.5 ml of the same for 2 hours at 37 °C and 5 % CO_2 . After 1 hour of the incubation, 250 μCi ^{32}P i was added to each well to be assayed behind a lead-glass shield and then transferred to the CO_2 incubator for a further 1 h. The radioactive medium was then removed from the cells behind the lead-glass shield and placed in a beaker containing Decon for subsequent appropriate disposal. 0.5 ml HPFV buffer (Section 2.1.7) containing 1 % thesitol, supplemented with protease inhibitors was added per well. The cells were lysed by pipetting up and down, taking care avoid creating an aerosol, and transferred to screw-capped eppendorfs. The lysates were then incubated on ice for 15 min before centrifuging at 13, 000 rpm for 10 min at 4 °C in a microfuge. The solid and liquid contaminated waste was disposed of appropriately, according to current regulations.

2.4.1.3. Immunoprecipitation from HeLa and HEK 293 cells

Immunoprecipitation was carried out from ^{32}P i labelled HEK 293 lysates or unlabelled HeLa lysates as in Section 2.4.1.1 except HPFV buffer (Section 2.1.7) containing 1 % (or 0.1 % where appropriate) thesitol and supplemented with protease inhibitors, was used throughout in place of Lysis Buffer (Section 2.1.7) and appropriate care was exercised when ^{32}P i labelled lysates were used.

2.4.1.4. Activation of Sodium Orthovanadate

Sodium orthovanadate was activated for maximal inhibition of protein phosphotyrosyl-phosphatases by depolymerisation of the vanadate, converting it into a more potent inhibitor of the protein tyrosine phosphatases. This was carried out according to the

protocol given on the Upstate website (www.upstate.com) and summarised briefly here. A 200 mM solution was prepared of sodium orthovanadate. The pH was adjusted to 10.0 (yellow) using either 1 N NaOH or 1 N HCl, depending on the starting pH, which can vary with large amounts of the chemical. The solution was boiled in the flow-hood for ~ 10 min until it turned colourless. It was then cooled to room temperature and the pH was adjusted to 10.0. This process of boiling, cooling and returning the pH to 10.0 was repeated until the solution remained colourless and the pH stabilised at 10.0. The activated sodium orthovanadate was stored in aliquots at $-20\text{ }^{\circ}\text{C}$ until required.

2.4.2. Trichloroacetic acid (TCA) precipitation

Proteins could be precipitated from cell lysates or from Secretion Assay fractions (Section 5.4.1.1). The protein sample was first subjected to a slow spin of 2000 rpm in a bench-top centrifuge at $4\text{ }^{\circ}\text{C}$ for 20 min to pellet any whole cells, and the volume was adjusted to 500 μl with distilled water. 50 μl of 0.15 % (w/v) sodium deoxycholate was then added and the sample was subjected to vortexing followed by incubation for 5 min at room temperature. 100 μl of 72 % TCA was added and again, the sample was vortexed and incubated on ice for 1 hour, before spinning in a chilled bench top centrifuge at $4\text{ }^{\circ}\text{C}$ for 5 min at 14, 000 rpm. The supernatant was aspirated and the pellet was washed in 1 ml acetone (pre-cooled on dry ice) with vortexing. The sample was then centrifuged at 14, 000 rpm and $4\text{ }^{\circ}\text{C}$ for 5 min and the acetate was carefully aspirated. This process was repeated and the pellet was allowed to air-dry. Finally, the pellet was resuspended in 50 μl HU buffer (Section 2.1.7) for Secretion Assay samples or 50 μl $2 \times$ SDS-PAGE Sample Buffer (Section 2.1.7) for SDS-PAGE analysis (Section 2.4.3).

2.4.3. SDS gel electrophoresis / SDS-PAGE

Proteins were resolved by gel electrophoresis through polyacrylamide gels, owing to differences in their electrophoretic mobility. Protein samples were denatured in a solution of sodium dodecyl sulphate (SDS, an anionic detergent that disrupts non-covalent interactions) and dithiothreitol (DTT, reduces disulfide bonds) by adding an appropriate volume of $4 \times$ SDS sample buffer (Section 2.1.7) for a final concentration of $1 \times$ SDS sample buffer. The samples were then boiled in a water bath for 5 min (or at $65\text{ }^{\circ}\text{C}$ for GLUT4-containing samples) prior to loading on the SDS gel.

Bio-Rad Upright Gel Kits, consisting of two glass plates with a 1 mm space between, were generally used. Acrylamide, which polymerises with the addition of TEMED, was poured

between the two glass plates. The gel pore size was controlled by changing the concentration of acrylamide used, allowing the resolution of various sizes of proteins. In this study, resolving gels containing 10, 12 or 15 % acrylamide were used (Section 2.1.7) and stacking gels contained 4.5 % acrylamide (Section 2.1.7). The protein samples were loaded and 80 V was applied across the gel until the samples had passed through the stacking gel, into the resolving gel at which time the voltage was increased to up to 130 V until the dye front reached the base of the gel or until the proteins were sufficiently resolved. Resolved proteins were compared to protein markers of known sizes.

2.4.4. Transfer to nitrocellulose

Proteins were transferred to nitrocellulose membrane using wet blotting apparatus. Two sections of filter paper and one section of nitrocellulose were cut to fit the blotting apparatus and soaked in transfer buffer prior to use. Starting from the black surface of the blotting case, a sponge soaked in transfer buffer was placed down, followed by filter paper. The SDS-PAGE gel (Section 2.4.3) was then carefully removed from between the glass plates using a plastic spatula and placed on top of the filter paper. The nitrocellulose membrane was placed on top of the gel and smoothed down before another sheet of filter paper and a sponge were placed on top. Air bubbles were removed at each stage by rolling over the surface with a cylindrical tube. The case was then closed and placed in a tank filled with Transfer Buffer (Section 2.1.7) in order that the current ran from the gel to the nitrocellulose in the positive direction. The current (70 mA overnight or at 250 mA for 1 h 45 min) was then applied and the negatively charged SDS-protein complexes migrated from the gel and bound to the nitrocellulose membrane.

2.4.5. Immunoblotting (Western blotting)

The nitrocellulose containing the bound proteins (Section 2.4.4) was washed twice in PBS-T for 5 min before incubation in blocking buffer (PBS-T, 5 % marvel) for 45 min. This was then incubated with primary antibody (at appropriate concentration in PBS-T, 1 % marvel) for 1 hour. The nitrocellulose was then washed five times in PBS-T for 5 min before incubation with appropriate HRP-conjugated secondary antibody (1:1000 in PBS-T, 1 % marvel) for 45 min. The blots were then washed twice in PBS-T for 5 min, once in high salt (0.5 M NaCl) PBS-T for 30 min and twice again in PBS-T for 5 min. The blots were then developed using ECL Western Blotting Detection Reagents.

Quantification of immunoblot signals was performed using a Bio-Rad (Hercules, CA) scanner and Scion Imaging software. In all cases, multiple exposures of x-ray film were analysed to be certain of studying immunoreactive signals within the linear range of both the detection antibodies and film.

2.4.6. Stripping nitrocellulose

Protein bound to nitrocellulose used for Western Blotting could be stripped of antibody and re-probed with a different primary antibody. 50 mM glycine pH 2.5 (pH with HCl) was applied to the nitrocellulose with shaking for exactly one minute. The nitrocellulose was then washed with PBS-T prior to further immunoblotting (Section 2.4.5).

2.4.7. Protein concentration determination (Bradford Assay)

Protein concentrations were measured using the Bradford Assay (Bradford, 1976) using Bio-Rad Brilliant Coomassie Blue Reagent. Protein samples were prepared in duplicate in plastic 1 ml cuvettes, according to the manufacturers instructions, and absorbance at 595 nm was measured using a UV-1201 UV-VIS Spectrophotometer. A standard curve was generated using 1-5 μ g BSA and sample volumes were used within the linear range of the standard curve. Unknown protein concentrations were calculated from the standard values.

Chapter 3

Phosphorylation of STX16

3. Phosphorylation of STX16

3.1. Introduction

There is much evidence to implicate STX16 as a potential regulator of GLUT4 trafficking in 3T3-L1 adipocytes (Section 1.8, Chapter 1), perhaps involving a SNARE complex with STX6. This Chapter aimed to investigate if the intriguing dephosphorylation of STX16 in response to insulin could be responsible for regulating the assembly of this SNARE complex. Indeed, phosphorylation has been shown to control the formation of many other SNARE complexes (Gerst, 2003). Section 3.1 provides an introduction to phosphorylation and its role in regulating the assembly of SNAREs into functional SNARE complexes.

3.1.1. Phosphorylation

3.1.1.1. Regulation by phosphorylation

Phosphorylation is the most common and ubiquitous type of reversible covalent modification, involved in regulating the activity of enzymes, membrane channels and other target proteins (reviewed in Cohen, 2002). A protein kinase catalyses the covalent attachment of phosphate groups, donated by ATP, to the hydroxyl groups on the side chains of specific amino acid residues. The process can then be reversed by a protein phosphatase, which restores the unmodified hydroxyl group by catalysing the hydrolysis of the phosphate group with the generation of orthophosphate. This reversible process is utilised by cells to modify the function of a protein by altering its structural, thermodynamic and kinetic properties to increase or decrease its biological activity and initiate or disrupt protein-protein interactions (Cohen, 2002).

There are over 500 protein kinases in the human genome, with 130 homologs identified in yeast (Manning et. al., 2002; Pawson et. al., 2003; Pawson et. al., 2005). The greatest majority of the mammalian protein kinases phosphorylate proteins on specific serine, threonine or tyrosine residues. Indeed, the majority of phosphatases are known to be associated with these residues, with over 100 genes in the human genome representing tyrosine phosphatases alone (Alonso et. al., 2004).

Almost every aspect of cellular function can be controlled by reversible phosphorylation and as such, kinases and phosphatases have a plethora of targets throughout the cell and varying degrees of specificity (Cohen, 2002). Some protein kinases phosphorylate just one or several closely related proteins and are referred to as dedicated protein kinases, whereas others referred to as multifunctional protein kinases, modify many different targets, with the ability to coordinate diverse processes. Multifunctional kinases recognise related sequences, known as consensus motifs, surrounding the phosphorylated residue.

Many protein kinases are themselves regulated by phosphorylation, leading to so-called phosphorylation cascades (Cohen, 2002) in which one protein kinase activates another, such as the MAP kinase pathway (Ray and Sturgill, 1987), which is activated by insulin signalling among other stimuli. In addition, many proteins are now known to exhibit multisite phosphorylation, being phosphorylated on two or more residues by two or more kinases (Cohen, 2002).

3.1.1.2. Phosphorylation of SNAREs

SNARE complex formation is fundamental to cell survival and so is subject to regulation (Section 1.5). From studies of phosphorylated SNARE proteins, it is clear that phosphorylation plays a key role in the regulation of the assembly of many SNARE complexes and the resulting cellular effects. It appears that phosphorylation can increase the affinity of SNAREs for other SNAREs or for SNARE regulators, such as SM proteins (Gerst, 2003) as described below.

At the mammalian synapse (Section 1.5.2), SNAP-25 binding to STX1a is reduced by *in vitro* phosphorylation of SNAP-25 by PKC (Shimazaki et al., 1996) and phosphorylation of Munc18 by cyclin-dependent kinase 5 also displays reduced affinity for STX1a (Shuang et al., 1998). STX1a itself can be phosphorylated by Casein Kinase II, increasing its affinity for the SNARE regulator synaptotagmin 1 (Risinger and Bennett, 1999).

Gerst and co-workers carried out a number of studies that demonstrate that regulation of SNARE assembly by phosphorylation is also apparent in yeast. They demonstrated that yeast utilize the PKA (Section 3.1.2) / CAPP (a sphingoid base- and ceramide- activated protein phosphatase) kinase / phosphatase pathway to regulate exo- and endocytosis by means of the dephosphorylation of the Sso and Tlg t-SNAREs respectively and their subsequent assembly into SNARE complexes (Gurunathan et al., 2002; Marash and Gerst, 2001). Not only did PKA phosphorylation of the autoinhibitory (H_{abc}) domain of the Sso t-

SNAREs inhibit SNARE complex assembly and exocytosis (Marash and Gerst, 2001), it also promoted the binding of Vsm1, a potential SNARE regulator (Marash and Gerst, 2003). Interestingly, when bound to Vsm1, Sso was unable to bind to its cognate t-SNARE, Sec9 (a yeast SNAP-25 homolog), and vice versa. Dephosphorylation of Sso, on the other hand, promoted SNARE complex assembly with Sec9 *in vitro* and *in vivo* (Marash and Gerst, 2001).

3.1.1.3. Tlg2p is phosphorylated in yeast

Perhaps most significant with regard to my study is the phosphorylation data regarding the STX16 and STX6 yeast homologs, Tlg2p and Tlg1p respectively (Section 1.6.4), which, among other functions, mediate endocytosis yeast in conjunction with the Snc v-SNAREs (Paumet et al., 2001). It was shown that, in yeast, PKA phosphorylation of Tlg2p and Tlg1p inhibited SNARE complex assembly and, as a result, blocked endocytosis (Gurunathan et al., 2002). The addition of ceramide precursors was able to rescue yeast mutants defective in endocytosis by activation of CAPP and subsequent dephosphorylation of the t-SNAREs, followed by their assembly into SNARE complexes (Gurunathan et al., 2002). Because the restoration of endocytosis by CAPP activation correlated with dephosphorylation of Tlg1p and Tlg2p, mutants bearing alanine substitutions at potential phosphorylation sites in the H_{abc} domains were generated and tested for their ability to confer the uptake of the vacuolar staining dye, FM4-64, in yeast cells defective in endocytosis in the absence of CAPP activation. It was found that alanine substitutions at position 31 of Tlg1p and position 90 of Tlg2p restored uptake of FM4-64 to the vacuole (Gurunathan et al., 2002), suggesting that these residues correspond to the sites of phosphorylation in Tlg1p and Tlg2p.

3.1.1.4. STX16 is a phosphoprotein in 3T3-L1 adipocytes

Previous work in our laboratory demonstrated that STX16 is a phosphoprotein in 3T3-L1 adipocytes and, intriguingly, that dephosphorylation appears to occur in response to acute insulin stimulation (Perera et al., 2003). The phosphorylation status of both endogenous STX16 and STX6 were examined by immunoprecipitation from 3T3-L1 adipocytes labelled with ³²Pi. STX16 was highlighted as a phosphoprotein, displaying a 50 % reduction in phosphorylation in response to acute insulin treatment (1 μM insulin for 30 min) compared to basal cells. STX6, on the other hand, was not observed to be phosphorylated in either basal or insulin stimulated cells (Perera et al., 2003).

The SM protein mVps45 (Section 1.6.5) was shown to interact weakly with STX6 (Bock et al., 1997; Tcllam et al., 1997), and more recently to bind directly to STX16 (Dulubova et al., 2002; Yamaguchi et al., 2002). Interestingly, recent data from our laboratory suggests that the yeast homolog of mVps45, Vps45p (Section 1.6.4) is a phosphoprotein (Scott Shanks, unpublished data).

3.1.2. Is STX16 phosphorylated by PKA?

3.1.2.1. PKA

The cyclic AMP activated kinase / protein kinase A (PKA) is a multifunctional kinase that phosphorylates specific serine or threonine residues (Cohen, 2002). PKA is responsible for propagating the effects of the intracellular messenger cyclic AMP, the formation of which is triggered by many hormones. PKA is widely distributed in animal tissues and other organisms and has been shown to phosphorylate a vast number of substrates with an extensive range of functions (Cohen, 2002).

3.1.2.2. Insulin-stimulated GLUT4 trafficking and regulation of PKA

As mentioned previously (Section 1.3.2, Chapter 1), insulin exerts its effects by binding to a cell surface receptor expressed in insulin-responsive cells, such as muscle and fat cells. The insulin receptor is a heterotetramer that is comprised of two α - and two β -subunits. When insulin binds to the extracellular portion of the α -subunits, a conformational change is induced in the receptor, leading to activation of its tyrosine-kinase domain, which is located within the intracellular portion of its β -subunits. On activation, the receptor phosphorylates several proximal substrates, translating the signal into an intracellular cascade responsible for the many cellular effects of insulin (reviewed in Saltiel and Kahn, 2001).

Most relevant to this study is the insulin-stimulated translocation of GLUT4 and insulin-regulation of PKA. The lipid kinase phosphatidylinositol 3-kinase (PI3K) has been implicated in both these signalling pathways (Saltiel and Kahn, 2001; Bryant et al. 2002; Conti, 2000; Carmen et al. 2005) (Figure 3.0). The insulin-regulated PI3K pathway is initiated by tyrosine phosphorylation of members of the insulin-receptor-substrate (IRS) family, which recruit PI3K to the PM. IRS-1 and IRS-2 are the most important insulin-receptor substrates in muscle and fat cells (Saltiel and Kahn, 2001).

There is considerable evidence to suggest that the Class 1a PI3K may be required for insulin-stimulated GLUT4 translocation, although other isoforms may potentially be involved (Bryant et al., 2002; Saltiel and Kahn, 2001; Tengholm and Meyer, 2002). PI3K exerts its effects on GLUT4 translocation through activation of the serine/threonine kinase Akt/PKB and the atypical protein kinase C (PKC) isoform PKC ζ , both of which have been directly implicated in the process (Bryant et al., 2002; Saltiel and Kahn, 2001). The mechanism by which PKC ζ is activated is currently unknown, however, its presence on intracellular GLUT4-containing vesicles suggests this may involve its recruitment to intracellular membranes. PKB is activated by binding to phosphoinositides, generated by PI3K, in the inner leaflet of the PM, bringing it into close apposition with its upstream regulatory kinase phosphatidylinositol-dependent kinase-1 (PDK-1).

Insulin regulation of PKA activity also utilises a PI3K signalling cascade to activate phosphodiesterases (PDEs) which impinge upon the cyclic nucleotide-regulated pathway (reviewed in Conti, 2000; Carmen et. al. 2005). PDEs are enzymes which inactivate cAMP by hydrolysis to 5'-ATP, therefore, insulin exerts a negative regulatory effect on PKA activity. Activation of PI3K by insulin is associated with an increase in PDE3 activity in adipocytes (Rahn et. al., 1994) and it has been shown that PDE3 is directly phosphorylated by PKB (Wijkander et. al., 1998). However, recently it was suggested that an additional mechanism of PDE3 activation by insulin might directly involve phosphorylation of PDE3B by the PI3K associated with the insulin receptor (Rondinone et. al., 2000).

This pathway is utilized in adipocytes to mediate the insulin-stimulated inhibition of lipolysis (Conti et. al., 2000). The hydrolysis of triglycerides stored in adipocytes is catalysed by PKA phosphorylation of hormone-sensitive lipase (HSL). Insulin-stimulation results in phosphorylation and activation of PDE3B, decreasing cAMP levels. The subsequent inactivation of PKA and dephosphorylation of HSL leads to inhibition of lipolysis.

It could be envisaged that regulation of PKA activity by insulin in this manner may also contribute to the dephosphorylation of STX16 following insulin stimulation observed in 3T3-L1 adipocytes (Section 3.1.1.4) (Pecera et. al., 2003), particularly in light of the fact that the yeast homolog of STX16, Tlg2p, was shown to be phosphorylated by PKA (Section 3.1.1.3) (Gurunathan et al., 2002). This scenario is depicted in Figure 3.0.

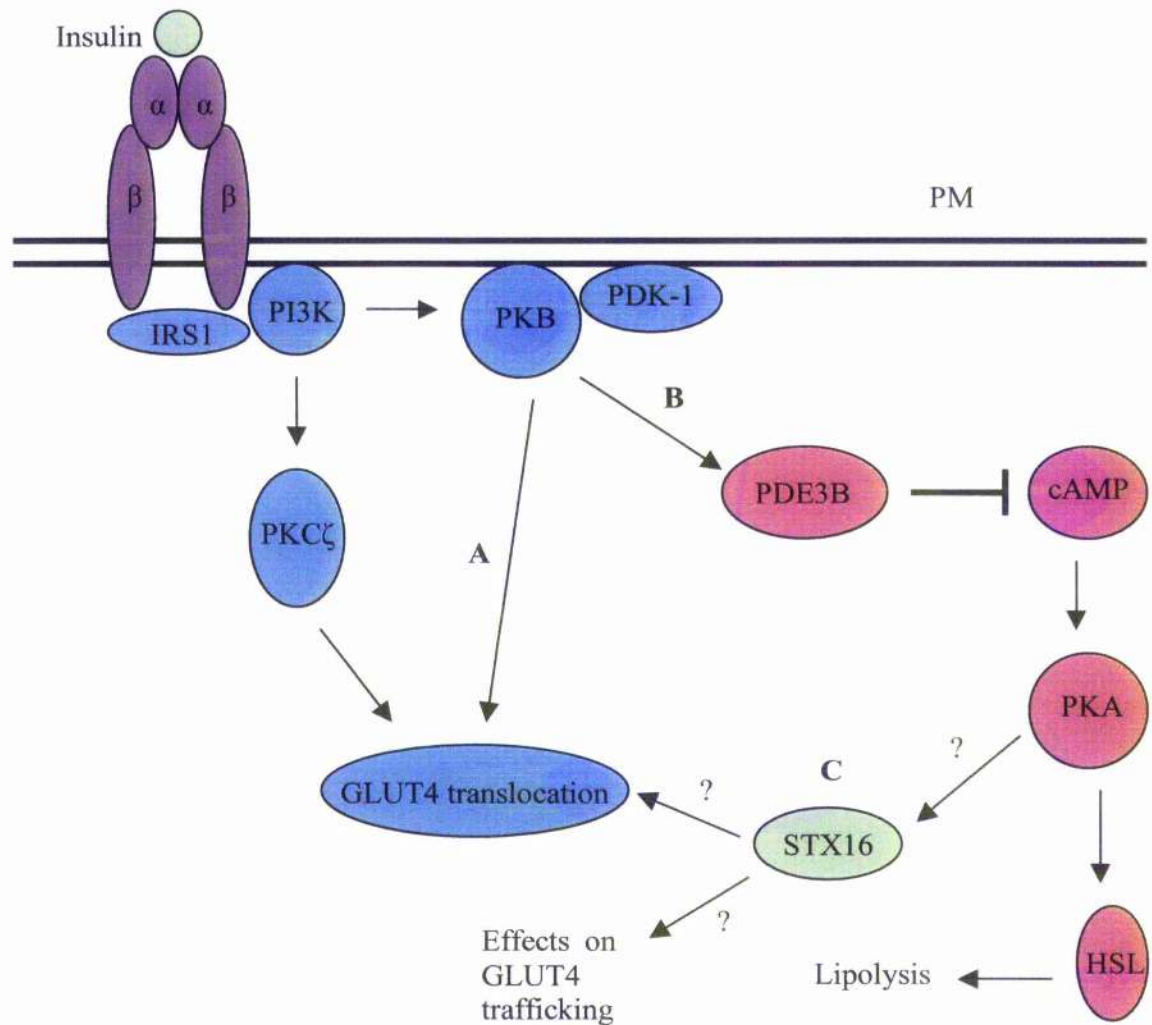


Figure 3.0 Insulin regulation of GLUT4 translocation and PKA activity in adipocytes (adapted from Bryant et. al., 2002 and Conti, 2000)

Binding of insulin to the α -subunits of the insulin receptor results in a conformational change in the receptor and subsequent activation of its tyrosine-kinase domain, located within the intracellular portion of its β -subunits. Phosphorylation of IRS-1 activates the PI3K pathway, which has been implicated both in GLUT4 translocation and PKA regulation. PI3K generates phosphoinositides in the PM, which act as a docking site for PKB via its pleckstrin homology domain, bringing it into close apposition to its upstream activator PDK-1.

A) PKB has been implicated in insulin-stimulated GLUT4 translocation, along with PKC ζ , which may be recruited to intracellular GLUT4 containing membranes.

B) PKB phosphorylation of PDE3B activates the enzyme to hydrolyse cAMP, thus acting as a negative regulator of PKA activity. In adipocytes, this results in inhibition of HSL phosphorylation and subsequent lipolysis.

C) The dephosphorylation of STX16 observed in response to insulin could be due to deactivation of PKA. It is hypothesised that the phosphorylation status of STX16 could ultimately be involved in controlling the translocation and / or intracellular trafficking of GLUT4.

3.2. Hypothesis

After considering examples of SNARE complex assembly regulated by phosphorylation and / or associated SM proteins, I offer the following hypothesis for this Chapter: The phosphorylation status of STX16 (perhaps controlled by PKA, Section 3.1.2) regulates binding of mVps45, which in turn regulates SNARE complex assembly with its cognate SNAREs, perhaps including STX6. Figure 3.1 demonstrates this hypothesis. Ultimately, I hypothesise that this SNARE complex may be responsible for the regulated trafficking of GLUT4, however, this will be investigated further in Chapters 4 and 5.

3.3. Aims

This Chapter aimed to directly investigate the STX16-containing SNARE complex that may be involved in GLUT4 trafficking. The specific aims of this Chapter were:

1. To identify the site of insulin-regulated phosphorylation in STX16
2. To identify the members of the STX16 containing SNARE complex
3. To address whether the phosphorylation status of STX16 (regulated by insulin) regulates SNARE complex assembly and mVps45 binding

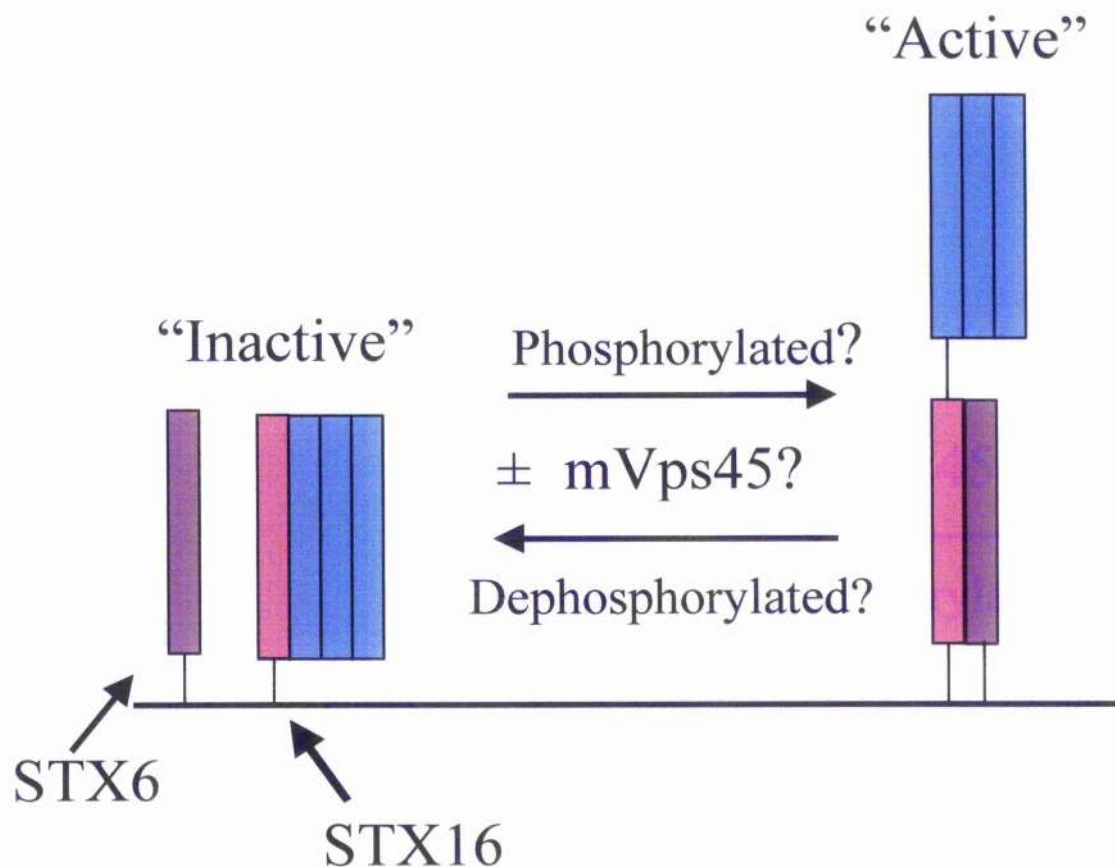


Figure 3.1 Model for the regulation of a SNARE complex involving STX16 and STX6 by phosphorylation (adapted from Gerst, 2003).

This model is based on current knowledge of SNARE complexes and also on my assumption that the phosphorylation status of STX16 determines its existence in an active or inactive conformation, depicted here as the so-called "open" and "closed" conformations. In the closed conformation, the N-terminal three-helix bundle or H_{abc} domain (blue) folds over and interacts with the SNARE or H3 domain (pink), whereas in the open conformation, the SNARE motif is exposed. When in the inactive conformation, STX16 is unable to bind to the SNARE domain of its partner t-SNARE, SNAP-25 homolog, STX6 (purple). At present, it is not known if this inactive conformation is rendered by the action of the kinase or the corresponding phosphatase. Based on the corresponding system at the mammalian synapse (Section 1.5.2), I speculate that mVps45 binding to this inactive conformation would be permitted. Then in response to a change in the phosphorylation status of STX16, mVps45 may facilitate the transition of STX16 to the active conformation and permit binding to STX6 and other members of the SNARE complex.

Pink: STX16 SNARE domain
 Blue: STX16 H_{abc} domain
 Purple: STX6 SNARE domain

3.4. Methods

3.4.1. *PhosphoProtein Purification Kit*

Phosphorylated proteins were purified from HEK 293 cell lysates as described in the *PhosphoProtein Purification Handbook* (Qiagen) and summarised briefly here.

Approximately 10^7 cells were required for each condition. This was estimated to be approximately equal to three confluent 10 cm^2 dishes of cells. HEK 293 cells were trypsinised as in Section 2.3.2, and an equal amount was plated into each of nine 10 cm^2 dishes 24 hours prior to transfection. The cells were plated so as to be approximately 50 % confluent and therefore to reach a confluence of 90 – 100 % 72 h later on the day of the experiment. The cells were transfected using the calcium phosphate method (Section 2.3.6.3). 48 h later, the cells were harvested. HEK 293 cells are notoriously fragile and easily become detached from the dish. Therefore, to ensure that no cells were lost (resulting in uneven cell numbers), they were not subjected to washes directly in the dishes, as suggested in the protocol. Instead, the cells were scraped from the dish in the original culture medium, pelleted by centrifugation and washed twice in HES buffer (Section 2.1.7) with subsequent spins.

The harvested HEK 293 cells were gently lysed in the lysis buffer provided (PhosphoProtein Lysis Buffer, 0.25 % (w/v) CHAPS, protease inhibitors, Benzonase). The lysate was cleared by centrifugation before the protein concentration was determined by Bradford Assay (Section 2.4.7) and adjusted to 0.1 mg/ml (to ensure that all phosphate groups were accessible during purification). The lysate was then loaded onto the PhosphoProtein Purification Column, pre-equilibrated with lysis buffer (PhosphoProtein Lysis Buffer, 0.25 % (w/v) CHAPS, protease inhibitors, Benzonase) and the flow-through fraction containing the non-phosphorylated proteins was collected. After a wash step to remove any unphosphorylated proteins, the proteins containing phosphate groups were eluted in the buffer provided (PhosphoProtein Elution Buffer, 0.25 % CHAPS) in four 500 μl fractions. The protein concentrations of the fractions were determined and those with the highest concentration (fractions 3 and 4 in each case) were pooled and concentrated to a volume of 50 μl using the Nanosep Ultrafiltration columns provided.

3.4.2. Immunoprecipitation of STX6 from 3T3-L1 adipocytes +/- insulin +/- NEM

3.4.2.1. Cell treatment and preparation of lysates

3T3-L1 fibroblasts were cultured as in Section 2.3.4.1. The cells (between P3 and P10) were trypsinised as in Section 2.3.2, plated out into 12-well plates and grown to confluence at which time they were differentiated into adipocytes as in Section 2.3.4.2. On day 8 post differentiation, 3T3-L1 adipocytes were incubated in 1 ml serum-free DMEM per well for 2 hours prior to the experiment. Four plates were assayed in the following way: 1) Basal, 2) Basal + NEM, 3) Insulin, 4) Insulin + NEM. 100 μ l 50 mM NEM was added to the appropriate wells (final concentration 5 mM) for 15 min and incubated at 37 °C and 5 % CO₂, after which time 1 μ M insulin was added to the appropriate wells for a further 15 min with incubation at 37 °C. The cells were then washed rapidly into ice-cold Wash Buffer (Section 2.1.7) by three additions with subsequent aspiration of 1 ml Wash Buffer. Solubilisation was achieved by adding 1 ml Lysis Buffer (Section 2.1.7) \pm 5 mM NEM as appropriate between three wells (~ 330 μ l / well). The cells from each set of three wells were then scraped with a cell scraper and transferred into a clean eppendorf. The lysates were incubated on ice for 30 min before centrifugation in a bench top centrifuge for 20 min at 14,000 rpm and 4 °C. The supernatants (the soluble lysates) were then transferred to clean cryo-vials and stored at - 80 °C until required for immunoprecipitation.

3.5. Results

3.5.1. Identification of phosphorylation site in STX16

3.5.1.1. Overview

It was reasoned that identification of the site of insulin-regulated phosphorylation in STX16 would be the first step towards elucidation of its function in 3T3-L1 adipocytes. Although this study will ultimately be carried out in 3T3-L1 adipocytes, the initial studies described in this Chapter were carried out in HeLa or HEK 293 cells, since 3T3-L1 adipocytes are notoriously difficult to transfect using standard techniques (Gnudi et al., 1997).

As mentioned previously, STX16 has been shown to exist in various spliced forms: STX16A, B, C, D and H (Figure 1.8, Chapter 1) (Dulubova et al., 2002; Simonsen et al., 1998; Tang et al., 1998a). This phosphorylation study involved the cloning and mutagenesis of STX16A, a full-length splice variant (Section 1.6, Figure 1.8), however, for simplicity, it will be referred to here as STX16.

The study began by analysing the STX16 sequence *in silico* to pinpoint candidate sites of phosphorylation. Mutants were then generated bearing alanine substitutions at these potential sites and tested for phosphorylation using the PhosphoProtein Purification Kit (Section 3.5.1.8) and ^{32}P analysis (Section 3.5.1.9).

3.5.1.2. *in silico* analysis of possible phosphorylation sites

It was decided to base the *in silico* investigation on Tlg2p, the yeast homolog of STX16. The first step was, therefore, to generate a sequence alignment of STX16 with Tlg2p (Figure 3.2) using ClustalW (<http://www.ebi.ac.uk/clustalw/>). Tlg2p sequence was obtained from NCBI (Accession number NP_014624). The nucleotide sequence of STX16A published by Simonsen *et. al.* (Simonsen et al., 1998) and submitted to the GenBank (Accession number AF008935), did not match the sequence of the cDNA used in this study (kindly provided by H. Stenmark, The Norwegian Radium Hospital, Montebello, Oslo/Norway). The sequences were identical except for five point-mutations (base number, cDNA base - published base; 233, C-T; 474, A-G; 615, G-C; 663, G-T; 758, T-C) and a

frame shift error caused by an "extra" G at base 360 in the cDNA. Therefore the STX16 sequence presented in this thesis (Figure 3.2) was obtained by the direct sequencing of the STX16A cDNA used in my study (verified by multiple sequencing runs on both strands at MWG-Biotech). As mentioned previously, Tlg2p has a putative PKA site at serine residue 90 (Gurunathan et al., 2002); however, sequence alignment of Tlg2p with STX16 did not reveal high homology in this region (Figure 3.2).

Therefore NetPhos 2.0 (<http://www.cbs.dtu.dk/services/NetPhos/>) was utilised to analyse the STX16 protein sequence for potential phosphorylation sites (Figure 3.3). At first it was hypothesised that STX16 would be phosphorylated on a serine residue, evolutionarily conserved from Tlg2p. The search implicated S94 and S95 as the most likely candidates of the serine residues with output scores of 0.996 and 0.998 respectively (on a scale of 0.000 to 1.000). These sites were favoured over other high scoring serine residues (S80, S131 and S224) because they were closest in sequence to the S90 phosphorylation site in Tlg2p. However, careful analysis of the threonine residues generated revealed another strong candidate - T90. Although the probability (0.601) was not as high as for the serine residues chosen (S94 and S95) or some of the other threonine residues implicated (T3, T105, T178, T197), it corresponded well with the site in Tlg2p and occurred within the predicted H_{abc} domain. T90 was therefore included in the list of residues to be investigated further. Residues of interest were then examined using the Scansite (Obenauer et al., 2003) (<http://scansite.mit.edu>) program Motif Scan (http://scansite.mit.edu/motifscan_seq.phtml) which searches for motifs within proteins that are likely to be phosphorylated by specific protein kinases (Figure 3.4). The analysis focused mainly on identifying potential PKA sites within the STX16 sequence, as, in addition to Tlg2p being phosphorylated by PKA (Gurunathan et al., 2002), it was envisaged that insulin regulation of PKA could be responsible for the dephosphorylation of STX16 (Section 3.1.2) observed upon insulin-stimulation (Perera et al., 2003). Only two potential PKA phosphorylation sites were identified, S17 and intriguingly, T90, adding further weight to the argument in support of this residue. S17 was not considered further at this stage as its output score in the previous search (0.026) was below the threshold of 0.500 (Figure 3.3). This program linked S94 and S95 with Casein Kinase II.

```

STX16      MATRRLTDAFLLLRNNSIQNRQLLA--EQLADDR---MALVSGISLDPEAAIGVTKRP-- 53
Tlg2p      -MFRDRTNLFLSYRRTFPHNITFSSGKAPLGDDQDIEMGTYPMMNMSHDISARLTDERKN 59
          *  * : * * * . . : * : : * . * : : . : : : * . .

STX16      -----PPKWVDGVDEIQYDVGRKIQKMKESASLHDKHLNRP●●●TLDDSS●●●EEHAIETI104
Tlg2p      KHENHSDALPPIFIDIAQVDVDDYLLLEVRRLSEQLAKVYRKNS-LPGFEDKSHDEALIEDL118
          * * : * * . . : : : : * : : * : * : * : * . * . * *

STX16      TQBEITQLFHRRCRAVQPCRAGP-----GPAPSRGGCLGT--WCLVAQALQELSTSFRH156
Tlg2p      SFKVIQMLQKCYAVMKRLKTIYNSQFVDGKQLSREELIILDNLQKIYAEKIQTESNKFRV178
          : : : * : : * : : : : : : * * : : : : : * : * : * * . * . *

STX16      AQSGLYLRMKNRER--SQHFFDTSVPLMDDGDD-----NTLYHRGFTE●●●DQLV202
Tlg2p      LQNNYLKFLNKDDLKPIRNKASAENTLLLDDEEEEAAREKREGLDIEDYSKRTLQRQQQL238
          * . * * * : : : : : : : . . * : * * : : : : : * : : : * :

STX16      LVEQNTLMVEEREREIRQMVQSISDLNEIFRDLGAMIVEQGTVLDRIDYNVEQSCIKTED262
Tlg2p      HDTSAEAYLREERDEEITQLARGVLEVSTIFREMQLVVDQGTIVDRIDYNLENTVVELKS298
          . : * * : * * * : : : : : : : * * : : * : * * : * * : * : : :

STX16      GLKQLHKAEQYQKKNRKMVLVILILFVIIIVLIVVLVGVKSR-----303
Tlg2p      ADKELNKATHYQKRTQKCVILLLTLCVIALFFFVMLKPHGGGSGGRNNGSNKYNNDDNK358
          . * : * * * : * * : * * * * : : * . * . . . :

STX16      -----
Tlg2p      TVNNSHDDGSNTHINDEESNLPSIVEVTESENDALDDLL 397
    
```

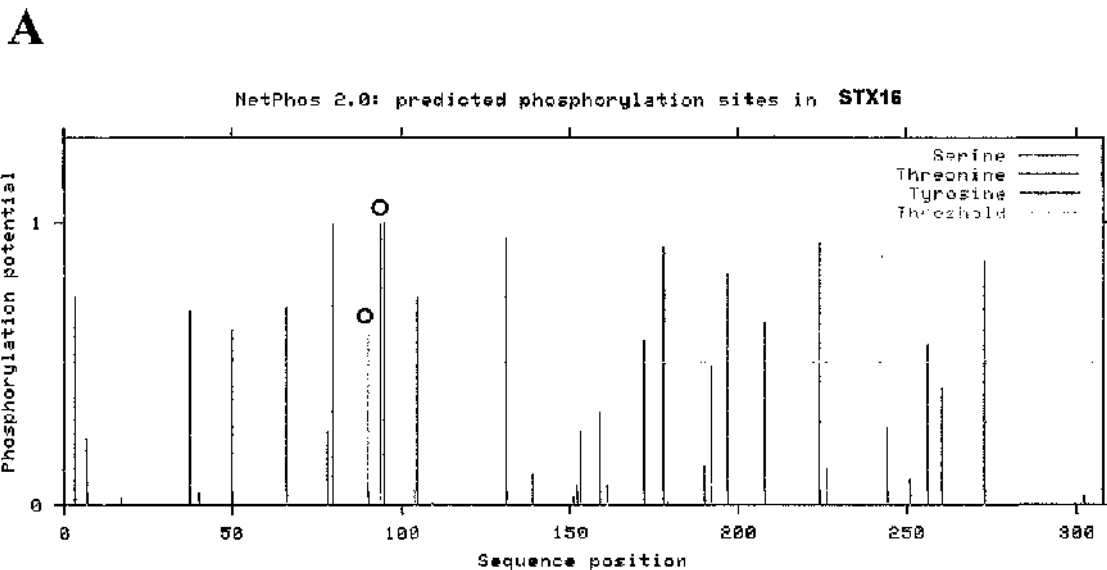
AVFPMILW	RED	Small (small+ hydrophobic (incl.aromatic -Y))
DE	BLUE	Acidic
RHK	MAGENTA	Basic
STYHCNGQ	GREEN	Hydroxyl + Amine + Basic - Q
Others	Gray	

Figure 3.2 Sequence alignment of STX16 with Tlg2p

Sequence alignment of STX16A and yeast Tlg2p, generated using ClustalW. Identical residues are indicated by an asterisk, conserved residues by double dots and semi-conserved residues by a single dot. The STX16 sites tested for phosphorylation in this study (T90, S94 and S95) are denoted by red dots while a red star highlights the Tlg2p PKA site (S90) (Gurunathan et al., 2002). The transmembrane domains of both proteins, consisting of mostly small hydrophobic residues, are highlighted with a red arrow. The Tlg2p extracellular domain can be observed at the C- terminus.

Figure 3.3 Analysis of STX16 sequence for potential phosphorylation sites

NetPhos 2.0 was utilized to analyse the STX16 sequence for potential phosphorylation sites. **A)** Graph illustrating the predictions in B. The potential sites chosen (T90, S94 and S95) and their output scores are denoted by red dots. **B)** Output format: Column 1: sequence name, Column 2: position of residue being analysed, Column 3: sequence context (shown as a 9- residue sequence centred on the residue being analysed), Column 4: output score (value in the range [0.000-1.000]), Column 5: assignment (scores above the threshold of 0.500 are assigned as “*S*”, “*T*” or “*Y*”). A red star indicates sites of interest chosen for this study. S94 and S95 were chosen, as they were the most likely serine residues with the highest output scores. T90 was chosen because it correlated well with the '1g2p phosphorylation site. Although its output score is lower than the serine residues chosen, it is, nonetheless, above the threshold of 0.500.



B**NetPhos 2.0 Server - prediction results**

Technical University of Denmark

Serine predictions

Name	Pos	Context	Score	Pred
		v		
STX16	17	LRNNSIQNR	0.026	.
STX16	37	MAIVSGISL	0.685	*S*
STX16	40	VSGISLDPE	0.041	.
STX16	78	KMKESASLH	0.260	.
STX16	80	KESASLHDK	0.992	*S*
STX16	94	TLDDSSEEE	0.996	*S* ☆
STX16	95	LDDSSEEEH	0.998	*S* ☆
STX16	131	GPAPSRGG	0.945	*S*
STX16	151	LQELSTSER	0.031	.
STX16	153	ELSTSEFRHA	0.260	.
STX16	159	RHAQSGYLK	0.328	.
STX16	172	REERSQHFF	0.581	*S*
STX16	179	FFDTSVPLM	0.006	.
STX16	224	QMVQSISDL	0.928	*S*
STX16	226	VQSISDLNE	0.130	.
STX16	256	NVEQSCIKT	0.562	*S*
STX16	302	VGVKSR---	0.032	.
		^		

Threonine predictions

Name	Pos	Context	Score	Pred
		v		
STX16	3	--MATRRLT	0.737	*T*
STX16	7	TRRLTDAFL	0.236	.
STX16	50	AIGVTKRPP	0.621	*T*
STX16	90	LNRPTLDDS	0.601	*T* ☆
STX16	104	AIEITTQEI	0.052	.
STX16	105	IEITTQEIT	0.734	*T*
STX16	109	TQEITQLFH	0.005	.
STX16	139	GCLGTWCIV	0.108	.
STX16	152	QELSTSEFRH	0.070	.
STX16	178	HFFDTSVPL	0.915	*T*
STX16	190	GQENTLYHR	0.137	.
STX16	197	HRGFTEDQL	0.813	*T*
STX16	208	VEQNTLMVE	0.646	*T*
STX16	244	VEQGTVLDR	0.271	.
STX16	260	SCIKTEDGL	0.408	.
		^		

Tyrosine predictions

Name	Pos	Context	Score	Pred
		v		
STX16	66	DEIQYDVGR	0.701	*Y*
STX16	161	AQSGYLKRM	0.073	.
STX16	192	DNTLYHRGF	0.490	.
STX16	251	DRIDYNVEQ	0.093	.
STX16	273	KAEQYQKKN	0.863	*Y*
		^		

Figure 3.4 STX16 sequence analysed for consensus motifs pertaining to a particular kinase

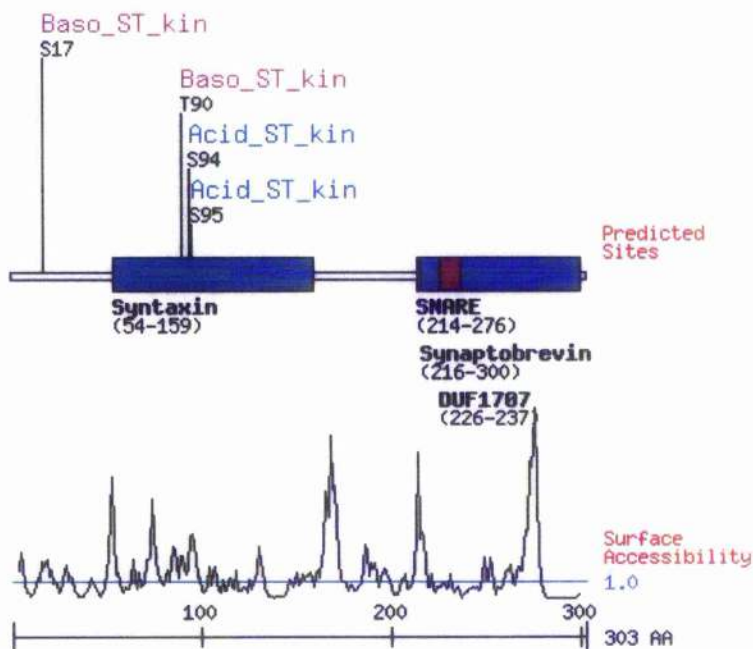
Generated using the Scansite Motif Scan option. Scansite was used to identify short protein sequence motifs that could be phosphorylated by protein Serine / Threonine or Tyrosine kinases. STX16 sequence was analysed for potential phosphorylation sites with low stringency. The analysis focused on identifying potential PKA sites, as well as assigning possible kinases to the previously identified residues of interest. **A)** A search for potential PKA sites revealed two candidates, T90 and S17. A further search suggested S94 and S95 could be phosphorylated by Casein Kinase II. Residues T90, S94 and S95 are indicated by red stars. **B)** Graphical representation of sites in (A) indicating that the sites of interest fall in the syntaxin homology region (the H_{abc} domain).

Scores in Scansite start at 0.000 if the sequence optimally matches the given motif, and the scores increase for sequences as they diverge from the optimal match (<http://scansite.mit.edu>). The score histograms and the percentile are the main ways to tell how good a score is for a given motif. It is considered to be quite good if the site ranks in the best 0.2% of all sites (<http://scansite.mit.edu>). For the Motif Scan program, the percentile is calculated from a reference database search, which is the vertebrate section of the Swiss-Prot database.

A

Basophilic serine/threonine kinase group (Baso_ST_kin)					
Protein Kinase A			Gene Card PRKACG		
Site	Score	Percentile	Sequence	SA	
S17	0.5791	2.913 %	FLLLRNNSIQNRQLL	1.736	
Protein Kinase A			Gene Card PRKACG		
Site	Score	Percentile	Sequence	SA	
★ T90	0.5524	2.079 %	DKHLNRPTLDDSSEE	2.304	
Acidophilic serine/threonine kinase group (Acid_ST_kin)					
Casein Kinase 2			Gene Card CSNK2B		
Site	Score	Percentile	Sequence	SA	
★ S95	0.4079	0.187 %	RPTLDDSSEEEHAIE	3.570	
Casein Kinase 2			Gene Card CSNK2B		
Site	Score	Percentile	Sequence	SA	
★ S94	0.4546	0.401 %	NRPTLDDSSEEEHAI	3.442	

B



3.5.1.3. Construction of STX16 pCR3.1

STX16A cDNA was cloned into the mammalian expression vector pCR3.1 (see Appendix) for subsequent transfection into mammalian cells. The phosphorylation mutants were then generated in this construct.

STX16A cDNA was PCR amplified using the conditions and cycling parameters described in Section 2.2.1. The template DNA was used at a concentration of 0.5 mg/ml. Primers were designed to amplify the entire STX16A open reading frame (915 bp) including the N-terminal myc-tag (63 bp), and restriction sites compatible with pCR3.1 (*KpnI* at the N-terminus and *XbaI* at the C-terminus). The primers were as follows (restriction sites underlined; start and stop codons in bold):

Fwd: 5'-CCGGTACCATGGCCCATATGGAAC-3'

Rev: 5'-CCTCTAGATTA'CGAGACTTCAC-3'

The resulting PCR product was gel purified as described in Sections 2.2.3 and 2.2.4 (Figure 3.5A). Digestion of the PCR fragment (Figure 3.5B) and pCR3.1 (not shown) with *KpnI* and *XbaI* (Section 2.2.7) preceded the ligation of myc-tagged STX16 into pCR3.1 as described in Section 2.2.8. Ligated product was transformed into TOP-10 cells and colonies were selected in the presence of Kanamycin (Section 2.2.9). Plasmid DNA was isolated as described in Section 2.2.11 and successful transformants were identified by restriction digest (Section 2.2.7) with *KpnI* and *XbaI* (Figure 3.5C). Plasmids found to contain the insert were ethanol precipitated (Section 2.2.15) and fully sequenced on both strands (Section 2.2.16) to confirm the veracity of the PCR experiment.

3.5.1.4. Transfection of HeLa cells with STX16 pCR3.1

The STX16 pCR3.1 plasmid was first tested for expression in HeLa cells. Cells were transfected with STX16 pCR3.1 or empty pCR3.1 (negative control) when 50 % confluent using Lipofectamine 2000 (Section 2.3.5.2). Cells treated with Lipofectamine 2000 alone provided a further negative control. Lysates were prepared after 24 hours (Section 2.3.5.3) and expression of myc-tagged STX16 was examined by SDS-PAGE electrophoresis on a 12 % SDS gel (Section 2.4.3) followed by Western Blotting (Section 2.4.4) using

monoclonal anti-myc (Figure 3.6) antibody. The construct was found to successfully express myc-tagged STX16. As a STX16 specific antibody was not obtained until later in the study, the level of expressed protein was not compared to that of the endogenous protein.

3.5.1.5. Immunoprecipitation of myc-tagged STX16 expressed in HeLa cells

It was necessary to ensure that myc-tagged STX16 could be immunoprecipitated from HeLa cells. HeLa cells were transfected using Lipofectamine 2000 as above. 1 ml lysates were prepared (Section 2.3.5.3) and immunoprecipitations were carried out according to the protocol in Section 2.4.1.3 using 2 μ g monoclonal anti-myc antibody or random IgG as a control. Immunoprecipitates and post-immunoprecipitation supernatants were analysed by immunoblotting (Section 2.4.4) with polyclonal anti-myc (Figure 3.7) antibody. This experiment demonstrated that myc-tagged STX16, expressed in HeLa cells, could be immunoprecipitated by means of its functional myc-tag. The interaction with the myc antibody was specific as STX16 was not immunoprecipitated with a random IgG.

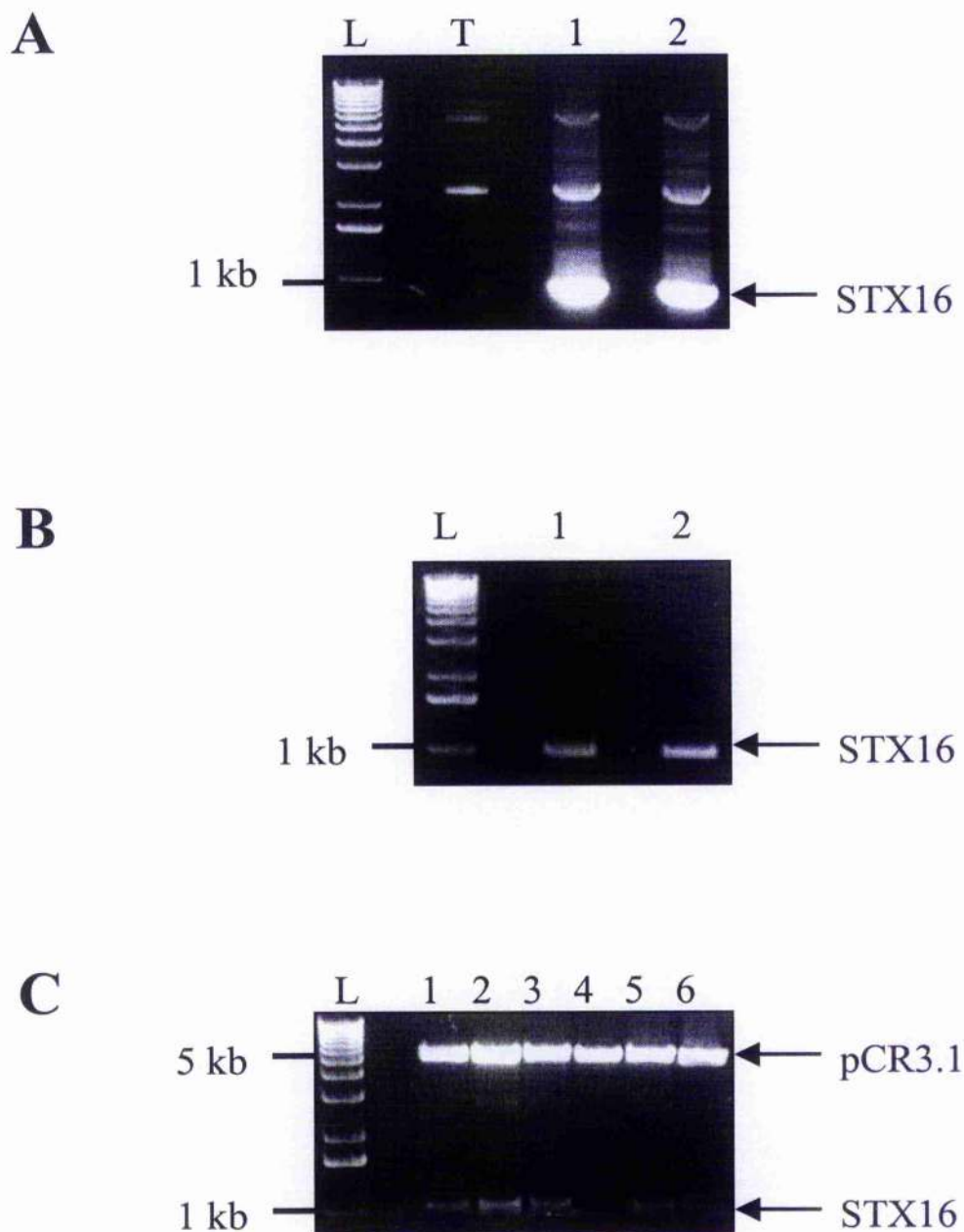


Figure 3.5 Construction of STX16 pCR3.1 plasmid

A) Uncut template DNA (T) used for PCR alongside the products of two independent PCRs (Lanes 1 and 2) resolved on a 1 % agarose gel. The template DNA present in each sample is of equal concentration. The strongly stained bands at ~ 1 kb correspond to STX16A cDNA. **B)** Restriction digests of the 1 kb bands in (A) with *KpnI* and *XbaI* (Lanes 1 and 2). pCR3.1 vector was also digested (not shown). **C)** Restriction digests with *KpnI* and *XbaI* of six potential ligation products (Lanes 1-6) following ligation of STX16 into pCR3.1. The bands at 5 kb can be attributed to pCR3.1; the insert, freed by the restriction digest, is observed in samples 1,2,3,5 and 6.

L: 1 kb DNA ladder. The 1 kb mark is indicated.

In (A) and (B) Lanes 1 and 2 contain the products of two independent PCRs.

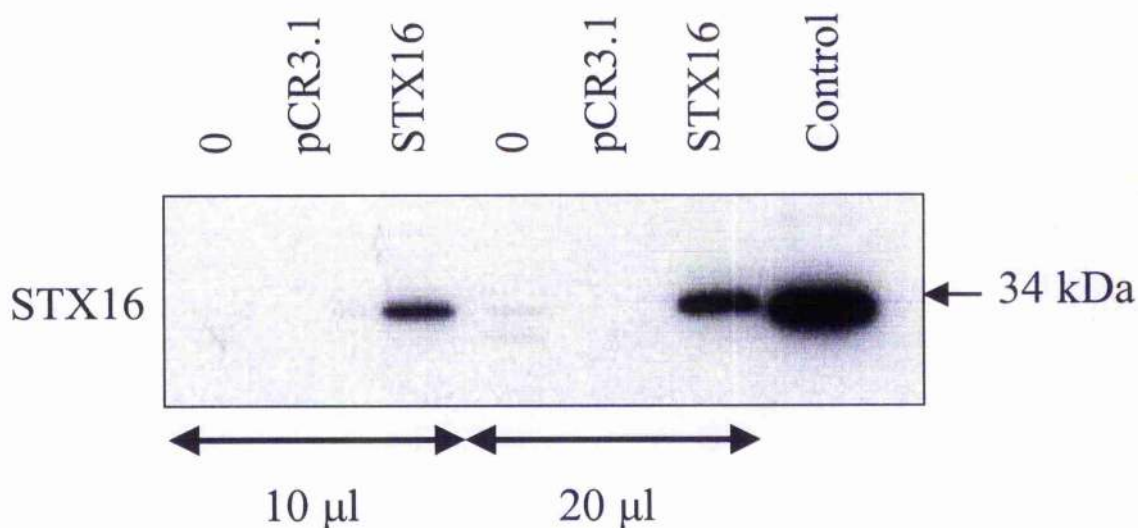


Figure 3.6 Western Blot of myc-tagged STX16 expressed in HeLa cells

Cells were transfected using Lipofectamine 2000 either in the absence of DNA (0), or in the presence of pCR3.1 (pCR3.1) or STX16 pCR3.1 (STX16) and lysates were prepared 24 h after transfection (Section 2.3.5.3). The lysates were separated by SDS-PAGE on a 12 % gel and immunoblotted with monoclonal anti-myc.

The first three lanes of the 12 % SDS-PAGE gel were loaded with 10 µl of the appropriate sample, followed by 20 µl of each in the remaining three wells. The lysate loaded in each well corresponds to 2 % of the total lysate obtained from one well of a 12-well plate.

Control: 36 kDa protein bearing a myc-tag and known to be successfully visualised by Western Blotting with anti-myc.

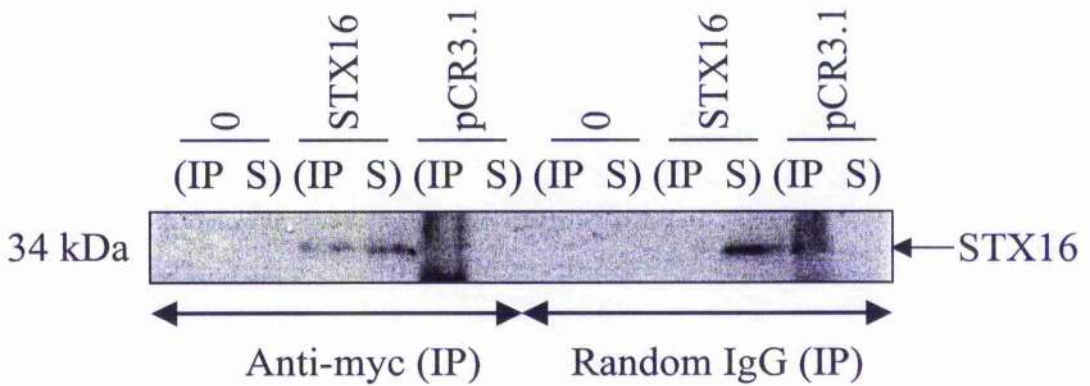


Figure 3.7 Immunoprecipitation of myc-tagged STX16 expressed in HeLa cells

Immunoprecipitation was carried out from HeLa cells, which had been transfected with STX16 pCR3.1 (STX16), empty pCR3.1 (pCR3.1) or treated with Lipofectamine 2000 alone (0), with 2 μ g monoclonal anti-myc or random IgG. The immunoprecipitates and post-immunoprecipitate supernatants were resolved on a 12 % SDS-PAGE gel, followed by immunoblotting with polyclonal anti-myc. Myc-tagged STX16 can be observed at 34 kDa as indicated and was partially immunoprecipitated using 2 μ g monoclonal anti-myc. The interaction with the myc antibody is specific as STX16 is not immunoprecipitated with a random IgG.

IP: immunoprecipitate

S: supernatant collected after immunoprecipitation

Fractions loaded: **IP**, 2/5 of total immunoprecipitate from 1 well of a 6-well plate;
S, 1/20 of the total S obtained from one well of a 6-well plate

The mutagenesis PCR was carried out as in Section 2.2.13. 5 μ l were then electrophoresed on a 1 % agarose gel (Section 2.2.3) to verify that the resulting plasmid was of the correct size (not shown), while 1 μ l of the product was transformed into TOP-10 cells and colonies were selected in the presence of Kanamycin (Section 2.2.9). The plasmid DNA was extracted from 20 individual colonies (Section 2.2.11), which were then screened for mutations by sequencing fully on both strands (Section 2.2.16). Stocks of plasmids found to contain the correct mutations were generated from the corresponding glycerol stocks (Section 2.2.17) by carrying out large-scale DNA preparations (Section 2.2.12). The resulting mutants will be referred to as T90 and S94&95.

3.5.1.7. Expression of STX16 and T90 in HEK 293 cells

Transfection of HEK 293 cells with Lipofectamine 2000 often caused them to become unhealthy; therefore the calcium phosphate method of transfection (Section 2.3.6.3) was utilized. The transfection efficiency was optimised by expressing GFP-tagged SNAP-25 and viewing the cells directly with an upright fluorescent microscope (results not shown). The optimum quantity of DNA was found to be 3.75 μ g per well of a 12 well plate to achieve 70 – 80 % transfection efficiency at these conditions. Cells were transfected with STX16 pCR3.1, T90 and empty pCR3.1 and lysates were analysed for expression by immunoblotting with either anti- STX16 or anti-myc antibodies. Figure 3.8 shows that the T90 mutant and STX16 were expressed at comparable levels. Both were expressed to a level exceeding that of endogenous STX16 in these cells.

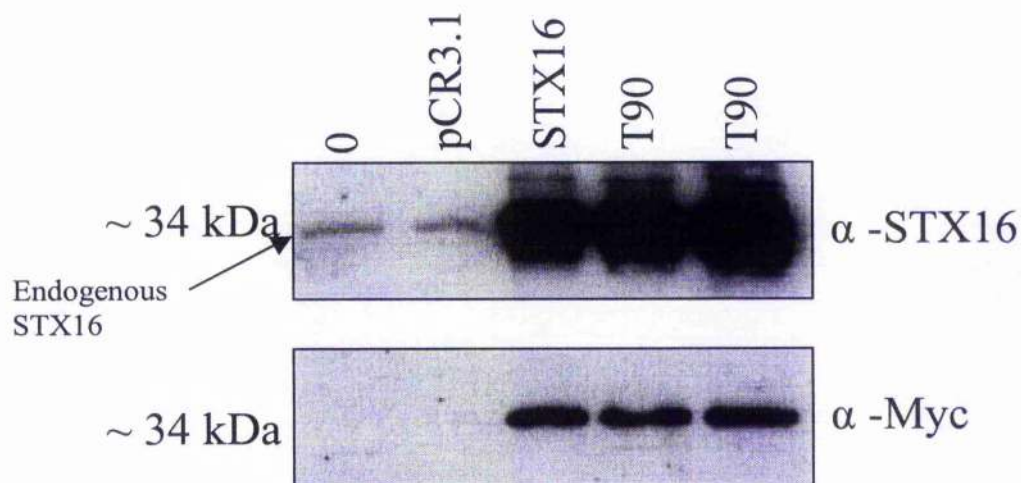


Figure 3.8 Expression of STX16 and STX16 T90 in HEK cells

The calcium phosphate method (Section 2.3.6.3) was utilised to express STX16 and T90 in HEK 293 cells. The expressed proteins could be observed by means of the N-terminal myc-tag by Western Blotting with anti-myc (lower panel) and by a STX16 specific antibody (upper panel). Endogenous STX16, myc-tagged STX16 and myc-tagged T90 are all recognised by the STX16 specific antibody, highlighting that the myc-tagged proteins are expressed to a level exceeding that of the endogenous protein.

The lysate on the gel corresponds to 2 % of the total lysate from cells in one well of a 12 well plate.

3.5.1.8. PhosphoProtein purification kit

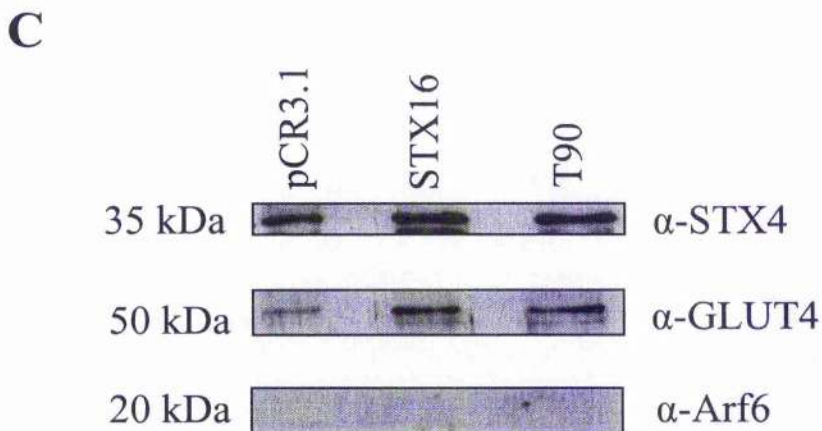
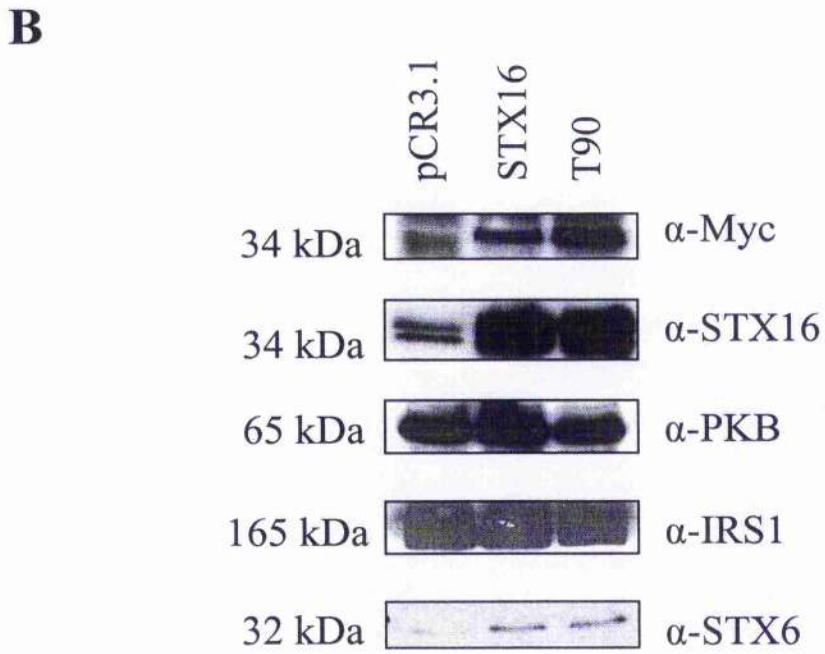
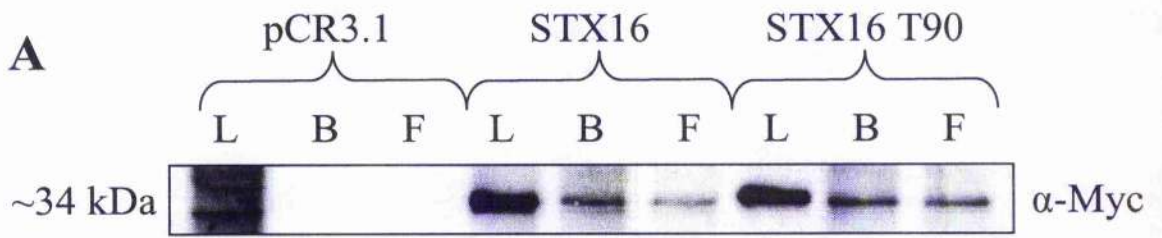
The PhosphoProtein Purification Kit (Qiagen) is designed to specifically purify phosphorylated proteins from complex cell lysates. Proteins that carry a phosphate group on any amino acid are bound with high specificity to a PhosphoProtein Purification Column, while proteins without phosphate groups do not bind to the column and can therefore be found in the column flow-through fraction. Phosphorylated proteins were purified from HEK 293 cell lysates as described in Section 3.4.1.

Samples were collected from the original cell lysates, from the lysates after concentration normalisation to 0.1 mg / ml prior to loading on the column, and the flow-through from the column (the non-phosphorylated proteins). The proteins were resolved by SDS-PAGE electrophoresis on a 12 % SDS gel (Section 2.4.3), followed by Western Blotting using anti-myc antibody (1:1000 dilution) (Figure 3.9A). Figure 3.9A highlights that a large fraction of the myc-tagged STX16 and T90 did not bind to the column, perhaps suggesting that this fraction of the total protein present was not phosphorylated or that the capacity of the column had been exceeded.

The concentrated eluants were analysed in the same way by Western Blotting with anti-STX16 and anti-myc antibodies (Figure 3.9B). Endogenous STX16, myc-tagged STX16 and STX16 T90 were all observed in the eluant, perhaps suggesting that a fraction of each was indeed phosphorylated and therefore that T90 is not the sole site of phosphorylation. The phosphorylated protein fractions were probed for IRS1, PKB and STX6, all of which were observed to one extent or another. IRS1 and PKB are both phosphorylated in response to insulin (Gual et al., 2005; Hill et al., 2001); therefore their presence in the eluant was expected. As mentioned previously, STX6 was not observed to be a phosphoprotein (Perera et al., 2003), however, its presence in the eluant may be due to binding to endogenous STX16, which is known to be a phosphoprotein. On the other hand, this may be evidence of non-specific binding to the column. The eluants were then probed for STX4, GLUT4, and Arf6 (Figure 3.9C). Previous work indicates that GLUT4 and STX4 are phosphorylated (Piper et al., 1993; Risinger and Bennett, 1999). All are observed except Arf6, which was not visible even after long exposure times. To date, no literature exists to implicate Arf6 as a phosphoprotein, however, it is not possible to be certain that this provides a reliable negative control and evidence that the binding is specific.

Figure 3.9 Fractions collected before and after the purification on the Phosphoprotein-binding column

Phosphorylated proteins were purified from the HEK 293 lysates using the PhosphoProtein Purification Kit and analysed by gel electrophoresis and Western Blotting. **A)** Original cell lysates (L), lysates after concentration normalisation to 0.1 mg / ml prior to loading on the column (B), and the flow-through from the column (the non-phosphorylated proteins) (F) were analysed with anti-myc antibody. This highlights that a large fraction of STX16 and T90 did not bind to the column. **B)** The eluants were analysed in the same way with anti-myc and anti-STX16. Endogenous STX16 can be observed in the pCR3.1 lane probed with anti-STX16. The lysates were also probed with anti-bodies to IRS1 and PKB, both of which are phosphorylated in response to insulin (Gual et al., 2005; Hill et al., 2001), and STX6, which was previously shown not to be phosphorylated (Perera et al., 2003). **C)** Further controls involved looking for the presence of STX4, GLUT4 and Afr6 by probing with the appropriate antibodies.



3.5.1.9. Analysis of STX16, T90 and S94&95 with ^{32}P

Given that the results obtained from the PhosphoProtein Purification Kit were inconclusive, it was decided to go on and examine the phosphorylation status of both mutants by ^{32}P analysis. This method was chosen allow the quantitative analysis of STX16 phosphorylation compared to that of the mutants, allowing for the possibility that STX16 is phosphorylated on more than one residue.

3.5.1.10. Expression of mutants

HEK 293 cells were transfected with STX16 pCR3.1, T90, S94&95 and empty pCR3.1 using the calcium phosphate method (Section 2.3.6.3). Figure 3.10A shows the expression levels prior to the experiment as visualised by Western Blotting with anti-myc antibody.

3.5.1.11. Analysis of mutants with ^{32}P

First it was ensured that the proteins could be immunoprecipitated by means of their N-terminal myc-tags (Figure 3.10B). Immunoprecipitation was carried out as in Section 2.4.1.3 using polyclonal anti-myc or random IgG, and the immunoprecipitates were compared by immunoblotting with monoclonal anti-myc antibody. 2 μg of polyclonal anti-myc immunoprecipitated more than 90 % of myc-tagged STX16 (not shown). The immunoprecipitation was selective as no immunoprecipitated material was observed in a cell-free control or cells transfected with empty vector.

3.5.1.12. Labelling with ^{32}Pi and immunoprecipitation

48 hours after transfection, the cells were washed and labelled using 250 μCi ^{32}Pi per well of a 6-well plate as described in Section 2.4.1.2. The cells were treated with or without 1 μM insulin for 30 min prior to the experiment. The immunoprecipitation was then carried out from labelled cells as in Section 2.4.1.3. The immunoprecipitated material from the ^{32}Pi labelled cells was subjected to electrophoresis on two separate 12 % SDS-PAGE gels. One gel was dried, and the phosphorylation status of the proteins examined by autoradiography while the other was transferred to nitrocellulose and analysed by Western Blotting with monoclonal anti-myc antibody. Figure 3.11A shows the autoradiograph. It is clear that no significant or specific phospho-bands are observed in these experiments.

Figure 3.11B shows the Western Blot analysis of the immunoprecipitates and indicates that although the proteins are not observed by autoradiography, the immunoprecipitations were carried out successfully. Therefore, it is likely that the proteins have not been labelled by the ^{32}P i. The conditions used for ^{32}P i labelling have previously been shown to be sufficient to equilibrate the ATP pool of 3T3-L1 adipocytes (G.Gould, unpublished observation) (Gibbs et al., 1986). This strongly suggests that STX16, T90 and S94&95 are not posttranslationally modified in HEK 293 cells.

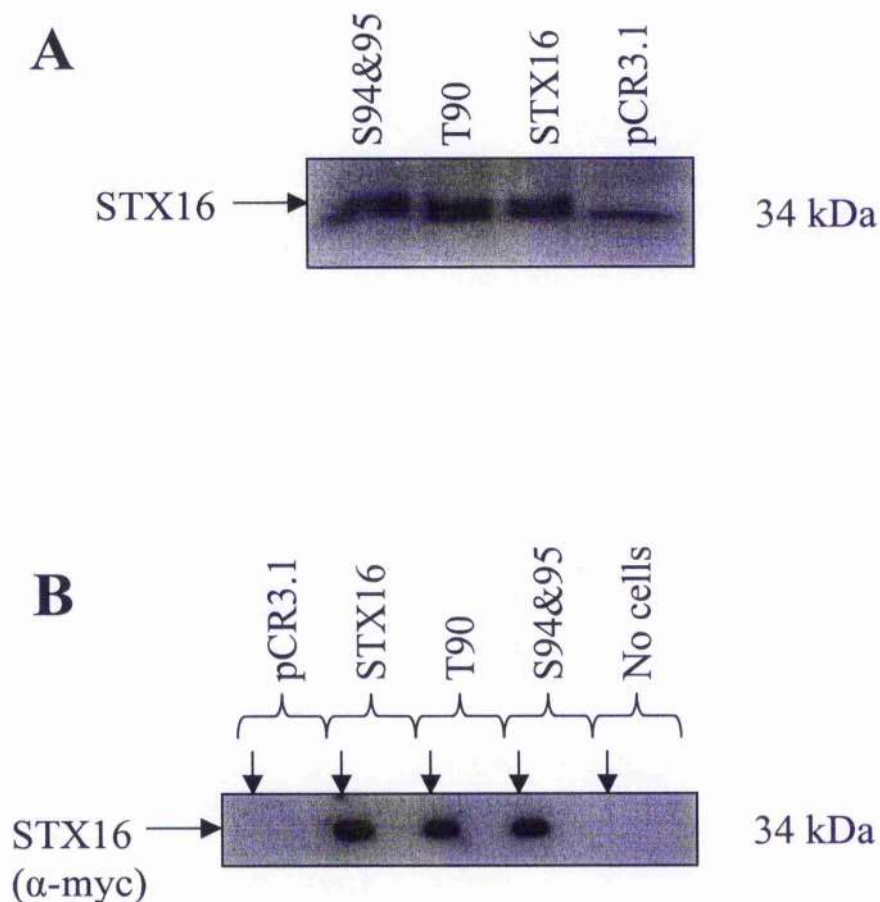


Figure 3.10 Expression and immunoprecipitation of myc-tagged STX16, T90 and S94&95 in HEK 293 cells

A) STX16, T90 and S94&95 were expressed in HEK 293 cells and visualised by Western Blotting with monoclonal anti- myc and compared to cells transfected with empty vector (pCR3.1). **B)** Immunoprecipitation of the proteins with polyclonal anti-myc (black arrow) or random IgG (no arrow). The myc-tagged proteins were immunoprecipitated successfully as shown by Western Blotting with monoclonal anti-myc. The immunoprecipitation was specific since the proteins were not immunoprecipitated with the random IgG and no immunoprecipitated bands were observed in cells transfected with pCR3.1 only (pCR3.1) or in a no cell control (no cells).

Fractions loaded: **A)** 1/20 of the total lysate from one well of a 6-well plate; **B)** 2/5 of the total immunoprecipitated material from one well of a 6-well plate

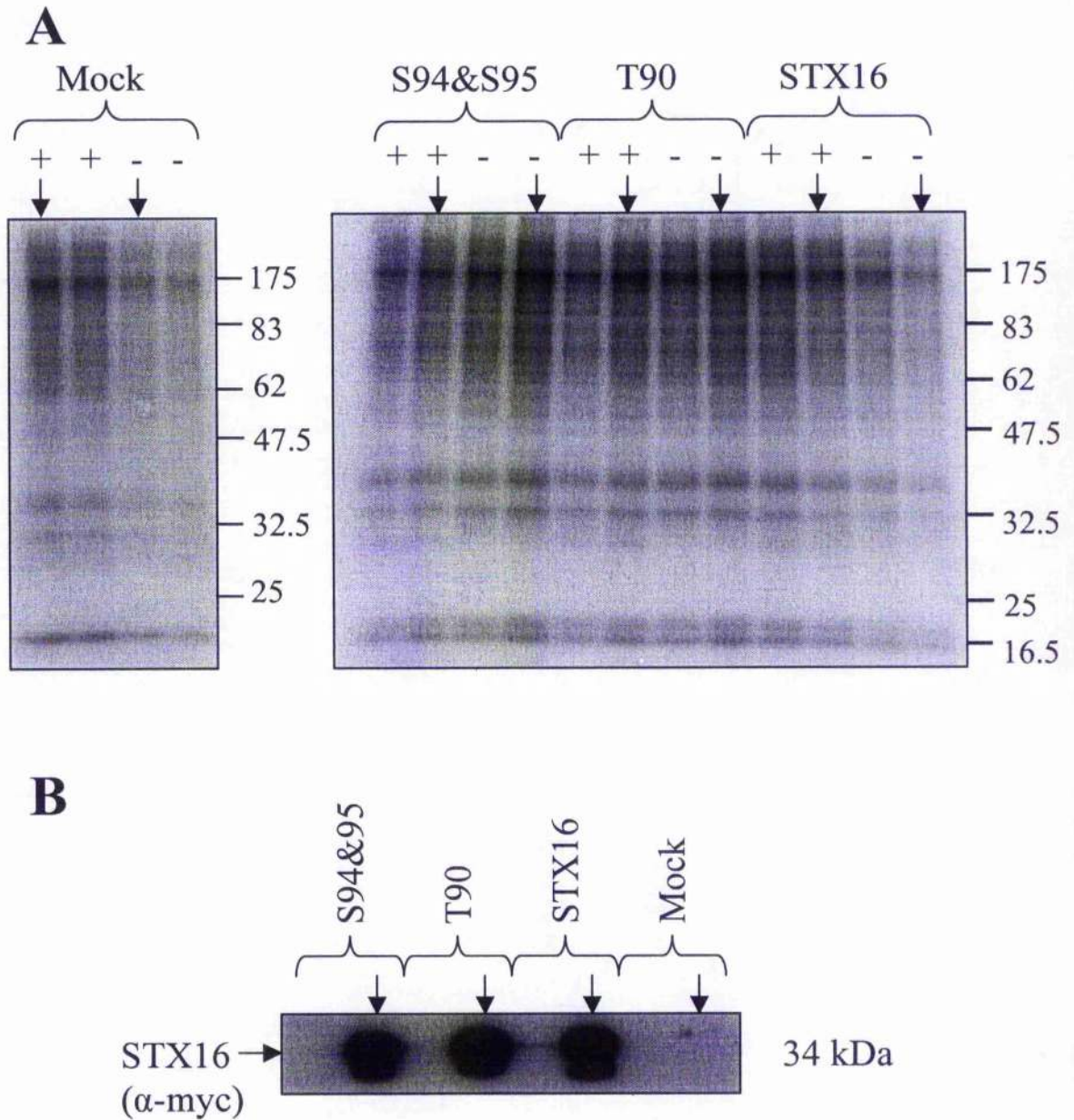


Figure 3.11 ^{32}P analysis of STX16 in HEK 293 cells

STX16, T90 and S94&95 were immunoprecipitated, using anti-myc (black arrow) or random IgG (no arrow), from ^{32}P -labelled HEK 293 cells treated acutely with (+) or without (-) 1 μM insulin for 30 min. **A**) The autoradiograph comparing the polyclonal anti-myc and IgG immunoprecipitates. STX16, T90 and S94&95 were not observed in anti-myc immunoprecipitates at ~ 34 kDa as anticipated. Molecular weight standards are shown. **B**) The corresponding immunoprecipitates from basal cells were analysed by Western Blotting with monoclonal anti-myc antibody. This demonstrates that although the proteins cannot be seen in the autoradiograph, it is not due to an unsuccessful immunoprecipitation but instead suggests that the proteins are not labelled with ^{32}P .

Fractions loaded: **A**) and **B**) 2/5 of the total immunoprecipitated material from one well of a 6-well plate.

3.5.2. Identification of STX16 SNARE binding partners in 3T3-L1 adipocytes

3.5.2.1. Overview

Immunoprecipitation studies were carried out in an effort to identify members of the insulin-regulated STX16-containing SNARE complex in 3T3-L1 adipocytes. Immunoprecipitations were carried out from 3T3-L1 adipocytes in the presence (STX16 is dephosphorylated) or absence (STX16 is phosphorylated) of insulin-stimulation. These studies attempted to address if binding to STX16 was altered by phosphorylation, and ultimately if the formation of a functional SNARE complex could be regulated by insulin.

The experiment was carried out both in the presence and absence of NEM (N-Ethyl-Maleimide), a reagent that prevents SNARE complex disassembly and therefore, favours the chances of pulling down intact complexes. Because a STX16 specific antibody was not obtained until later in the study, the immunoprecipitations were carried out using anti-STX6 and immunoprecipitates were probed for STX16 and other possible SNARE binding partners.

3.5.2.2. Immunoprecipitation of STX6 from 3T3-L1 adipocytes

3T3-L1 adipocytes were treated as described in Section 3.4.2, \pm 5 mM NEM and + 1 μ M insulin for 15 min. Lysates were prepared as in Section 2.3.4.3 and immunoprecipitation was carried out as in Section 2.4.1.1 using monoclonal anti-STX6 or random IgG per 500 μ l lysate. Immunoprecipitates and post- immunoprecipitation supernatants were resolved on a 12 % SDS-PAGE gel, and analysed by immunoblotting with polyclonal anti-STX6 (Figure 3.12). STX6 was immunoprecipitated both in the presence and absence of NEM and in both basal and insulin-stimulated cells. 2 μ g monoclonal anti-STX6 was found to be optimum for the immunoprecipitation, even although STX6 was not absorbed completely from the lysates. Using greater than 2 μ g antibody did not result in more STX6 in the immunoprecipitate and in fact was detrimental, resulting in strong signals from the heavy and light chains of the antibody in the Western Blot, which obscured the STX6

signal and the signals from its binding partners, when resolved by gel electrophoresis (not shown).

3.5.2.3. STX6 co-immunoprecipitates STX16

The first aim was to ensure that the STX6 immunoprecipitated from the lysates was in a complex with STX16. Figure 3.12 shows that STX16 does indeed co-immunoprecipitate with STX6. The interaction could be observed both in the presence and absence of insulin, suggesting perhaps that SNARE complex formation can occur in both basal and insulin-stimulated cells. Intact cells were treated with (Figure 3.12B) or without (Figure 3.12A) 5 mM NEM prior to lysis, to accumulate SNARE complexes. Comparison of Figure 3.12A and Figure 3.12B reveals that more STX16 was co-immunoprecipitated in the cells pre-treated with NEM (judged by the corresponding decrease in the amount of protein left in the post-immunoprecipitation supernatant). This is indicative that the complexes did not form after lysis (Galli et al., 1998).

3.5.2.4. STX6 co-immunoprecipitates Vti1a

The TGN-localised t-SNARE Vti1a forms a SNARE complex with both STX6 and STX16 in HeLa cells (Mallard et al., 2002). To check if this interaction is also viable in 3T3-L1 adipocytes, the immunoprecipitates were probed with antibodies to Vti1a. Figure 3.13A shows that Vti1a was co-immunoprecipitated with STX6, suggesting that it could indeed be the third member of a SNARE complex formed in adipocytes. As with STX16, the interaction was observed both in the presence and absence of insulin. In addition, preliminary data appeared to suggest that antibody to Vti1a also co-immunoprecipitates STX6 (not shown).

3.5.2.5. STX6 does not co-immunoprecipitate mVps45

As previous work has suggested that mVps45 interacts weakly with STX6 (Bock et al., 1997; Tellam et al., 1997), and directly with STX16 (Dulubova et al., 2002; Yamaguchi et al., 2002), the STX6 immunoprecipitates were probed for the presence of mVps45. Under my experimental conditions, mVps45 did not co-immunoprecipitate with STX6, either in the presence or absence of insulin, with all of the mVps45 remaining in the post-immunoprecipitation supernatant (Figure 3.13B). As well as suggesting that mVps45 does not bind to STX6 in 3T3-L1 adipocytes this result also suggests that no interaction occurs with STX16 (which is also present in the immunoprecipitate) when STX16 is part of the

STX6/STX16/Vti1a SNARE complex. However, it is highly plausible that the fraction of STX16 that remains in the post-immunoprecipitation supernatant (Figure 3.12) constitutes uncomplexed STX16 that may be bound to mVps45.

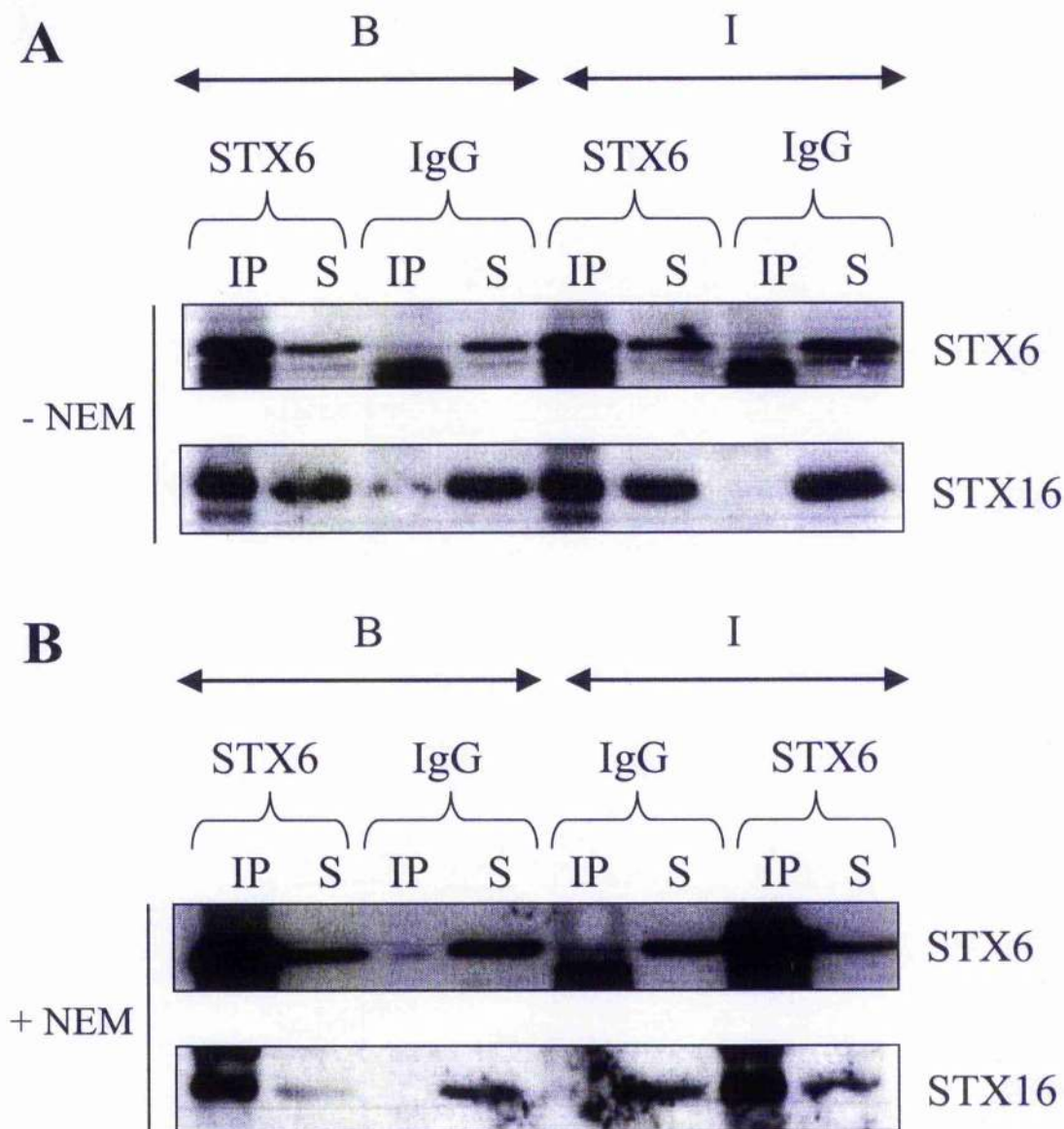


Figure 3.12 STX6 and STX16 co-immunoprecipitate in 3T3-L1 adipocytes

STX6 was immunoprecipitated from 3T3-L1 adipocytes, which, after serum starving for 2 h, had been treated with (I) or without (B) 1 μ M insulin for 15 min and with (+ NEM) or without (- NEM) 5 mM NEM as indicated on the left. Lysates were prepared and STX6 was immunoprecipitated using 2 μ g monoclonal anti-STX6. The immunoprecipitates and corresponding post-immunoprecipitate supernatants were resolved by electrophoresis, transferred to nitrocellulose and analysed by Western Blotting with polyclonal anti-STX6 and anti-STX16 as indicated on the right. **A)** The monoclonal STX6 antibody was capable of immunoprecipitating STX6 itself from the cell lysates. STX16 was co-immunoprecipitated to a similar extent in the presence or absence of insulin stimulation. The interaction with the STX6 antibody was specific as neither STX6 nor STX16 interact with a random IgG. **B)** STX6 was immunoprecipitated from cells treated with NEM prior to lysis. A larger proportion of STX16 was coimmunoprecipitated in this case (judged by the corresponding decrease in protein in the post-immunoprecipitation supernatant), indicating that the complexes did not form after lysis (Galli et al., 1998).

IP: immunoprecipitate

S: supernatant collected after immunoprecipitation

Fractions loaded: IP, 2/5 of total immunoprecipitate from 1 well of a 12-well plate; S, 1/20 of the total supernatant obtained from one well of a 12-well plate

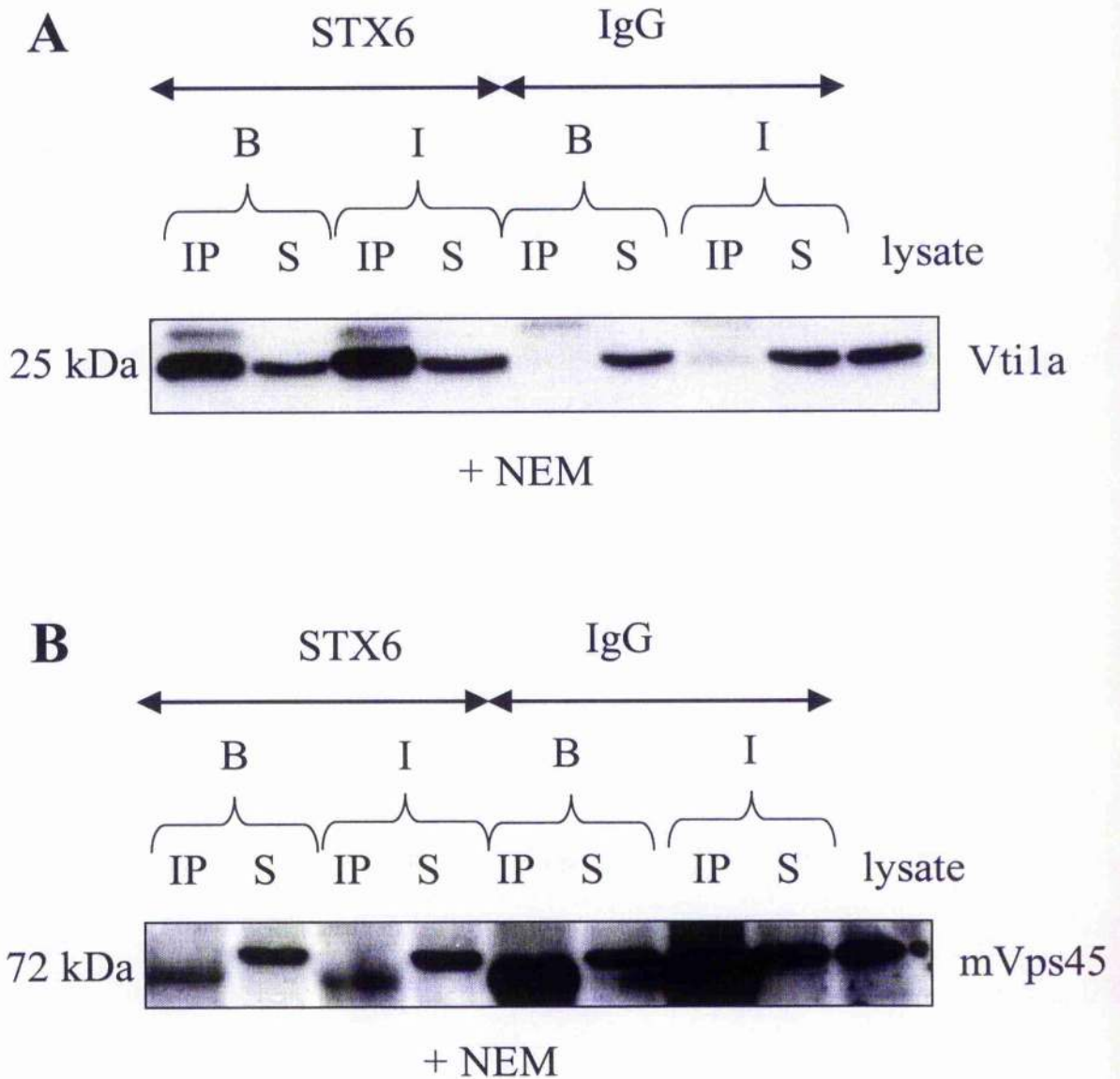


Figure 3.13 STX6 co-immunoprecipitates Vti1a but not mVps45 in 3T3-L1 adipocytes

3T3-L1 adipocytes treated with 5 mM NEM and with (I) or without (B) 1 μ M insulin for 15 min were lysed and STX6 was immunoprecipitated using 2 μ g monoclonal anti-STX6. The immunoprecipitates were compared to the post immunoprecipitation supernatants by resolving on a 12 % gel, and probing for possible binding partners by immunoblotting with specific antibodies. **A)** The blots were probed with anti-Vti1a, revealing that Vti1a co-immunoprecipitated with STX6 both in basal and insulin-stimulated cells. **B)** Analysis with anti-mVps45 indicated that STX6 did not co-immunoprecipitate mVps45 either in the presence or absence of insulin.

IP: immunoprecipitate

S: supernatant collected after immunoprecipitation

Lysate: lysate prior to immunoprecipitation

Fractions loaded: **IP**, 2/5 of total immunoprecipitate from 1 well of a 12-well plate; **S**, 1/20 of the total supernatant obtained from one well of a 12-well plate; **Lysate**, 1/20 of the total lysate obtained from one well of a 6-well plate

3.6. Discussion

Phosphorylation of t-SNAREs has been known for some time to regulate the formation of functional SNARE complexes and the binding of their respective SM proteins (Gerst, 2003). The intriguing dephosphorylation of STX16 in response to insulin (Perera et al., 2003) combined with this knowledge, led to the speculation that STX16 phosphorylation could be responsible for the regulation of a SNARE complex involved in GLUT4 trafficking. This Chapter describes the initial steps taken to identify the site of insulin-regulated phosphorylation, from which future studies can build, as well as the identification of STX16 binding partners in basal and insulin-stimulated 3T3-L1 adipocytes.

It was reasoned that the identification of the exact site insulin-regulated phosphorylation in STX16 would be the first step towards elucidating its function. The method employed by Gerst and co-workers was adopted, which involved the generation of specific STX16 mutants bearing alanine substitutions at potential sites of phosphorylation (Gurunathan et al., 2002) which were tested for phosphorylation in HEK 293 cells.

The yeast t-SNARE, Tlg2p has recently been shown to be a functional homolog of STX16 (Marion Struthers, unpublished data), and it was hypothesised that the site of PKA phosphorylation at S90 (Gurunathan et al., 2002) may have been evolutionally conserved in STX16. This hypothesis gained further credence by *in silico* investigation, which identified T90 as a potential PKA site in STX16 (Figures 3.3 and 3.4). The notion that STX16 could be phosphorylated by PKA is supported by the fact that insulin-stimulation leads to deactivation of PKA (Section 3.1.2) (Conti, 2000; Carmen et. al. 2005), a finding that could support the dephosphorylation of STX16 upon acute insulin-stimulation. Therefore, T90 was mutated to an alanine residue, the resulting mutant was expressed in HEK 293 cells and the phosphorylation status was examined by its ability to bind to a phosphoprotein-binding column. Figure 3.9B suggests that endogenous STX16, myc-tagged STX16 and T90 are all phosphorylated in HEK 293 cells and perhaps, that T90 is not the correct or only site of phosphorylation. However, careful analysis of the controls highlighted some important points. In the first instance, it proved difficult to find a reliable negative control, considering approximately 1/3 of all eukaryotic gene products can be posttranslationally phosphorylated. STX6 and Arf6 were chosen for this purpose as

previous work showed that STX6 was not phosphorylated (Perera et al., 2003), and Arf6 has not been reported to be phosphorylated to date. While Arf6 was not observed in the eluant from the phosphoprotein-binding column, STX6 was observed, (Figures 3.9B and 3.9C) however, it was reasoned that STX6 could be evident through its interaction with phosphorylated endogenous STX16. Positive controls were supplied by looking for the presence of STX4, PKB and IRS1. Both STX4 and GLUT4 are known to be phosphorylated (Piper et al., 1993; Risinger and Bennett, 1999) and bound to the column as expected (Figure 3.9C). Both PKB and IRS1 are phosphorylated upon insulin stimulation (Gual et al., 2005; Hill et al., 2001). The fact that they are observed in the eluant under basal conditions suggests that perhaps the serum present during transfection was responsible for stimulating the insulin receptors and the subsequent phosphorylation of their substrates. If this was the case, however, STX16 would be dephosphorylated and binding to the column would not be observed. This led to the notion that there was perhaps a second site of phosphorylation in STX16, which is constitutively active and responsible for the binding observed in Figure 3.9B. Recall that only a 50 % reduction in phosphorylation is observed upon insulin stimulation (Perera et al., 2003). For this reason, it was not possible to conclude with certainty that T90 was not the correct site of phosphorylation. In addition, the possibility that there was simply non-specific binding to the column could not be ruled out. In effect, this experiment left more questions than answers.

^{32}P analysis was therefore utilised in an attempt to clarify the above by allowing the quantitative analysis of any changes in phosphorylation observed in the T90 mutant. In addition, two more sites were chosen for analysis. Tlg2p is phosphorylated on a serine residue, and as such, two serine residues (S94 and S95) with the highest probability of being phosphorylated were chosen (Figures 3.3 and 3.4), mutated to alanine residues and screened for phosphorylation in the same way. Unexpectedly, Figure 3.11A clearly demonstrates that neither wild type STX16 nor the mutants are labelled, strongly suggesting that STX16 is not phosphorylated in HEK 293 cells. It is therefore speculated that the phosphorylation of STX16 previously observed in adipocytes by the same method of $^{32}\text{P}_i$ labelling is in fact cell-type specific. This presents the intriguing possibility of a SNARE complex specifically regulated in highly insulin-responsive cells, a concept which will be discussed further below. Clearly, the next step in this investigation will be to test the phosphorylation status of the STX16 mutants in 3T3-L1 adipocytes.

I sought to find STX16 binding partners in 3T3-L1 adipocytes with the aim of identifying the insulin-regulated STX16 complex. It was found that STX16 was co-

immunoprecipitated with STX6 and that the t-SNARE, Vti1a, was also present in the immunoprecipitate (Figures 3.12 and 3.13). An interaction between STX6 and STX16 in 3T3-L1 adipocytes was identified previously (Perera et al., 2003; Shewan et al., 2003) and in the time since these immunoprecipitation studies were conducted, an interaction between Vti1a and STX16 has been reported in these cells (Bose et al., 2005).

Mallard *et al.* (Mallard et al., 2002) demonstrated that a SNARE complex is formed between STX6, STX16 and Vti1a in HeLa cells and that this complex, along with the v-SNAREs VAMP3/cellubrevin and VAMP4, controls trafficking between endosomes and the TGN. In this study, I have shown that the STX16/STX6/Vti1a complex also exists in 3T3-L1 adipocytes and that the interaction is viable in basal and insulin-stimulated cells (Figures 3.12 and 3.13). As such, the change in binding affinity anticipated between STX16 and its binding partners with a change in phosphorylation status (Figure 3.1) does not appear to apply to this complex. At present, it is not known if this complex has the same function in 3T3-L1 adipocytes as reported in HeLa cells. As GLUT4 may traffic from endosomes to the TGN in adipocytes (Bryant et al., 2002) (Figure 1.9, Chapter 1), it seems plausible that the STX6/STX16/Vti1a complex may be required to accomplish this trafficking step. On the other hand, as my data suggests that formation of this complex is not regulated by insulin, it may not represent the complex involved in regulated GLUT4 trafficking.

Perhaps the STX6/STX16/Vti1a complex is indeed involved in the general traffic from endosomes to the TGN in adipocytes and a distinct specialised complex controls GLUT4 trafficking, thus avoiding all cargo bound for the TGN being regulated by insulin. The upregulation of STX16 and STX6 observed upon differentiation of 3T3-L1 fibroblasts (Shewan et al., 2003) could be required for a specialised transport system in adipocytes corresponding with the biogenesis of the GSV compartment. In support of this theory is the observation that STX16 phosphorylation may be cell specific (Figure 3.11) suggesting that this regulation is only necessary in insulin-responsive cells.

What then would be the components of this specialised SNARE complex? I speculate that it includes STX6 and STX16 (due to the evidence presented in Section 1.8.1) with an alternative t- or v-SNARE. After all, many SNAREs are known to take part in more than one SNARE complex in more than one trafficking step. In HeLa cells, the STX6/STX16/Vti1a complex was shown to interact with two different v-SNAREs, VAMP3/cellubrevin and VAMP4, most likely in two distinct complexes (Mallard et al., 2002). STX6 has also been shown to interact with VAMP7 and VAMP8, along with Vti1b

and STX7, in a complex from melanoma cells (Wade et al., 2001). Perhaps in 3T3-L1 adipocytes, STX16, STX6 and Vti1a interact with one v-SNARE to accept incoming general traffic from endosomes to the TGN and with another v-SNARE, present on GLUT4 containing vesicles, in a complex that is regulated by insulin and STX16 phosphorylation. Unfortunately, no data were recorded in this study regarding the possible v-SNAREs involved in 3T3-L1 adipocytes due to lack of good specific antibodies. However, previous work in our laboratory identified, intriguingly, a weak but perhaps insignificant interaction between VAMP2 and STX6 (H.K.I. Perera, unpublished observation). GSVs are enriched in VAMP2 (Ramm et al., 2000), and although this v-SNARE is associated with the fusion of GSVs with the PM in adipocytes (Foster and Klip, 2000) could it also function as the v-SNARE for incoming GLUT4 containing vesicles to the TGN?

I then considered an alternative t-SNARE that could participate in a STX6 and STX16 containing complex. Of the 14 known mammalian syntaxins, only four are localised to the Golgi apparatus, with STX6, STX16 and STX10 localised to the TGN (Bock et al., 1997; Mallard et al., 2002; Simonsen et al., 1998; Tang et al., 1998a; Tang et al., 1998b). Although STX10 was shown to co-immunoprecipitate with STX6 and STX16, it was shown to act independently of STX6 and STX16 in a separate trafficking step (Wang et al., 2005). However, as mentioned above, STX6 was shown to interact with the t-SNARE Vti1b, in melanoma cells (Wade et al., 2001) and more recently, in activated macrophages. Vti1b is localised mostly on tubules and vesicles in the TGN area and on endosomes in synaptosomes (Kreykenbohm et al., 2002). Therefore, although STX16 did not co-immunoprecipitate Vti1b in HeLa cells (Mallard et al., 2002) it was decided to test Vti1b as a potential member of the SNARE complex in 3T3-L1 adipocytes. However, it was not possible to observe Vti1b in the STX6 immunoprecipitates due to the similarity in size of Vti1b and the light chain of the STX6 antibody used for the immunoprecipitation. Both resolved at approximately 25 kDa on the SDS-PAGE gel and the Vti1b signal was therefore obscured. Attempts to resolve the proteins using various percentages of acrylamide in the SDS gels (Section 2.4.3) were without success (not shown). Future studies will be required to address this issue, perhaps by carrying out the immunoprecipitation with antibody to Vti1b and probing for STX6 and STX16.

Figure 3.1 demonstrates the scenario anticipated between STX16 and its SM binding partner mVps45 with a change in phosphorylation status. Recent data from our laboratory suggests that the yeast homologue of mVps45, Vps45p (Section 1.6.4) is a phosphoprotein (Scott Shanks, unpublished data) in yeast. Perhaps the apparent phosphorylation of

Vps45p, if shared by mVps45, could add a further layer of regulation to the STX16-containing SNARE complex like its synaptic counterpart Munc18 (Shuang et al., 1998). Further work will be required to test this possibility. Previously, mVps45 was shown to bind weakly to STX6 (Bock et al., 1997; Tellam et al., 1997), however, under my experimental conditions, mVps45 does not co-immunoprecipitate with STX6 (Figure 3.13B). Correspondingly, it would seem that neither does it bind to the fraction of STX16 present in the STX6 immunoprecipitate, despite the fact that previous work has demonstrated a direct interaction between STX16 and mVps45 (Dulubova et al., 2002; Yamaguchi et al., 2002). The reason for this discrepancy could be that mVps45 is unable to bind STX16 when STX16 is participating in a SNARE complex. As mentioned previously, it is highly plausible that the fraction of STX16 left in the post-immunoprecipitation supernatant (Figure 3.12) could constitute uncomplexed STX16 and could be found associated with mVps45.

The suggestion that mVps45 binding to STX16 is incompatible with SNARE complex formation is in agreement with current knowledge of SNARE complexes involved in exocytosis but contrary to reports regarding intracellular complexes, in which t-SNAREs can simultaneously bind to SM proteins while participating in a ternary complex (Rizo and Sudhof, 2002) (Section 1.5.6). Perhaps my data is suggestive that STX16 can indeed adopt a so-called "open" and "closed" conformation (as depicted in Figure 3.1), like its synaptic counterpart STX1a (Dulubova et al., 1999) (Section 1.5.2), and mVps45 binding is dependent on the formation of the inactive closed conformation. This possibility will be investigated further in Chapters 4 and 5.

Chapter 4

Generation of Recombinant Adenoviruses and Optimisation of Adenovirus-Mediated Expression of STX16 mutants in 3T3-L1 Adipocytes

4. Generation of Recombinant Adenoviruses and Optimisation of Adenovirus-Mediated Expression of STX16 mutants in 3T3-L1 Adipocytes

4.1. Introduction

The main aim of this study was to elucidate the role, if any, of STX16 in GLUT4 trafficking in 3T3-L1 adipocytes. Experiments were therefore conducted to examine the effects on GLUT4 trafficking of expressing various domains of STX16 in 3T3-L1 adipocytes, the results of which are presented in Chapter 5. In order to make these experiments possible, it was first necessary to construct the tools required to conduct such an investigation. This Chapter, therefore, details the generation of recombinant adenoviruses to express the cytosolic domain, an N-terminal truncation mutant and full-length STX16, and to optimise the expression of these proteins in 3T3-L1 adipocytes. Section 4.1.1 provides an introduction to the adenovirus and its use as a vehicle for the expression of recombinant proteins in cell culture.

4.1.1. Introduction to adenovirus

4.1.1.1. General properties of the adenovirus

The adenovirus was first isolated from human adenoids in the early 1950s during a study into the cause of the common cold (ROWE et al., 1953). Members of the adenovirus family, or *Adenoviridae*, are known to infect a wide variety of post-mitotic cells, even those associated with highly differentiated tissues including skeletal muscle, lung, brain and heart (Russell, 2000). Human adenovirus serotypes 2 and 5 of subgroup C are the most extensively characterised and used as vectors (Hitt et al., 1997). The use of adenoviruses as vectors will be considered in more detail in Section 4.1.1.6.

4.1.1.2. Structure and genome

The characteristic morphology the adenovirus is defined by an icosahedral capsid, surrounded by protruding knobbed fibre domains at each of the 12 vertices (Stewart et al., 1993). The capsid, of diameter 80-90 nm, encloses the viral genome and is assembled from three major proteins, the hexon, penton base and knobbed fibre, along with a number of other minor proteins (Stewart et al., 1993) (Figure 4.1). 240 hexons make up the faces of the icosahedron, with a penton base residing at each of the 12 vertices. A fibre protein, ending in a globular tip known as the knob domain, extends from each penton base (Stewart et al., 1993). The adenovirus genome consists of a linear, double-stranded DNA molecule, which varies in size between groups from 30- 40 kb. The genome of the most commonly used human adenovirus (serotype 5) comprises a linear, 36 kb, double stranded DNA molecule (Chroboczek et al., 1992). Both strands are transcribed and nearly all transcripts are extensively spliced. Conventionally, viral transcription units are divided into regions that are expressed at an early (E1, E2, E3 and E4) (Section 4.1.1.4) or late stage of the infectious cycle.

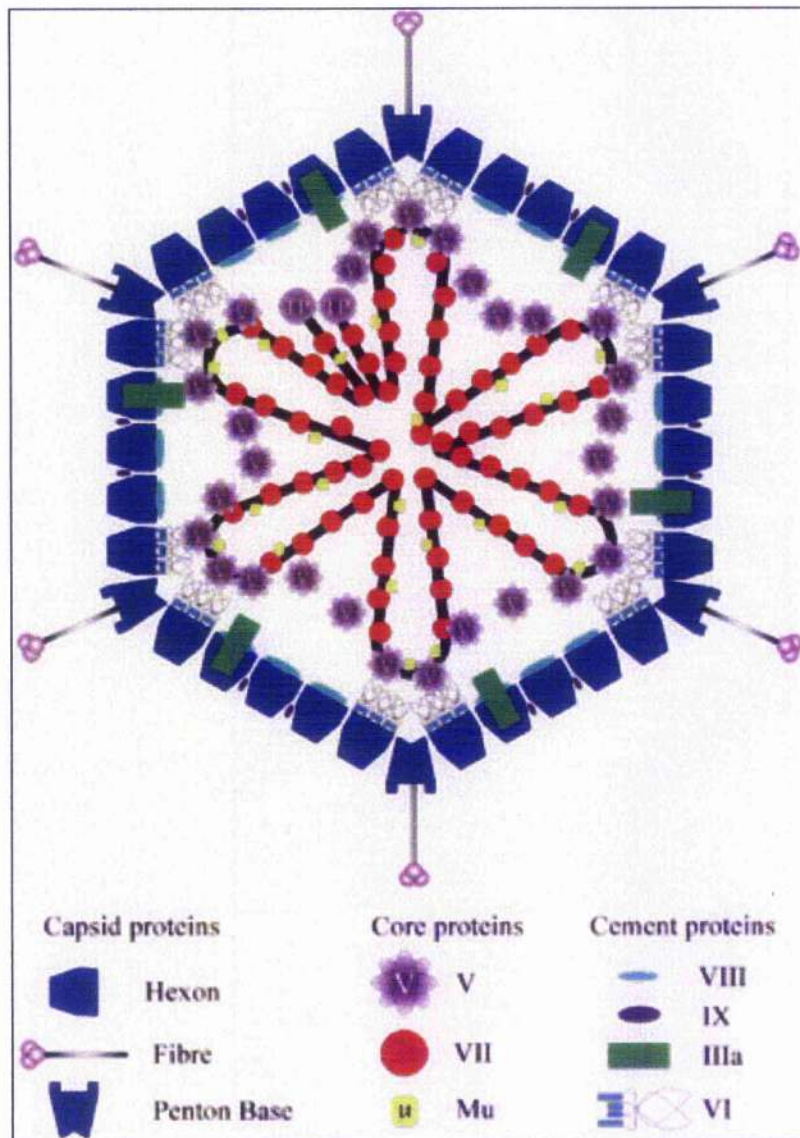


Figure 4.1 Structure of adenovirus (taken from (Russell, 2000))

The characteristic icosahedral morphology of the adenovirus, along with its main structural components. The positions of the capsid proteins (the hexon, fibre and penton base), core proteins and hypothetical locations of the cement proteins are as indicated.

TP- terminal proteins, containing the inverted terminal repeats at the 5' end of the virus DNA, the hypothetical arrangement of which is depicted in black.

4.1.1.3. Infectious cycle of the adenovirus

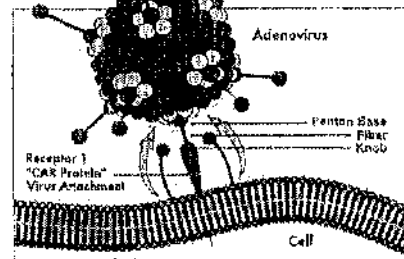
The infectious cycle of the adenovirus can be clearly divided into an “early” and a “late” phase, which occur before and after virus replication, respectively. The early phase in a permissive cell takes about 6-8 hours and involves the entry of the virus into the host cell and subsequent transport of the virus into the nucleus, where the selective transcription and translation of the early genes can occur (Russell, 2000). These early events serve to modify the host cell functions to create favourable conditions for replication of the virus DNA and the resultant transcription and translation of the late genes. The late phase can yield virus in a further 4-6 hours (Russell, 2000).

4.1.1.4. Cell receptors for the adenovirus

The entry of the adenovirus into cells is mediated by interactions with two distinct cell-surface receptors (Figure 4.2). The initial contact of the adenovirus with the host cell is via the knobbed fibre domain. In the case of the human subgroup C adenoviruses, the knobbed fibre domain binds to the coxsackie / adenovirus receptor (CAR), so called because it is identical to the receptor for the coxsackie B virus (Bergelson et al., 1997). The next step involves an interaction of the virus with the cellular integrins, which normally react with the extracellular matrix to facilitate adhesion, differentiation and other cell-cell phenomena (Meredith, Jr. et al., 1996). The virus interacts with the cellular $\alpha\beta3$ or $\alpha\beta5$ integrins (Bai et al., 1993; Takayama et al., 1998; Wickham et al., 1993) through an exposed RGD (arginine-glycine-aspartate) motif on the penton base (Stewart et al., 1993) and entry of the virus proceeds via clathrin-mediated endocytosis. Both $\alpha\beta3$ and $\alpha\beta5$ support adenovirus internalisation (Bai et al., 1993; Takayama et al., 1998; Wickham et al., 1993) and interestingly, $\alpha\beta5$ is expressed on human bronchial epithelial cells, a major site of adenovirus infection *in vivo* (Mette et al., 1993).

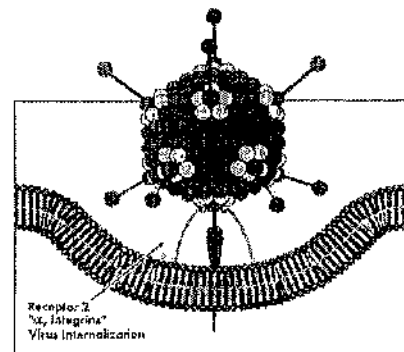
Following endocytosis, the virus escapes into the cytosol by lysis of the endosomal membrane, induced by the penton base. The viron is then disassembled stepwise during the process of internalisation and import to the nucleus, where transcription, replication and viral packaging take place (Russell, 2000).

A)



1) Attachment to cell surface receptor.

B)



2) Receptor-mediated endocytosis

Figure 4.2 Binding and internalisation of the adenovirus (taken from AdenoVator Applications Manual, Version 1.1, QBIogene)

A) The virus attaches to the target cell by binding of the knobbed fibre to the CAR proteins on the cell surface. **B)** The exposed RGD motif on the penton base interacts with the αv integrins and mediates endocytosis of the virus into the host cell.

4.1.1.5. Use of adenoviral vectors to confer gene transfer into mammalian cells

The ability of adenovirus to infect a wide variety of cell types and tissues in both dividing and non-dividing cells, combined with their relative ease of preparation and purification, has led to their extensive use as gene vectors. Recombinant adenoviruses can transfer genes to a broad spectrum of cell types with the major advantage that gene transfer is not dependent on active cell division. Additionally, high titres of viruses and high levels of transgene expression generally can be obtained.

The adenovirus can incorporate only about 2 kb of foreign DNA without significant effects on its stability or its infectivity. Adenoviral vectors have been designed to allow for the introduction of longer sequences by the removal of some or all of the virus genes. The various methods for the construction of adenovirus vectors are reviewed in Hitt et al., 1997. In most recombinant vectors, transgenes are introduced in place of E1 and/or E3 genes, allowing the introduction of up to 6.5 kb of foreign DNA. Deletion of the E1 gene removes the ability of the virus to replicate in target cells and therefore prevents propagation of infectious viral particles. The E3 region encodes proteins involved in evading host immunity and is not required for the replication of virus in tissue culture. A further generation of vectors have been developed, which involve the deletion of the E2 genes, or in some cases, nearly all of the virus genes in so-called "gutless vectors" (see Russell, 2000 and references within).

4.1.1.6. HEK 293 cells

HEK 293 cells constitute a cell line that provides E1 genes *in trans* (Graham et al., 1977) and as such are used to allow the propagation of replication deficient viruses lacking the E1 genes. Human embryonic kidney cells were transformed by exposing the cells to sheared fragments of adenovirus type 5 DNA (Graham et al., 1977). High titres of recombinant adenovirus lacking the E1 genes can be therefore be obtained by infection and propagation in HEK 293 cells.

4.1.1.7. Construction recombinant adenoviruses

There is a range of techniques for the construction of recombinant adenoviruses and these are described in detail elsewhere (Hitt et al., 1997; Tashiro et al., 1999; Zhang, 1999). Generally, the gene of interest is cloned into a suitable “shuttle” vector, which serves the standard purpose of “shuttling” cDNAs of interest from a plasmid vector to a viral construct, followed by homologous recombination with a larger vector constituting the viral backbone. Homologous recombination can occur by co-transfection of the shuttle vector and the viral backbone into bacteria (He et al., 1998), followed by production of viral particles in HEK 293 cells, or co-transfection directly in HEK 293 cells. Finally, the virus can be amplified in HEK 293 cells (Graham et al., 1977) and the titre accurately determined by a range of methods such as plaque unit forming assay (AdEasy Adenoviral Vector System Instruction Manual, Stratagene, USA, www.stratagene.com).

Although rendered defective for replication as a result of deletion of the E1 genes, the potential exists for recombinant adenoviruses to regain the ability to replicate in a non-complimenting cell line. Replication competent adenoviruses can emerge within a population of replication deficient adenoviruses as a result of a double crossover event between the homologous overlapping sequences present in the recombinant adenovirus and the HEK 293 genome (Lochmuller et al., 1994), resulting in the loss of the transgene and its replacement by the E1 region (Zhu et al., 1999). The method used to generate recombinant adenoviruses in my study was the RAPAd.I system, developed by Anderson and co-workers (Anderson et al., 2000). The system makes use of a novel adenovirus backbone devoid of the left-hand inverted terminal repeat, the packaging signal and E1 sequences. The investigators reasoned that an adenoviral genome devoid of sequences necessary for packaging and replication would greatly reduce or eliminate production of wild-type virus. Thus the RAPAd.I system allowed for generation of a recombinant adenovirus containing virtually no contaminating E1 sequences and no detectable wild-type virus contamination (Anderson et al., 2000).

4.1.1.8. Receptor availability may affect protein expression

Clearly the first step in achieving successful protein expression in target cells involves the ability of the adenovirus to enter that particular cell. This relates to the availability of the cell-surface receptors discussed in Section 4.1.1.4. Although CAR and αv integrins are

widely distributed among most cell types, some tissues and cells, such as lymphocytes, express very little if any of these receptors, (Hitt et al., 1997; Leon et al., 1998). Evidently, the availability of these receptors is a crucial factor that must be taken into account when considering adenovirus mediated gene transfer in a particular cell.

4.1.1.9. Why use adenovirus in this study?

My study into elucidating a role for STX16 in GLUT4 trafficking required the use of terminally differentiated 3T3-L1 adipocytes, a cell line which would allow native GLUT4 trafficking to be studied. Gene transfer via standard transfection methods has been shown to be very inefficient in these highly differentiated cells (Gnudi et al., 1997). Adenovirus vectors, on the other hand, are able to transfer genes even to highly differentiated cells and gene transfer is not dependent on active cell division (Russell, 2000). As such adenovirus vectors have been successfully used to transfer genes into 3T3-L1 adipocytes (Bosc et al., 2001; Emoto et al., 2001; Sakaue et al., 1997).

4.2. Aims

My ultimate goal was to study the function of STX16 in 3T3-L1 adipocytes. Crucial to my study, therefore, was the identification and design of the STX16 mutants that would provide functional information and ultimately test the hypothesis described Section 1.9, Chapter 1. The second hurdle was to be able to express these proteins in 3T3-L1 adipocytes, notoriously difficult to transfect using standard techniques (Gnudi et al., 1997). Therefore recombinant adenoviruses were required to drive expression. Nevertheless, despite an efficient transfection system, the expression of STX16 in 3T3-L1 adipocytes was subject to limitations that had to be overcome to achieve optimum expression. Therefore the aims of this Chapter were as follows:

1. To design STX16 mutants to test the hypothesis in 3T3-L1 adipocytes
2. To clone these mutants into the adenoviral vector pShuttle-CMV for subsequent generation of recombinant adenovirus
3. To optimise adenovirus-mediated expression of the STX16 mutants in 3T3-L1 adipocytes

4.3. Materials and Methods

4.3.1. Generation of recombinant adenoviruses

4.3.1.1. ViraQuest

Homologous recombination and amplification were carried out by Ronald B. Haskell at ViraQuest Inc., 310 West Zeller, North Liberty, IA, USA. The RAPAd.1 system (Section 4.1.1.8.) was used as described in Anderson et al., 2000. The general procedure is summarised briefly here and in Figure 4.3.

The “shuttle” vector, housing the gene of interest (Section 4.4.2.1), and the adenoviral backbone, RAPAdTM, were linearised by enzymatic digestion with *PacI* and the mixture was transfected into HEK 293 cells using standard calcium phosphate methods. Viral foci were observed 6 days later, with more foci evident in the following days. The cells were harvested 8 days after transfection, pelleted by low speed centrifugation, and the virus liberated by three cycles of freeze/thaw. The cell lysate (1 ml in 10 mM Tris, pH 8.1) containing the recombinant virus was amplified and purified. The infectious titre of the resultant purified virus particles was determined by HEK 293 plaque assay as described (Anderson et al., 2000). A549 cell overlay and PCR methods to detect potential E1 sequences were used as described in Anderson et al., 2000 to ensure that no wild-type virus was detectable after amplification.

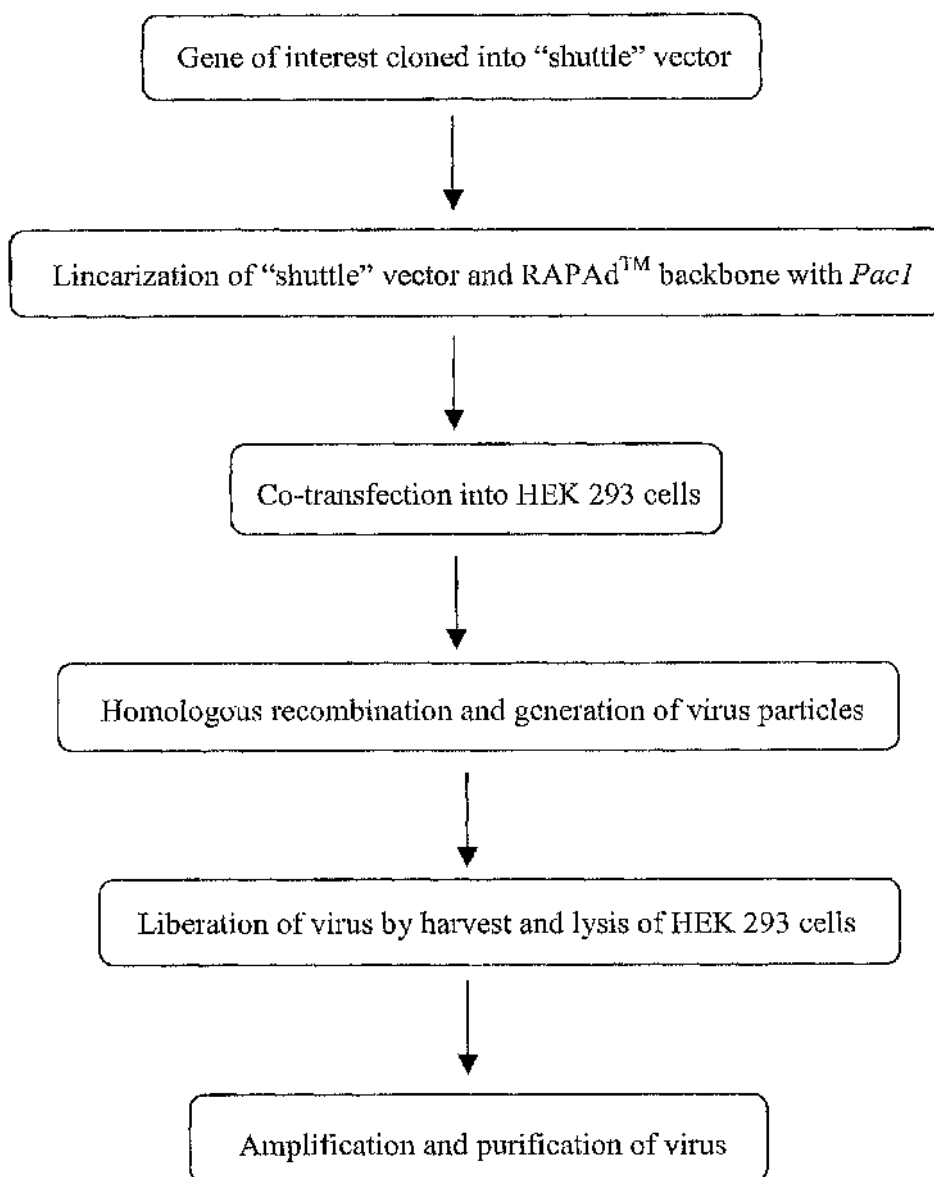


Figure 4.3 Generation of recombinant adenovirus using the RAPAd.1 system (adapted from Anderson et. al. 2000).

The gene of interest was cloned into the "shuttle" vector (Section 4.4.2.1). At ViraQuest Inc., this plasmid was linearised by digestion with *PacI*. The RAPAd™ viral backbone (described in Anderson et. al. 2000) was also digested with *PacI*. The digested products were then co-transfected into HEK 293 cells, where homologous recombination occurred. Viral foci were observed six days later. Eight days after transfection, the cells were harvested and lysed by three cycles of freeze/thaw. The cell lysate, containing recombinant virus was amplified and purified. Large-scale amplification resulted in a high titre of virus capable of expressing the gene of interest.

4.3.1.2. Amplification of pShuttle-CMV virus in HEK 293 cells

5 μ l of control virus ("empty" pShuttle-CMV), diluted in 10 ml of HEK 293 growth media, were used to infect one 75 cm flask of HEK 293 cells, which were ~ 90 % confluent. The cells were incubated at 37 °C and 5 % CO₂ for ~ 4 days. After this time, the cells were detached by gently tapping the flask, and harvested by centrifugation at 1000 rpm for 5 min in a bench-top centrifuge. The viral growth medium was decanted and, after dilution in HEK 293 growth medium, was used to infect further flasks of HEK 293 cells (~ 90 % confluent). This process was repeated until there was enough viral media to infect thirty 150 cm² flasks of HEK 293 cells. The viral medium was mixed with normal HEK 293 growth medium at a ratio of 1 : 5. 5 ml of this mixture were pipetted into each flask and allowed to completely cover the cells. The cells were incubated at 37 °C and 5 % CO₂ for 1 h before the addition of an additional 20 ml HEK 293 growth medium. This was followed by incubation at 37 °C and 5 % CO₂ for ~ 4 days or until the cells began to show the cytopathic effects of rounding up detaching from the flask. The flasks were gently tapped to remove all remaining attached cells, which were then harvested by centrifugation at 1000 rpm for 5 min. The viral medium was carefully decanted and aliquots were stored at -80 °C until required for further infections of HEK 293 cells and virus preparations. The virus was extracted from the cell pellets as described in Section 4.3.1.4 below.

4.3.1.3. Purification of viral particles from HEK 293 cells

HEK 293 cells from thirty 150 cm² flasks were combined and resuspended in 10 ml PBS. An equal volume of ARKcloneP was added to the cell suspension, which was mixed thoroughly and allowed to stand for 10 min until the layers separated. The mixture was then subjected to centrifugation at 1000 rpm for 5 min, after which time the top lysed layer was removed and gently pipetted onto the CsCl₂ gradient prepared as follows. 3 ml 30 % CsCl₂ (Section 2.1.7) was added to a Beckman 14 × 95 mm tube and this was carefully under-layered with 1.5 ml 60 % CsCl₂ (Section 2.1.7). The CsCl₂ gradient was poured directly prior to use and after the addition of the top lysed layer it was immediately spun in an ultracentrifuge at 27 K, zero deceleration at 8 °C for 90 min in an SW40 swing-out rotor. The white viral band was identified and removed by piercing the tube with an 18 G needle and withdrawing the virus into a 5 ml syringe. The viral band was then dialysed

against 1 L TE buffer (Section 2.1.7) at 4 °C overnight. The CsCl₂ gradient and dialysis steps were repeated and the purified virus was stored in 50 µl aliquots in cryo-vials at - 80 °C until required.

4.3.1.4. Calculation of virus titre for accurate infections

It was essential that the virus be accurately quantified following the preparation of each batch of control virus to ensure consistency between samples. The quantification of the viral stocks was determined using the Adeno-X™ Rapid Titre Kit as described in the Adeno-X™ Rapid Titre Kit Manual and described briefly here.

1 ml of healthy HEK 293 cells (5×10^5 cells/ml) in HEK 293 growth medium was added to each well of a 12-well plate. The number of cells was accurately determined using a haemocytometer. 10-fold serial dilutions of the viral sample to be quantified were prepared in PBS from 10^{-2} to 10^{-6} ml (10^{-2} , 10^{-3} , 10^{-4} , 10^{-5} , 10^{-6} ml). 100 µl of each dilution were added drop-wise to the appropriate wells. Duplicate infections were performed at each dilution to ensure accurate assay results. The cells were incubated at 37 °C and 5 % CO₂ for 48 h, after which time the medium was aspirated and the cells were allowed to dry in the flow-hood for 5 min.

The cells were fixed by the addition of 1 ml ice-cold 100 % methanol to each well and incubation at -20 °C for 10 min. The methanol was then carefully aspirated and the wells were rinsed three times with 1 ml PBS + 1 % BSA. Anti-Hexon primary antibody (provided) was diluted 1:1000 in PBS + 1 % BSA and when the final rinse had been aspirated from the cells, 0.5 ml of the antibody dilution were added per well. After incubation for 1 h at 37 °C on an orbital shaker, the antibody was aspirated and the cells were gently rinsed three times with 1 ml PBS + 1 % BSA. HRP conjugated secondary antibody (provided) was then diluted 1:500 in PBS + 1 % BSA and 0.5 ml of this dilution were added to each well, followed by incubation at 37 °C for 1 h on an orbital shaker. During this incubation, the DAB working solution was prepared by diluting 10 × DAB substrate (provided) 1:10 with 1 × Stable Peroxidase Buffer (provided) and the DAB working solution was allowed to come to room temperature. The secondary antibody was removed and each well was gently rinsed three times with PBS + 1 % BSA. 500 µl of the DAB working solution was added to each well and incubated at room temperature for 10 min, after which time the DAB was aspirated and 1 ml PBS was added to each well. The DAB solution caused the labelled cells to be stained brown/black. The cells were then viewed on a microscope with a 20 × objective lens. Four fields were selected at random

and the numbers of brown/black positive cells were counted per field. Dilutions with 10 % or fewer positive cells were counted and ideal fields contained 5 to 50 positive cells. The mean number of positive cells in each well were calculated.

The number of infectious units (ifu)/ ml were calculated as follows:

$$\text{Ifu} = \frac{(\text{infected cells/field}) \times (\text{fields / well})}{\text{Volume virus (ml)} \times \text{dilution factor}}$$

4.3.1.5. Multiplicity of infection (MOI)

The titre of the resulting adenovirus is expressed as infectious units or plaque forming units per ml (pfu/ml). The amount of virus used in infections in cell culture is often expressed as the ratio of cells to pfu, known as the multiplicity of infection (MOI). Therefore, an MOI of 1:100 is equivalent to 100 pfu per cell.

To calculate the volume of a particular virus to add to each well of a 12-well plate, the following formula was used:

$$\frac{\text{Number of virus particles}}{\text{pfu per } \mu\text{l}} \longrightarrow \mu\text{l virus per well}$$

Where:

Number of virus particles is calculated from the MOI used, assuming 2×10^4 3T3-L1 adipocytes per well of a 12- well plate, in a confluent monolayer.

4.3.2. Infection of 3T3-L1 adipocytes with adenovirus

3T3-L1 adipocytes, differentiated as described in Section 2.3.4.2 were infected on day 6 post-differentiation unless otherwise stated and the assay was carried out on day 8. On the day of infection, the growth medium was aspirated and the cells were gently rinsed twice in serum-free DMEM. After removal of the final wash, 350 μl serum-free DMEM (to maximise contact of the virus with the cells) was added to each well. The desired amount of virus was then added directly to each well and the plate was swirled gently to induce mixing. This was then incubated for 24 hours, after which time the virus was removed and replaced with normal 3T3-L1 adipocyte growth medium. This was then incubated for a further 24 h at 37 °C and 5 % CO₂ prior to assay.

4.3.3. Infection of HeLa cells with adenovirus

Infection of HeLa cells was carried out as for 3T3-L1 adipocytes (Section 4.3.2) except the infection was carried out entirely in HeLa growth medium.

4.3.4. Treatment of infected 3T3-L1 adipocytes with MG132

A 10 mM stock solution was prepared by dissolving MG132 in DMSO. 3T3-L1 adipocytes were infected on day 6 post-differentiation as described in Section 4.3.2. The virus was removed 24 h after infection (day 7) and replaced with 500 μ l normal 3T3-L1 adipocyte growth medium per well. 8 h later, 2.5 μ l of MG132 were added directly to each well (final concentration 50 μ M) and the plate was swirled gently to induce mixing. The cells were incubated with MG132 at 37 °C and 5 % CO₂ for times from 4 – 16 hours. The 16-hour treatment began on the evening of day 7 and proceeded until the morning of day 8.

4.3.5. Adenovirus use and safety considerations

Adenoviruses are stable at room temperature for a number of days and should never be stored at 4 °C. For long-term storage virus stocks were stored in aliquots at – 80 °C in designated, clearly labelled areas. Prior to use, viruses were defrosted at room temperature and were maintained at room temperature during use. If an experiment was carried out over a number of days (such as day 4 and 6 infections, Section 4.4.4.6), viruses were stored at room temperature during this period. As a rule, viruses should not be subjected to more than two freeze / thaw cycles to maintain optimum infectivity.

All infections were carried out in a Type II Cell Culture facility designated for adenoviral work. Double latex gloves and designated laboratory coats were worn when handling virus stocks. Vials containing viral stocks were opened only inside a designated flow hood and virus was added directly from the vial to cells to be infected using a sterile pipette tip. All virally contaminated plasticware was steeped in Vircon for 30 min before disposal in designated waste bags for subsequent autoclaving procedures. Virally infected cells were incubated in designated incubators.

4.4. Results

4.4.1. Design of STX16 mutants

The STX16 proteins described below were either full-length or truncated versions of the STX16A sequence given in Chapter 3 (Figure 3.2), obtained by direct sequencing of the cDNA used in this study (Section 3.5.2). The proteins are described in detail in Sections 4.4.1.1 – 4.4.1.3 and summarised in Figure 4.4.

4.4.1.1. The cytosolic domain (STX16cyt)

In order to define the role of STX16 in GLUT4 trafficking in 3T3-L1 adipocytes, it was sought to study the effects of inhibition of STX16 function. SNARE protein function can be inhibited by means of expressing only the cytosolic domain of the SNARE protein in question. A protein lacking the transmembrane domain competes with the endogenous protein for binding to its SNARE partners thus reducing their interactions with the membrane-bound endogenous protein. Other SNAREs have been studied using these so-called “poison proteins” to inhibit endogenous protein function, for example the plasma membrane localised STX1a and STX4 (Olson et al., 1997; Tellam et al., 1997; Volchuk et al., 1996). In particular, previous work in our laboratory involved the study of STX6 by expressing the cytosolic domain of the protein (Perera et al., 2003). Therefore a construct expressing only the cytosolic domain of STX16 (denoted STX16cyt) was generated.

DNA strider (www.cellbiol.com) was utilised to generate a Kyte/Doolittle hydropathy plot in order to locate the residues comprising the transmembrane domain (Figure 4.5). The full-length STX16 sequence was analysed. The plot predicted that the transmembrane domain begins approximately at residue M280. It was therefore decided to truncate the protein after residue R278 to ensure that no hydrophobic residues remained and all membrane associations had been abolished. Therefore the STX16cyt mutant comprised residues 1-278 of the full-length STX16A sequence (Figure 4.4), plus an N-terminal myc-tag.

4.4.1.2. N-terminal deletion mutant (STX16T)

It was hypothesised that, like STX1a (Dulubova et al., 1999; Misura et al., 2001) (Section 1.5.2), STX16 could adopt an active and inactive conformation in which the N-terminal

H_{abc} domain may self-associate with the functional SNARE domain, preventing SNARE complex assembly with other SNAREs. Figure 4.6 demonstrates how these so-called open and closed conformations, if adopted by STX16, could be regulated either by phosphorylation or mVps45 binding. In order to test this model, and to determine whether each conformation exerts a different effect on GLUT4 trafficking, an N-terminal truncation mutant of STX16 lacking the H_{abc} domain, denoted STX16T, was constructed (Figures 4.4 and Figure 4.6).

Previous work has shown that deletion of the N-terminal H_{abc} domain of either STX1a or Sso1p significantly increases the rate of SNARE complex formation and / or membrane fusion compared to the full-length proteins (Nicholson et. al., 1998; Parlati et. al., 1999). It is assumed that in the absence of the inhibitory action of the H_{abc} helices, the SNARE motif is more readily available for binding to other SNAREs.

Similarly, it was hypothesised that removal of the STX16 H_{abc} domain would prevent formation of the closed conformation (if indeed a closed conformation exists) rendering STX16T a constitutively active version of wild-type STX16. Removal of the H_{abc} domain would also have the effect of removing the mVps45 binding site (Dulubova et al., 2002) and the hypothesised sites of phosphorylation (Chapter 3). This construct was therefore anticipated to mimic the open active conformation with the SNARE motif available for binding at all times.

A similar mutant was made previously in the yeast homolog, Tlg2p, (Bryant and James, 2001) in which the N-terminal 230 residues (constituting the H_{abc} domain) were removed. This mutant was shown to bypass the requirement for Vps45p in SNARE complex assembly in yeast. Binding to Vps45p was abolished but the truncated Tlg2p was still able to form complexes with its cognate SNAREs Tlg1p and Vti1p in cells lacking the SM protein (Bryant and James, 2001). The sequence alignment of STX16 with Tlg2p generated in Chapter 3 (Figure 3.2) was utilised to compare the position of the domains. Figure 4.7 highlights the first residue of the Tlg2p N-terminal truncated mutant (residue T231). The corresponding STX16 threonine residue in the homology plot is T197. Figure 3.4B (in Chapter 3), demonstrates that this residue is predicted to occur within the linker region between the H_{abc} and SNARE domains. Therefore STX16T was truncated before residue T197, and so constitutes residues 197 – 303 of wild-type STX16A (Figure 4.4). This mutant was cloned bearing an N-terminal HA tag.

4.4.1.3. Full-length STX16 (STX16F)

It has been shown that expression of full-length Syntaxins can amplify the effects of these Syntaxins (Pagan et al., 2003; Thurmond et al., 1998). Therefore, it was decided to compare the effects of expressing truncated STX16 (STX16T) with those of expressing full-length STX16 and so an adenovirus construct expressing full-length STX16 was prepared (denoted STX16F) to provide a control in experiments involving the expression of STX16T. The sequence of STX16F was identical to the sequence of STX16A (Figure 3.2, Chapter 3), constituting all 303 residues (Figure 4.4), and an N-terminal myc-tag.

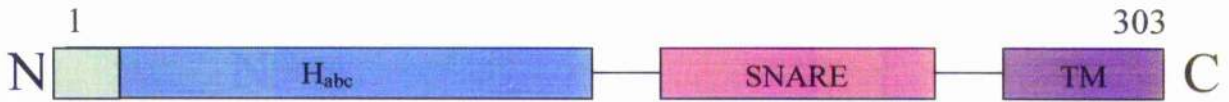
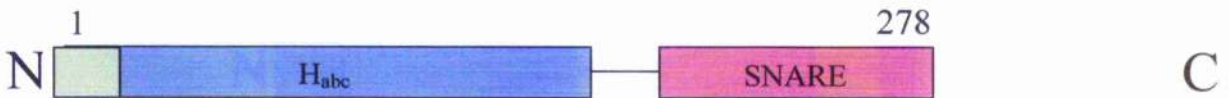
A) STX16F**B) STX16cyt****C) STX16T**

Figure 4.4 Comparison of domain structures of STX16F, STX16cyt and STX16T

Schematic diagram of full-length STX16 and the STX16 mutants. STX16 mutants were designed to allow the effects of GLUT4 trafficking to be studied in 3T3-L1 adipocytes. The N- and C-termini are indicated, including the residue numbers. Coloured boxes correspond to different structural elements in STX16. **A)** STX16F, full length STX16, comprising all 303 residues. **B)** STX16cyt, cytosolic domain of STX16, comprising residues 1-278, and consisting of the N-terminal mVps45 binding motif, the intact H_{abc} and SNARE domains but lacking the transmembrane domain. **C)** STX16T, truncation mutant lacking the N-terminal H_{abc} domain and mVps45 binding motif, and comprising residues 197-303.

N-terminal motif (green)	- N-terminal 55 residues predicted to bind to mVps45 (Dulubova et al., 2002)
H _{abc} (blue)	-Syntaxin homology or autoinhibitory domain, characteristic of syntaxins
SNARE (pink)	-SNARE homology domain, the defining feature of SNAREs and facilitative of their assembly into SNARE complexes
TM (purple)	-C-terminal transmembrane domain, which confers membrane attachment

Hydrophobicity of STX16

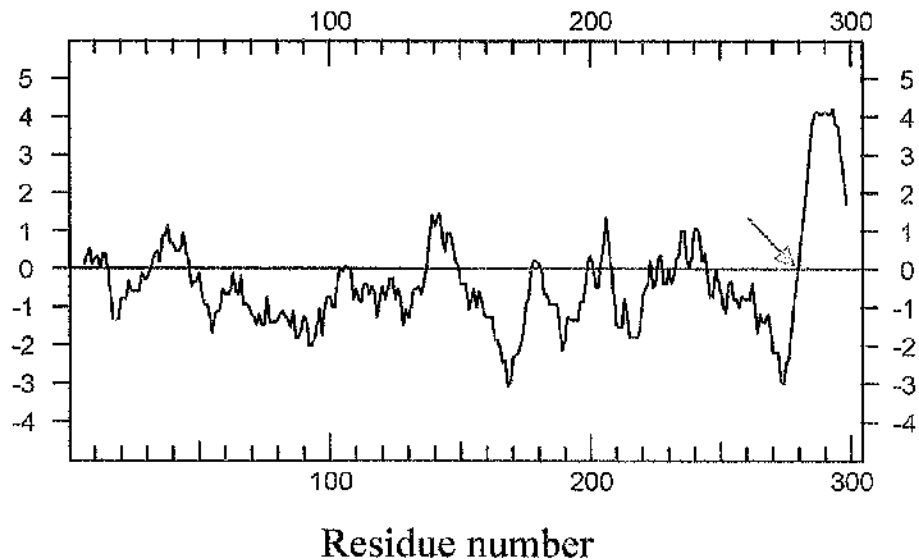


Figure 4.5 STX16 Kyte-Doolittle Plot, indicating the position of the transmembrane domain

DNA Strider (www.cellbiol.com) was used to generate a Kyte/Doolittle hydrophobicity plot. Hydrophobic domains are plotted as positive numbers, indicated by peaks above the black line. A red arrow indicates the predicted location of the transmembrane domain at residue M280. STX16_{cyt} was therefore truncated after R278.

A hydrophobicity plot is an approximate method to determine the higher order structure of a protein. It is based on the principle that 20-30 consistently hydrophobic residues are required to constitute a membrane-spanning α -helix. For each amino acid residue, a weighted average of the hydrophobicity of the residue and its immediate neighbours are calculated. Hydrophobic domains are plotted as positive numbers (Lackie and Dow, 2003).

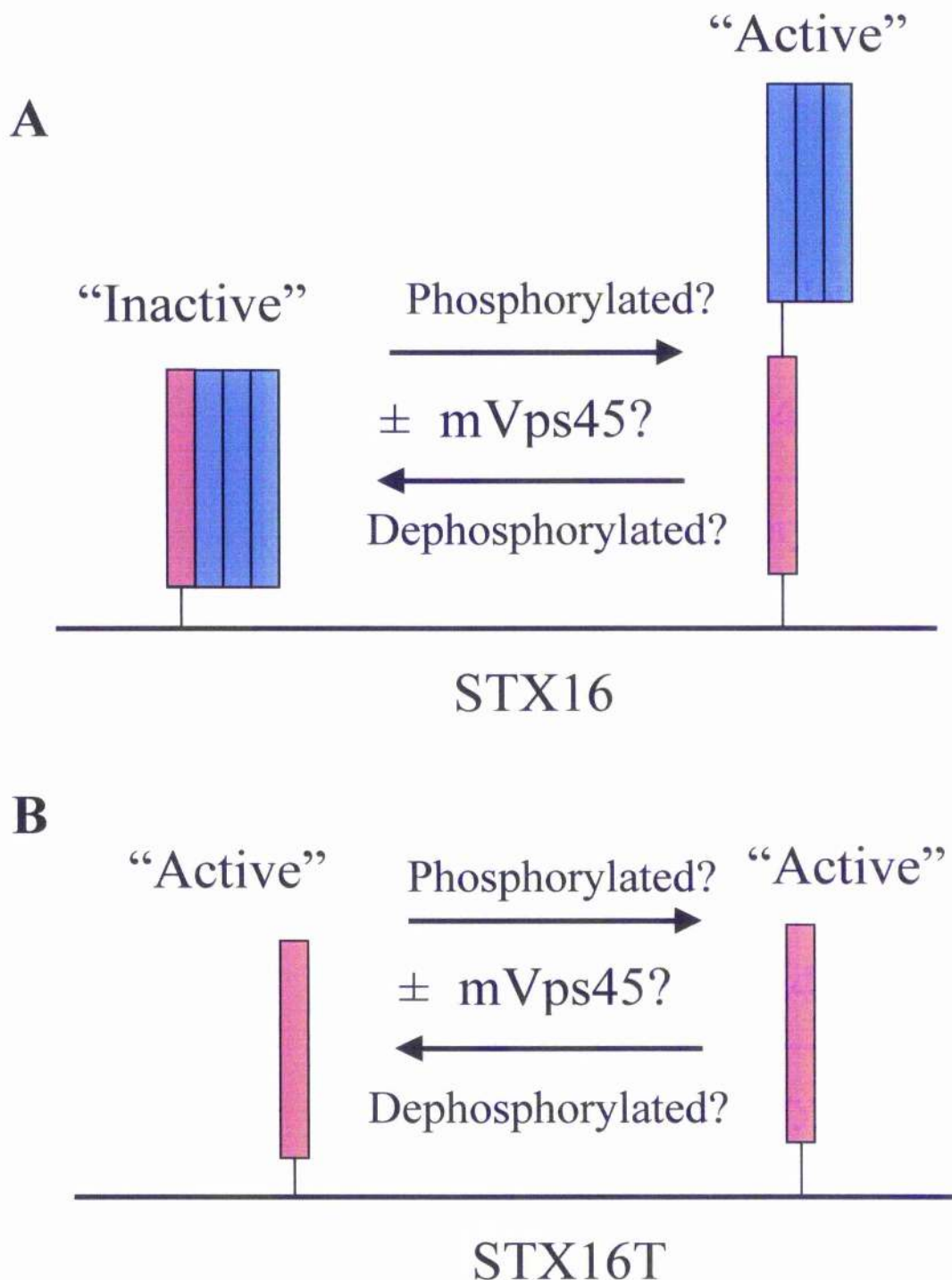


Figure 4.6 Comparative models of wild-type STX16 and STX16T

A) STX16 may exist in a closed “inactive” or an open “active” conformation, in which the availability of the SNARE domain (pink) for binding to other SNAREs is regulated by mVps45 binding and /or phosphorylation. **B)** Removal of the H_{abc} domain (blue) prevents the formation of a closed conformation. The mVps45 binding site (Dulubova et al., 2002) and hypothesised sites of phosphorylation (Chapter 3) will also be absent in this mutant, therefore bypassing the requirement for a regulated shift to the active state, mediated either by mVps45 or phosphorylation. This construct is anticipated to mimic the active “open” conformation with the SNARE motif available for binding at all times.

```

STX16      MATRRLLTDAFLLLRNNSIQNRQLLA--EQLADDR---MALVSGISLDPEAAIGVTKRP-- 53
Tlg2p      -MFRDRTNLFLSYRRTFPFHNITFSSGKAPLGDDQDIEMGTYPMMNMSHDISARLTDERKN 59
          *  * : * * * . . : * : : * . * : * . . . . : : : * . .
STX16      -----PPKWVDGVDEIQYDVGRIKQKMKESASLHDKHLNRPTLDDSSSEEHAIEIT104
Tlg2p      KHENHSDALPPIFIDIAQDVDDYLLVRRRLSEQLAKVYRKNS-LPGFEDKSHDEALIEDL118
          * * : * * : : : : : : : : * : * : * : * * * * * * * *
STX16      TQEITQLFHRCQRAVQPCRAGP-----GPAPSRRGGLGT--WCLVAQALQELSTSFRH156
Tlg2p      SFKVIQMLQKCYAVMKRLKTIYNSQFVDGKQLSREELIILDNLQKIYAEKIQTESNKFRV178
          : : * : * : * : : : : : : * * * : : : * : * * * . . * *
STX16      AQS●GYLKR●MKNREER--SQHFFDTSVPLMDDGDD-----NTLYHRGFTEDQLV202
Tlg2p      LQNNYLKFLNKDDLKPIRNKASAENTLLLDDDEEEEAAAREKREGLDIEDYSKRTLQRQQQL238
          * . * * * : : : : : : . . * * * : : : : * : * : : * :
STX16      LVEQNTLMVEEREREIRQMVSISDLNEIFRDLGAMIVEQGTVLDRIDYNVEQSCIKTED262
Tlg2p      HDTSAEAYLRERDEEITQLARGVLEVSTIFREMQLVVDQGTIVDRIDYNLENTVVELKS298
          . : * * : * * : : : : : : * * : : : * * * * * * * * * * : : .
STX16      GLKQLHKA●BQYQKKNR●KMLVILILFV●I●I●VLIVLV●GVKSR-----303
Tlg2p      ADKELNKA●THYQKRTQ●CKVILLLTLCVIALFFV●M●LKPHGGGSGGRNNGSNKYNNDDNK358
          . * * : * * : * * : * * * * * : * * * * * : : * * * : : :
STX16      -----
Tlg2p      TVNNSHDDGSNTHINDEESNLPSIVEVTESENDALDDLL 397
    
```

AVFPMILW	RED	Small (small+ hydrophobic (incl.aromatic -Y))
DE	BLUE	Acidic
RHK	MAGENTA	Basic
STYHCNGQ	GREEN	Hydroxyl + Amine + Basic - Q
Others	Gray	

Figure 4.7 Sequence alignment of STX16 with Tlg2p

Sequence alignment of STX16A and yeast Tlg2p, generated using ClustalW and used here to design STX16T. Identical residues are indicated by an asterisk, conserved residues by double dots and semi-conserved residues by a single dot. A red dot indicates the beginning of the Tlg2p N-terminal truncation mutant (Bryant and James, 2001) at residue T231, which occurs within the linker region between the H_{abc} domain and the SNARE domain. According to Figure 3.4 (Chapter 3) the STX16 H_{abc} domain ends ~ at residue S159 and the SNARE domain begins ~ at residue R214, each denoted by purple dots. Therefore, the corresponding threonine residue in STX16, T197 (denoted by a blue star), also occurs within the linker region between the H_{abc} and SNARE domains. Therefore STX16T was truncated before residue T197. The transmembrane domains of both proteins are highlighted with a red arrow.

4.4.2. Construction of recombinant adenoviruses to express STX16cyt, STX16T and STX16F in 3T3-L1 adipocytes

4.4.2.1. Cloning of STX16cyt, STX16T and STX16F into pShuttle-CMV

The first step involved the cloning of the genes of interest into the “shuttle” vector pShuttle-CMV (See Appendix) (He et al., 1998), which makes use of the heterologous cytomegalovirus (CMV) promoter.

The c-DNAs encoding STX16cyt (834 bp), STX16T (318 bp) and STX16F (915 bp) were PCR amplified using the conditions and cycling parameters described in Section 2.2.1. The full-length STX16 open reading frame including the N-terminal myc-tag, housed in pCR3.1 (Section 3.5.2.1) was used as the template DNA for each PCR at a concentration of 0.5 mg/ml. Primers were designed to each domain appropriately, including an N-terminal myc (63 bp) or HA (27 bp) tag and restriction sites compatible with pShuttle-CMV (*BglIII* at the N-terminus and *HindIII* at the C-terminus).

The forward primer for both STX16cyt and STX16F was simply the first 18 bp encoding the N-terminal myc-tag. Since STX16T contained an N-terminal truncation, the myc-tag could not be amplified directly from STX16 pCR3.1. Therefore an N-terminal HA-tag was included in the forward primer, followed by a start codon inserted before base 197 (corresponding to the start of the SNARE domain). The HA-tag was chosen due to it having a short recognition sequence, in keeping with an appropriate primer length.

The reverse primer for both STX16F and STX16T was simply the bases encoding the C-terminal 21 residues of STX16, including the stop codon. In the reverse primer for STX16cyt, a stop codon was inserted after residue 278 (corresponding to the end of the cytosolic domain).

Therefore, the primers were as follows (restriction sites underlined; start and stop codons in bold):

STX16_{cyt}

Fwd: 5'-AAAGATCTATGGCCCATATGGAACAAAAA-3'

Rev: 5'-GGAAGCTTTTACCGATTCTTCTTTTGA-3'

STX16_T

The sequence of the HA tag is indicated.

Fwd:

5'- AGATCTATGTACCCTTACGATGTGCCTGATTACGCAACAGAGGACCAGTTA - 3'

← HA tag →

Rev: 5'-GGAAGCTTTTATCGAGACTTCACGCCAAC -3'

STX16_F

Fwd: 5'-AAAGATCTATGGCCCATATGGAACAAAAA-3'

Rev: 5'-GGAAGCTTTTATCGAGACTTCACGCCAAC -3'

The resulting PCR products were gel purified as described in Sections 2.2.3 and 2.2.4 (Figure 4.8A and Figure 4.9A), Taq-treated (Section 2.2.5) and TA cloned into pCR2.1 as described in Section 2.2.6. White colonies, positive for the introduction of the insert were selected and propagated as in Section 2.2.10. The pCR2.1 plasmids were sequenced fully on both strands before proceeding. The inserts were freed from pCR2.1 by enzymatic digestion with *Bgl*III and *Hind*III (Section 2.2.7), gel purified and ligated (Section 2.2.8) into pShuttle-CMV which had been digested with the same enzymes (Figure 4.9B). Ligation products were then transformed into TOP-10 cells and colonies were selected in the presence of Kanamycin (Section 2.2.9). Plasmid DNA was isolated as described in Section 2.2.11 and successful transformants were identified by restriction digest with *Bgl*III and *Hind*III (Figure 4.8B and Figure 4.9C). These were ethanol precipitated (Section 2.2.15) and fully sequenced on both strands (Section 2.2.16) to confirm that no unwanted point mutations had been introduced by the PCR.

4.4.2.2. ViraQuest

100 µl of each plasmid, at a concentration of 1 mg / ml was required for recombination. Large-scale DNA preparations (Section 2.2.12) were therefore carried out to generate large amounts of the desired plasmids, after which the plasmid DNA was resuspended in TE buffer pH 8.0 (Section 2.1.7). Recombination and amplification were then carried out at ViraQuest Inc. as described in Section 4.3.1.1 (Figure 4.3). The titre of the resulting recombinant adenoviruses was 3.0×10^{10} PFU/ml.

4.4.3. Control virus

A recombinant adenovirus generated previously in our laboratory by H.K.I. Perera (Perera et al., 2003) was used as the control for my functional studies. This adenovirus was generated using “empty” pShuttle-CMV vector i.e. no insert was cloned into the vector prior to recombination. Amplification, purification and quantification of this virus were carried out routinely in this study as required as described in Sections 4.3.1.3 to 4.3.1.5.

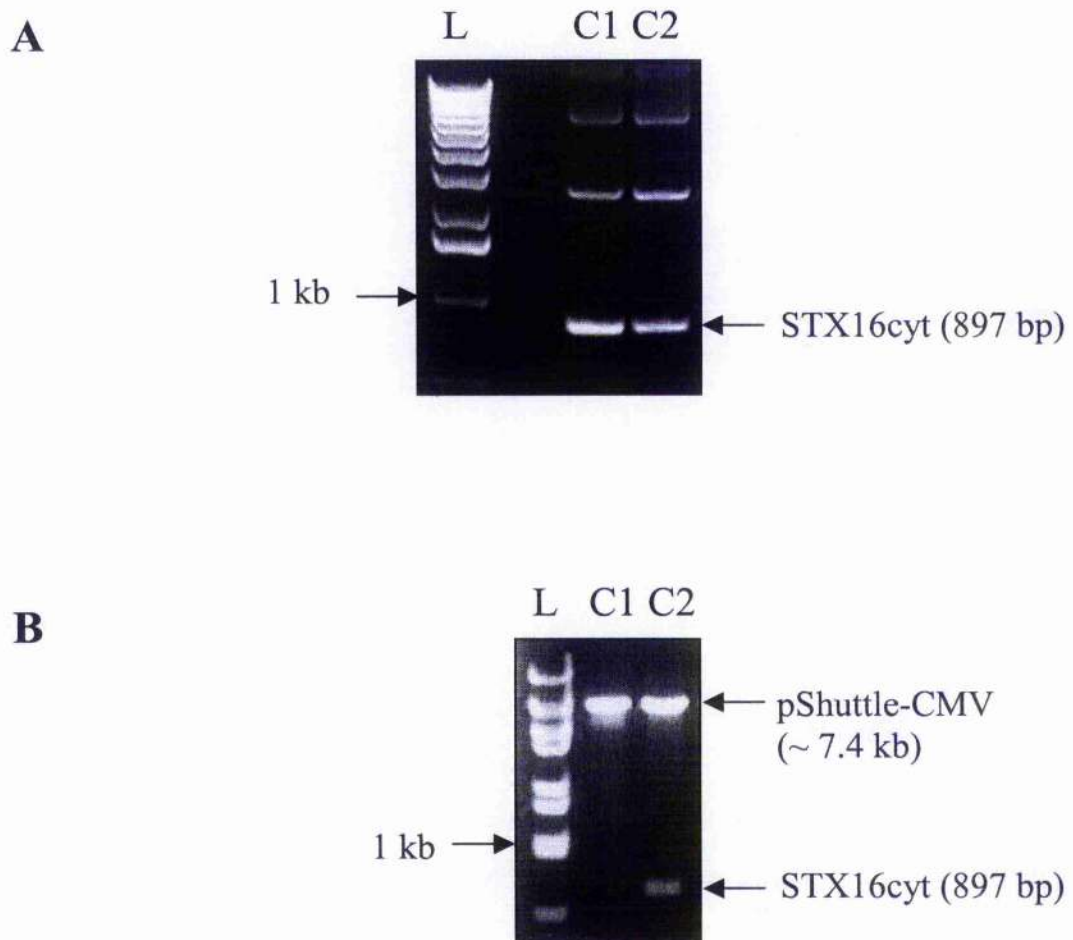


Figure 4.8 Construction of STX16cyt pShuttle-CMV plasmid

A) Products of two independent PCRs (C1 and C2) resolved on a 1 % agarose gel. The strongly stained bands at ~ 0.9 kb correspond to STX16cyt cDNA. This was then TA cloned into pCR2.1 for propagation in bacterial cells, and the STX16cyt insert was freed by restriction digests with *Bgl*III and *Hind*III (not shown). pShuttle-CMV vector was also digested (not shown). **B)** Restriction digests with *Bgl*III and *Hind*III of two potential ligation products (Lanes C1 and C2) following ligation of STX16cyt into pShuttle-CMV. The bands at ~ 7.4 kb can be attributed to pShuttle-CMV; the insert, freed by the restriction digest, is observed in sample C2. L: 1 kb DNA ladder. The 1 kb mark is indicated.

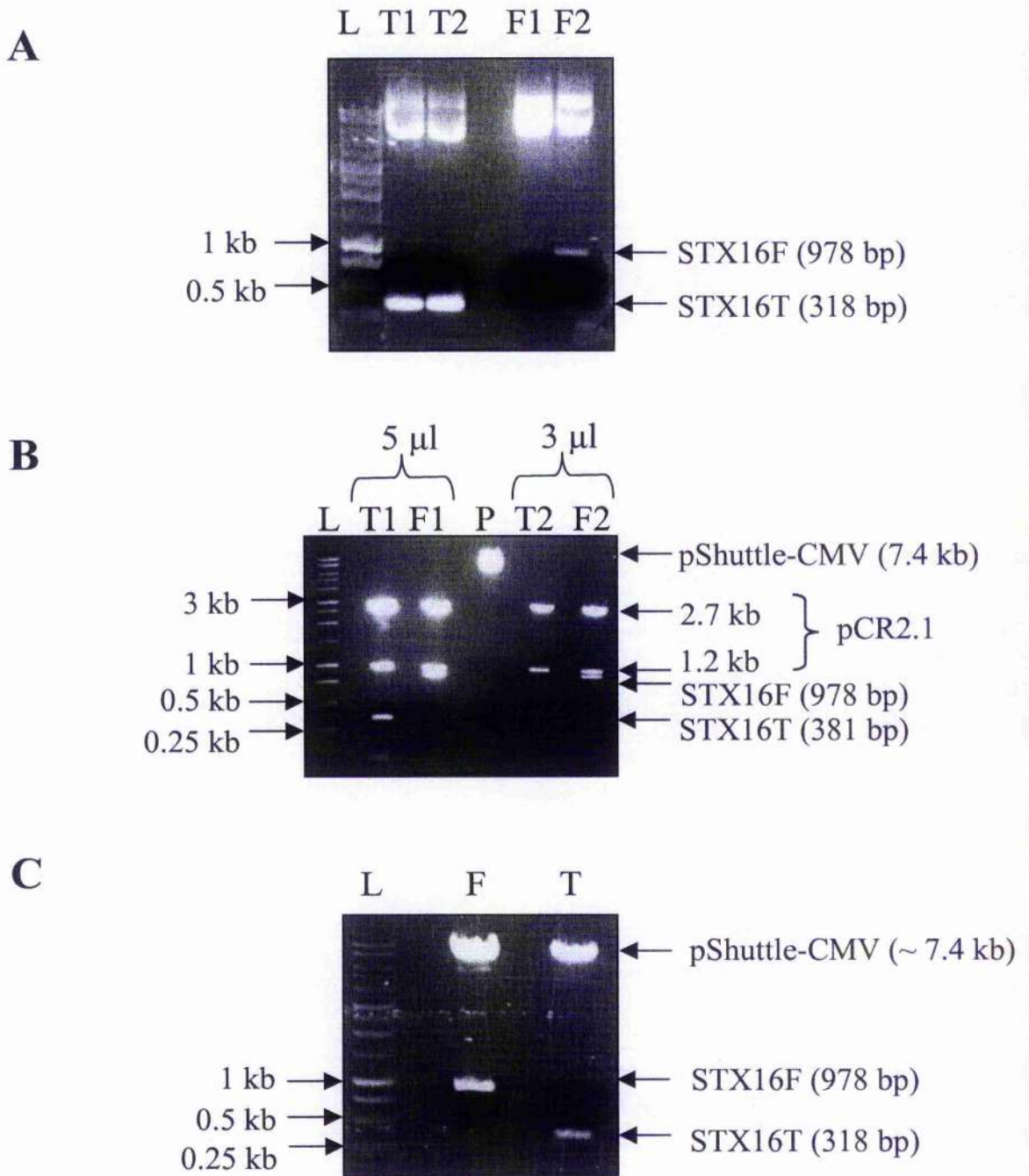


Figure 4.9 Construction of STX16T and STX16F pShuttle-CMV plasmid

A) STX16T (Lanes T1 and T2) and STX16F (Lanes F1 and F2) were PCR amplified and the resulting products were resolved on a 1 % agarose gel. Lane F2 contains a 1 kb band corresponding to STX16F and lanes T1 and T2 contain bands at 0.3 kb corresponding to STX16T cDNA. **B)** Restriction digests with *Bgl*III and *Hind*III of 5 μ l and 3 μ l respectively of STX16T (T1 and T2) and STX16F (F1 and F2) TA-cloned into pCR2.1. pCR2.1 contains an internal *Bgl*III site and as such is observed as two bands at 2.7 and 1.2 kb. STX16T can be observed at 0.3 kb in T1 and STX16F at 1 kb in F2. pShuttle-CMV vector (P) was also digested with the same enzymes. **C)** Restriction digests with *Bgl*III and *Hind*III of ligation products following ligation of STX16F (F) and STX16T (T) into pShuttle-CMV. pShuttle-CMV can be observed at ~ 7.4 kb and STX16T and STX16F at 0.3 and 1 kb respectively. L: 1 kb DNA ladder. The 3, 1, 0.5 and 0.25 kb marks are indicated.

4.4.4. Optimisation of infection of STX16cyt in 3T3-L1 adipocytes

4.4.4.1. Trial infection of HeLas

As HeLas are easier to infect, expression of STX16cyt was verified in these cells first. HeLa cells, grown to ~ 70 % confluence in 12-well plates, were infected with increasing amounts of STX16cyt adenovirus as described in Section 4.3.3 at MOIs (Section 4.3.1.6) of 1:3, 1:9, 1:33, 1:99 and 1:300 (Figure 4.10). 48 h after infection, lysates were prepared (Section 2.3.4.3) and separated on a 12 % SDS-PAGE gel. This was transferred to nitrocellulose and immunoblotted with anti- myc (Sections 2.4.4 and 2.4.5). It appeared that optimum expression was reached with an MOI of 1:99. An MOI of 1:300 perhaps resulted in cytopathic effects, resulting in less efficient expression. This experiment verified that the virus was capable of expressing myc-tagged STX16cyt.

4.4.4.2. Infection of 3T3-L1 adipocytes

3T3-L1 adipocytes were infected similarly with increasing amounts of STX16cyt adenovirus from MOIs of 1:150 to 1:300 (Figure 4.11). The infections were carried out in serum-free DMEM as described in Section 4.3.2. The optimum MOI for infection of 3T3-L1 adipocytes was found to be 1:225. This experiment verified that the virus was able to confer expression of STX16cyt in 3T3-L1 adipocytes and that this protein was successfully labelled with anti-STX16. Although myc-tagged STX16cyt has a predicted molecular weight of 34.48 kDa, it was observed to run faster through the SDS-PAGE gel than endogenous STX16 (predicted molecular weight 34.78 kDa).

4.4.4.3. Infection in 3T3-L1 adipocytes +/- 0.5 % BSA

Infection of 3T3-L1 adipocytes with adenovirus is generally carried out in the presence of 0.5 % BSA. However, previous work in our laboratory suggested that the presence of BSA during infection might interfere with GLUT4 trafficking, increasing the basal level of glucose uptake (unpublished data). Therefore, infection was carried out using the optimum MOI of STX16cyt adenovirus, (1:225) both in the presence and absence of 0.5 % BSA. Lysates were prepared (Section 2.3.4.3) and probed for the presence of STX16cyt by

immunoblotting with anti-STX16 (Sections 2.4.4 and 2.4.5). STX16cyt was expressed at similar levels in cells infected in media \pm 0.5% BSA, indicating that infections could be carried out successfully in serum-free media. This was advantageous for my study, as the infected cells were to ultimately be used to investigate GLUT4 trafficking.

However, this experiment highlighted another important point. It showed that STX16cyt was expressed to a level less than that of endogenous STX16. In order to produce effective inhibition of the endogenous protein, it was considered that it may be necessary to increase this level of expression.

4.4.4.4. $\alpha\beta$ 5 integrins

I therefore set out to investigate why the levels of STX16cyt expressed were lower than anticipated. Section 4.1.1.5 describes the process of internalisation of the adenovirus into target cells, mediated by the CAR and cellular integrins. Both $\alpha\beta$ 3 and $\alpha\beta$ 5 integrins support adenovirus internalisation (Wickham *et al.* 1993). It was suggested that the levels of these integrins can vary considerably between cell-types and that the quantification of the $\alpha\beta$ 5 integrins may be a good way of predicting the susceptibility of cells to adenovirus vectors (Takayama *et al.*, 1998). It was also reported that the expression level of integrins and the efficiency of adenovirus-mediated gene transfer varied during differentiation of a skeletal muscle cell line (Acsadi *et al.*, 1994). Therefore, I set out to determine the most favourable time post-differentiation to infect the cells with regard to the availability of the $\alpha\beta$ 3 and $\alpha\beta$ 5 integrins.

The relative quantities of $\alpha\beta$ 5 and $\alpha\beta$ 3 were measured from day 2 to day 10 post-differentiation. Therefore, 3T3-L1 fibroblasts were differentiated as described in Section 2.3.4.2 and lysates were prepared (Section 2.3.4.3) from day 2 to day 10 post-differentiation. These lysates were analysed by immunoblotting with appropriate antibodies (Figure 4.12). The bands were quantified using Scion Image software.

When exposed to heat and SDS, the integrins denature into the individual subunits, α v (150 kDa), β 3 (90-110 kDa) and β 5 (80 kDa) and so the lysates were probed with antibodies specific to each individual subunit. The α v subunit (150 kDa) further dissociates into two subunits (125 kDa and 25 kDa). The lysates were probed using anti- β 5 (80 kDa), anti- α v (125 kDa), anti- α v (25 kDa) and anti- β 3 (90-110 kDa). The antibody to the 25 kDa subunit of α v did not produce a clear result, therefore this protein was quantified by means of the

antibody specific to its 125 kDa subunit. Similarly, the $\beta 3$ subunit could not be studied, as the quality of the antibody binding was poor.

This experiment highlighted, importantly, that the αv and $\beta 5$ subunits are indeed expressed in 3T3-L1 adipocytes. It also demonstrated that the levels of both subunits do in fact change during differentiation. Figure 4.12 demonstrates an increase in the levels of each subunit, particularly the $\beta 5$ subunit, from day 2 to day 5 followed by a decrease from day 5 to day 10. Since a peak in integrin expression was reached at day 5 post-differentiation (with a 3.5-fold increase in $\beta 5$ expression over expression on day 2), infection on this day was attempted, however, the levels of STX16cyt produced were identical to those observed from day 6 infection (not shown). Maximum expression of each subunit was observed between days 4 and 6, indicating that it was indeed advantageous to carry out infections at this time (as in Section 4.4.6). Therefore, it was concluded that it was not possible to improve the expression levels of STX16cyt by changing the time of infection.

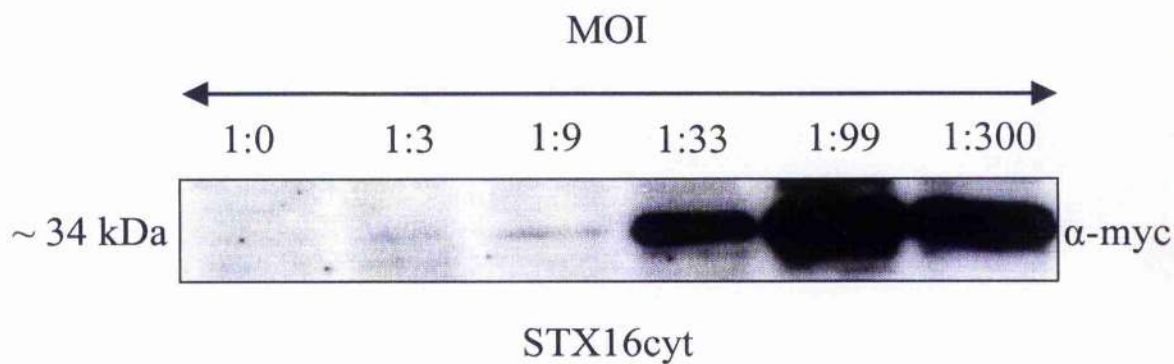


Figure 4.10 Expression of STX16cyt in HeLa cells

HeLa cells were infected with STX16cyt adenovirus as described in Section 4.3.3. Increasing MOIs were used as indicated, from no virus (1:0) to MOI 1:300. Lysates were resolved on a 12 % SDS-PAGE gel. Myc-tagged STX16cyt was visualised by Western Blotting with anti-myc.

The lysate loaded in each well corresponds to 2 % of the total lysate obtained from one well of a 12-well plate.

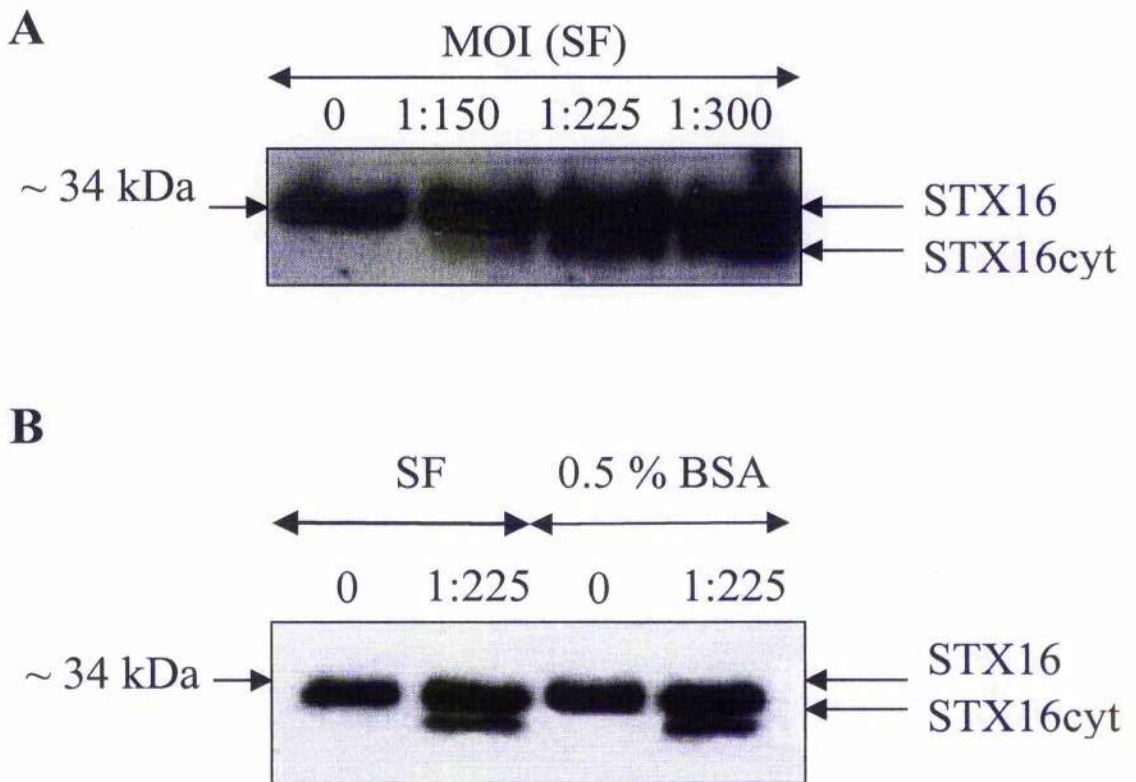


Figure 4.11 Infection of 3T3-L1 adipocytes with STX16cyt in the presence and absence of 0.5 % BSA

A) 3T3-L1 adipocytes were infected in serum-free DMEM (SF) on day 6 post-differentiation as described in Section 4.3.2 with MOIs of 1:150 to 1:300 STX16cyt adenovirus per well of a 12-well plate. Lysates were analysed by electrophoresis through a 12 % SDS-PAGE gel followed by Western Blotting with anti STX16. Both endogenous STX16 and STX16cyt can be observed. **B)** 3T3-L1 adipocytes were infected on day 6 post-differentiation with MOI 1:225 of adenovirus per well (1:225) or no virus (0), in either serum free DMEM (SF) or DMEM supplemented with 0.5 % BSA (0.5 % BSA). The lysates from this experiment were probed with anti-STX16 as above. STX16cyt is observed at similar levels when cells are infected either with or without 0.5 % BSA, indicating that infection can be carried out in serum-free medium thus avoiding the complications associated with infection in the presence of exogenous serum.

Endogenous STX16 is observed in all lysates in (A) and (B) at ~ 34 kDa as indicated. This highlights that the level of expression of STX16cyt is < 50 % of that of the endogenous protein.

The lysate loaded in each well corresponds to 2 % of the total lysate obtained from one well of a 12-well plate.

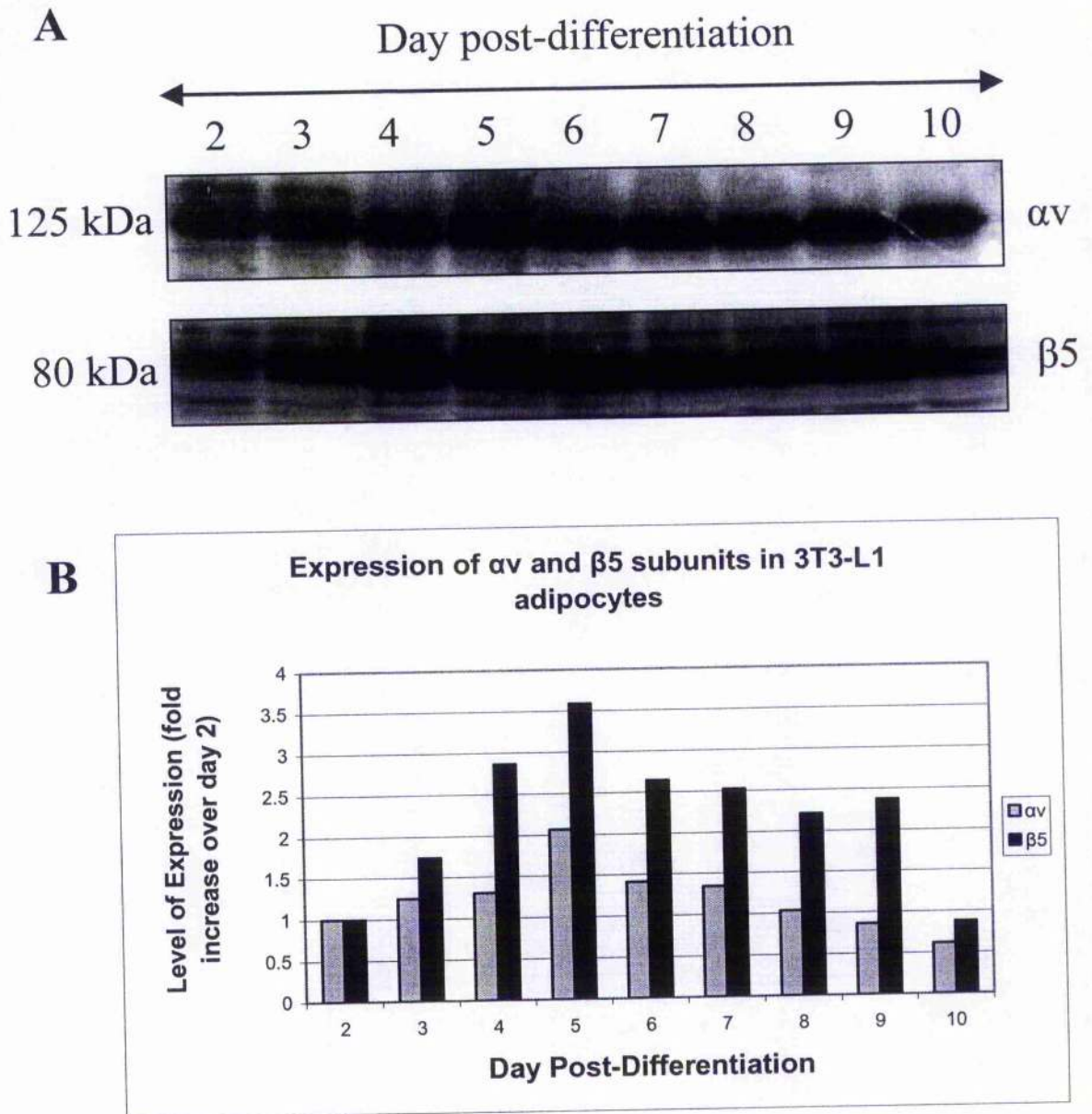


Figure 4.12 Expression of the αv and β5 subunits in 3T3-L1 adipocytes from day 2 to day 10 post-differentiation

3T3-L1 fibroblasts were differentiated as in Section 2.3.4.2. **A)** Lysates were prepared from 3T3-L1 adipocytes from day 2 to day 10 post-differentiation. These were separated by electrophoresis through a 12 % SDS-PAGE gel and probed for the β5 and the 125 kDa αv integrin subunits by immunoblotting. The lysate loaded in each well corresponds to 2 % of the total lysate obtained from one well of a 12-well plate.

B) Quantification of the data in (A) generated using Scion Image software. This highlights an increase in the expression level of αv and β5 from day 2 to day 5, followed by a decrease from day 5 to 10. Although the quantification of each receptor can be compared from day to day, the levels of the αv should not be compared to that of the β5 due to differences in the binding affinities of the antibodies.

This experiment was repeated three times with similar results. Data from a representative experiment is shown.

4.4.4.5. Why such low expression?

After confirming that the integrin mediated endocytosis of the virus was maximal, it was anticipated that the reason for poor expression of STX16cyt could relate to its cognate SM protein, mVps45 (Section 1.6.5). It has been shown that SM proteins and their t-SNAREs are expressed at 1:1 stoichiometry (Hickson et al., 2000) and that deletion of Vps45p, the yeast homologue of mVps45, results in rapid proteasomal degradation of its cognate t-SNARE, STX16 homologue Tlg2p (Bryant and James, 2001). As STX16 is upregulated post-differentiation (Shewan et al., 2003), it was speculated that perhaps the additional protein expressed by the virus exceeded the level of mVps45 and was subsequently degraded by the proteasome.

Two methods were employed to address this possibility. The first involved carrying out multiple infections earlier in the differentiation process and the second involved inhibition of proteasome function. These methods are detailed in sections 4.4.4.6 and 4.4.4.7 below.

4.4.4.6. Expression of STX16cyt is increased by infection of 3T3-L1 adipocytes on days 4 and 6 post-differentiation

As mentioned previously, infections were generally carried out on day 6 post-differentiation to allow for 48 h incubation time before the assay on day 8 when the cells should be fully differentiated. Previous work indicated that STX16 was upregulated by 4.6 ± 2.1 fold ($n=4 \pm$ SEM) upon differentiation of 3T3-L1 fibroblasts into adipocytes, by day 8 post-differentiation (Shewan et al., 2003). It was reasoned that if the cells were infected before or during the upregulation of STX16, perhaps more STX16cyt would be expressed by the virus at the expense of endogenous STX16. Therefore, cells were subjected to multiple, duplicate or single infections, 48 h apart, on days 2, 4, and 6, days 4 and 6 or day 6 only post-differentiation. Each infection was carried out using an MOI of 1:225 per well of a 12-well plate as described in Section 4.3.2.

Figure 4.13 shows that infection on days 2, 4 and 6 post-differentiation increased the expression of STX16cyt most dramatically with ~ 2.75-fold increase in protein produced, compared to infection on day 6 alone. However, these multiple infections, beginning only

one day after differentiation was induced, appeared to interfere with the differentiation process. Assessment of these cells under a 20 × objective lens indicated that they possessed fibroblast-like morphology, even at day 10 post-differentiation (not shown). However, cells infected on days 4 and 6 post-differentiation differentiated well and produced more STX16cyt (~ 1.5-fold increase) compared to those infected on day 6 only. Therefore this was the chosen method to carry out the functional assays detailed in Chapter 5. Surprisingly, the anticipated reduction in the level of endogenous protein with the corresponding increase in STX16cyt was not observed. This will be discussed below in Section 4.5.

4.4.4.7. Expression of STX16cyt is increased when 3T3-L1 adipocytes are treated with Proteasome Inhibitors (MG132) following infection on day 6 post-differentiation

The proteasome is the second major cellular compartment for proteolysis. Located abundantly in both the cytoplasm and nucleoplasm, often accounting for up to 1 % of total cellular protein, proteasomes are large, cylindrical structures composed of multiple protein subunits. There are several proteolytic active sites in the structure, which combine to degrade proteins to small peptides (Bochtler et al., 1999). The best-characterised targeting mechanism to the proteasome involves the reversible, covalent linkage of a small protein, ubiquitin, onto the target protein (Bonifacino and Weissman, 1998). Tlg2p could be stabilised in cells lacking Vps45p by inhibition of proteasome function. (Bryant and James, 2001).

Therefore, in the second method employed to increase expression of STX16cyt in 3T3-L1 adipocytes, the cells were treated with proteasome inhibitors. MG132 (Z-Leu-Leu-Leu-CHO, C₂₆H₄₁N₃O₅) is a potent, cell permeable and selective proteasome inhibitor (BIOMOL International, product data). MG132 was prepared as described in Section 4.3.4 by dissolving in DMSO.

3T3-L1 adipocytes were infected with MOI 1:225 STX16cyt adenovirus on day 6 post-differentiation (Section 4.3.2.). Treatment with 50 μM MG132 on day 7 post-differentiation was carried out as described in Section 4.3.4 for 4 to 16 h as indicated in Figure 4.14. The cells remained healthy throughout the treatment as judged by morphological analysis under a 20 × objective lens (not shown). Lysates were prepared 48

h after infection and analysed by gel electrophoresis and immunoblotting with anti-STX16 (Figure 4.14). The level of STX16cyt expressed was dramatically increased with MG132 treatment. Treatment of the cells with MG132 for 16 h was capable of increasing the level of STX16cyt produced by almost 10-fold. The level of endogenous STX16 remained constant during the treatment. STX16cyt was not observed in cells treated with 50 μ M MG132 only or DMSO only (the solvent for MG132) in the absence of virus and no change in the level of endogenous STX16 was observed. This indicates that the additional STX16cyt observed in infected cells treated with MG132 was indeed expressed by the virus and was not a product of any other treatment.

4.4.4.8. Levels of IRAP, mVps45, STX4, Vti1a, VAMP2 and endogenous STX16 remain constant with MG132 treatment

Figure 4.14 demonstrates that the level of endogenous STX16 was not affected when cells were exposed to MG132 proteasome inhibitors. It was decided to investigate if the treatment altered expression of a range of representative proteins relevant to my study or if the effect was indeed specific to STX16cyt. Therefore the lysates prepared in Section 4.4.4.7 were analysed by Western Blotting for the presence of IRAP, mVps45, STX4, Vti1a and VAMP2 by probing with appropriate antibodies. Figure 4.15 shows that the levels of all these proteins remained constant with MG132 treatment.

As mentioned above, the level of endogenous protein remained constant, suggesting that STX16 is not normally subject to proteasomal degradation, as inhibiting proteasome function did not result in an increase in this protein. Similarly, the levels of Vti1a, a t-SNARE known to interact with STX16 in a functional SNARE complex (Bose et al., 2005; Mallard et al., 2002) (this study, Chapter 3) and VAMP2 and STX4, chosen as representative examples of v- and t-SNAREs known to be involved in GLUT4 trafficking (Foster and Klip, 2000), were unchanged.

It has been reported that inhibition of proteasome function, mediated by MG132, decreased the level of GLUT4 in the cell (Cooke and Patel, 2005), a finding that could potentially be detrimental to my functional studies. The lysates were therefore probed with antibodies to GLUT4; however, the results were unclear due to poor quality of antibody binding at this time. IRAP is known to traffic similarly to GLUT4 (Garza and Birnbaum, 2000) and as

such the levels of this protein were analysed and found to remain uniform in the absence of proteasome function.

Given that t- SNAREs and their SM proteins were shown to be expressed at a 1:1 ratio (Hickson et al., 2000), it was deemed necessary to investigate how the levels of mVps45 were affected. Surprisingly, the level of mVps45 remained constant although the level of its cognate t-SNARE increases significantly. This will be discussed in more detail in Section 4.5.

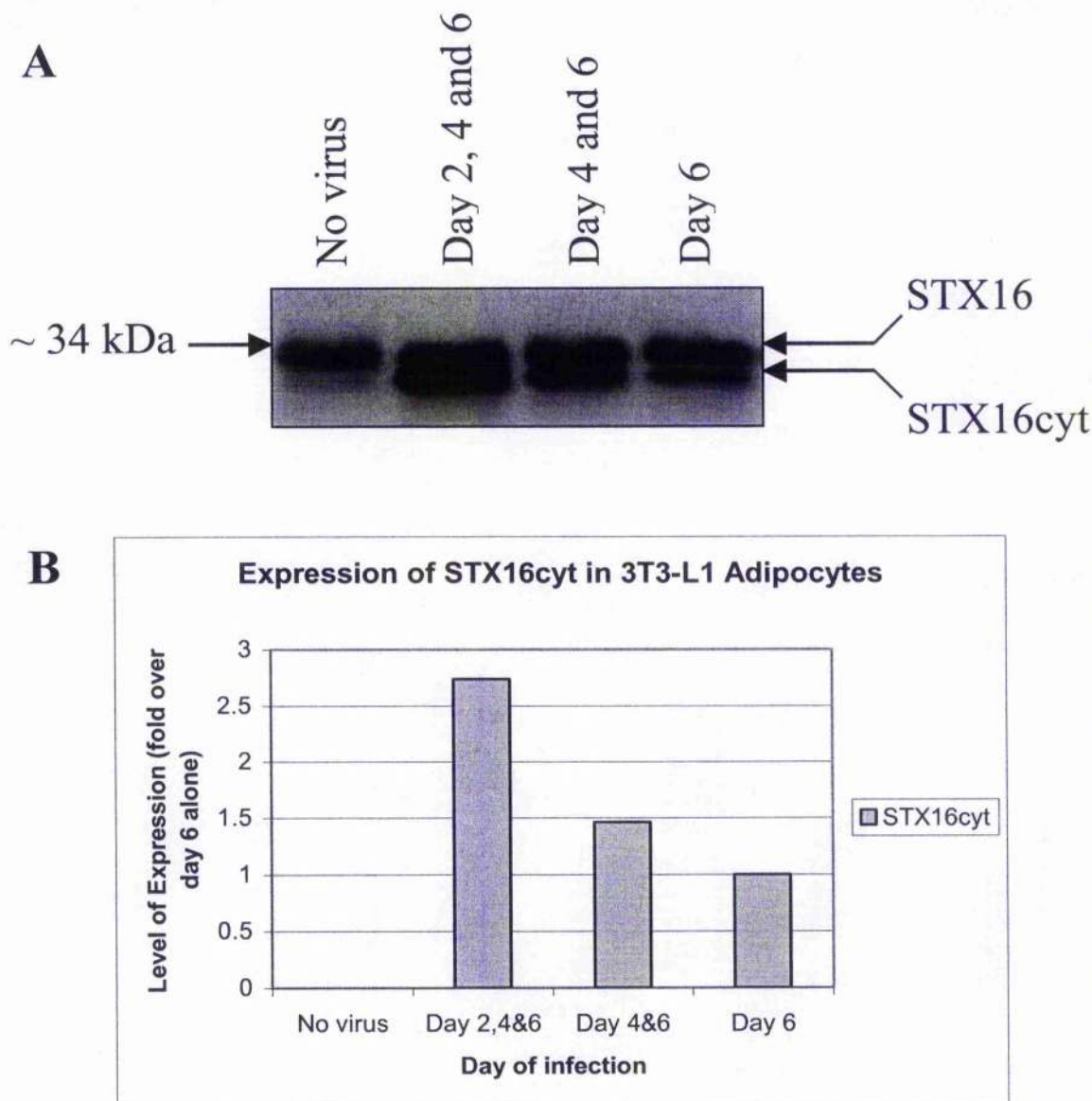


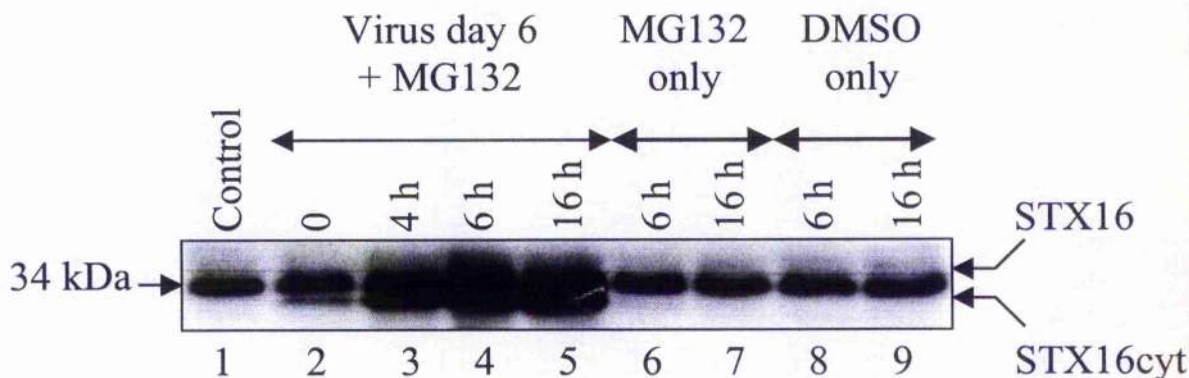
Figure 4.13 Expression of STX16cyt in 3T3-L1 adipocytes is increased when cells are infected on days 4 and 6 post-differentiation

3T3-L1 adipocytes, differentiated as described in Section 2.3.4.2, were subjected to infection with MOI 1:225 STX16cyt adenovirus (Section 4.3.2) on days 2, 4 and 6, days 4 and 6 or day 6 only, as indicated. Cells treated in the same way but without virus provided a control (no virus). **A**) Immunoblot of the cell lysates with anti-STX16. **B**) Quantification of data in (A). Although cells infected on days 2, 4 and 6 post-differentiation displayed the most dramatic increase in the expression of STX16cyt compared to infecting on day 6 only (> 2.5 fold increase), the morphology of these cells remained fibroblastic during the differentiation process, suggesting that infection early in the differentiation process interferes with the process. Infections on days 4 and 6 post-differentiation increased the level of expression of STX16cyt, compared to infecting on day 6 only (~ 1.5 fold). Cells treated in this way were observed to differentiate normally and expression of STX16cyt was approximately equal to that of endogenous STX16. The level of endogenous protein (indicated at 34 kDa) was not significantly altered by multiple infections.

The lysate loaded in each well corresponds to 2 % of the total lysate obtained from one well of a 12-well plate.

This experiment was repeated multiple times with similar results. Data from a representative experiment is shown.

A



B

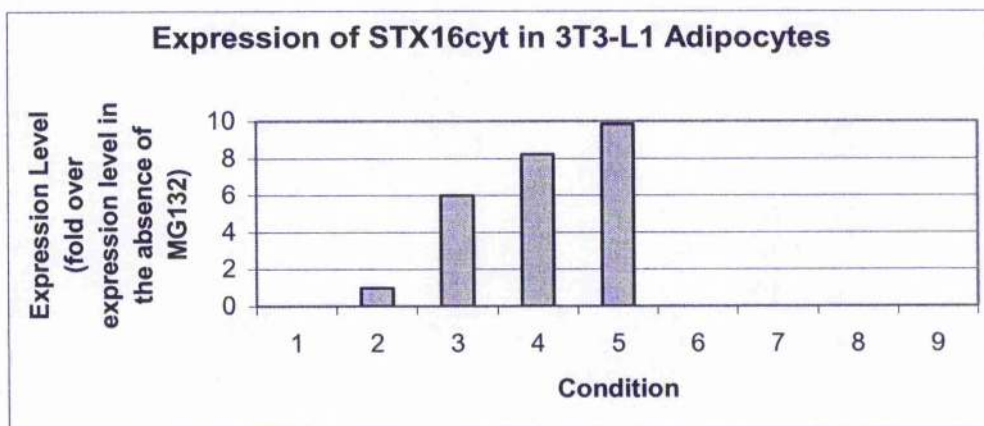


Figure 4.14 Stabilisation of STX16cyt expression with MG132

Lysates prepared from 3T3-L1 adipocytes treated as indicated were resolved on a 12 % SDS-PAGE gel and analysed by Western Blotting with anti- STX16. **A)** 3T3-L1 adipocytes were infected with MOI 1:225 STX16cyt adenovirus on day 6 post-differentiation as described in Section 4.3.2. 50 μ M MG132 was then added for 0, 4, 6 or 16h (lanes 2 - 5). Control cells were untreated (Lane 1), treated with 50 μ M MG132 only (Lanes 6 and 7) or DMSO only (Lanes 8 and 9) for 6 or 16 h. **B)** Quantification of the levels of STX16cyt produced in cells treated as in (A). The numbers on the x-axis correspond to the numbers below each lane in (A). This indicates that treatment with MG132 for 16 h increases the expression of STX16cyt by ~10-fold compared to infection on day 6 alone.

The lysate loaded in each well corresponds to 2 % of the total lysate obtained from one well of a 12-well plate.

This experiment was repeated three times with similar results. Data from a representative experiment is shown.

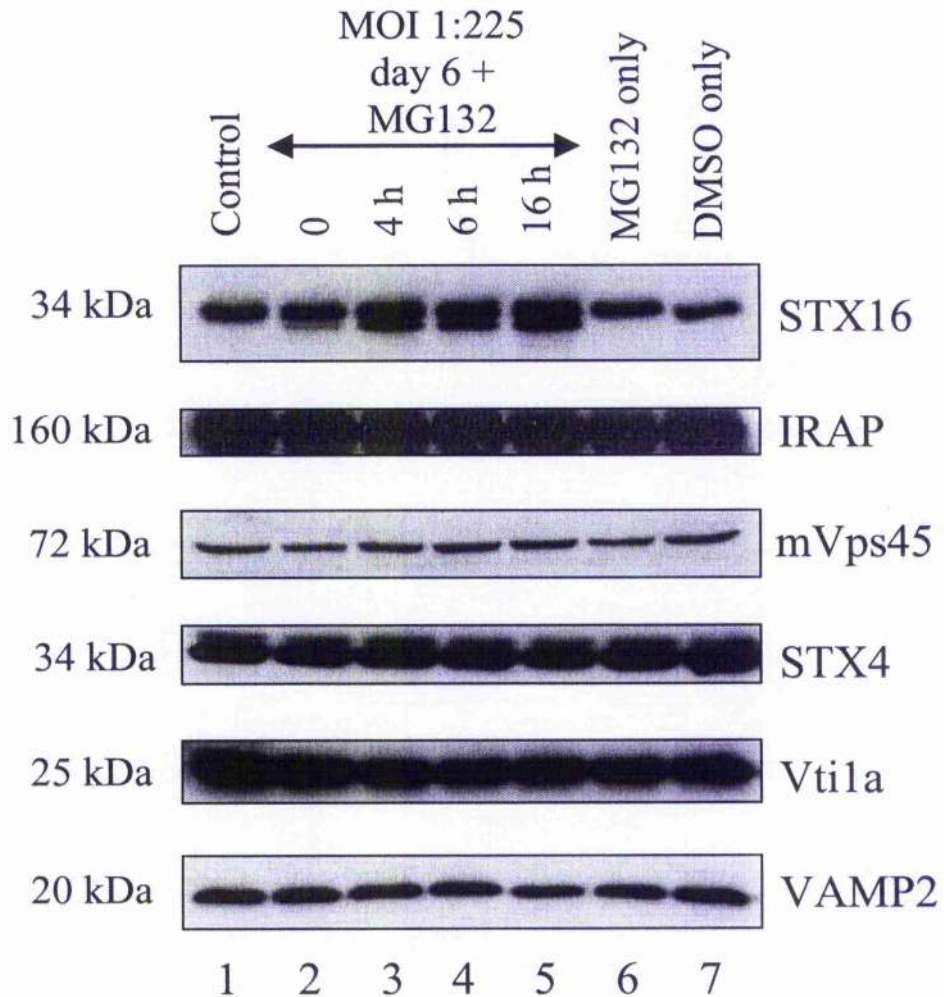


Figure 4.15 Levels of IRAP, mVps45, STX4, Vti1a, VAMP2 and endogenous STX16 remain constant following treatment with MG132 proteasome inhibitors

Lysates prepared from 3T3-L1 adipocytes treated as indicated were resolved on a 12 % SDS-PAGE gel and the levels of IRAP, mVps45, STX4, Vti1a, VAMP2 and STX16 were analysed by immunoblotting with relevant antibodies. 3T3-L1 adipocytes were infected with MOI 1:225 STX16cyt adenovirus on day 6 post-differentiation as described in Section 4.3.2. 50 μ M MG132 was then added for 0, 4, 6 or 16h (lanes 2 - 5). Control cells were untreated (Lane 1), treated with 50 μ M MG132 only for 16h (Lane 6) or DMSO only for 16 h (Lane 7).

The lysate loaded in each well corresponds to 2 % of the total lysate obtained from one well of a 12-well plate.

4.4.4.9. Optimisation of STX16F in 3T3-L1 adipocytes

Expression of STX16F was optimised based on the findings for STX16cyt above (Section 4.4.4). It was anticipated that expression of STX16F might be subject to the same limitations experienced when expressing STX16cyt, requiring stabilisation by mVps45. In support of this notion, Bryant and James (Bryant and James, 2001) were unable to overproduce Tlg2p significantly in wild-type cells, presumably because levels of Vps45p became rate limiting.

STX16F expression was optimised in 3T3-L1 adipocytes, using the conditions indicated in Figure 4.16. Lysates were analysed for the presence of STX16F by immunoblotting with anti-STX16 (Figure 4.16). Although myc-tagged-STX16F (predicted molecular weight 37.25) is effectively heavier than endogenous STX16 (predicted molecular weight 34.78) it was observed to resolve at a lower molecular weight on a 12 % SDS-PAGE gel. This could indicate that the confirmation of STX16F is different from that of endogenous STX16, perhaps caused by the presence of the myc-tag. A similar phenomenon was observed for STX16cyt (Section 4.4.4.2) and the cytosolic domain of STX6, which also resolved at lower molecular weights than anticipated (Percera et al., 2003).

In contrast to STX16cyt, infection with an MOI of only 1:90 STX16F adenovirus on day 6 post-differentiation was capable of producing levels of STX16F almost equalling that of the endogenous protein. However, as for the cytosolic domain, it appeared that the maximum protein expressed during one infection was reached with an MOI of 1:225, with no significant increase in protein expression observed with an MOI of 1:300.

As anticipated, double infection of the cells on days 4 and 6 with MOI 1:225 increased the level of STX16F produced, compared to infection on day 6 alone, and appears to be accompanied by a small decrease in endogenous STX16. This finding perhaps supports the theory that infection before or during the upregulation of STX16, induced by differentiation (Shewan et al., 2003), results in more STX16F expressed by the virus at the expense of endogenous STX16.

Expression of STX16F was dramatically enhanced by treatment with MG132 following infection. Cells infected with MOI 1:225 STX16F virus per well on day 6 (Section 4.3.2.) were exposed to 50 μ M MG132 overnight from the evening of day 7 to day 8 (Section

4.3.4). As for STX16cyt, this large increase in STX16F observed with the inhibition of proteasome activity, supports the hypothesis that t-SNARE in excess of and therefore not stabilised by its cognate SM protein is subject to proteasomal degradation. Intriguingly, in these cells a significant decrease in the level of endogenous STX16 is also observed. The reason for this is at present unclear but will be discussed in more detail in Section 4.5.

4.4.4.10. Optimisation of STX16T in 3T3-L1 adipocytes

It was anticipated that the expression of STX16T would not present the same problems encountered with STX16cyt or STX16F. It was hypothesised that removal of the potential autoinhibitory H_{abc} domain, including the mVps45 binding-site (Dulubova et al., 2002) and the hypothesised phosphorylation site (Chapter 3) would remove any need for regulation or stabilisation (Figure 4.6). Bryant and James found that expression of the similarly truncated Tlg2p, bypassed the need for stabilisation by Vps45p (Bryant and James, 2001).

Once again the methods used to optimise the expression of STX16cyt (Section 4.4.4) were utilised here. 3T3-L1 adipocytes were subjected to the conditions indicated in Figure 4.17. Lysates were analysed for the presence of STX16T by immunoblotting with anti-STX16 (Figure 4.17). Importantly, Figure 4.17 shows that the heavily truncated STX16T is recognised by anti-STX16, an extremely important feature in my study to allow detection of both STX16T and endogenous STX16. However, it should be noted that the binding affinity of the antibody for STX16T is unknown. HA-tagged STX16T is a small 14.8 kDa protein that resolves at ~ 15 kDa on an SDS-PAGE gel and therefore was too small to be observed on a 12 % gel. As such, a 15 % gel was used to visualise this protein, and although full length STX16 (~34 kDa) is best resolved on a 12 % gel, it is, nonetheless, still observed.

Figure 4.17 shows that infection on day 6 alone with MOI 1:225 of virus could not be detected compared to the level of endogenous protein in the cell lysate. Double infection with an MOI of 1:225 on days 4 and 6 increased this to detectable levels, therefore, this method was used to optimise the expression, with increasing MOI in each infection. Intriguingly, the expression of STX16T, unlike STX16cyt or STX16F (Figures 4.11 and 4.16), was dose dependent, with a steady increase in protein produced from MOI 1:225 to 1:900 on days 4 and 6 post-differentiation. An MOI higher than 1:900 was not attempted, due to the potential adverse effects that could be experienced by the cells with such a high

dose of virus. However, it is highly probable that the level of STX16T would have continued to rise with higher MOI.

Unexpectedly, treatment with MG132 following infection (Section 4.3.4) also increased the level of STX16T expressed compared to infection in the absence of proteasome inhibitors (Figure 4.17), but with no obvious decrease in the level of endogenous STX16 as noted for STX16F in the same experiment.

These intriguing effects will be discussed in Section 4.5.

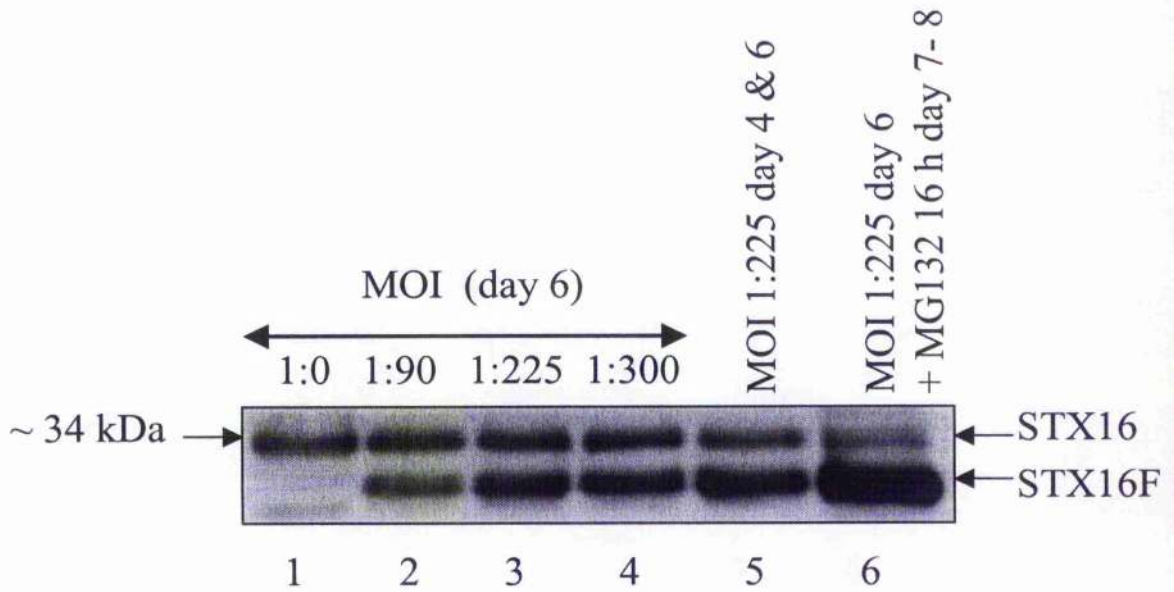


Figure 4.16 Optimisation of expression of STX16F in 3T3-L1 adipocytes

3T3-L1 adipocytes were infected as described in Section 4.3.2 with MOIs of 1:0, 1: 90, 1:225 or 1:300 STX16F adenovirus per well as indicated on day 6 post-differentiation (lanes 1-4), MOI 1:225 per well on both days 4 and 6 post-differentiation (lane 5) or MOI 1:225 day 6, followed by treatment with 50 μ M MG132 for 16 h overnight from day 7 to day 8 post-differentiation (lane 6). Lysates prepared from these cells on day 8, 48 h after infection, were subjected to SDS-PAGE electrophoresis and analysed for the presence of STX16F by immunoblotting with anti-STX16. Endogenous STX16 can be observed at 34 kDa as indicated. Although STX16F is heavier than endogenous STX16, due to the presence of the N-terminal myc tag, it was found to resolve at a lower molecular weight on the 12 % SDS-PAGE gel.

The lysate loaded in each well corresponds to 2 % of the total lysate obtained from one well of a 12-well plate.

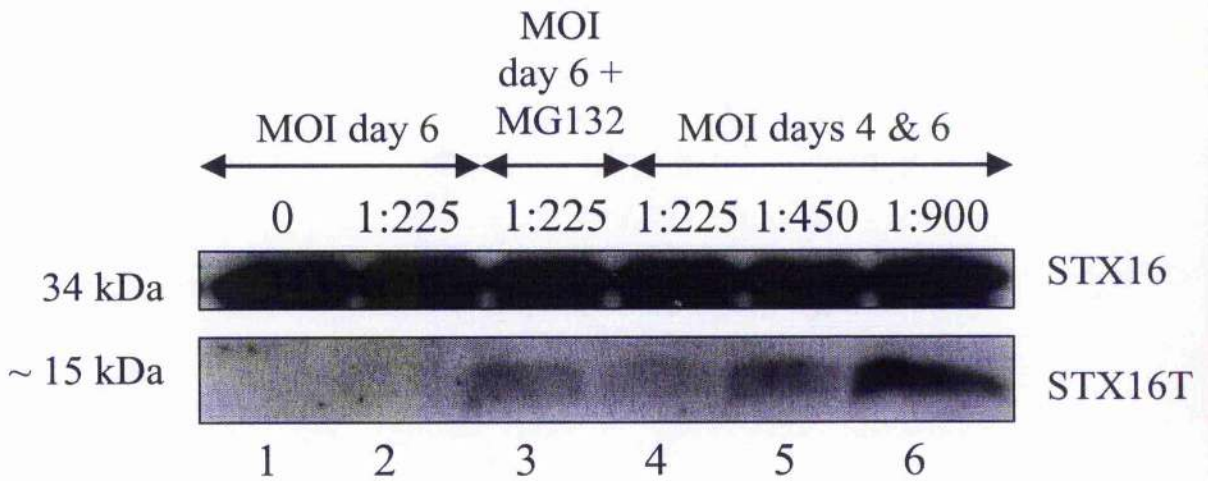


Figure 4.17 Optimisation of STX16T expression in 3T3-L1 adipocytes

3T3-L1 adipocytes were infected as described in Section 4.3.2 with MOIs of 1:0 or 1:225 day 6 (Lanes 1 and 2), MOI 1:225 day 6, followed by treatment with 50 μ M MG132 proteasome inhibitors for 16 h overnight on day 7 to day 8 post-differentiation (lane 3), or MOIs of 1:225, 1:450 or 1:900 STX16T adenovirus per well on both days 4 and 6 post-differentiation (Lanes 4-6). Lysates prepared from these cells on day 8, 48 h after infection, were subjected to SDS-PAGE electrophoresis on a 15 % gel and analysed for the presence of STX16T by immunoblotting with anti-STX16. Endogenous STX16 (upper panel) is better resolved on a 12 % gel; however, a 15 % gel was used to allow successful detection of STX16T (lower panel). Both panels are from the same gel, however, they should not be directly compared, as the affinity of the STX16 antibody to STX16T is unknown.

The lysate loaded in each well corresponds to 2 % of the total lysate obtained from one well of a 12-well plate.

4.5. Discussion

Previous work suggested a possible role for STX16 in GLUT4 trafficking in 3T3-L1 adipocytes (Perera et al., 2003; Shewan et al., 2003) (Section 1.8, Chapter 1). I set out to investigate its precise function by analysing the effects of expressing STX16 mutants in 3T3-L1 adipocytes. Transfection of 3T3-L1 adipocytes by standard transfection methods is poor (Gnudi et al., 1997) and would not produce the required levels of protein for my study. Adenovirus vectors, on the other hand, are known to be highly efficient in their ability to transfer genes into even highly differentiated cells and the efficiency is not limited in non-dividing cells (Russell, 2000). As such this method has been used for the successful introduction of transgenes into 3T3-L1 adipocytes (Bose et al., 2001; Emoto et al., 2001; Sakaue et al., 1997). This Chapter describes the generation of recombinant adenoviruses capable of expressing STX16 mutants and the optimisation of their expression in 3T3-L1 adipocytes.

Of course, adenovirus-mediated gene transfer is subject to limitations such as the availability of the CAR proteins and $\alpha\beta 5$ integrins, which allow the internalisation of the virus, on the cell type in question (Takayama et al., 1998; Wickham et al., 1993). Furthermore, much overlooked during the development of adenovirus technology was the immune response provided by the host (Russell, 2000). Nonetheless, the adenovirus remains a pivotal tool in the transfer of genes to cells that would be otherwise inaccessible. Homologous recombination and production of the adenoviruses used in this study was carried out at ViraQuest Inc., because their patented technology (Anderson et al., 2000) allows for the production of adenoviruses considerably quicker than the standard current methods available for laboratory use and have little to no wild-type contamination or unwanted complicating E1 sequences.

Recombinant adenoviruses were generated to express full length STX16 (STX16F), the cytosolic domain (STX16cyt) and an N-terminal truncation mutant (STX16T) (Figure 4.4). STX16cyt was required to inhibit the effects of the endogenous protein (Olson et al., 1997; Perera et al., 2003; Tellam et al., 1997; Volchuk et al., 1996); STX16T, lacking the putative H_{abc} domain, was anticipated to act as a constitutively active version of the wild type protein (Bryant and James, 2001), by mimicking a hypothetical open conformation; and STX16F, with its ability to amplify the effects of the endogenous protein (Pagan et al.,

2003; Thurmond et al., 1998) was generated to provide a control for experiments involving STX16T. The effects of these proteins on GLUT4 trafficking are described in Chapter 5. However, I found that the expression capabilities of STX16cyt, STX16T and STX16F were very informative in terms of the properties of those particular STX16 domains, the associated proteins and their environment.

The study began by looking at the infection capabilities of the adenovirus in 3T3-L1 adipocytes. Infection of the cells in serum free media produced levels of STX16cyt almost identical to those produced by standard infection conditions in the presence of exogenous serum (Figure 4.11). Infection in serum free media limited any potentially detrimental effects on GLUT4 trafficking, which may occur in cells infected in exogenous serum. In addition, it was shown that 3T3-L1 adipocytes are in possession of the $\alpha\beta 5$ integrins, required for internalisation of the virus, and that the levels of these proteins are elevated between days 4 and 6 post-differentiation (Figure 4.12), corresponding to the time infections were carried out. It is likely that a number of additional factors could be responsible for the low expression levels, as discussed below.

After exhausting the possibilities regarding limitations of the virus and the expression system, it was decided to look at the properties of STX16 with regard to its ability to be overproduced in adipocytes. As mentioned previously, it has been shown that SM proteins and their t-SNAREs are expressed at 1:1 stoichiometry (Hickson et al., 2000), a finding that could suggest that, at steady state, STX16 and mVps45 are present at an equal level. It has not yet been shown that mVps45 is directly related to / required for STX16 stability, however, I think that this possibility is highly likely with regard to my virus studies (discussed below). The results suggest that STX16F and STX16cyt require stabilisation from mVps45. STX16 is upregulated post-differentiation, however, it is not currently known if this is also the case for mVps45. Further experiments will be required to test this possibility. Nonetheless, it is probable that the upregulation of STX16, combined with protein produced by the virus (STX16F or STX16cyt), eventually exceeds the level of mVps45. Deletion of Vps45p in yeast resulted in the rapid proteasomal degradation of its cognate t-SNARE, Tlg2p (Bryant and James, 2001). This could imply that the excess STX16F or STX16cyt would be targeted for proteasomal degradation. STX16T, on the other hand was not anticipated to be subject to such limitations. Truncation of the N-terminal 230 residues of Tlg2p abolished binding to Vps45p and was found to bypass the requirement for Vps45p stabilisation (Bryant and James, 2001). As such, it was anticipated that the similarly truncated STX16T, devoid of the mVps45 binding site (Dulubova et al., 2002) and inhibitory H_{abc} domain (Figure 4.6) would be capable of overexpression.

Recombinant adenoviruses were used previously in our laboratory to express the cytosolic domains of STX6, STX8 and STX12 in 3T3-L1 adipocytes (Perera et al., 2003). The expression level of each SNARE protein was found to vary but the reasons for these differences were not fully explored in terms of the individual properties of the target proteins. STX16cyt could not be expressed to a similar level as that of the cytosolic domain of its partner SNARE, STX6 (Perera et al., 2003), using the same method of adenoviral mediated gene transfer. Both proteins are known to be upregulated during differentiation (Shewan et al., 2003), yet STX6 overexpression is not limited because of this. I anticipate that the main difference in expression capability of these two proteins is due to the fact that STX16, but not STX6, interacts directly with mVps45 (Dulubova et al., 2002) and correlate this to a requirement for stabilisation, not required by STX6. The requirement for a 1:1 stoichiometry of the t-SNARE and SM protein (Hickson et al., 2000) will become rate limiting for STX16. Interestingly, Bryant and James were unable to overproduce Tlg2p significantly in wild-type cells, presumably because levels of Vps45p become rate limiting (Bryant and James, 2001).

Expression of STX16cyt and STX16F could be increased by infecting the cells on days 4 and 6 post-differentiation, compared to day 6 alone (Figures 4.13 and 4.16). It was hypothesised that infection of the cells earlier in the differentiation process would allow greater expression of STX16cyt or STX16F by the virus at the expense of endogenous STX16. In favour of this hypothesis, a small corresponding decrease in the level of endogenous STX16 was observed in cells producing STX16F. However, this effect was not observed when STX16cyt was overproduced. The difference could be due to the fact that STX16F requires membrane insertion and is therefore in more direct competition with the endogenous protein.

Similarly, the expression levels of STX16cyt and STX16F were increased dramatically when proteasome function was inhibited using MG132 (Figures 4.14 and 4.16). This is in agreement with the suggestion that any t-SNARE (Qa-SNARE) in excess of its SM protein is subject to proteasomal degradation (Bryant and James, 2001). Very intriguing is the fact that the level of endogenous STX16 decreased significantly with proteasome inhibitor treatment in cells expressing STX16F (Figure 4.16). The reason for this is at present unclear. However, it could suggest that the endogenous STX16 must somehow be disposed of to support the large increase in STX16F. Clearly, this route of disposal is not via the proteasome but perhaps another pathway for the degradation of this unstabilised protein exists. It is particularly important to notice here that the level of mVps45 remained constant with proteasome inhibitor treatment (Figure 4.15), adding weight to the theory

that endogenous STX16 in excess of mVps45 had to be degraded. The absence of this effect in STX16cyt could once again be due to its cytosolic nature.

Although it was anticipated that expression of STX16T would not be subject to such limitations, the levels produced were unexpectedly poor in cells infected on day 6 alone. Equally surprising was the fact that expression could be increased using the same methods as STX16cyt and STX16F, by infection on days 4 and 6 or by treatment with MG132 (Figure 4.17). Some possible explanations for these effects will be discussed below. It is important to note, however, that the increase in STX16T expression using these methods could not be quantified, as the level of STX16T produced from infection on day 6 alone could not be detected by the antibody. It is not therefore possible to determine if the increases in expression of STX16T occur to the same extent as for STX16cyt and STX16F, and as such, it is possible that additional factors, such as those described above, are responsible for the increases observed for these proteins.

The increase in STX16T observed after double infection on days 4 and 6 may be simply due to the additive effects of protein produced from two infections, which, of course, could also be responsible for the increase observed in STX16cyt and STX16F. However, the decrease in endogenous STX16 with increasing expression of STX16F (Figure 4.16) is perhaps more indicative of the need for stabilisation described above. Most significant with regard to this theory is that, unlike STX16cyt and STX16F, the expression of STX16T was dose dependent and increased with increasing (MOI) virus (Figure 4.17). Expression of STX16cyt and STX16F appeared to reach a plateau, which could not be increased by the addition of more virus in a single infection (Figures 4.11 and 4.16). This plateau was not due to cytopathic effects because this would also have been apparent for STX16T, which was infected with a higher MOI. Although this notion is based on the comparison of single infections for STX16cyt and STX16F, and double infections for STX16T, I reasoned that expression of STX16cyt and STX16F would similarly reach a plateau with increasing levels of virus in a double infection. In fact this was shown to be the case for STX16F later in the study when double infection with an MOI greater than 1:225 in each infection did not increase the level of STX16F produced (Figure 5.5, Chapter 5). This could support the notion that STX16 in possession of an N-terminal domain requires stabilisation by mVps45 and the truncated form, lacking this domain and the mVps45 binding site bypasses the requirement for this stabilisation, a finding supported by the yeast homolog, Tlg2p (Bryant and James, 2001).

Surprisingly, proteasome inhibitor treatment also increased the level of STX16T produced (Figure 4.17). It was anticipated that STX16T would not be subject to proteasomal degradation as it was not dependent on mVps45 stabilisation. This highlights the possible alternative explanation that all adenoviral products are subject to proteasomal degradation, especially considering the levels of native proteins, such as mVps45, VAMP2, Vti1a, IRAP and STX4 are unaffected by the treatment (Figure 4.15). Perhaps the introduction of foreign genes into 3T3-L1 adipocytes results in their products being subject to degradation by the proteasome. However, this was not the case for the cytosolic domains of STX6 and STX12 (Perera et al., 2003), which could be expressed to 16-fold the level of the endogenous protein with one single infection. Perhaps there is a property inherent in STX16, which makes overexpression of even the truncated domain subject to limitations not observed for other Syntaxins such as STX6, STX8 or STX12 (Perera et al., 2003). So far, I have based my model of STX16 function on Tlg2p but have not addressed the possibility that STX16 may in fact be different from Tlg2p and that perhaps even STX16T requires stabilisation. Half-life studies could be very informative here, to compare the half-life of the STX16 mutants and other syntaxins expressed by the adenovirus.

In general, I feel that the differences in expression capabilities of the STX16 mutants provide the first shreds of evidence towards proving the existence of STX16 active and inactive conformations. I hypothesise that these conformations are stabilised by mVps45, which may also be required to facilitate its transition to an active state. Whether these conformations resemble the open and closed conformations described for STX1a with the SM binding to the closed conformation, or are more like those observed for other intracellular SNARE complexes (Dulubova et al., 1999; Rizo and Sudhof, 2002) (Section 1.5.6) is yet to be discovered, although my immunoprecipitation studies suggest that mVps45 does not bind to the intact SNARE complex (Section 3.5.2.5, Chapter 3). Further studies, for example NMR or protein crystallography will be required to fully test these possibilities. NMR studies of the N-terminal region of Tlg2p predicted that, although it shared little homology with the corresponding domains of other syntaxins known to be in possession of an H_{abc} domain, it adopted a structure characteristic of a three helical domain (Dulubova et al., 2002). Based on the homology between STX16 and Tlg2p, I predict that STX16 does also. However, the study also concluded that Tlg2p did not adopt a closed conformation (Dulubova et al., 2002). In the case of STX1a, the three α -helical N-terminal domain is believed to mimic the three helices provided by their cognate SNAREs in a functional SNARE complex (Dulubova et al., 1999; Misura et al., 2001). If Tlg2p, and correspondingly STX16, do not adopt a closed conformation, what then could be the

function of this three helical N-terminal domain? This is an intriguing question, which will require careful further studies.

The implications of expression of the STX16 domains on GLUT4 trafficking will be presented in Chapter 5.

Chapter 5

The role of STX16 in the intracellular trafficking of GLUT4

5. The role of STX16 in the intracellular trafficking of GLUT4

5.1. Introduction

In an effort to resolve the function of STX16 in GLUT4 trafficking, recombinant adenoviruses were prepared to express wild-type STX16, STX16F, and STX16 mutants, STX16cyt and STX16T, in 3T3-L1 adipocytes (Chapter 4). This Chapter details the effects of these proteins on GLUT4 trafficking in 3T3-L1 adipocytes as well as the effect of expression of STX16cyt on ACRP30 secretion from these cells. As a complimentary approach to measuring GLUT4 trafficking in cells overexpressing the dominant negative STX16cyt, STX16 expression was knocked-down using a specific Morpholino Antisense Oligonucleotide and the consequences for insulin-stimulated 2-Deoxy-D-glucose (deGlc) uptake were evaluated.

5.1.1. Morpholino Antisense Oligonucleotides (MAOs)

Morpholino Antisense Oligonucleotides (MAOs) are advanced tools for blocking sites on RNA to obstruct protein expression. With properties including stability, nuclease-resistance, efficacy, long-term activity, water solubility, low toxicity and high specificity, they have become widely used as gene knockdown reagents. MAOs are manufactured exclusively by GeneTools Inc. and are described in detail on the website (www.genetools.com). MAOs are short chains of Morpholino subunits (Figure 5.1) comprised of a nucleic acid base, a morpholine ring and a non-ionic phosphorodiamidate. The morpholino backbone differs from that of DNA and RNA in that morpholine rings replace ribose or deoxyribose sugar moieties, and non-ionic phosphorodiamidate linkages replace anionic phosphates. MAOs act via a steric block mechanism (RNase H-independent) with high mRNA binding affinity and specificity, either by blocking the translation initiation complex (by targeting 5' UTR through first 25 bases of coding sequence) or nuclear splicing machinery (by targeting splice junctions in pre-mRNA). These antisense reagents bind to the complementary strand of the RNA via Watson-Crick pairing. As the backbone is not recognised by cellular enzymes or signalling proteins, MAOs are stable to nucleases and do not trigger an immune response.

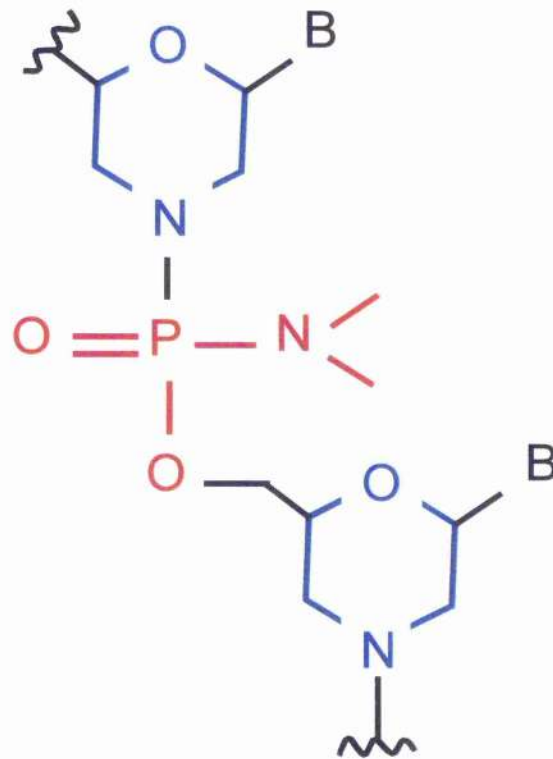


Figure 5.1 Structure of a Morpholino subunit

MAOs are short chains of Morpholino subunits, comprised of a nucleic acid base (B, black), a morpholine ring (blue) and a non-ionic phosphorodiamidate (red). The resulting morpholino backbone differs from that of DNA and RNA in that the morpholine rings replace ribose or deoxyribose sugar moieties, and the non-ionic phosphorodiamidate linkages replace anionic phosphates.

5.1.2. GLUT4 trafficking

Glut4 has a complex intracellular itinerary in adipocytes, which is described in detail in Section 1.7 (Chapter 1). Recent studies support a model in which the intracellular GLUT4 itinerary involves two intracellular cycles (Figure 1.9, Chapter 1). In the first cycle GLUT4 recycles through the fast cycling endosomal system. From there, unique sequences within GLUT4 direct it into a slowly recycling pathway, involving the *trans*-Golgi network (TGN) and GSVs. The selective routing of GLUT4 into this slowly recycling pathway results in the effective sequestration of GLUT4 away from the cell surface, in a population of vesicles available for rapid mobilisation upon insulin binding. The intracellular components that regulate the GLUT4 intracellular trafficking pathway remain largely unknown.

There is much evidence to implicate the TGN-localised t-SNARE, STX16 in the intracellular trafficking and/or translocation of GLUT4 to the cell surface in adipocytes (described in detail in Section 1.8, Chapter 1), which led to the development of my hypothesis and model for this thesis (Section 1.9, Chapter 1). STX16 was therefore directly tested for its involvement in GLUT4 trafficking in this Chapter.

5.1.3. Secretion of ACRP30 from adipocytes

ACRP30 (adipocyte complement-related protein of 30 kDa) is a protein secreted exclusively by adipocytes (Scherer et al., 1995) (Section 1.3.5) and its mRNA is induced over 100-fold during adipocyte differentiation (Scherer et al., 1995). ACRP30 is a relatively abundant serum protein and, paradoxically, circulating levels were found to decrease in parallel with increasing obesity and the progression of insulin resistance (Yang et al., 2001). Previous work suggests that ACRP30 is secreted from a distinct secretory compartment to GLUT4 (Bogan and Lodish, 1999), and that Vt1a, known to bind to STX16 (Mallard et al., 2002), may regulate a step common to both GLUT4 and ACRP30 trafficking in 3T3-L1 adipocytes (Bose et al., 2005). For this reason, ACRP30 secretion was chosen for investigation as another index of STX16 function.

5.2. Aims

The main aim of this Chapter was to study the effects of inhibition of STX16 function on GLUT4 trafficking in 3T3-L1 adipocytes. Inhibition was achieved both by overexpression of the dominant negative STX16cyt (Section 4.4.1.1) and MAO knockdown of endogenous STX16 in 3T3-L1 adipocytes. To assess GLUT4 trafficking, deGlc uptake was assayed in basal and insulin-stimulated cells and following insulin withdrawal from the cell receptors.

Additionally, I sought to study the effects of STX16T and STX16F (Sections 4.4.1.2 and 4.4.1.3) on GLUT4 trafficking in 3T3-L1 adipocytes and the effect of STX16cyt on ACRP30 secretion from these cells.

Therefore, the aims of this Chapter were as follows:

- To achieve knock down of STX16 in 3T3-L1 adipocytes via a Morpholino Antisense Oligonucleotide
- To determine the effect of perturbation of STX16 on basal and insulin-stimulated deGlc transport
- To determine the effect of perturbation of STX16 on the cells ability to return glucose transport to basal levels after the withdrawal of insulin (reversal of GLUT4 translocation)
- To determine the effect of perturbation of STX16 on secretion of ACRP30 in 3T3-L1 adipocytes
- To determine the effect of expression of STX16T and STX16F on basal and insulin-stimulated deGlc transport

5.3. Materials and Methods

5.3.1. Assays

All assays were carried out in 12-well plates of 3T3-L1 adipocytes on day 8 post-differentiation. All measurements and controls were conducted in triplicate. Cells were incubated in serum-free DMEM for 2 h prior to each assay at 37 °C and 5 % CO₂, and transferred to 37 °C hot-plates where the assays were carried out.

For assays measuring 2-Deoxy-D-glucose (deGlc) uptake, the classic inhibitor of glucose transport, Cytochalasin B (CB), was added to control wells to measure non-specific association of deGlc with the cells, which was subsequently subtracted from the appropriate measurements.

5.3.1.1. ACRP30 Secretion Assay

Cells were washed three times with 1 ml Krebs-Ringer-Phosphate (KRP, Section 2.1.7) buffer pH 7.4 pre-warmed to 37 °C. After aspiration of the final KRP wash, 500 µl KRP was added to each well then removed and transferred to an eppendorf tube after 0, 5, 10 and 20 min. The experiment was then repeated, this time adding KRP containing 1 µM insulin. The samples were then TCA precipitated as described in Section 2.4.2 and stored at - 80 °C prior to analysis by SDS-PAGE (Section 2.4.3). ACRP30 secretion was assayed by immunoblotting with an anti-peptide antibody raised against the C-terminal 15 amino acids of the murine protein (Ewart et al., 2005).

5.3.1.2. Glucose Transport Assay

Cells were rinsed three times in KRP buffer pre-warmed to 37 °C and then covered with 475 µl KRP ± 10 µM Cytochalasin B, ± 100 nM insulin as appropriate, and incubated for 30 min. Transport was then initiated by the addition of 25 µl of ³H deGlc such that the final concentration was 50 µM, with 0.25 µCi per well. Transport was assayed for 5 min, after which time, the contents of the wells were flipped out and the plates were rapidly washed by dipping in three consecutive beakers of ice-cold PBS. Cells were air-dried for approximately 1 h, and then solubilised in 500 µl 1% Triton X-100 for at least 2 h. The solubilised samples were then transferred to scintillation vials containing 5 ml scintillation

fluid and mixed thoroughly. The radioactivity associated with the cells was then determined by liquid scintillation spectrophotometry.

5.3.1.3. Reversal of GLUT4 translocation after insulin withdrawal

Cells were rinsed three times in KRP buffer pre-warmed to 37 °C. Control plates (measuring basal and insulin-stimulated glucose transport) were covered with 475 µl KRP ± 10 µM Cytochalasin B, ± 100 nM insulin as appropriate, incubated for 30 min and assayed straight away exactly as described in Section 5.4.1.2. For the insulin reversal experiments, cells were incubated in 475 µl KRP, + 100 nM insulin for 30 min. After this incubation, the cells were then rapidly washed into KRM buffer at pH 6.0 (as KRP except MES replaced the sodium phosphate) to cause dissociation of insulin from its receptor and the subsequent re-internalisation of GLUT4. Cells were gently washed in KRM pH 6.0 every 5 min for different times (from 5 to 40 min, as indicated) before a final wash in KRP pH 7.4 and subsequent assay in 475 µl KRP pH 7.4 ± 10 µM Cytochalasin B as outlined above (Section 5.4.1.2).

5.3.1.4. Statistical analysis

Data from glucose transport assays and quantified immunoblots were analysed using Excel software. Results are shown as mean ± SE (standard error). An unpaired Student's *t* test was carried out as a determination of statistical significance. Values of $p < 0.05$ were considered to be statistically significant for comparisons.

5.3.2. Electroporation of 3T3-L1 adipocytes with MAO

Morpholino Antisense Oligonucleotides (MAOs) designed to deplete cells of STX16 were generated by GeneTools Inc. (Philomath, OR) and introduced into 3T3-L1 adipocytes by electroporation as described in Jiang et al., 2003 and summarised here. Briefly, 3T3-L1 adipocytes were cultured in 10 cm² dishes as described in Section 2.3.4.1 and electroporation was carried out on day 6 post-differentiation. Cells were washed twice with Dulbecco's-PBS at room temperature then incubated at 37 °C in 2ml 1 × Trypsin-EDTA and 3ml 1 mg/ml Collagenase. After 10 min, the cells were gently shaken off the plate, 10 ml of 3T3-L1 adipocyte growth medium (Section 2.1.6) added and the cells centrifuged for 5 min. Cells were washed twice in D-PBS, then resuspended in 650 µl of the same and transferred to an electroporation cuvette prior to electroporation. 20 or 40 nmoles MAO

was added directly to the cells and the electroporation performed in a Bio-Rad GenePulser II at 0.18 kV, 950 μ F. Cells were then added to 15 ml of 3T3-L1 adipocyte growth medium (Section 2.1.6) and plated into 12-well plates. The cells were then incubated at 37 °C and 5 % CO₂ for 48 h prior to the assay on day 8 post-differentiation.

5.4. Results

5.4.1. Effect of STX16cyt, STX16T and STX16F on GLUT4 trafficking

5.4.1.1. Overview

STX16 mutants were designed to provide functional information about GLUT4 trafficking when expressed in 3T3-L1 adipocytes (Chapter 4). The cytosolic domain, STX16cyt, was anticipated to act as an inhibitor of the endogenous protein (Volchuk *et al.*, 1996; Tellam *et al.*, 1997b; Olson *et al.*, 1997), whereas an N-terminal truncation, STX16T, was designed to mimic the hypothesised open conformation of STX16 (Bryant and James, 2001) and therefore to represent a constitutively active version of the wild-type protein. The effects of STX16T were compared to those of expressing the full-length protein STX16F, anticipated to amplify the effects the endogenous protein (Pagan *et al.*, 2003; Thurmond *et al.*, 1998).

The adenovirus-mediated expression of STX16cyt, STX16T and STX16F in 3T3-L1 adipocytes was optimised in Chapter 4. Two methods were used to increase the expression of these mutants: infection of the cells on days 4 and 6 post-differentiation, and infection on day 6 alone followed by treatment with MG132 proteasome inhibitors (Sections 4.3.2 and 4.3.4). Cells treated in each way were used to carry out functional assays in which the effects of these mutants on GLUT4 trafficking could be measured.

Glucose transport and insulin withdrawal assays were carried out on day 8 post-differentiation as described in Section 5.4.1 (5.4.1.2 and 5.4.1.3).

5.4.1.2. Effect of MG132 Proteasome Inhibitors on basal and insulin-stimulated deGlc transport

MG132 proteasome inhibitors could be used to increase the expression of STX16cyt, STX16T and STX16F in 3T3-L1 adipocytes (Chapter 4). To check the compatibility of this method with deGlc transport assays, the effects of MG132 on basal and insulin-stimulated deGlc uptake were measured. 3T3-L1 adipocytes were treated with MG132 as described in Section 4.3.4 for 16 h overnight from day 7 to day 8 post-differentiation. Control cells were untreated. The results from a representative experiment are displayed in Figure 5.2.

Unexpectedly, this experiment highlighted that treatment of the cells with MG132 significantly decreased both basal and insulin-stimulated glucose uptake in 3T3-L1 adipocytes (Figure 5.2). It was previously reported that GLUT4 expression in 3T3-L1 adipocytes was repressed by proteasome inhibition by MG132 (Cooke and Patel, 2005). This loss of GLUT4 is likely to be responsible for reduced glucose transport into cells treated with MG132, however, this phenomenon will be discussed further in Section 5.7.

5.4.1.3. Effect of STX16cyt on deGlc transport in basal and insulin-stimulated cells and following insulin withdrawal

Since treatment of the cells with MG132 caused a decrease in the level of insulin-stimulated glucose uptake, the alternative method to achieve optimum expression of STX16cyt was utilised and deGlc transport was measured in cells infected on days 4 and 6. Therefore, cells were infected on days 4 and 6 as described in Section 4.3.2 with MOI 1:225 STX16cyt or empty pShuttle-CMV virus.

Figure 5.3 demonstrates that expression of STX16cyt did not perturb basal or insulin-stimulated deGlc transport rates significantly. However, expression of STX16cyt significantly slowed the rate of deGlc transport reversal after insulin withdrawal. Whereas in control cells (infected with empty pShuttle-CMV virus) insulin-stimulated deGlc transport returned essentially to basal levels 40 min after insulin withdrawal, in cells expressing STX16cyt transport remained significantly elevated at this time point, often as high as ~50% of the maximal insulin-stimulated rate.

The levels of STX16cyt and endogenous STX16 were compared to check if inhibition was achievable under these conditions. The expression levels were investigated thoroughly during the optimisation described in Chapter 4. However, to ensure that expression had been achieved, lysate was prepared (Section 2.3.4.3) just prior to the assay from cells treated in exactly the same way and at the same times as those to be assayed. The cell lysate was then subjected to SDS-PAGE electrophoresis (Section 2.4.3) and probed with anti-STX16. Figure 5.4 shows that during the experiment, STX16cyt and STX16 were present at approximately equal levels. In similar experiments involving STX6 (Perera et al., 2003), the STX6 cytosolic domain was expressed to 12-16 fold that of the endogenous protein (the reasons for low STX16 expression are discussed in detail in Chapter 4). However, it was reasoned that a 1:1 ratio of endogenous STX16 to STX16cyt may be sufficient to cause inhibition, at least during reversal conditions, when high levels of GLUT4 may be trafficking back into GSVs.

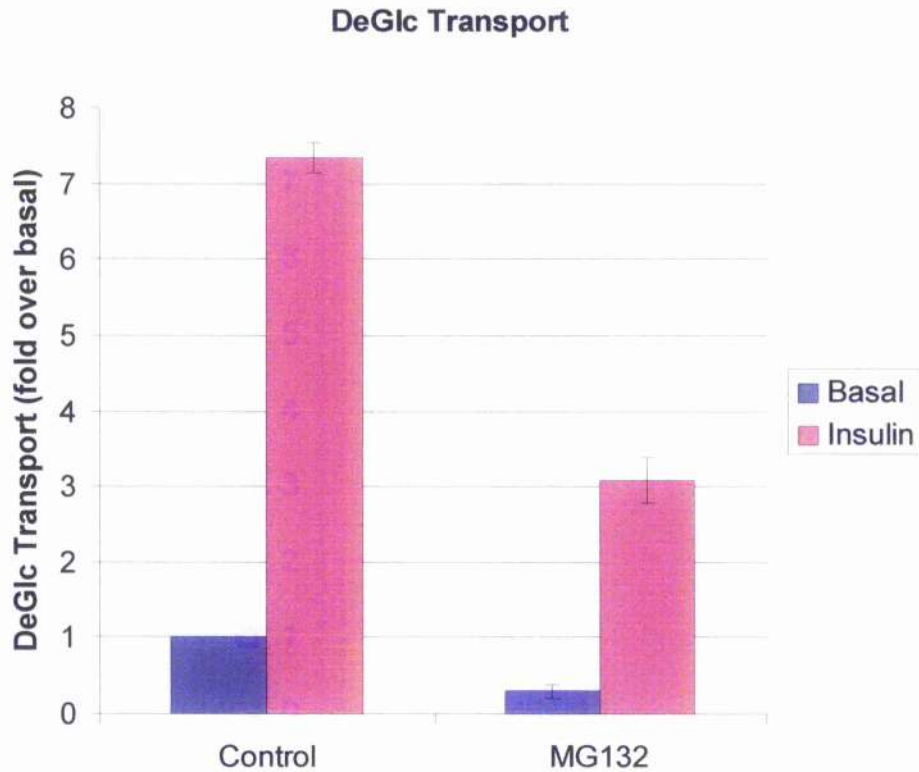


Figure 5.2 Effect of MG132 on basal and insulin-stimulated deGlc transport

DeGlc transport was assayed in cells treated with 50 μ M MG132 (Sections 4.3.2 and 4.3.4). Control cells were untreated. Basal and Insulin-stimulated deGlc transport was assayed in the presence or absence of 100 nM insulin (after stimulation for 30 min). Strikingly, MG132 treatment significantly inhibits basal and insulin-stimulated deGlc transport.

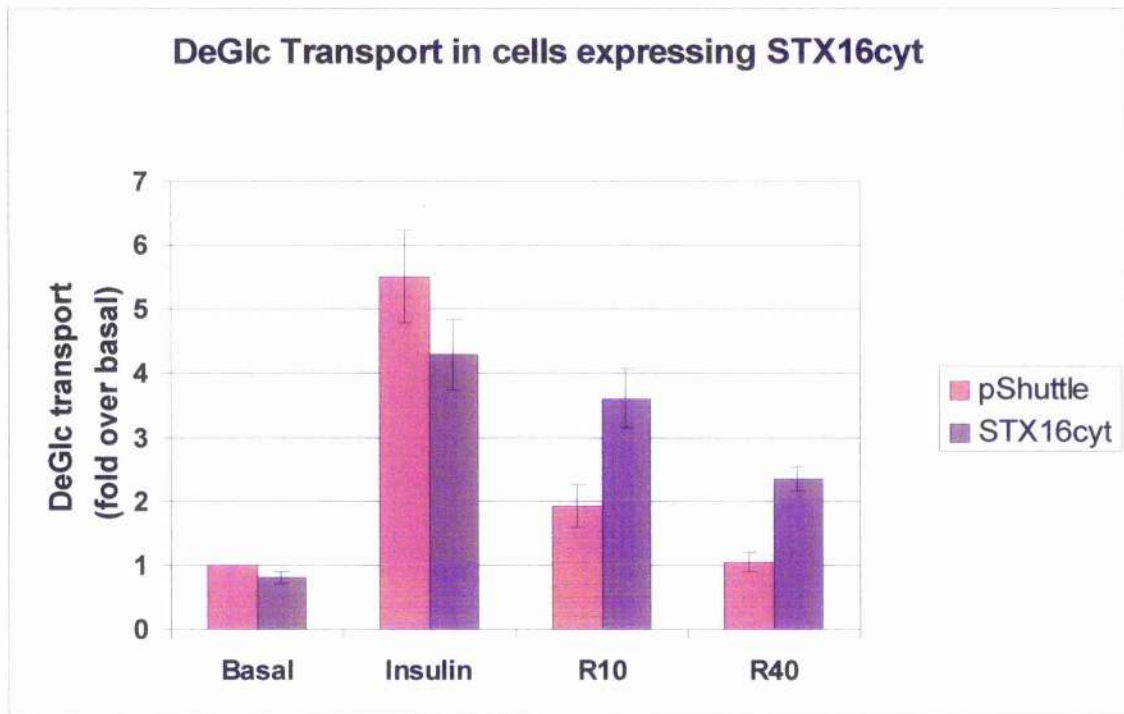
The data shown is from a representative experiment, repeated three times with similar results. Each point is the mean of triplicate determinations and the error bars are \pm standard error. The difference between control and MG132-treated cells is significant for basal ($p=0.001$) and insulin-stimulated ($p=0.0001$) deGlc transport.

Figure 5.3 Effect of STX16cyt on deGlc transport in basal and insulin-stimulated cells and following insulin withdrawal

DeGlc transport was assayed in cells infected with MOI 1:225 STX16cyt or empty pShuttle-CMV adenovirus on days 4 and 6 post-differentiation (Section 4.3.2). Cells were incubated in the presence or absence of 100 nM insulin for 30 min, after which time basal and insulin-stimulated deGlc transport were assayed over 5 min. Insulin-stimulation was reversed by low pH washes in parallel experiments, and the rate of reversal of insulin-stimulated deGlc transport assayed at 10 (R10) and 40 (R40) min after reversal. **A)** Expression of STX16cyt does not affect basal or insulin-stimulated glucose transport compared to control cells but significantly slows the reversal of insulin-stimulated deGlc transport during the 10 to 40 min period. **B)** Rate of reversal of insulin-stimulated glucose transport. The values in (A) are expressed as a percentage of the maximal insulin-stimulated value in each case and demonstrate that STX16cyt expression slows reversal of insulin-stimulated deGlc transport.

The data shown is from a representative experiment, repeated three times with similar results. Each point is the mean of triplicate determinations. The error bars are \pm standard error. The difference between control and STX16cyt expressing cells is significant at R10 ($p \sim 0.01$) and R40 ($p = 0.005$), but not significant under basal or insulin-stimulated conditions.

A



B



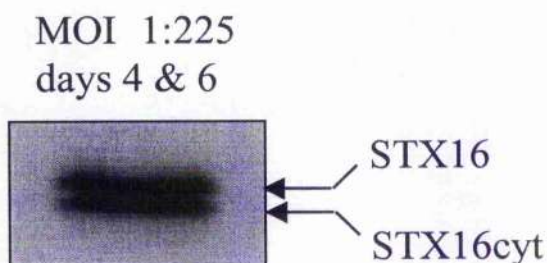
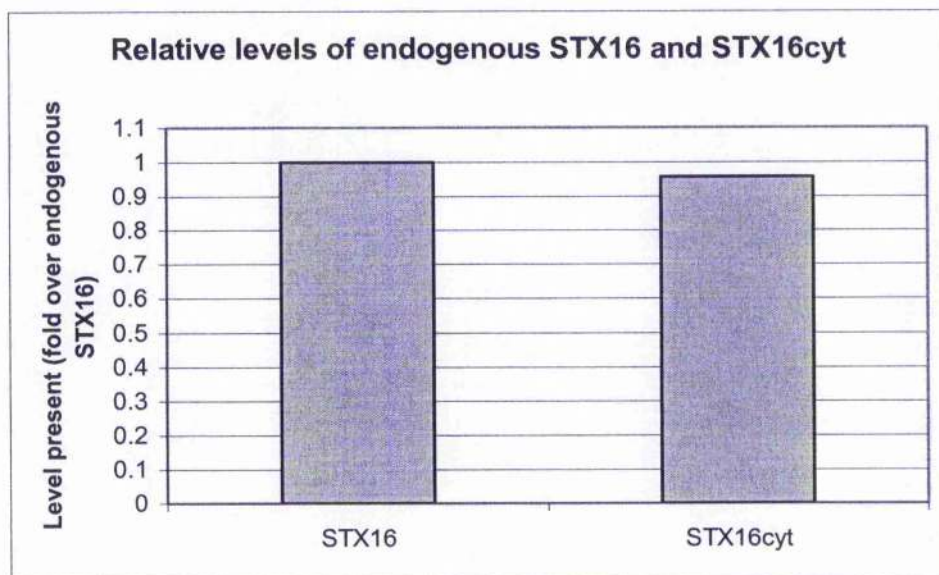
A**B**

Figure 5.4 Quantification of STX16cyt produced by cells infected day 4 and 6

Cells were infected on days 4 and 6 post-differentiation with MOI 1:225 STX16cyt adenovirus. Cells to be assayed were treated in exactly the same way at the same times. Just prior to the assay on day 8 post-differentiation, cells were lysed (Section 2.3.4.3) and resolved on an SDS-PAGE gel and analysed by immunoblotting with anti-STX16. **A)** A representative immunoblot demonstrates that STX16 and STX16cyt are present in approximately equal quantities. **B)** Quantification of the immunoblot in (A), confirming that STX16 and STX16cyt are indeed present in approximately equal quantities.

The lysate loaded in the well corresponds to 2 % of the total lysate obtained from one well of a 12-well plate.

5.4.1.4. Effect of STX16T and STX16F on basal and insulin-stimulated glucose transport

Cells were infected on days 4 and 6 as described in Section 4.3.2 with STX16T, STX16F or empty pShuttle-CMV adenovirus. The cells were infected at MOI 1:225 or 1:450. As for STX16cyt, expression of STX16T and STX16F at each MOI of virus was assessed prior to each experiment. Lysates were prepared as described in Section 2.3.4.3 and analysed by SDS-PAGE electrophoresis and Western Blotting with anti-STX16 (Figure 5.5). The levels of STX16T increased in a dose dependent manner from MOI 1:225 to MOI 1:450, whereas the levels of STX16F at each MOI were similar. It therefore proved difficult to express STX16T and STX16F at equal levels. In addition, it was not possible to achieve both equal exposure to virus and equal levels of protein present because the proteins were not expressed to the same extent at each MOI. However, cells infected with each virus at MOI 1:450 were used thereafter for the glucose transport assays, as it was advantageous to carry out the assay with optimum levels of STX16T. It is, however, likely that the levels of STX16T and STX16F were not equal during the experiment; hence the effects of each protein cannot be directly compared. In addition, as STX16T lacks a large part of the N-terminus, it is possible that a portion of the antibody-binding site is absent and as a result the binding affinity of anti-STX16 to STX16T may be different to that of STX16F or endogenous STX16.

Figure 5.6 demonstrates that expression of neither STX16T nor STX16F significantly affects basal or insulin stimulated glucose transport, with levels of glucose transport remaining essentially equal compared to control cells. A trend was observed, however, for modestly elevated levels of insulin-stimulated deGlc transport in cells expressing STX16F and STX16T, and decreased levels in basal cells expressing STX16F. These possible effects will be discussed further in Section 5.7.

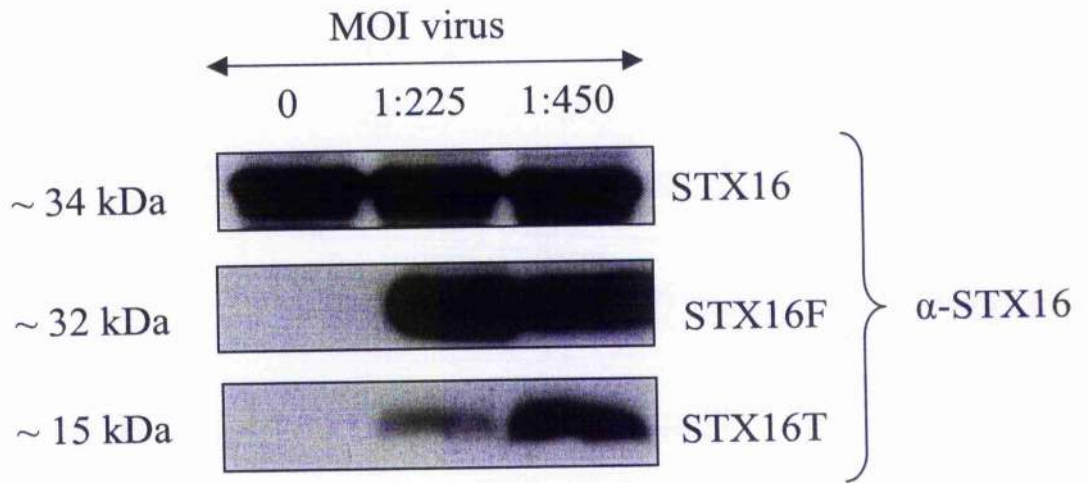


Figure 5.5 Quantification of STX16T and STX16F produced by cells infected day 4 and 6

Cells were infected on day 4 and 6 post-differentiation with MOIs of 1:225 or 1:450 STX16T or STX16F adenovirus as indicated, in parallel with cells to be assayed. Exactly prior to the assay on day 8, cells were lysed (Section 2.3.4.3). The lysates were then resolved on an SDS-PAGE gel and analysed by immunoblotting with anti-STX16. The level of STX16T produced increased in a dose dependent manner from MOI 1:225 to 1:450. In contrast, STX16F expression remained constant at each MOI. As the ability of each protein to recognise the STX16 antibody is unknown, the relative levels of each cannot be directly compared.

The lysate loaded in each well corresponds to 2 % of the total lysate obtained from one well of a 12-well plate.

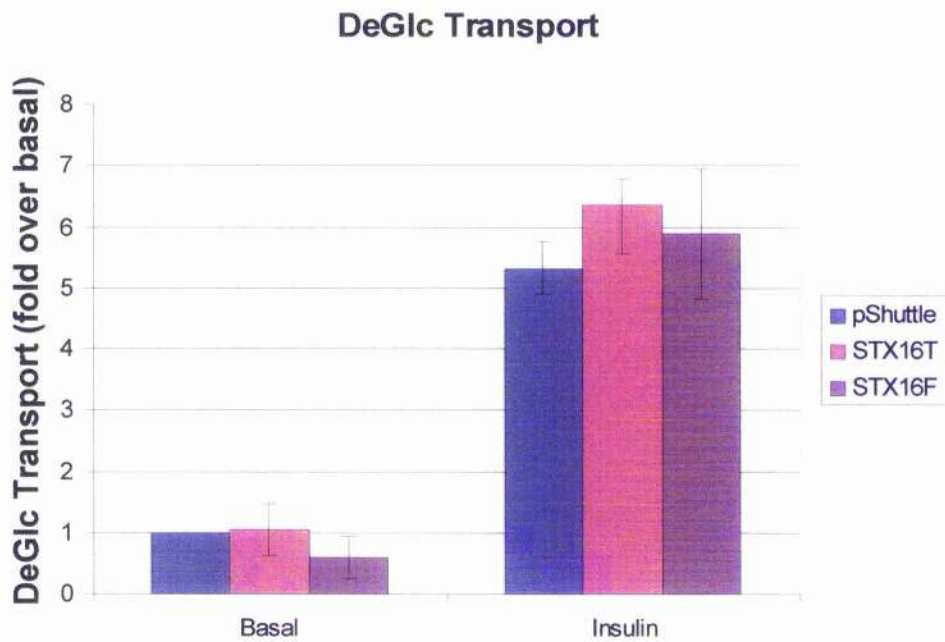


Figure 5.6 Effect of STX16T and STX16F on deGlc transport in 3T3-L1 adipocytes

DeGlc transport was assayed in cells infected with MOI 1:450 STX16T, STX16F or empty pShuttle-CMV adenovirus on days 4 and 6 post-differentiation (Section 4.3.2). Basal and insulin-stimulated deGlc transport was assayed in the presence or absence of 100 nM insulin (after 30 min stimulation). Neither STX16T nor STX16F have a significant effect on basal or insulin-stimulated deGlc transport compared to control cells.

The data shown is from a representative experiment, repeated three times with similar results. Each point is the mean of triplicate determinations. The error bars are \pm standard error.

5.4.2. Effect of STX16cyt on the secretion of ACRP30

5.4.2.1. Overview

Next, the effect of inhibition of STX16 function on ACRP30 secretion was examined. Secretion of ACRP30 from adipocytes is described in Section 5.1.2. ACRP30 secretion from 3T3-L1 adipocytes was measured as described by Kitagawa and co-workers (Kitagawa et al., 1989). Secretion assays were carried out on day 8 post-differentiation as described in Section 5.4.1 (5.4.1.1) in the presence or absence of 1 μ M insulin. Secretion samples, collected at various time points, from 0 to 20 min, were resolved by gel electrophoresis and immunoblotted with anti-ACRP30. Each time-point was performed in triplicate and each experiment was carried out three times with similar results. In each case, representative immunoblots are shown.

5.4.2.2. Effect of MG132 on ACRP30 secretion

As mentioned previously, expression of STX16cyt could be enhanced by treatment of the cells with MG132 proteasome inhibitors (Section 4.4.4.7, Chapter 4). As for glucose transport assays, the suitability of this method for the analysis of ACRP30 secretion was investigated.

3T3-L1 adipocytes were treated with 50 μ M MG132 as described in Section 4.3.4 for 16 h overnight from day 7 to day 8 post-differentiation. Controls cells were differentiated in parallel but were not treated with MG132. Strikingly, Figure 5.7 shows that there is a dramatic reduction in ACRP30 secretion in both basal and insulin-stimulated cells treated with MG132. The reasons for this intriguing effect are at present unclear but will be discussed further in Section 5.7 below. ACRP30 secretion appears to be decreased to a greater extent by MG132 treatment of basal cells. This could be due to the enhancement in ACRP30 secretion previously reported in response to insulin (Bogan and Lodish, 1999; Scherer et al., 1995).

5.4.2.3. Effect of STX16cyt on ACRP30 secretion

Due to the adverse effects of MG132 on ACRP30 secretion, the alternative method to produce optimum STX16cyt expression was then utilised. Cells were therefore infected on

days 4 and 6 post-differentiation as described in Section 4.3.2 with MOI 1:225 STX16cyt, empty pShuttle-CMV adenovirus or no virus. No appreciable difference was observed in secretion of ACRP30 in cells expressing STX16cyt compared to cells infected with empty pShuttle-CMV (Figure 5.8A) or no virus control cells (not shown) after 0, 5, 10 or 20 min.

It was then decided to compare the secretion of ACRP30 from cells expressing STX16cyt to cells expressing the cytosolic domain of another Syntaxin, STX12 (Tang et al., 1998c), which was previously shown to have no effect on ACRP30 secretion in 3T3-L1 adipocytes (H.K.I. Perera, unpublished data). This was achieved by infecting cells with a recombinant adenovirus generated previously in our laboratory by H.K.I. Perera (Perera et al., 2003), capable of expressing the cytosolic domain of STX12 (STX12cyt). Once again, no appreciable difference was observed in the levels of ACRP30 secreted from cells expressing STX16cyt compared to STX12cyt after 10 min either in the presence or absence of insulin (Figure 5.8B).

These data suggest that that STX16cyt and therefore STX16 has no effect on the secretion of ACRP30 from 3T3-L1 adipocytes.

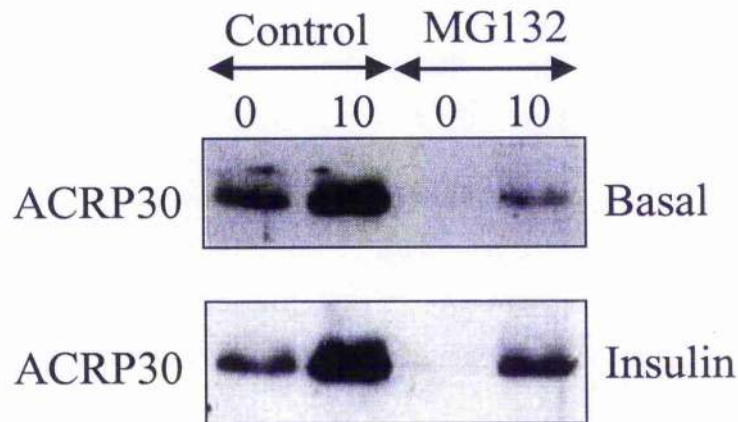


Figure 5.7 Effect of MG132 treatment on ACRP30 secretion in 3T3-L1 adipocytes

3T3-L1 adipocytes were treated with 50 μM MG132 (Section 4.3.3) for 16 h overnight from day 7 to day 8 post-differentiation. Control cells were differentiated in parallel but not treated with MG132. The secretion assay was carried out on day 8 post-differentiation as described in Section 5.4.1.1, in the presence or absence of 1 μM insulin and secretion samples were collected after 0 and 10 min. The samples were resolved by SDS-PAGE electrophoresis and analysed by immunoblotting with anti-ACRP30.

Upper Panel: Samples collected from basal cells after 0 and 10 min indicated that MG132 treatment dramatically inhibited ACRP30 secretion from 3T3-L1 adipocytes. **Lower panel:** Secretion samples collected from insulin-stimulated cells after 0 and 10 min also showed that MG132 treatment decreases ACRP30 secretion.

The upper and lower panels are from different exposures of separate immunoblots and therefore should not be directly compared. The experiment was carried out three times with similar results. A representative immunoblot is shown. Each lane was loaded with 2/5 of the secreted proteins from one well of a 12-well plate, collected after the times indicated.

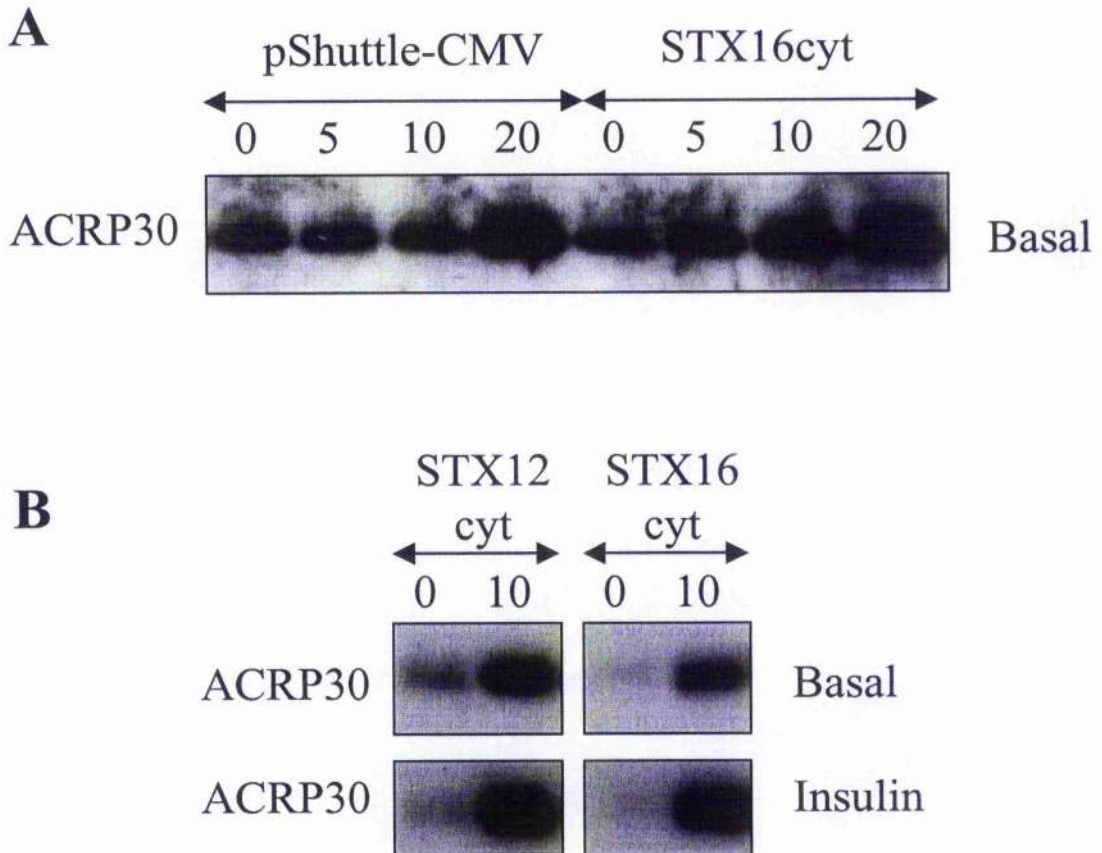


Figure 5.8 Effect of STX16cyt on ACRP30 secretion in 3T3-L1 adipocytes

3T3-L1 adipocytes were infected on days 4 and 6 post-differentiation (Section 4.3.2) with MOI 1:225 STX16cyt, empty pShuttle-CMV adenovirus or an adenovirus expressing the cytosolic domain of STX12 (STX12cyt). The secretion assay was carried out on day 8 post-differentiation as described in Section 5.4.1.1, and secretion samples were collected at the time points indicated. The samples were resolved by SDS-PAGE electrophoresis and analysed by immunoblotting with anti-ACRP30. **A)** Samples collected after 0, 5, 10 and 20 min indicated that STX16cyt had no effect on ACRP30 secretion compared to control cells (infected with empty pShuttle-CMV virus) in basal cells. **B)** Secretion samples collected after 0 and 10 min in cells expressing STX16cyt or STX12cyt in the presence (Insulin, bottom panel) or absence (Basal, top panel) of 1 μ M insulin were compared. No appreciable difference in ACRP30 secretion was observed in cells expressing STX16cyt compared to STX12cyt, either in the presence or absence of insulin.

The experiments were carried out three times with similar results. Representative immunoblots are shown. Each lane was loaded with 2/5 of the secreted proteins from one well of a 12-well plate, collected after the times indicated.

5.5. Knockdown of STX16 in 3T3-L1 adipocytes

5.5.1. Overview

In Section 5.5.1, the effects of inhibiting STX16 function were studied by means of expressing the dominant negative cytosolic domain, STX16_{cyt}. As a complimentary approach to probe the function of STX16 in GLUT4 trafficking, Morpholino Antisense Oligonucleotides (MAOs) were employed to knockdown levels of this protein in 3T3-L1 adipocytes. MAOs are described in Section 5.1.3.

5.5.2. STX16 specific MAO

5.5.2.1. Blast search and design of STX16 MAO

A Blast search was carried out to identify the murine STX16 sequence (not shown). The accession number was identified as NM_172675. The murine STX16 specific MAO was then designed according to this sequence and manufactured at GeneTools Inc. (Philomath, OR). The sequence of the STX16 MAO was as follows:

5'-GCCATGCGGTCATCAGCAAGCTCGT-3'

5.5.3. Internalisation of fluoresceinated MAO using Endo-Porter reagent

Although MAOs have a high success rate of knocking down target genes in various cell types, the limiting factor is their successful delivery into target cells. The Endo-Porter delivery reagent (GeneTools Inc.) delivers substances into the cytosol of cultured cells via an endocytic pathway, avoiding toxicity due to disruption of the plasma membrane, and has been shown to successfully deliver MAOs into a number of cell types (www.genetools.com).

The Endo-Porter delivery reagent was therefore tested for its ability to internalise a standard control MAO with a fluorescent tag (3'-Carboxyfluorescein end modification) into 3T3-L1 adipocytes. 1, 5 or 10 μ M fluoresceinated MAO were added, along with 10

μM Endo-Porter reagent per well of a 12 well plate, to 3T3-L1 adipocytes on day 6 post-differentiation. Cells were viewed using an upright fluorescent microscope at various times for up to 48 h after treatment. 48 h after treatment, cells were imaged using AxioVision 4.3 software and the results of representative fields are shown in Figure 5.9. Whereas diffuse fluorescence is indicative of successful delivery into the cytosol, it appeared that only punctate spots were observed at all concentrations of MAO. This suggests that the MAOs were trapped at the cell surface or in endosomes. 20 and 40 μM fluoresceinated MAO were then tested for endocytosis with similar results (not shown).

In support of this finding, 3T3-L1 adipocytes treated with Endo-Porter reagent and STX16 specific MAO displayed no change in the level of STX16 compared to control cells as shown by Western Blotting (not shown).

5.5.4. Electroporation of 3T3-L1 adipocytes to achieve delivery of MAO

Electroporation was therefore employed to achieve delivery of the MAO into adipocytes. This method was used previously to successfully deliver RNAi into 3T3-L1 adipocytes and achieve successful gene knockdown (Jiang et al., 2003). However, the success of delivering uncharged MAOs, with different properties to RNA, was unknown. Electroporation was carried out as described Section 5.4.2 with 20 or 40 nmoles STX16 or control MAO on day 6 post-differentiation. 48 h later, the cells were either used for glucose transport assay (Section 5.6.4.2, below) or lysates were prepared as in Section 2.3.4.3 and analysed by Western Blotting with anti- STX16 (Section 5.6.4.1, below).

5.5.4.1. STX16 is knocked down by > 90 % in 3T3-L1 adipocytes using STX16 MAO

Lysates prepared from cells electroporated with 20 nmoles STX16 MAO (Section 5.4.2) were analysed by gel electrophoresis and Western Blotting with anti-STX16. Figure 5.10 demonstrates that using 20 nmoles of MAO per 10cm plate of adipocytes was sufficient to reduce STX16 levels by > 90%. The lysates were also probed for the presence of other Syntaxin family members, STX4, STX8 and STX12, using appropriate specific antibodies. The levels of these Syntaxins were unchanged with MAO treatment (Figure 5.10), indicating that the effect was indeed specific to STX16.

5.5.4.2. Knockdown of STX16 expression reduces insulin-stimulated deGlc transport

3T3-L1 adipocytes, electroporated as described above were then used to carry out a glucose transport assay. 20 or 40 nmolcs of MAO were used per 10 cm² dish to knockdown levels of STX16. The higher concentration was used in this case to maximise knockdown, since the sensitivity of the anti-STX16 antibody is unknown. The glucose transport assay was carried out as described in Section 5.4.1 (5.4.1.2), except insulin-stimulation was achieved using 1, 10 and 100 nM insulin. This was to assay insulin-stimulated deGlc transport at both maximal and sub-maximal insulin concentrations. As shown in Figure 5.11, knockdown of STX16 resulted in decreased rates of insulin-stimulated deGlc transport, evident at both maximal and sub-maximal doses of insulin.

5.5.4.3. Knockdown of STX16 expression reduces total cell GLUT4 levels

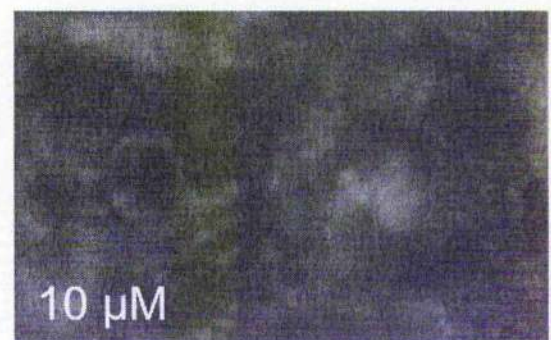
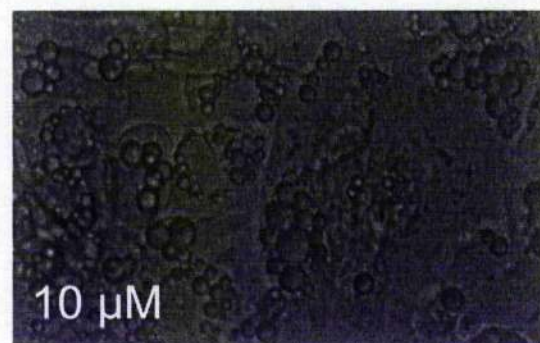
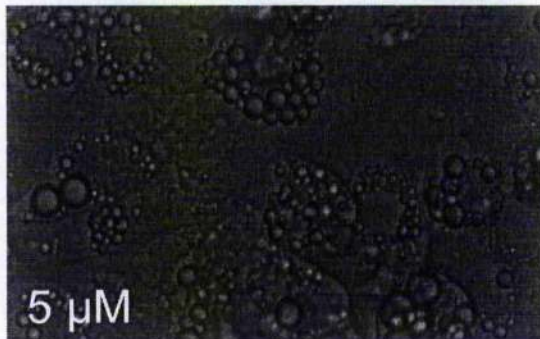
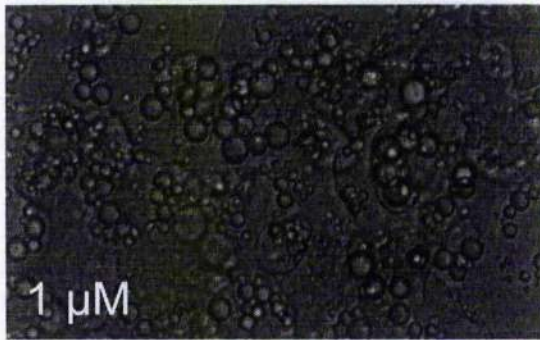
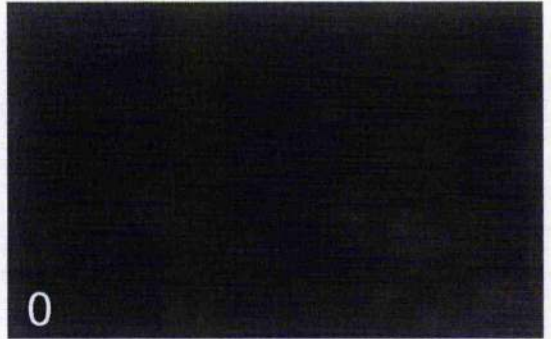
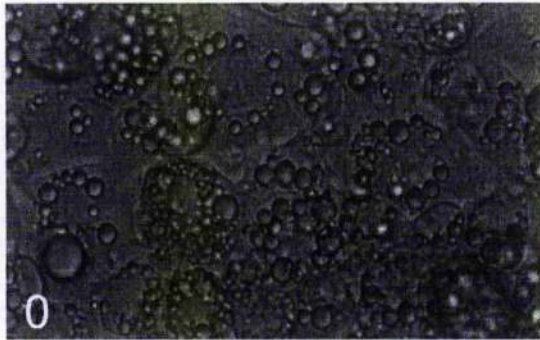
It was thought that this reduction in insulin-stimulated deGlc uptake in cells depleted of STX16 could correlate with depleted levels of GLUT4, and as such, the levels of GLUT4 in cells depleted of STX16 were examined. 48 h after electroporation with STX16 MAO or control, on day 8 post-differentiation, cell lysates were probed with anti-GLUT4 (Figure 5.12). It was found that depletion of STX16 indeed resulted in a $30.6 \pm 7.2\%$ reduction in total cell GLUT4 levels. The possible reasons for this decrease will be discussed in Section 5.7.

Figure 5.9 Delivery of a fluoresceinated MAO at various concentrations into 3T3-L1 adipocytes

Endo-Porter delivery reagent was tested for its ability to internalise a standard control MAO with a fluorescent tag into 3T3-L1 adipocytes. 3T3-L1 adipocytes were exposed to 0, 1, 5 or 10 μM fluoresceinated MAO (as indicated), along with 10 μM Endo-Porter reagent per well of a 12 well plate, on day 6 post-differentiation. 48 h after treatment, cells were viewed using an upright fluorescent microscope and imaged using AxioVision 4.3 Software. Representative fields are shown. Bright field images (left hand panels) are displayed along with their corresponding fluorescent images (right hand panels). Punctuate spots of fluorescence at all concentrations of MAO were indicative that the MAOs were trapped at the cell surface or in endosomes.

Bright field

Fluorescence



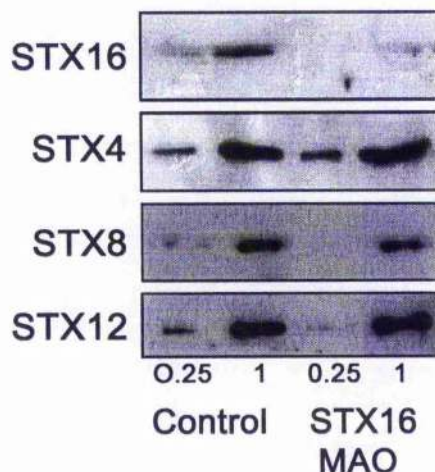


Figure 5.10 MAO-depletion of STX16 expression in 3T3-L1 adipocytes.

3T3-L1 adipocytes were electroporated (Section 5.4.2) in the presence of 20 nmoles of STX16-MAO or control per 10 cm² dish. 48h later, cell lysates were prepared (Section 2.3.4.3) and immunoblotted with antibodies to STX16, STX4, STX8 and STX12. STX16 levels were reduced by >90% with 20 nmoles MAO per plate, whereas the levels of STX4, STX8 and STX12 were unchanged.

This experiment was repeated three times with similar results. Representative immunoblots are shown.

Fractions loaded: 1.0 is equivalent to 4×10^4 cells. 0.25 × and 1.0 × samples were loaded as indicated.

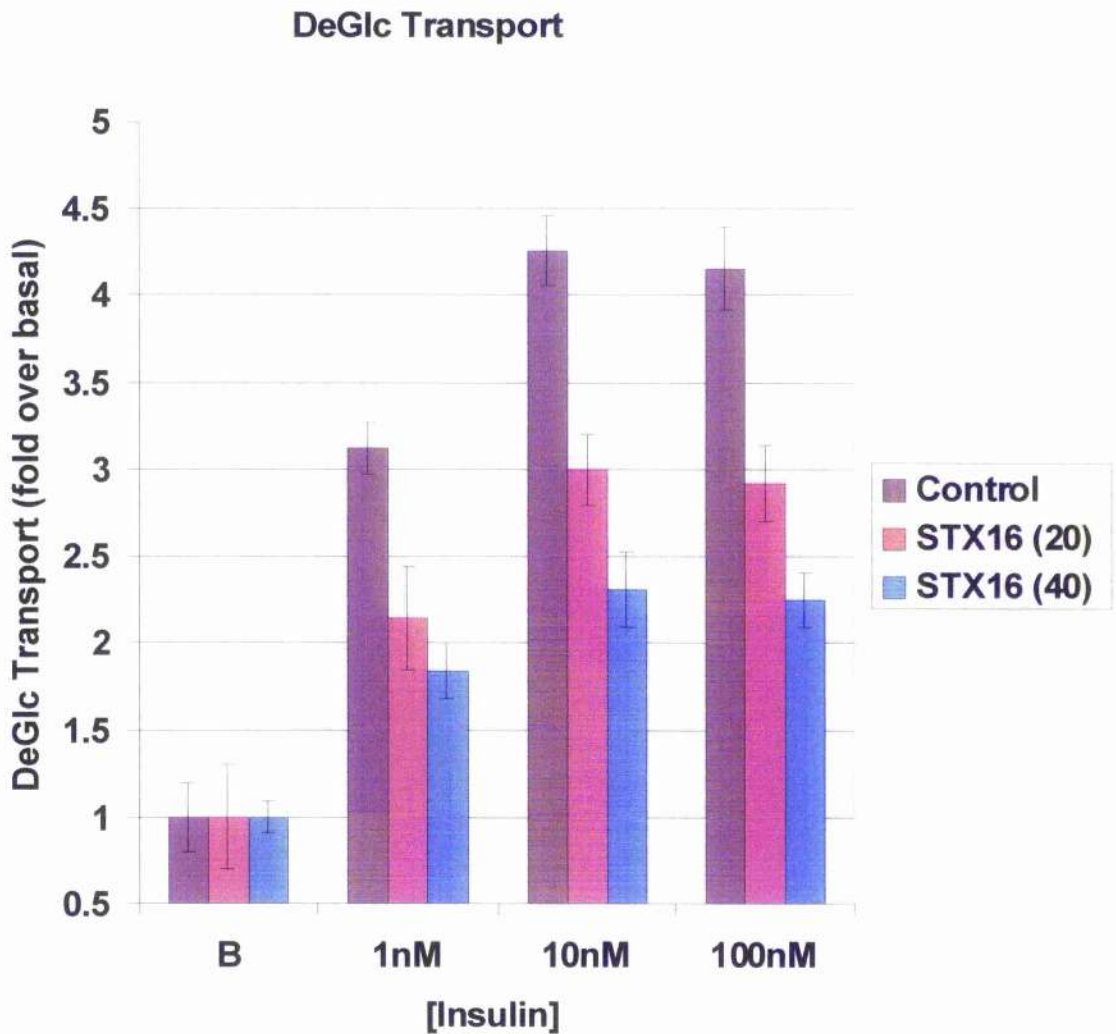


Figure 5.11 Insulin-stimulated deGlc transport is inhibited by MAO-depletion of STX16 in 3T3-L1 adipocytes

3T3-L1 adipocytes were electroporated with 20 or 40 nmoles of STX16-MAO or control per 10 cm² dish (Section 5.4.2) on day 6 post-differentiation. 48h later, basal and insulin-stimulated deGlc transport was assayed (Section 5.4.1.2) in triplicate at the concentrations of insulin shown (1 nM, 10 nM, 100 nM), following 30 min stimulation. Depletion of STX16 had no effect on basal deGlc uptake but significantly inhibited insulin-stimulated deGlc transport at each concentration of insulin.

Data shown is from a typical experiment of this type, repeated three times with similar results. MAO's specific for STX16 resulted in a statistically significant inhibition of deGlc uptake at all insulin concentrations tested ($p < 0.05$ for all comparisons).

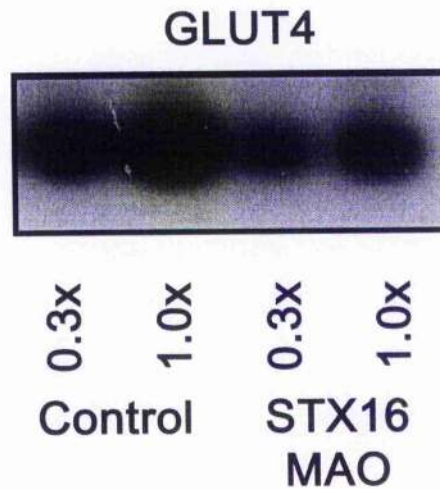


Figure 5.12 GLUT4 levels are decreased in 3T3-L1 adipocytes depleted of STX16 in 3T3-L1 adipocytes

3T3-L1 adipocytes were electroporated with 40 nmoles STX16 MAO or control on day 6 post-differentiation. Lysates were prepared 48 h later and immunoblotted for GLUT4. This demonstrates that levels of GLUT4 are $\sim 30.6 \pm 7.2\%$ depleted in cells lacking STX16 compared to control cells. 0.3 and 1.0 equivalents of lysates were added (as indicated) to demonstrate the linearity of the immunoblot.

This experiment was repeated three times with similar results. A representative immunoblot is shown.

Fractions loaded: 1.0 is equivalent to 4×10^4 cells. 0.3 \times and 1.0 \times samples were loaded as indicated.

5.6. Discussion

GLUT4 trafficking is described in detail in Section 1.7 and my discussion of the results obtained in this Chapter is based upon the model shown in Chapter 1 (Figure 1.9), taken from (Bryant et al., 2002), which highlights the existence of two GLUT4 trafficking pathways in 3T3-L1 adipocytes: a fast recycling pathway between the cell surface and endosomes and a slowly recycling pool, which sequesters GLUT4 away from the general endosomal traffic and may involve the TGN and insulin-responsive GSVs.

To address the function of STX16 in GLUT4 trafficking directly, two complementary approaches were used, each of which involved the inhibition of endogenous STX16 function. The first method involved the construction of a recombinant adenovirus to express a mutant form of STX16, STX16cyt, lacking its transmembrane domain (Section 4.4.1.1). Previous studies of SNARE protein function have shown that endogenous SNARE protein function can be effectively inhibited by expression of the corresponding cytosolic domain (Olson et al., 1997; Tellam et al., 1997b; Volchuk et al., 1996). Expression of STX16cyt in fully differentiated 3T3-L1 adipocytes was found to have little or no significant effect on either basal or insulin-stimulated deGlc uptake (Figure 5.3). However, STX16cyt expression significantly slowed the rate of reversal of insulin-stimulated deGlc transport (Figure 5.3). Insulin-stimulated deGlc transport was reversed by rinsing cells with a low pH buffer, which causes insulin to dissociate with its receptor resulting in the re-sequestration of GLUT4 into intracellular compartments. In control cells, insulin-stimulated deGlc transport returned essentially to basal levels 40 min after insulin withdrawal. On the other hand, in cells expressing STX16cyt, deGlc transport remained significantly elevated during the 10-40 minute withdrawal period time point, often as high as ~50% of the maximal insulin-stimulated rate after 40 min (Figure 5.3). This could suggest that inhibition of STX16 function results in defects in either the endocytosis of GLUT4 from the cell surface or the intracellular sorting of GLUT4 from the endosomal system into the slowly recycling intracellular pool. Although it is not possible to formally distinguish between these possibilities, I hypothesise that, as previously reported for STX6, this corresponds with an inability of GLUT4 to be sequestered from the fast recycling endosomal system into the slow cycling intracellular compartment involving the TGN and the GSVs. This therefore implies a role for STX16 in the intracellular

sequestration of GLUT4 from the endosomal recycling pathway, contributing to its exclusion from the cell surface in the absence of insulin.

In order to consolidate this data, a second method to inhibit endogenous STX16 function was employed. A specific Morpholino Antisense Oligonucleotide (MAO) was used to knockdown STX16 in 3T3-L1 adipocytes. Using this method, cellular levels of STX16 were reduced by more than 90 % (Figure 5.10). In 3T3-L1 adipocytes depleted of STX16 in this way, a marked decrease in the magnitude of insulin-stimulated deGlc uptake was observed (Figure 5.11). This finding adds further support to the model described above in which STX16 functions to control sorting of GLUT4 from the recycling endosomal pathway into the slowly recycling arm housing the insulin-responsive GSVs. It was thought that cells depleted of STX16 may be unable to sequester GLUT4 into this compartment, resulting in reduced levels of GLUT4 in the insulin-responsive vesicles. In an attempt to resolve where the miss-sorted GLUT4 then resided in the cell, cell lysates treated with STX16 specific MAO were probed with antibodies to GLUT4. Strikingly, the levels of GLUT4 in cells depleted of STX16 were reduced by ~ 30% (Figure 5.12). This suggests that when sorting into the slowly recycling compartment is blocked, GLUT4 may be diverted into a degradative pathway. Interestingly, insulin resistance in adipose tissue was shown to correlate most strongly with reduced GLUT4 expression and decreased GLUT4 mRNA (Shepherd and Kahn, 1999).

A decrease in insulin-stimulated deGlc transport was not observed upon over-expression of STX16_{cyt} perhaps because the levels produced were not high enough to produce complete inhibition of the endogenous molecule. STX16_{cyt} was expressed to a level equal to that of endogenous STX16, whereas in similar experiments, the cytosolic domain of STX6 was expressed to levels of 12-16 fold that of the endogenous protein (Perera et al., 2003). As a result of this relatively low expression, GLUT4 could presumably still be sorted into the slowly recycling compartment, avoiding degradation, due to the active presence of endogenous STX16. A significant inhibitory effect was perhaps only observed after insulin withdrawal because this step would require the re-sequestration of a large proportion of GLUT4 from the cell surface into intracellular compartments.

Nonetheless, I suggest that these two complementary approaches both argue that STX16 is involved in sorting of GLUT4 from the general endosomal traffic into the slowly recycling pathway. This model would be consistent with a role for STX16 in EE to TGN trafficking as reported in HeLas (Mallard et al., 2002) and correlates well with its description as a TGN localised t-SNARE (Simonsen et al., 1998; Tang et al., 1998a). Perhaps STX16 is

involved in a general trafficking step at this location, accepting incoming traffic from the EE arriving at the TGN or perhaps its role becomes more specific to GLUT4 trafficking in 3T3-L1 adipocytes. This will be considered further in Chapter 6.

Secretion of ACRP30 (Section 5.1.2) from 3T3-L1 adipocytes is enhanced by insulin (Scherer et al., 1995; Bogan and Lodish, 1999). Despite initial results suggesting the existence of a common insulin-regulated secretory pathway in adipocytes (Scherer et al., 1995), more recent work suggested the existence of at least two distinct compartments that undergo insulin-stimulated exocytosis in adipocytes: one for ACRP30 and one for GLUT4 (Bogan and Lodish, 1999). However, Bose *et. al.* demonstrated that Vti1a is involved in insulin-stimulated glucose transport as well as ACRP30 secretion, and offer the hypothesis that it is involved in the regulation of a common step between the two pathways (Bose et al., 2005). Vti1a was previously shown to bind to STX16 (Mallard et al., 2002) in a complex that controls trafficking between the EE and the TGN. My study was therefore extended by determining if STX16 was involved in the intracellular trafficking or the sorting of this molecule into a secretory compartment.

Once again, STX16cyt was expressed in 3T3-L1 adipocytes and ACRP30 secretion was measured at various time points. Experiments showed that expression of STX16cyt had no effect on ACRP30 secretion in either basal or insulin-stimulated cells (Figure 5.8). I therefore concluded that, like STX6 (Perera et al., 2003), STX16 is not involved in the intracellular trafficking or secretion of ACRP30. This is consistent with a model that suggests both STX6 and STX16 operate in the same SNARE complex, which is involved in GLUT4 trafficking but not ACRP30 secretion in 3T3-L1 adipocytes.

The role of STX16 was further investigated with a study into how the molecule may structurally act to regulate GLUT4 trafficking. A recombinant adenovirus was constructed to express another mutant protein, STX16T (Section 4.4.1.2), which lacked the potential autoinhibitory H_{abc} domain. A similar mutant in Tlg2p was shown to bypass the requirement for Vps45p in SNARE complex assembly in yeast (Bryant and James, 2001). The effects of STX16T were compared to those of expressing the full-length protein, STX16F (Section 4.4.1.3), in an attempt to identify if STX16T represented a constitutively active version of the wild-type protein by accelerating the effects of expressing the full-length protein. However, expression of STX16T or STX16F did not alter basal or insulin-stimulated deGlc uptake significantly (Figure 5.5). Although this could suggest that neither STX16T nor STX16F have any effect GLUT4 trafficking, the effects of STX16cyt expression were similarly not observed on basal or insulin-stimulated deGlc uptake but on

the endocytic retrieval following insulin withdrawal. Future work will be required to address whether these proteins affect GLUT4 trafficking following insulin withdrawal. Before future work can proceed, however, it will be necessary to equalise the levels of STX16T and STX16F produced. The proteins are not expressed to the same level at the same MOI virus (Figure 5.6), and given that the recognition of STX16T to the STX16 antibody is unknown, it would, with hindsight, have been prudent to express the proteins bearing the same N-terminal tag (Section 4.4.1).

However, it is worth noting that, consistently, the levels of insulin-stimulated glucose transport were modestly elevated in cells expressing STX16F and STX16T compared to control cells, with those expressing STX16T exhibiting higher levels still (Figure 5.5). This may correlate with increased sequestration of GLUT4 into the insulin-responsive GSV compartment resulting in a larger fraction being mobilised to the PM in response to insulin. The elevated response of STX16T compared to STX16F may be indicative of a lack of regulation. Whereas STX16F may be subject to regulation by dephosphorylation in response to insulin and /or the autoinhibitory H_{abc} domain, STX16T, lacking this domain and potential sites of phosphorylation (Chapter 3), may not. Also worth noting is the modest decrease in deGlc transport consistently observed in basal cells expressing STX16F (Figure 5.5). Again, this would correlate with increased levels of GLUT4 being sequestered from the endosomal pool and subsequently away from the cell surface in the basal state. It would be anticipated that STX16T would also exhibit decreased basal deGlc uptake; however, the absence of this effect could once again be due to a lack of regulation. Once again, further studies will be required to explore these possibilities, and it should be clearly noted that despite this trend, the data do not reach statistical significance.

MG132 functions as a competitive inhibitor of proteasome function. Since MG132 proteasome inhibitors could be used to increase adenoviral-mediated expression of the STX16 mutants, the effects of these inhibitors on deGlc transport and ACRP30 secretion were assessed. Intriguingly and unexpectedly, cells treated with MG132 displayed both inhibition of deGlc transport and ACRP30 secretion (Figures 5.2 and 5.7). Most intriguing is the fact that both effects are observed in type II diabetes.

Insulin-stimulated glucose uptake in adipocytes is highly correlated with the expression level of GLUT4, and it has been suggested that altered expression of GLUT4 in adipocytes may play a role in the insulin resistance of type II diabetes (Shepherd and Kahn, 1999). Indeed, GLUT4 protein and mRNA levels are decreased in adipocytes in most cases of

insulin resistance, including that present in human obesity and type II diabetes (Shepherd and Kahn, 1999).

A recent study reported that the treatment of cells with proteasome inhibitors, including MG132, results in a decrease in the cellular levels of GLUT4 (Cooke and Patel, 2005), a finding that most likely explains the reduced deGlc uptake observed in response to insulin in my study. The direct effect of inhibition of proteasome function might be expected to increase protein levels. The authors hypothesise that proteasome inhibition stabilized an inhibitor of GLUT4 expression and implicate a number of potential transcription factors including PPAR γ and its coactivator PGC-1 α , which have been shown to inhibit GLUT4 expression (Armoni et al., 2003; Miura et al., 2003), as likely candidates of factors that mediated the repression of GLUT4 expression with proteasome inhibition. In my study, MG132 samples were not tested for GLUT4 levels to verify this theory, however, future work should address this important issue.

ACRP30 is an abundant protein in human plasma (Maeda et al., 1996), and circulating levels decrease in parallel with increasing obesity and the progression of insulin resistance (Yang et al., 2001). The expression of ACRP30 mRNA is significantly reduced in the adipose tissue of obese humans (Hu et al., 1996) and fat loss in obese patients causes ACRP30 levels to increase (Yang et al., 2001). Insulin resistant patients also display lower levels of ACRP30 (Hotta et al., 2000; Maeda et al., 2001) and when these patients are administered thiazolidinediones (TZD), an insulin-sensitising drug, ACRP30 levels increase (Maeda et al., 2001). Most intriguing, then, is the decrease observed in ACRP30 secretion in my study after MG132 treatment (Figure 5.7). I hypothesise that this decrease in secreted protein correlates with a decrease of protein expression in a manner similar to that observed for GLUT4 (Cooke and Patel, 2005), however, it is plausible that the ACRP30 secretion pathway is perturbed by proteasome inhibition. This could be resolved by immunoblotting cell lysates for total levels of ACRP30.

So could the decreases observed in insulin-stimulated glucose transport and ACRP30 secretion be related? As mentioned above, circulating ACRP30 levels were found to decrease in parallel with increasing obesity and the progression of insulin resistance (Yang et al., 2001). However, it is not currently known whether decreased levels of ACRP30 secretion are a cause or effect of the insulin resistance. My results could suggest that there may be factors that regulate a connecting step in the two pathways, which are degraded by the proteasome. Although to discuss this further would be beyond the scope of this thesis,

it nonetheless remains intriguing that inhibition of proteasome function leads to both of these significant effects.

In conclusion, I suggest that the data presented in this Chapter, particularly that from the experiments involving STX16^{cyt} expression and MAO STX16 knockdown, provides evidence that STX16 is involved in the intracellular sorting of GLUT4. I suggest that STX16 plays a key role in delivering GLUT4 from the general endosomal system to a slowly recycling intracellular trafficking pathway, which may involve the TGN and GSVs, thus sequestering GLUT4 away from the cell surface in the absence of insulin. These findings are summarised in Figure 5.13. Whether STX16 has a further role to play in GLUT4 trafficking, such as in the biogenesis of GSVs or translocation to the PM will require careful further study, an issue which will be addressed in Chapter 6.

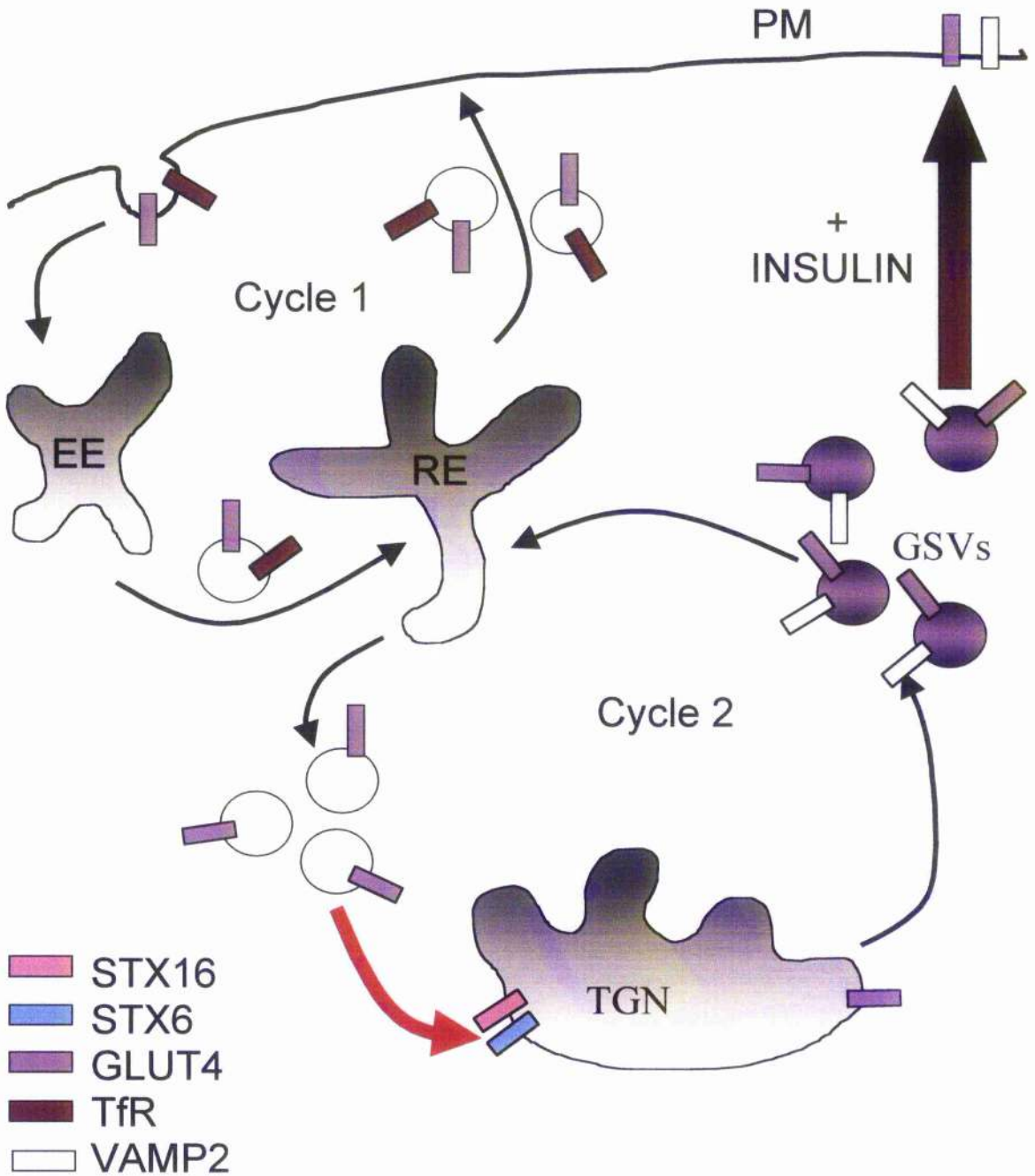


Figure 5.13 A model depicting the involvement of STX16 in GLUT4 trafficking in adipocytes (adapted from (Bryant et al., 2002))

In this model, GLUT4 occupies two main intracellular recycling pathways. **Cycle 1:** GLUT4 recycles between the cell surface and endosomes, showing co-localisation with molecules such as the TfR. **Cycle 2:** GLUT4 is sequestered away from the endosomal system and recycles more slowly between the TGN and endosomes. Insulin-responsive GSVs, enriched with VAMP2 may bud from the TGN.

A red arrow depicts the step that I anticipate to be regulated by STX16, possibly in concert with STX6. It is likely that STX16 would be involved in a SNARE complex that would allow the fusion of GLUT4-containing vesicles from the endosomal system with the TGN.

Chapter 6

Conclusions and future directions

6. Conclusions and future directions

Insulin promotes glucose uptake in muscle and adipose tissue by stimulating the translocation of the glucose transporter GLUT4 from an intracellular location to the plasma membrane (Bryant et al., 2002; Watson et al., 2004). Recent studies support a model in which the intracellular GLUT4 itinerary involves two intracellular cycles (Figure 1.9, Chapter 1). In the basal state, GLUT4 recycles between the PM and endosomes in the fast recycling endosomal system. However, a large population of GLUT4 is sorted away from the endosomal system, into a slowly recycling intracellular pathway between endosomes and the TGN. This pathway involves the sorting of GLUT4 into unique storage vesicles, GSVs, which are mobilised in response to insulin, and are responsible for the majority of GLUT4 that is delivered to the cell surface upon insulin-stimulation. The intracellular sorting of GLUT4 is therefore essential for the maintenance of blood glucose homeostasis, both to direct GLUT4 into the insulin-responsive compartment and to effectively sequester GLUT4 from the cell surface in the basal state. However, the molecules responsible for regulating this intracellular sorting remain largely unknown.

There is a substantial pool of evidence to suggest a role for the TGN localised t-SNARE STX16 in the regulated trafficking of GLUT4 in 3T3-L1 adipocytes (Perera et al., 2003; Shewan et al., 2003) (Section 1.8, Chapter 1). In this thesis, I aimed to elucidate the role of STX16 in GLUT4 trafficking and to determine whether STX16 phosphorylation played a role in the regulation of this process. The experiments described in Chapters 3-5 are discussed in detail at the end of these Chapters. This Chapter aims to summarise the main conclusions drawn and suggest the future direction of the project.

6.1. Phosphorylation of STX16

STX16 is a phosphoprotein in 3T3-L1 adipocytes and this phosphorylation is decreased by ~ 50 % following acute insulin-stimulation (Perera et al., 2003). It was decided that identification of the exact site of insulin-regulated phosphorylation in STX16 would be the first step towards the elucidation of its function. Three potential sites were identified (based on the putative PKA site in the yeast homolog, Tlg2p), mutated to alanine residues and tested for phosphorylation in HEK 293 cells. These initial studies were carried out in HEK 293 cells because they are easier to transfect than fully differentiated adipocytes. It was thought that the generation of recombinant adenoviruses (Chapter 4) at this stage would be much too time consuming and cost inefficient, and electroporation had not yet

been optimised as a method to deliver the plasmids into adipocytes. However, ^{32}P labelling suggested that neither these mutants nor wild type STX16 (expressed in the same way as the mutants) were phosphorylated in these cells. It was concluded that STX16 phosphorylation might be specific to adipocytes.

Clearly then, the next step will be to test these mutants for expression and phosphorylation directly in 3T3-L1 adipocytes. Electroporation can now be used to deliver the mutant plasmids into adipocytes and phosphorylation can be assessed by ^{32}P labelling as before. If this approach is unsuccessful, or if the hypothesised phosphorylation sites prove to be incorrect, an alternative method could be utilised to identify the site of phosphorylation in STX16. For example, STX16 could be immunoprecipitated from 3T3-L1 adipocytes and analysed for phosphorylation by tryptic digest and mass spectrometry analysis. Initially, it was anticipated that the phosphorylation site was likely to correspond directly to that in Tlg2p and therefore that it would be a simple matter to test this possibility using the phosphorylation mutants. However, with hindsight, it may have been more prudent to screen the STX16 sequence for phosphorylation sites in this way from the beginning. Nonetheless, once the site(s) has been identified, both phosphorylation-null (phospho-site to alanine) and phosphorylation-mock (phospho-site to aspartate) mutants could be generated, expressed in adipocytes and glucose transport assays (Chapter 5) performed to determine their effects on GLUT4 trafficking. Expression of these mutants in adipocytes could be achieved either by electroporation of expression vectors or adenoviral mediated gene-transfer (Chapter 4). The ability to achieve < 90 % knockdown of endogenous STX16 in adipocytes using a specific MAO (Chapter 5) provides the additional possibility to express these mutants in cells depleted of endogenous STX16.

In order to determine whether STX16 phosphorylation played a role in regulating the formation of a SNARE complex that may be involved in GLUT4 trafficking, it was deemed necessary to identify STX16 binding partners, and whether binding was affected by insulin-stimulation. These studies revealed the existence of a STX16/STX6/Vti1a SNARE complex in 3T3-L1 adipocytes, the formation of which was not altered in response to insulin and, intuitively, neither by STX16 phosphorylation. STX16 did not appear to bind to mVps45 when part of this complex, either in the presence or absence of insulin.

Due to a lack of a STX16 specific antibody at this time, these binding studies were carried out by immunoprecipitation of STX6, and not STX16, from 3T3-L1 adipocytes. SNARE pairing is known to be promiscuous, particularly in the case of STX6 (Wendler and Tooze, 2001), and it is highly plausible that the population of STX16 present in the STX6

immunoprecipitate does not correspond to that in the insulin-regulated complex. Future studies could immunoprecipitate STX16 directly, and as well as looking for potential SNARE partners, should perhaps be extended to looking at non-SNARE proteins, to allow for the possibility that STX16 phosphorylation serves another function other than to regulate SNARE complex formation. Once generated, the phosphorylation-null and phosphorylation-mock mutants described above could also be used to look for binding partners in adipocytes by means of immunoprecipitation with N-terminal tags.

In conclusion, I anticipate that STX6, STX16 and Vti1a certainly do form a complex in 3T3-L1 adipocytes but, since binding is not altered by insulin-stimulation, this does not represent the insulin-regulated complex involved in GLUT4 trafficking. It is possible that this in fact represents the complex responsible for accepting incoming traffic to the TGN from the EE as described by Mallard *et al.* (Mallard *et al.*, 2002), which would of course suggest that STX16 is involved in a general trafficking step at this location. This could be investigated by testing STX16 for its involvement in the trafficking of other molecules known to follow this route in 3T3-L1 adipocytes. However, due to the promiscuous nature of SNARE proteins, it is highly plausible that STX16 may be involved in a separate SNARE complex at another stage of GLUT4 trafficking (discussed in Chapter 3). This insulin-regulated complex may still involve STX6 and STX16 and perhaps even Vti1a, but with a different v-SNARE on the incoming vesicle. The identity of these v-SNAREs and the possible nature of this complex are discussed in Chapter 3.

6.2. Effect of STX16 on GLUT4 trafficking in 3T3-L1 adipocytes

STX16 mutants (STX16cyt and STX16T, described in detail in Chapter 4) were designed to test the function of STX16 in GLUT4 trafficking in 3T3-L1 adipocytes. Adenoviral vectors have been used in previous studies to successfully introduce genes into 3T3-L1 adipocytes (Bose *et al.*, 2001; Emoto *et al.*, 2001; Sakaue *et al.*, 1997), a cell line which is only poorly transfected using standard transfection methods (Gnudi *et al.*, 1997). Recombinant adenoviruses were therefore prepared to express these STX16 mutants and full-length STX16, STX16F. The cytosolic domain, STX16cyt, was anticipated to act as an inhibitor of the endogenous protein (Olson *et al.*, 1997; Perera *et al.*, 2003; Tellam *et al.*, 1997; Volchuk *et al.*, 1996), whereas an N-terminal truncation, STX16T, was designed to mimic the hypothesised open conformation of STX16 and therefore to represent a constitutively active version of the wild-type protein (Bryant and James, 2001). The effects

of STX16T were compared to those of expressing the full-length protein STX16F, anticipated to amplify the effects the endogenous protein (Pagan et al., 2003; Thurmond et al., 1998).

Expression of these proteins in 3T3-L1 adipocytes proved to be problematic, but perhaps informative in terms of the properties of STX16 (discussed in detail in Chapter 4). In the case of STX16cyt, which consisted of the SNARE domain and the H_{abc} domain, an apparent need for stabilisation by its cognate SM protein, mVps45, was identified. It appeared that STX16 expressed in excess of mVps45 was subject to proteasomal degradation, as expression could be increased dramatically by inhibition of proteasome function. This method of expression, however, could not be used to carry out functional assays, as treatment of cells with proteasome inhibitors dramatically decreased both insulin-stimulated glucose transport and ACRP30 secretion (discussed in detail in Chapter 5). An alternative method, involving double infection of the cells was utilised to achieve optimum expression.

When each of the proteins was expressed in 3T3-L1 adipocytes, neither basal nor insulin-stimulated glucose transport was significantly affected. Since depletion of STX16 in these cells proved that STX16 does in fact play a role in GLUT4 trafficking, it seems likely that the absence of an effect in cells expressing STX16cyt, STX16F and STX16T was due to inefficient levels of protein produced. The proteins were expressed to approximately one-fold of the level of the endogenous protein, compared to 12-16 fold for STX16 expressed in the same way (Perera et al., 2003). In the case of STX16cyt, which was designed to perturb endogenous STX16 function, the level was perhaps inefficient to achieve complete inhibition of the endogenous protein. In the case of STX16T and STX16F, the effects of these proteins on glucose transport were perhaps not observed over those of the endogenous molecule, which was still able to function correctly.

As mentioned above, the reasons for poor levels of expression appear to be due the properties of STX16, rather than a problem with the adenovirus method of expression. A complementary approach to inhibition of STX16 function via STX16cyt expression was achieved by knockdown of endogenous STX16 using a specific MAO (Chapter 5). An alternative method could have involved the generation of a recombinant adenovirus to co-express mVps45 with STX16cyt to provide the necessary stabilisation. However, the future of this study relies on the development of alternative methods to answer the questions posed by STX16T and STX16F. Expression of STX16T and STX16F attempted to address whether STX16 could adopt an open and closed conformation and, indeed, whether these

conformations could influence GLUT4 trafficking. As a starting point, homology comparisons with other Syntaxins known to adopt these conformations could be informative. These studies could lead to further structural investigations by NMR or crystallisation studies. As mentioned previously, electroporation of adipocytes was not optimised until very late this study, however this may now provide the opportunity to eliminate endogenous STX16 function when expressing STX16T and STX16F using adenovirus. Perhaps the absence of the endogenous protein will allow these mutants to be expressed to a higher level or at least will remove the interfering effects of endogenous STX16.

Finally, as the expressed mutant proteins do not run at the expected molecular weight on an SDS-PAGE gel, this could suggest that the conformations are different than that of the wild-type protein. Future work should perhaps address the exact localisation and functionality of the expressed STX16 mutants in 3T3-L1 adipocytes. To check if they are functional, the domains could be tested for their ability to interact with wild-type STX16 SNARE partners, STX6 and Vti1a, and mVps45 (Mallard et al., 2002; Perera et al., 2003; Shewan et al., 2003)(Chapter 3). This could be achieved by immunoprecipitation using antibodies specific to the HA- or myc-tags present on N-terminus of each mutant. In addition, fractionation / compartmentalisation studies could be carried out to ensure that the proteins are accurately targeted to the correct compartment in 3T3-L1 adipocytes. Preliminary results suggest that STX16_{cyt} is present in both a cytosolic and a membrane fraction (not shown) in adipocytes, in keeping with its cytosolic nature and ability to bind to membrane-bound SNAREs. This could be repeated to ensure that STX16T and STX16F are inserted into membranes. Immunofluorescence studies would allow the comparison of the localisation of the mutants in 3T3-L1 adipocytes with endogenous STX16.

Despite the low levels of protein produced, expression of STX16_{cyt} significantly slowed the reversal of GLUT4 trafficking after insulin withdrawal but did not affect ACRP30 secretion. In the complementary method, depletion of STX16 significantly reduced insulin-stimulated deGlc transport, corresponding to a decrease in GLUT4 expression in these cells. These results are discussed in detail in Chapter 5 but in summary, they were explained within a model in which STX16 plays an important role in the intracellular sorting of GLUT4 but not ACRP30. It was hypothesised that STX16 functions to sequester GLUT4 away from the fast recycling endosomal system into a slowly recycling intracellular loop involving the TGN and GSVs. When STX16 is depleted, GLUT4 is no longer sorted into this pathway and appears to be rerouted to a degradative pathway.

6.3. Model of STX16 in GLUT4 trafficking

A model is described in Chapter 5 (Section 5.7, Figure 5.13), which suggests that the intracellular GLUT4 sorting step involving STX16 may involve the sorting of GLUT4 away from the endosomal system to the TGN. To expand on this model, this trafficking step may constitute a general trafficking step at this location, as described by Mallard *et al.* (Mallard *et al.*, 2002) or perhaps a more specific route taken exclusively by GLUT4 to the TGN subdomain enriched in STX16 and STX6 described by Shewan *et al.* (Shewan *et al.*, 2003). Vti1a has also been reported to colocalise with GLUT4 in such a TGN subdomain (Bose *et al.*, 2005), suggesting this could indeed be the third t-SNARE involved in this complex. Of course, the presence of STX16 in GSVs and its apparent translocation to the cell surface upon insulin-stimulation (Bose *et al.*, 2005; Perera *et al.*, 2003) must also be addressed. I offer the hypothesis that since STX16 is involved in the sorting of GLUT4 to the TGN or a TGN subdomain, perhaps from which GSVs bud, then STX16 might become incorporated into these vesicles during the budding of GSVs from this compartment in a manner similar to the inclusion of unnecessary cargo molecules, such as MPRs, during the budding of immature secretory granules from the TGN (Tooze *et al.*, 2001). The nature of GSVs remains controversial (Section 1.7.4) (Bryant *et al.*, 2002), however, supposing GSVs do not undergo a process of maturation similar to secretory granules during which unnecessary molecules are removed, then this could explain the translocation of STX16 to the cell surface in these vesicles. This theory may also apply to STX6 and Vti1a, which also appear to demonstrate insulin-stimulated translocation to the cell surface (Bose *et al.*, 2005; Perera *et al.*, 2003).

I also offer a hypothesis for the phosphorylation of STX16, given the trafficking step that I predict it to be involved in, from which future studies can build. I hypothesise that in the basal state, when STX16 is phosphorylated, it forms a SNARE complex which functions to sort GLUT4 from the fast recycling endosomal system into the slowly recycling intracellular pathway, thus sequestering GLUT4 away from the cell surface. Then in response to insulin, when STX16 becomes dephosphorylated, assembly of this SNARE complex is inhibited, blocking traffic into this slowly recycling compartment. This could either cause GLUT4 to re-enter the endosomal system and increase its delivery to the cell surface in this way or perhaps this is responsible for the modest slowing of GLUT4 endocytosis observed in insulin-stimulated cells (Jhun *et al.*, 1992; Yang and Holman, 1993). In fact, this slowing down of the endocytic retrieval of GLUT4 was observed when STX16 function was partially inhibited using STX16cyt. On the other hand, when STX16

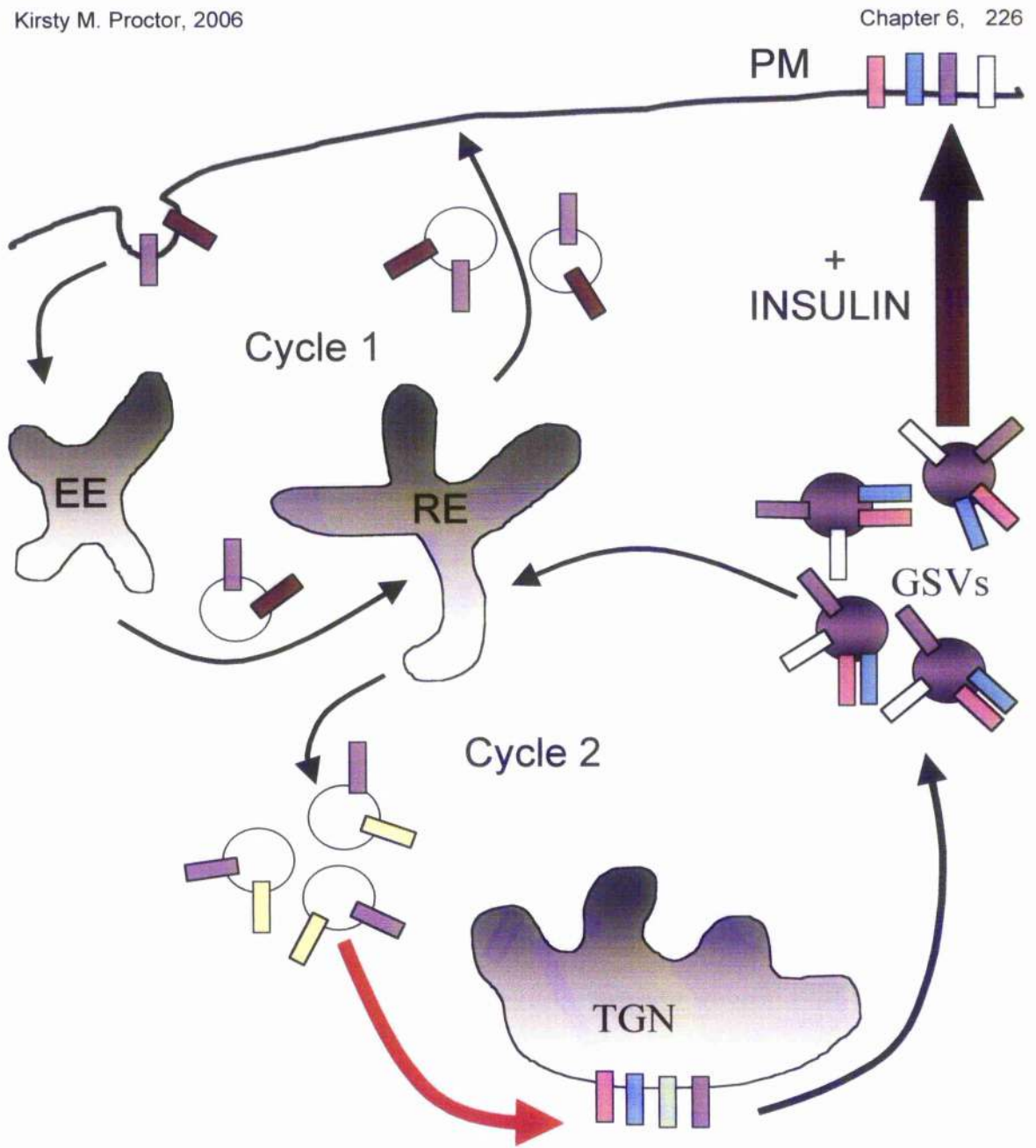
was almost completely depleted in fat cells, insulin-stimulated glucose transport was reduced, apparently owing to the rerouting of GLUT4 to a degradative pathway. This is perhaps why only a 50 % reduction in phosphorylation is observed upon insulin-stimulation (Perera et al., 2003). This would be sufficient to slow the intracellular sequestration of GLUT4 without completely inhibiting the pathway.

To conclude my thesis, I would like to present a model in which I have put together both the data from my own experiments, along with the current literature, to suggest a possible role for STX16 in GLUT4 trafficking (Figures 6.1 and 6.2). The full testing of these models will require careful future study.

Figure 6.1 A possible model depicting the involvement of STX16 in GLUT4 trafficking in adipocytes (adapted from Bryant et al., 2002)

In this model, GLUT4 occupies two main intracellular recycling pathways. In the basal state, GLUT4 recycles between the PM and endosomes in the fast recycling endosomal system and shows co-localisation with recycling molecules such as the TfR (**Cycle 1**). A large population of GLUT4 is sequestered away from the endosomal system into a slowly recycling pathway between endosomes and the TGN (**Cycle 2**). This pathway involves the sorting of GLUT4 into unique storage vesicles (GSVs) enriched in VAMP2, which are mobilised in response to insulin and are responsible for the majority of GLUT4 that is delivered to the cell surface in response to insulin.

A red arrow depicts the step that I anticipate to be regulated by STX16. I hypothesise that STX16 would be involved in a SNARE complex, perhaps involving STX6 and Vti1a, which would allow the fusion of sequestered GLUT4-containing vesicles from the endosomal system with a region of the TGN. This may constitute the TGN subdomain enriched in STX6 and STX16 previously described (Shewan et al., 2003). GSVs may bud from this region, thus incorporating STX16 and STX6 into these vesicles and explaining their translocation to the PM upon insulin-stimulation (Perera et al., 2003).



- STX16
- STX6
- GLUT4
- VAMP3/4
- TfR
- VAMP2
- Vti1a

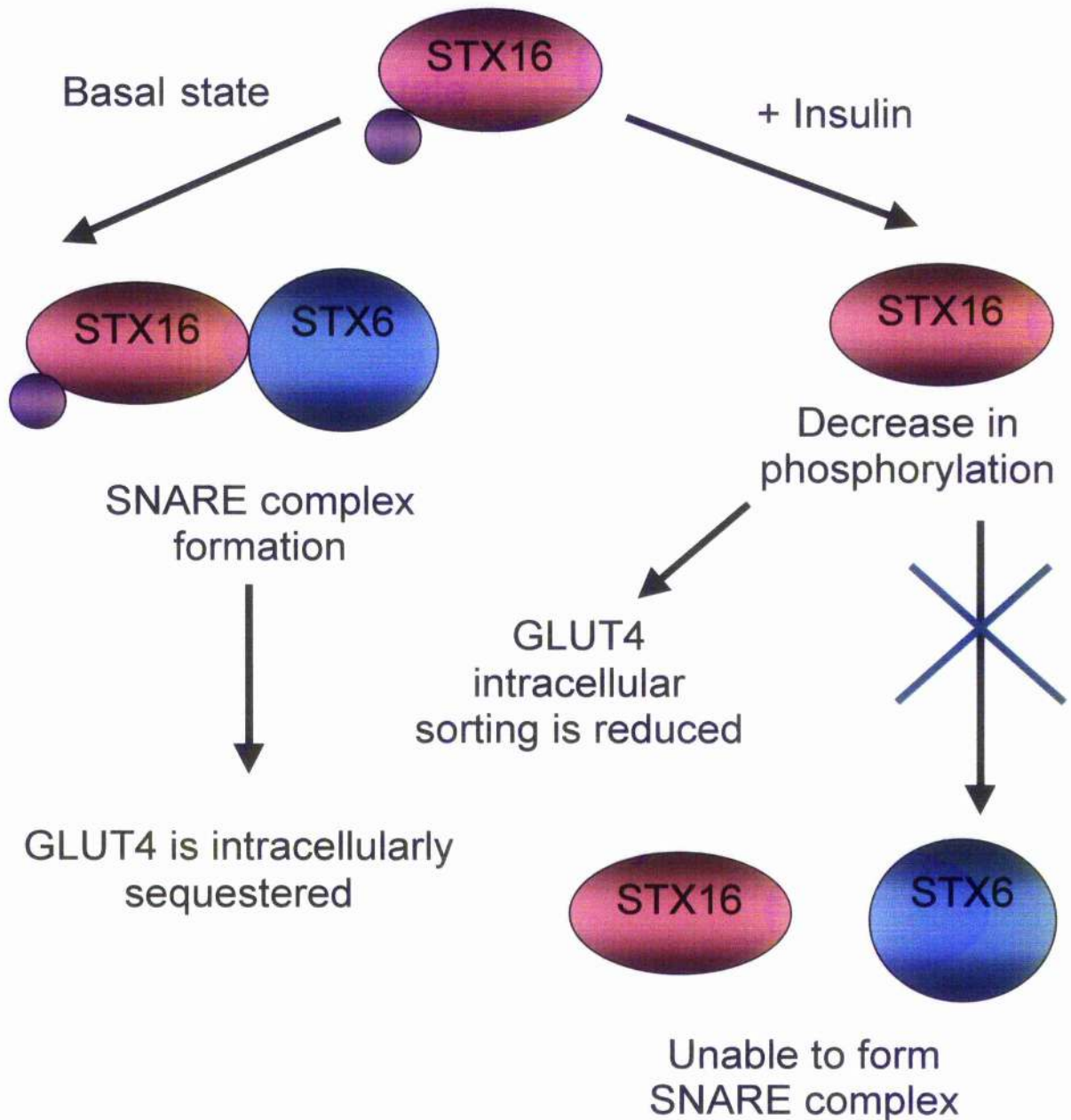
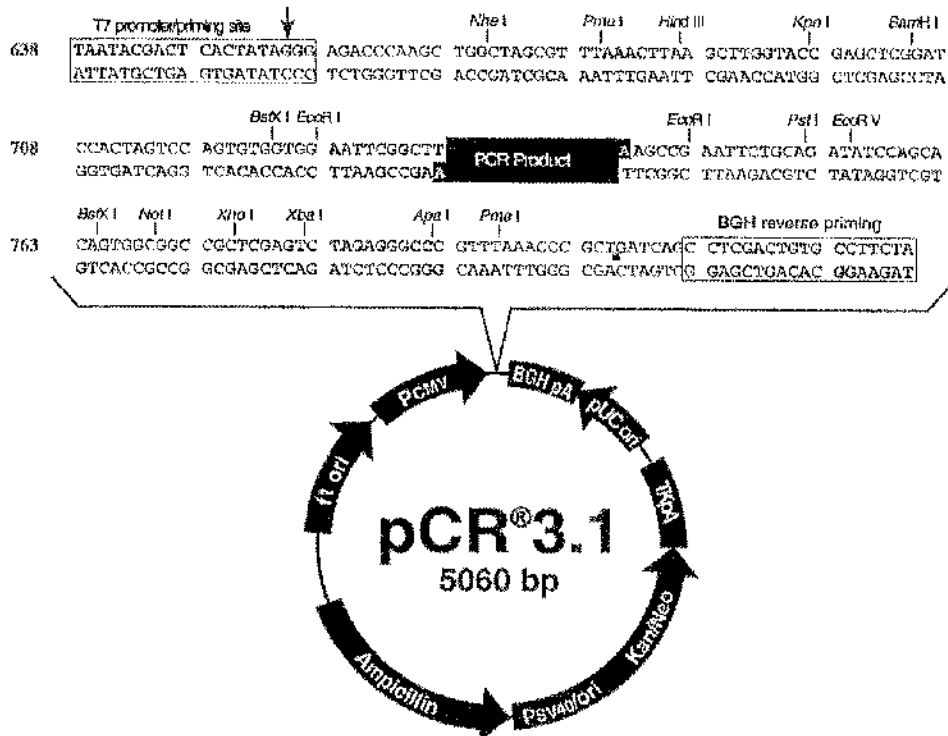


Figure 6.2 Model depicting the possible role of STX16 phosphorylation in regulation of GLUT4 trafficking

In the basal state STX16 is phosphorylated and able to bind to its SNARE partner, STX6. This SNARE complex may be involved in the intracellular sorting of GLUT4 into the slowly recycling compartment as described in Figure 6.1. Upon insulin-stimulation, phosphorylation of STX16 is decreased by ~ 50 % and SNARE complex formation is inhibited. Blockade of this trafficking step may slow the intracellular sorting of GLUT4 into slowly recycling compartment, thus increasing its presence at the cell surface during insulin-stimulation.

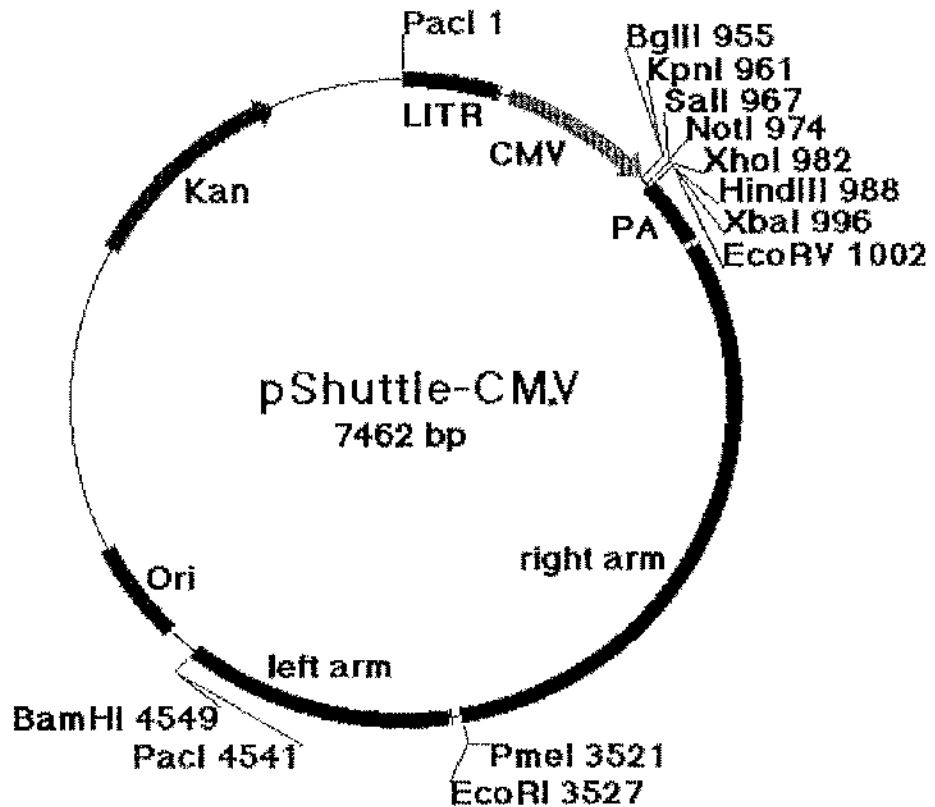
Previous work has suggested that (de)phosphorylation of t-SNAREs could regulate the formation of functional SNARE complexes (Gerst, 2003). This model is based on my assumption that phosphorylation of STX16 will promote SNARE complex assembly.

Appendix

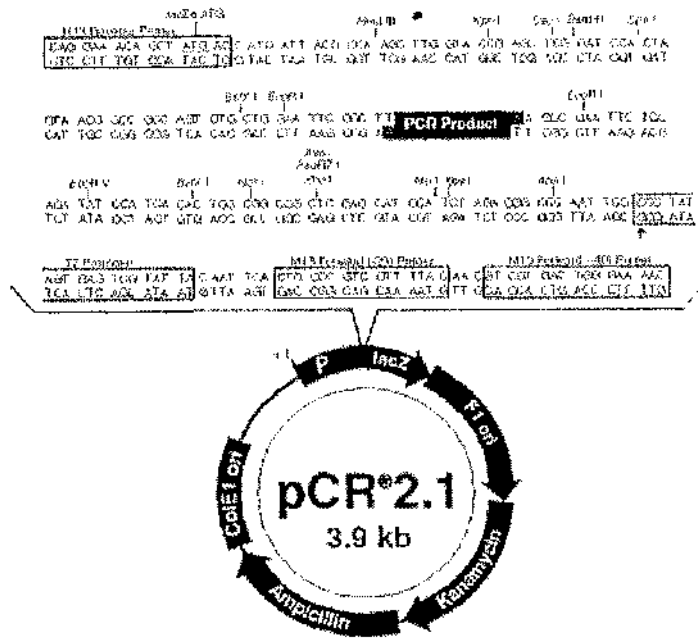


PCR3.1 vector for expression in mammalian cells

pCR3.1 is a 5 kb cloning vector containing Ampicillin and Neomycin/Kanamycin resistance genes for selection. The gene of interest is inserted in the multiple cloning region (bases 670-801), following the CMV promoter (bases 1-596).



pShuttle-CMV vector is described by He *et. al.* (He *et. al.*, 1998). This vector contains a multiple cloning site for insertion of exogenous transgenes between the cytomegalovirus (CMV) promoter and a polyadenylation site. It contains a polylinker for the expression of transgenes, surrounded by adenoviral sequences (“arms”) that allow homologous recombination with the adenovirus backbone. Artificially created *PacI* sites surround both arms. The pShuttle plasmid also contains a Kanamycin resistance gene and the origin of replication from pBR322.



pCR2.1 for TA cloning

pCR2.1 is a 3.9 kb vector containing Ampicillin and Kanamycin resistance genes for selection. The gene of interest is TA cloned into this vector as described in Section 2.2.6. pCR2.1 contains the lacZ-alpha complementation fragment for blue-white colour screening.

References

- Abel, E.D., Peroni, O., Kim, J.K., Kim, Y.B., Boss, O., Hadro, E., Minnemann, T., Shulman, G.I., and Kahn, B.B. (2001). Adipose-selective targeting of the GLUT4 gene impairs insulin action in muscle and liver. *Nature* 409, 729-733.
- Abeliovich, H., Darsow, T., and Emr, S.D. (1999). Cytoplasm to vacuole trafficking of aminopeptidase I requires a t-SNARE-Sec1p complex composed of Tlg2p and Vps45p. *EMBO J.* 18, 6005-6016.
- Abeliovich, H., Grote, E., Novick, P., and Ferro-Novick, S. (1998). Tlg2p, a yeast syntaxin homolog that resides on the Golgi and endocytic structures. *J. Biol. Chem.* 273, 11719-11727.
- Acsadi, G., Jani, A., Huard, J., Blaschuk, K., Massie, B., Holland, P., Lochmuller, H., and Karpati, G. (1994). Cultured human myoblasts and myotubes show markedly different transducibility by replication-defective adenovirus recombinants. *Gene Ther.* 1, 338-340.
- Allan, B.B. and Balch, W.E. (1999). Protein sorting by directed maturation of Golgi compartments. *Science* 285, 63-66.
- Alonso, A., Sasin, J., Bottini, N., Friedberg, I., Friedberg, I., Osterman, A., Godzik, A., Hunter, T., Dixon, J., and Mustelin, T. (2004). Protein tyrosine phosphatases in the human genome. *Cell* 117, 699-711.
- Amos, A.F., McCarty, D.J., and Zimmet, P. (1997). The rising global burden of diabetes and its complications: estimates and projections to the year 2010. *Diabet. Med.* 14 Suppl 5, S1-85.
- Anderson, R.D., Haskell, R.E., Xia, H., Roessler, B.J., and Davidson, B.L. (2000). A simple method for the rapid generation of recombinant adenovirus vectors. *Gene Ther.* 7, 1034-1038.
- Antonin, W., Fasshauer, D., Becker, S., Jahn, R., and Schneider, T.R. (2002). Crystal structure of the endosomal SNARE complex reveals common structural principles of all SNAREs. *Nat. Struct. Biol.* 9, 107-111.
- Armoni, M., Kritiz, N., Harel, C., Bar-Yoseph, F., Chen, H., Quon, M.J., and Karnieli, E. (2003). Peroxisome proliferator-activated receptor-gamma represses GLUT4 promoter activity in primary adipocytes, and rosiglitazone alleviates this effect. *J. Biol. Chem.* 278, 30614-30623.
- Bai, M., Harfe, B., and Freimuth, P. (1993). Mutations that alter an Arg-Gly-Asp (RGD) sequence in the adenovirus type 2 penton base protein abolish its cell-rounding activity and delay virus reproduction in flat cells. *J. Virol.* 67, 5198-5205.
- Barlow, C. (2000). Traffic COPs of the Early Secretory Pathway. *Traffic.* 1, 371-377.
- Barr, V.A., Malide, D., Zarnowski, M.J., Taylor, S.I., and Cushman, S.W. (1997). Insulin stimulates both leptin secretion and production by rat white adipose tissue. *Endocrinology* 138, 4463-4472.

- Baumert, M., Maycox, P.R., Navone, F., De Camilli, P., and Jahn, R. (1989). Synaptobrevin: an integral membrane protein of 18, 000 daltons present in small synaptic vesicles of rat brain. *EMBO J.* 8, 379-384.
- Bennett, M.K., Calakos, N., and Scheller, R.H. (1992). Syntaxin: a synaptic protein implicated in docking of synaptic vesicles at presynaptic active zones. *Science* 257, 255-259.
- Bennett, M.K., Garcia-Araras, J.E., Elferink, L.A., Peterson, K., Fleming, A.M., Hazuka, C.D., and Scheller, R.H. (1993). The syntaxin family of vesicular transport receptors. *Cell* 74, 863-873.
- Bennett, M.K. and Scheller, R.H. (1993). The molecular machinery for secretion is conserved from yeast to neurons. *Proc. Natl. Acad. Sci. U. S. A* 90, 2559-2563.
- Bergelson, J.M., Cunningham, J.A., Droguett, G., Kurt-Jones, E.A., Krithivas, A., Hong, J.S., Horwitz, M.S., Crowell, R.L., and Finberg, R.W. (1997). Isolation of a common receptor for Coxsackie B viruses and adenoviruses 2 and 5. *Science* 275, 1320-1323.
- Bochtler, M., Ditzel, L., Groll, M., Hartmann, C., and Huber, R. (1999). The proteasome. *Annu. Rev. Biophys. Biomol. Struct.* 28, 295-317.
- Bock, J.B., Klumperman, J., Davanger, S., and Scheller, R.H. (1997). Syntaxin 6 functions in trans-Golgi network vesicle trafficking. *Mol. Biol. Cell* 8, 1261-1271.
- Bock, J.B., Lin, R.C., and Scheller, R.H. (1996). A new syntaxin family member implicated in targeting of intracellular transport vesicles. *J. Biol. Chem.* 271, 17961-17965.
- Bock, J.B., Matern, H.T., Peden, A.A., and Scheller, R.H. (2001). A genomic perspective on membrane compartment organization. *Nature* 409, 839-841.
- Bogan, J.S. and Lodish, H.F. (1999). Two compartments for insulin-stimulated exocytosis in 3T3-L1 adipocytes defined by endogenous ACRP30 and GLUT4. *J. Cell Biol.* 146, 609-620.
- Bonifacino, J.S. and Weissman, A.M. (1998). Ubiquitin and the control of protein fate in the secretory and endocytic pathways. *Annu. Rev. Cell Dev. Biol.* 14, 19-57.
- Bose, A., Cherniack, A.D., Langille, S.L., Nicoloso, S.M., Buxton, J.M., Park, J.G., Chawla, A., and Czech, M.P. (2001). G(alpha)11 signaling through ARF6 regulates F-actin mobilization and GLUT4 glucose transporter translocation to the plasma membrane. *Mol. Cell Biol.* 21, 5262-5275.
- Bose, A., Guilherme, A., Huang, S., Hubbard, A.C., Lane, C.R., Soriano, N.A., and Czech, M.P. (2005). The γ -SNARE Vtila regulates insulin-stimulated glucose transport and Acp30 secretion in 3T3-L1 adipocytes. *J. Biol. Chem.* 280, 36946-36951.
- Bradford, M.M. (1976). A rapid and sensitive method for the quantitation of microgram quantities of protein utilizing the principle of protein-dye binding. *Anal. Biochem.* 72, 248-254.
- Brickner, J.H., Blanchette, J.M., Sipos, G., and Fuller, R.S. (2001). The Tlg SNARE complex is required for TGN homotypic fusion. *J. Cell Biol.* 155, 969-978.

- Brownlee, M. (2001). Biochemistry and molecular cell biology of diabetic complications. *Nature* 414, 813-820.
- Bruning, J.C., Michael, M.D., Winnay, J.N., Hayashi, T., Horsch, D., Accili, D., Goodyear, L.J., and Kahn, C.R. (1998). A muscle-specific insulin receptor knockout exhibits features of the metabolic syndrome of NIDDM without altering glucose tolerance. *Mol. Cell* 2, 559-569.
- Bryant, N.J., Govers, R., and James, D.E. (2002). Regulated transport of the glucose transporter GLUT4. *Nat. Rev. Mol. Cell Biol.* 3, 267-277.
- Bryant, N.J. and James, D.E. (2001). Vps45p stabilizes the syntaxin homologue Tlg2p and positively regulates SNARE complex formation. *EMBO J.* 20, 3380-3388.
- Carmen, G.Y. and Victor, S.M. (2006). Signalling mechanisms regulating lipolysis. *Cell Signal.* 18, 401-408.
- Carr, C.M., Grote, E., Munson, M., Hughson, F.M., and Novick, P.J. (1999). Sec1p binds to SNARE complexes and concentrates at sites of secretion. *J. Cell Biol.* 146, 333-344.
- Cheatham, B., Volchuk, A., Kahn, C.R., Wang, L., Rhodes, C.J., and Klip, A. (1996). Insulin-stimulated translocation of GLUT4 glucose transporters requires SNARE-complex proteins. *Proc. Natl. Acad. Sci. U. S. A* 93, 15169-15173.
- Chen, F., Foran, P., Shone, C.C., Foster, K.A., Melling, J., and Dolly, J.O. (1997). Botulinum neurotoxin B inhibits insulin-stimulated glucose uptake into 3T3-L1 adipocytes and cleaves cellubrevin unlike type A toxin which failed to proteolyze the SNAP-23 present. *Biochemistry* 36, 5719-5728.
- Chen, Y.A. and Scheller, R.H. (2001). SNARE-mediated membrane fusion. *Nat. Rev. Mol. Cell Biol.* 2, 98-106.
- Chroboczek, J., Bieber, F., and Jacrot, B. (1992). The sequence of the genome of adenovirus type 5 and its comparison with the genome of adenovirus type 2. *Virology* 186, 280-285.
- Claguc, M.J. (1998). Molecular aspects of the endocytic pathway. *Biochem. J.* 336 (Pt 2), 271-282.
- Coe, J.G., Lim, A.C., Xu, J., and Hong, W. (1999). A role for Tlg1p in the transport of proteins within the Golgi apparatus of *Saccharomyces cerevisiae*. *Mol. Biol. Cell* 10, 2407-2423.
- Cohen, P. (2002). The origins of protein phosphorylation. *Nat. Cell Biol.* 4, E127-E130.
- Conti, M. (2000). Phosphodiesterases and cyclic nucleotide signaling in endocrine cells. *Mol. Endocrinol.* 14, 1317-1327.
- Cooke, D.W. and Patel, Y.M. (2005). GLUT4 expression in 3T3-L1 adipocytes is repressed by proteasome inhibition, but not by inhibition of calpains. *Mol. Cell Endocrinol.* 232, 37-45.
- Daro, E., van der, S.P., Galli, T., and Mellman, I. (1996). Rab4 and cellubrevin define different early endosome populations on the pathway of transferrin receptor recycling. *Proc. Natl. Acad. Sci. U. S. A* 93, 9559-9564.

- Dascher, C., Matteson, J., and Balch, W.E. (1994). Syntaxin 5 regulates endoplasmic reticulum to Golgi transport. *J. Biol. Chem.* 269, 29363-29366.
- Dulubova, I., Sugita, S., Hill, S., Hosaka, M., Fernandez, I., Sudhof, T.C., and Rizo, J. (1999). A conformational switch in syntaxin during exocytosis: role of munc18. *EMBO J.* 18, 4372-4382.
- Dulubova, I., Yamaguchi, T., Gao, Y., Min, S.W., Huryeva, I., Sudhof, T.C., and Rizo, J. (2002). How Tlg2p/syntaxin 16 'snares' Vps45. *EMBO J.* 21, 3620-3631.
- Dulubova, I., Yamaguchi, T., Wang, Y., Sudhof, T.C., and Rizo, J. (2001). Vam3p structure reveals conserved and divergent properties of syntaxins. *Nat. Struct. Biol.* 8, 258-264.
- El Jack, A.K., Kandror, K.V., and Pilch, P.F. (1999). The formation of an insulin-responsive vesicular cargo compartment is an early event in 3T3-L1 adipocyte differentiation. *Mol. Biol. Cell* 10, 1581-1594.
- Ellgaard, L., Molinari, M., and Helenius, A. (1999). Setting the standards: quality control in the secretory pathway. *Science* 286, 1882-1888.
- Emoto, M., Langille, S.E., and Czech, M.P. (2001). A role for kinesin in insulin-stimulated GLUT4 glucose transporter translocation in 3T3-L1 adipocytes. *J. Biol. Chem.* 276, 10677-10682.
- Errede, B. and Levin, D.E. (1993). A conserved kinase cascade for MAP kinase activation in yeast. *Curr. Opin. Cell Biol.* 5, 254-260.
- Ewart, M.A., Clarke, M., Kane, S., Chamberlain, L.H., and Gould, G.W. (2005). Evidence for a role of the exocyst in insulin-stimulated Glut4 trafficking in 3T3-L1 adipocytes. *J. Biol. Chem.* 280, 3812-3816.
- Fasshauer, D., Eliason, W.K., Brunger, A.T., and Jahn, R. (1998a). Identification of a minimal core of the synaptic SNARE complex sufficient for reversible assembly and disassembly. *Biochemistry* 37, 10354-10362.
- Fasshauer, D., Sutton, R.B., Brunger, A.T., and Jahn, R. (1998b). Conserved structural features of the synaptic fusion complex: SNARE proteins reclassified as Q- and R-SNAREs. *Proc. Natl. Acad. Sci. U. S. A* 95, 15781-15786.
- Fernandez, I., Ubach, J., Dulubova, I., Zhang, X., Sudhof, T.C., and Rizo, J. (1998). Three-dimensional structure of an evolutionarily conserved N-terminal domain of syntaxin 1A. *Cell* 94, 841-849.
- Ferro-Novick, S. and Jahn, R. (1994). Vesicle fusion from yeast to man. *Nature* 370, 191-193.
- Foran, P.G., Fletcher, L.M., Oatey, P.B., Mohammed, N., Dolly, J.O., and Tavaré, J.M. (1999). Protein kinase B stimulates the translocation of GLUT4 but not GLUT1 or transferrin receptors in 3T3-L1 adipocytes by a pathway involving SNAP-23, syntaxobrevin-2, and/or cellubrevin. *J. Biol. Chem.* 274, 28087-28095.

Foster, L.J. and Klip, A. (2000). Mechanism and regulation of GLUT-4 vesicle fusion in muscle and fat cells. *Am. J. Physiol Cell Physiol* 279, C877-C890.

Galli, T., Zahraoui, A., Vaidyanathan, V.V., Raposo, G., Tian, J.M., Karin, M., Niemann, H., and Louvard, D. (1998). A novel tetanus neurotoxin-insensitive vesicle-associated membrane protein in SNARE complexes of the apical plasma membrane of epithelial cells. *Mol. Biol. Cell* 9, 1437-1448.

Ganda, O.P. (2000). Lipoatrophy, lipodystrophy, and insulin resistance. *Ann. Intern. Med.* 133, 304-306.

Garippa, R.J., Johnson, A., Park, J., Petrush, R.L., and McGraw, T.E. (1996). The carboxyl terminus of GLUT4 contains a serine-leucine-leucine sequence that functions as a potent internalization motif in Chinese hamster ovary cells. *J. Biol. Chem.* 271, 20660-20668.

Garippa, R.J., Judge, T.W., James, D.E., and McGraw, T.E. (1994). The amino terminus of GLUT4 functions as an internalization motif but not an intracellular retention signal when substituted for the transferrin receptor cytoplasmic domain. *J. Cell Biol.* 124, 705-715.

Garza, L.A. and Birnbaum, M.J. (2000). Insulin-responsive aminopeptidase trafficking in 3T3-L1 adipocytes. *J. Biol. Chem.* 275, 2560-2567.

Gerst, J.E. (2003). SNARE regulators: matchmakers and matchbreakers. *Biochim. Biophys. Acta* 1641, 99-110.

Ghosh, P., Dahms, N.M., and Kornfeld, S. (2003). Mannose 6-phosphate receptors: new twists in the tale. *Nat. Rev. Mol. Cell Biol.* 4, 202-212.

Gibbs, E.M., Allard, W.J., and Lienhard, G.E. (1986). The glucose transporter in 3T3-L1 adipocytes is phosphorylated in response to phorbol ester but not in response to insulin. *J. Biol. Chem.* 261, 16597-16603.

Gillingham, A.K., Koumanov, F., Pryor, P.R., Reaves, B.J., and Holman, G.D. (1999). Association of $\Delta P1$ adaptor complexes with GLUT4 vesicles. *J. Cell Sci.* 112 (Pt 24), 4793-4800.

Gnudi, L., Frevert, E.U., Houseknecht, K.L., Erhardt, P., and Kahn, B.B. (1997). Adenovirus-mediated gene transfer of dominant negative ras(asn17) in 3T3L1 adipocytes does not alter insulin-stimulated P13-kinase activity or glucose transport. *Mol. Endocrinol.* 11, 67-76.

Gould, G.W. and Bell, G.I. (1990). Facilitative glucose transporters: an expanding family. *Trends Biochem. Sci.* 15, 18-23.

Graham, F.L., Smiley, J., Russell, W.C., and Nairn, R. (1977). Characteristics of a human cell line transformed by DNA from human adenovirus type 5. *J. Gen. Virol.* 36, 59-74.

Gruenberg, J. and Kreis, T.E. (1995). Membranes and sorting. *Curr. Opin. Cell Biol.* 7, 519-522.

Gual, P., Marchand-Brustel, Y., and Tanti, J.F. (2005). Positive and negative regulation of insulin signaling through IRS-1 phosphorylation. *Biochimie* 87, 99-109.

- Gurunathan, S., Chapman-Shimshoni, D., Trajkovic, S., and Gerst, J.E. (2000). Yeast exocytic v-SNAREs confer endocytosis. *Mol. Biol. Cell* 11, 3629-3643.
- Gurunathan, S., Marash, M., Weinberger, A., and Gerst, J.E. (2002). t-SNARE phosphorylation regulates endocytosis in yeast. *Mol. Biol. Cell* 13, 1594-1607.
- Hanks, S.K. and Hunter, T. (1995). Protein kinases 6. The eukaryotic protein kinase superfamily: kinase (catalytic) domain structure and classification. *FASEB J.* 9, 576-596.
- Hanson, P.I., Roth, R., Morisaki, H., Jahn, R., and Heuser, J.E. (1997). Structure and conformational changes in NSF and its membrane receptor complexes visualized by quick-freeze/deep-etch electron microscopy. *Cell* 90, 523-535.
- Harrison, S.D., Broadie, K., van de, G.J., and Rubin, G.M. (1994). Mutations in the *Drosophila* Rop gene suggest a function in general secretion and synaptic transmission. *Neuron* 13, 555-566.
- Hashiramoto, M. and James, D.E. (2000). Characterization of insulin-responsive GLUT4 storage vesicles isolated from 3T3-L1 adipocytes. *Mol. Cell Biol.* 20, 416-427.
- Hata, Y., Slaughter, C.A., and Sudhof, T.C. (1993). Synaptic vesicle fusion complex contains unc-18 homologue bound to syntaxin. *Nature* 366, 347-351.
- Hatsuzawa, K., Hirose, H., Tani, K., Yamamoto, A., Scheller, R.H., and Tagaya, M. (2000). Syntaxin 18, a SNAP receptor that functions in the endoplasmic reticulum, intermediate compartment, and cis-Golgi vesicle trafficking. *J. Biol. Chem.* 275, 13713-13720.
- Hay, J.C. (2001). SNARE complex structure and function. *Exp. Cell Res.* 271, 10-21.
- Hayashi, T., McMahon, H., Yamasaki, S., Binz, T., Hata, Y., Sudhof, T.C., and Niemann, H. (1994). Synaptic vesicle membrane fusion complex: action of clostridial neurotoxins on assembly. *EMBO J.* 13, 5051-5061.
- He, T.C., Zhou, S., da Costa, L.T., Yu, J., Kinzler, K.W., and Vogelstein, B. (1998). A simplified system for generating recombinant adenoviruses. *Proc. Natl. Acad. Sci. U. S. A.* 95, 2509-2514.
- Hickson, G.R., Chamberlain, L.H., Maier, V.H., and Gould, G.W. (2000). Quantification of SNARE protein levels in 3T3-L1 adipocytes: implications for insulin-stimulated glucose transport. *Biochem. Biophys. Res. Commun.* 270, 841-845.
- Hill, M.M., Andjelkovic, M., Brazil, D.P., Ferrari, S., Fabbro, D., and Hemmings, B.A. (2001). Insulin-stimulated protein kinase B phosphorylation on Ser-473 is independent of its activity and occurs through a staurosporine-insensitive kinase. *J. Biol. Chem.* 276, 25643-25646.
- Hitt, M.M., Addison, C.L., and Graham, F.L. (1997). Human adenovirus vectors for gene transfer into mammalian cells. *Adv. Pharmacol.* 40, 137-206.
- Hodel, A. (1998). SNAP-25. *Int. J. Biochem. Cell Biol.* 30, 1069-1073.

- Hohl, T.M., Parlati, F., Wimmer, C., Rothman, J.E., Sollner, T.H., and Engelhardt, H. (1998). Arrangement of subunits in 20 S particles consisting of NSF, SNAPs, and SNARE complexes. *Mol. Cell* 2, 539-548.
- Holman, G.D., Lo, L.L., and Cushman, S.W. (1994). Insulin-stimulated GLUT4 glucose transporter recycling. A problem in membrane protein subcellular trafficking through multiple pools. *J. Biol. Chem.* 269, 17516-17524.
- Holthuis, J.C., Nichols, B.J., Dhruvakumar, S., and Pelham, H.R. (1998a). Two syntaxin homologues in the TGN/endosomal system of yeast. *EMBO J.* 17, 113-126.
- Holthuis, J.C., Nichols, B.J., and Pelham, H.R. (1998b). The syntaxin Tlg1p mediates trafficking of chitin synthase III to polarized growth sites in yeast. *Mol. Biol. Cell* 9, 3383-3397.
- Hosono, R., Hekimi, S., Kamiya, Y., Sassa, T., Murakami, S., Nishiwaki, K., Miwa, J., Taketo, A., and Kodaira, K.I. (1992). The unc-18 gene encodes a novel protein affecting the kinetics of acetylcholine metabolism in the nematode *Caenorhabditis elegans*. *J. Neurochem.* 58, 1517-1525.
- Hotta, K., Funahashi, T., Arita, Y., Takahashi, M., Matsuda, M., Okamoto, Y., Iwahashi, H., Kuriyama, H., Ouchi, N., Maeda, K., Nishida, M., Kihara, S., Sakai, N., Nakajima, T., Hasegawa, K., Muraguchi, M., Ohmoto, Y., Nakamura, T., Yamashita, S., Hanafusa, T., and Matsuzawa, Y. (2000). Plasma concentrations of a novel, adipose-specific protein, adiponectin, in type 2 diabetic patients. *Arterioscler. Thromb. Vasc. Biol.* 20, 1595-1599.
- Hu, E., Liang, P., and Spiegelman, B.M. (1996). AdipoQ is a novel adipose-specific gene dysregulated in obesity. *J. Biol. Chem.* 271, 10697-10703.
- Inoue, A., Obata, K., and Akagawa, K. (1992). Cloning and sequence analysis of cDNA for a neuronal cell membrane antigen, HPC-1. *J. Biol. Chem.* 267, 10613-10619.
- Jahn, R. and Sudhof, T.C. (1999). Membrane fusion and exocytosis. *Annu. Rev. Biochem.* 68, 863-911.
- Jhun, B.H., Rampal, A.L., Liu, H., Lachaal, M., and Jung, C.Y. (1992). Effects of insulin on steady state kinetics of GLUT4 subcellular distribution in rat adipocytes. Evidence of constitutive GLUT4 recycling. *J. Biol. Chem.* 267, 17710-17715.
- Jiang, Z.Y., Zhou, Q.L., Coleman, K.A., Chouinard, M., Boese, Q., and Czech, M.P. (2003). Insulin signaling through Akt/protein kinase B analyzed by small interfering RNA-mediated gene silencing. *Proc. Natl. Acad. Sci. U. S. A* 100, 7569-7574.
- Kahn, B.B. and Flier, J.S. (2000). Obesity and insulin resistance. *J. Clin. Invest* 106, 473-481.
- Kandror, K.V. and Pilch, P.F. (1996a). Compartmentalization of protein traffic in insulin-sensitive cells. *Am. J. Physiol* 271, E1-14.
- Kandror, K.V. and Pilch, P.F. (1996b). The insulin-like growth factor II/mannose 6-phosphate receptor utilizes the same membrane compartments as GLUT4 for insulin-dependent trafficking to and from the rat adipocyte cell surface. *J. Biol. Chem.* 271, 21703-21708.

- Kao, A.W., Ceresa, B.P., Santeler, S.R., and Pessin, J.F. (1998). Expression of a dominant interfering dynamin mutant in 3T3L1 adipocytes inhibits GLUT4 endocytosis without affecting insulin signaling. *J. Biol. Chem.* 273, 25450-25457.
- Kitagawa, K., Rosen, B.S., Spiegelman, B.M., Lienhard, G.E., and Tanner, L.I. (1989). Insulin stimulates the acute release of adiponectin from 3T3-L1 adipocytes. *Biochim. Biophys. Acta* 1014, 83-89.
- Klumpperman, J., Kuliawat, R., Griffith, J.M., Geuze, H.J., and Arvan, P. (1998). Mannose 6-phosphate receptors are sorted from immature secretory granules via adaptor protein AP-1, clathrin, and syntaxin 6-positive vesicles. *J. Cell Biol.* 141, 359-371.
- Kopelman, P.G. and Hitman, G.A. (1998). Diabetes. Exploding type II. *Lancet* 352 Suppl 4, SIV5.
- Kreykenbohm, V., Wenzel, D., Antonin, W., Atlachkine, V., and von Mollard, G.F. (2002). The SNAREs vti1a and vti1b have distinct localization and SNARE complex partners. *Eur. J. Cell Biol.* 81, 273-280.
- Kuehn, M.J. and Schekman, R. (1997). COPII and secretory cargo capture into transport vesicles. *Curr. Opin. Cell Biol.* 9, 477-483.
- Lackie, J.M. and Dow, J.A.T. (2003). *The Dictionary of Cell and Molecular Biology*.
- Lampson, M.A., Schmoranzler, J., Zeigerer, A., Simon, S.M., and McGraw, T.E. (2001). Insulin-regulated release from the endosomal recycling compartment is regulated by budding of specialized vesicles. *Mol. Biol. Cell* 12, 3489-3501.
- Lenzen, C.U., Steinmann, D., Whiteheart, S.W., and Weis, W.I. (1998). Crystal structure of the hexamerization domain of N-ethylmaleimide-sensitive fusion protein. *Cell* 94, 525-536.
- Leon, R.P., Hedlund, T., Meech, S.J., Li, S., Schaack, J., Hunger, S.P., Duke, R.C., and DeGregori, J. (1998). Adenoviral-mediated gene transfer in lymphocytes. *Proc. Natl. Acad. Sci. U. S. A* 95, 13159-13164.
- Levin, D.E. and Errede, B. (1995). The proliferation of MAP kinase signaling pathways in yeast. *Curr. Opin. Cell Biol.* 7, 197-202.
- Lewis, M.J., Nichols, B.J., Prescianotto-Baschong, C., Riezman, H., and Pelham, H.R. (2000). Specific retrieval of the exocytic SNARE Snclp from early yeast endosomes. *Mol. Biol. Cell* 11, 23-38.
- Lim, S.N., Bonzelius, F., Low, S.H., Wille, H., Weimbs, T., and Herman, G.A. (2001). Identification of discrete classes of endosome-derived small vesicles as a major cellular pool for recycling membrane proteins. *Mol. Biol. Cell* 12, 981-995.
- Lin, R.C. and Scheller, R.H. (1997). Structural organization of the synaptic exocytosis core complex. *Neuron* 19, 1087-1094.
- Lin, R.C. and Scheller, R.H. (2000). Mechanisms of synaptic vesicle exocytosis. *Annu. Rev. Cell Dev. Biol.* 16, 19-49.

- Livingstone, C., James, D.E., Rice, J.E., Hanpeter, D., and Gould, G.W. (1996). Compartment ablation analysis of the insulin-responsive glucose transporter (GLUT4) in 3T3-L1 adipocytes. *Biochem. J.* 315 (Pt 2), 487-495.
- Lochmuller, H., Jani, A., Huard, J., Prescott, S., Simoncau, M., Massie, B., Karpati, G., and Acsadi, G. (1994). Emergence of early region 1-containing replication-competent adenovirus in stocks of replication-defective adenovirus recombinants (delta E1 + delta E3) during multiple passages in 293 cells. *Hum. Gene Ther.* 5, 1485-1491.
- Maeda, K., Okubo, K., Shimomura, I., Funahashi, T., Matsuzawa, Y., and Matsubara, K. (1996). cDNA cloning and expression of a novel adipose specific collagen-like factor, apM1 (AdiPose Most abundant Gene transcript 1). *Biochem. Biophys. Res. Commun.* 221, 286-289.
- Maeda, N., Takahashi, M., Funahashi, T., Kihara, S., Nishizawa, H., Kishida, K., Nagaretani, H., Matsuda, M., Komuro, R., Ouchi, N., Kuriyama, H., Hotta, K., Nakamura, T., Shimomura, I., and Matsuzawa, Y. (2001). PPARgamma ligands increase expression and plasma concentrations of adiponectin, an adipose-derived protein. *Diabetes* 50, 2094-2099.
- Mallard, F., Tang, B.L., Galli, T., Tenza, D., Saint-Pol, A., Yue, X., Antony, C., Hong, W., Goud, B., and Johannes, L. (2002). Early/recycling endosomes-to-TGN transport involves two SNARE complexes and a Rab6 isoform. *J. Cell Biol.* 156, 653-664.
- Manning, G., Whyte, D.B., Martinez, R., Hunter, T., and Sudarsanam, S. (2002). The protein kinase complement of the human genome. *Science* 298, 1912-1934.
- Marash, M. and Gerst, J.E. (2001). t-SNARE dephosphorylation promotes SNARE assembly and exocytosis in yeast. *EMBO J.* 20, 411-421.
- Marash, M. and Gerst, J.E. (2003). Phosphorylation of the autoinhibitory domain of the Sso t-SNAREs promotes binding of the Vsm1 SNARE regulator in yeast. *Mol. Biol. Cell* 14, 3114-3125.
- Martin, L.B., Shewan, A., Millar, C.A., Gould, G.W., and James, D.E. (1998). Vesicle-associated membrane protein 2 plays a specific role in the insulin-dependent trafficking of the facilitative glucose transporter GLUT4 in 3T3-L1 adipocytes. *J. Biol. Chem.* 273, 1444-1452.
- Martin, S., Millar, C.A., Lyttle, C.T., Meerloo, T., Marsh, B.J., Gould, G.W., and James, D.E. (2000a). Effects of insulin on intracellular GLUT4 vesicles in adipocytes: evidence for a secretory mode of regulation. *J. Cell Sci.* 113 Pt 19, 3427-3438.
- Martin, S., Ramm, G., Lyttle, C.T., Meerloo, T., Stoorvogel, W., and James, D.E. (2000b). Biogenesis of insulin-responsive GLUT4 vesicles is independent of brefeldin A-sensitive trafficking. *Traffic*. 1, 652-660.
- Martin, S., Reaves, B., Banting, G., and Gould, G.W. (1994). Analysis of the co-localization of the insulin-responsive glucose transporter (GLUT4) and the trans Golgi network marker TGN38 within 3T3-L1 adipocytes. *Biochem. J.* 300 (Pt 3), 743-749.
- Martin, S., Teflam, J.T., Livingstone, C., Slot, J.W., Gould, G.W., and James, D.E. (1996). The glucose transporter (GLUT-4) and vesicle-associated membrane protein-2 (VAMP-2)

are segregated from recycling endosomes in insulin-sensitive cells. *J. Cell Biol.* 134, 625-635.

Martin-Martin, B., Nabokina, S.M., Blasi, J., Lazo, P.A., and Mollinedo, F. (2000). Involvement of SNAP-23 and syntaxin 6 in human neutrophil exocytosis. *Blood* 96, 2574-2583.

May, A.P., Misura, K.M., Whiteheart, S.W., and Weis, W.I. (1999). Crystal structure of the amino-terminal domain of N-ethylmaleimide-sensitive fusion protein. *Nat. Cell Biol.* 1, 175-182.

Mayor, S., Presley, J.F., and Maxfield, F.R. (1993). Sorting of membrane components from endosomes and subsequent recycling to the cell surface occurs by a bulk flow process. *J. Cell Biol.* 121, 1257-1269.

McNew, J.A., Parlati, F., Fukuda, R., Johnston, R.J., Paz, K., Paumet, F., Sollner, T.H., and Rothman, J.E. (2000). Compartmental specificity of cellular membrane fusion encoded in SNARE proteins. *Nature* 407, 153-159.

Mellman, I. (1996). Endocytosis and molecular sorting. *Annu. Rev. Cell Dev. Biol.* 12, 575-625.

Mercedith, J.E., Jr., Winitz, S., Lewis, J.M., Hess, S., Ren, X.D., Renshaw, M.W., and Schwartz, M.A. (1996). The regulation of growth and intracellular signaling by integrins. *Endocr. Rev.* 17, 207-220.

Mette, S.A., Pilewski, J., Buck, C.A., and Albelda, S.M. (1993). Distribution of integrin cell adhesion receptors on normal bronchial epithelial cells and lung cancer cells in vitro and in vivo. *Am. J. Respir. Cell Mol. Biol.* 8, 562-572.

Miesenbock, G. and Rothman, J.E. (1995). The capacity to retrieve escaped ER proteins extends to the trans-most cisterna of the Golgi stack. *J. Cell Biol.* 129, 309-319.

Millar, C.A., Meerloo, T., Martin, S., Hickson, G.R., Shimwell, N.J., Wakelam, M.J., James, D.E., and Gould, G.W. (2000). Adipsin and the glucose transporter GLUT4 traffic to the cell surface via independent pathways in adipocytes. *Traffic* 1, 141-151.

Minokoshi, Y., Kahn, C.R., and Kahn, B.B. (2003). Tissue-specific ablation of the GLUT4 glucose transporter or the insulin receptor challenges assumptions about insulin action and glucose homeostasis. *J. Biol. Chem.* 278, 33609-33612.

Misura, K.M., Bock, J.B., Gonzalez, L.C., Jr., Scheller, R.H., and Weis, W.I. (2002). Three-dimensional structure of the amino-terminal domain of syntaxin 6, a SNAP-25 C homolog. *Proc. Natl. Acad. Sci. U. S. A* 99, 9184-9189.

Misura, K.M., Scheller, R.H., and Weis, W.I. (2000). Three-dimensional structure of the neuronal-Sec1-syntaxin 1a complex. *Nature* 404, 355-362.

Misura, K.M., Scheller, R.H., and Weis, W.I. (2001). Self-association of the H3 region of syntaxin 1A. Implications for intermediates in SNARE complex assembly. *J. Biol. Chem.* 276, 13273-13282.

- Miura, S., Kai, Y., Ono, M., and Ezaki, O. (2003). Overexpression of peroxisome proliferator-activated receptor gamma coactivator-1alpha down-regulates GLUT4 mRNA in skeletal muscles. *J. Biol. Chem.* 278, 31385-31390.
- Moller, D.E. (2001). New drug targets for type 2 diabetes and the metabolic syndrome. *Nature* 414, 821-827.
- Mora, S. and Pessin, J.E. (2002). An adipocentric view of signaling and intracellular trafficking. *Diabetes Metab Res. Rev.* 18, 345-356.
- Mueckler, M. (1994). Facilitative glucose transporters. *Eur. J. Biochem.* 219, 713-725.
- Munson, M., Chen, X., Cocina, A.E., Schultz, S.M., and Hughson, F.M. (2000). Interactions within the yeast t-SNARE Sso1p that control SNARE complex assembly. *Nat. Struct. Biol.* 7, 894-902.
- Nabi, I.R. and I.e, P.U. (2003). Caveolae/raft-dependent endocytosis. *J. Cell Biol.* 161, 673-677.
- Nicholson, K.L., Munson, M., Miller, R.B., Filip, T.J., Fairman, R., and Hughson, F.M. (1998). Regulation of SNARE complex assembly by an N-terminal domain of the t-SNARE Sso1p. *Nat. Struct. Biol.* 5, 793-802.
- Obenauer, J.C., Cantley, L.C., and Yaffe, M.B. (2003). Scansite 2.0: Proteome-wide prediction of cell signaling interactions using short sequence motifs. *Nucleic Acids Res.* 31, 3635-3641.
- Olson, A.L., Knight, J.B., and Pessin, J.E. (1997). Syntaxin 4, VAMP2, and/or VAMP3/cellubrevin are functional target membrane and vesicle SNAP receptors for insulin-stimulated GLUT4 translocation in adipocytes. *Mol. Cell Biol.* 17, 2425-2435.
- Olson, A.L. and Pessin, J.E. (1996). Structure, function, and regulation of the mammalian facilitative glucose transporter gene family. *Annu. Rev. Nutr.* 16, 235-256.
- Ossig, R., Dascher, C., Trepte, H.H., Schmitt, H.D., and Gallwitz, D. (1991). The yeast SLY gene products, suppressors of defects in the essential GTP-binding Ypt1 protein, may act in endoplasmic reticulum-to-Golgi transport. *Mol. Cell Biol.* 11, 2980-2993.
- Oyler, G.A., Higgins, G.A., Hart, R.A., Battenberg, E., Billingsley, M., Bloom, F.E., and Wilson, M.C. (1989). The identification of a novel synaptosomal-associated protein, SNAP-25, differentially expressed by neuronal subpopulations. *J. Cell Biol.* 109, 3039-3052.
- Pagan, J.K., Wylie, F.G., Joseph, S., Widberg, C., Bryant, N.J., James, D.E., and Stow, J.L. (2003). The t-SNARE syntaxin 4 is regulated during macrophage activation to function in membrane traffic and cytokine secretion. *Curr. Biol.* 13, 156-160.
- Palacios, S., Lalioti, V., Martinez-Arca, S., Chattopadhyay, S., and Sandoval, I.V. (2001). Recycling of the insulin-sensitive glucose transporter GLUT4 - Access of surface internalized GLUT4 molecules to the perinuclear storage compartment is mediated by the Phe(5)-Gln(6)-Gln(7)-Ile(8) MOTIF. *J. Biol. Chem.* 276, 3371-3383.
- Panek, H.R., Conibear, E., Bryan, J.D., Colvin, R.T., Goshorn, C.D., and Robinson, L.C. (2000). Identification of Rgp1p, a novel Golgi recycling factor, as a protein required for efficient localization of yeast casein kinase 1 to the plasma membrane. *J. Cell Sci.* 113 Pt 24, 4545-4555.

Parlati, F., Varlamov, O., Paz, K., McNew, J.A., Hurtado, D., Sollner, T.H., and Rothman, J.E. (2002). Distinct SNARE complexes mediating membrane fusion in Golgi transport based on combinatorial specificity. *Proc. Natl. Acad. Sci. U. S. A* 99, 5424-5429.

Paumet, F., Brugger, B., Parlati, F., McNew, J.A., Sollner, T.H., and Rothman, J.E. (2001). A t-SNARE of the endocytic pathway must be activated for fusion. *J. Cell Biol.* 155, 961-968.

Pawson, T. and Scott, J.D. (2005). Protein phosphorylation in signaling--50 years and counting. *Trends Biochem. Sci.* 30, 286-290.

Pelham, H.R. (2001). SNAREs and the specificity of membrane fusion. *Trends Cell Biol.* 11, 99-101.

Perera, H.K., Clarke, M., Morris, N.J., Hong, W., Chamberlain, L.H., and Gould, G.W. (2003). Syntaxin 6 regulates Glut4 trafficking in 3T3-L1 adipocytes. *Mol. Biol. Cell* 14, 2946-2958.

Pessin, J.E. and Saltiel, A.R. (2000). Signaling pathways in insulin action: molecular targets of insulin resistance. *J. Clin. Invest* 106, 165-169.

Pessin, J.E., Thurmond, D.C., Elmendorf, J.S., Coker, K.J., and Okada, S. (1999). Molecular basis of insulin-stimulated GLUT4 vesicle trafficking. Location! Location! Location! *J. Biol. Chem.* 274, 2593-2596.

Piper, R.C., James, D.E., Slot, J.W., Puri, C., and Lawrence, J.C., Jr. (1993). GLUT4 phosphorylation and inhibition of glucose transport by dibutyryl cAMP. *J. Biol. Chem.* 268, 16557-16563.

Ploug, T., van Deurs, B., Ai, H., Cushman, S.W., and Ralston, E. (1998). Analysis of GLUT4 distribution in whole skeletal muscle fibers: identification of distinct storage compartments that are recruited by insulin and muscle contractions. *J. Cell Biol.* 142, 1429-1446.

Poirier, M.A., Hao, J.C., Malkus, P.N., Chan, C., Moore, M.F., King, D.S., and Bennett, M.K. (1998a). Protease resistance of syntaxin.SNAP-25.VAMP complexes. Implications for assembly and structure. *J. Biol. Chem.* 273, 11370-11377.

Poirier, M.A., Xiao, W., Macosko, J.C., Chan, C., Shin, Y.K., and Bennett, M.K. (1998b). The synaptic SNARE complex is a parallel four-stranded helical bundle. *Nat. Struct. Biol.* 5, 765-769.

Rahn, T., Ridderstrale, M., Tornqvist, H., Manganiello, V., Fredrikson, G., Belfrage, P., and Degerman, E. (1994). Essential role of phosphatidylinositol 3-kinase in insulin-induced activation and phosphorylation of the cGMP-inhibited cAMP phosphodiesterase in rat adipocytes. Studies using the selective inhibitor wortmannin. *FEBS Lett.* 350, 314-318.

Ralston, E. and Ploug, T. (1996). GLUT4 in cultured skeletal myotubes is segregated from the transferrin receptor and stored in vesicles associated with TGN. *J. Cell Sci.* 109 (Pt 13), 2967-2978.

- Ramm, G., Slot, J.W., James, D.E., and Stoorvogel, W. (2000). Insulin recruits GLUT4 from specialized VAMP2-carrying vesicles as well as from the dynamic endosomal/trans-Golgi network in rat adipocytes. *Mol. Biol. Cell* 11, 4079-4091.
- Randhawa, V.K., Bilan, P.J., Khayat, Z.A., Daneman, N., Liu, Z., Ramlal, T., Volchuk, A., Peng, X.R., Coppola, T., Regazzi, R., Trimble, W.S., and Klip, A. (2000). VAMP2, but not VAMP3/cellubrevin, mediates insulin-dependent incorporation of GLUT4 into the plasma membrane of L6 myoblasts. *Mol. Biol. Cell* 11, 2403-2417.
- Ray, L.B. and Sturgill, T.W. (1987). Rapid stimulation by insulin of a serine/threonine kinase in 3T3-L1 adipocytes that phosphorylates microtubule-associated protein 2 in vitro. *Proc. Natl. Acad. Sci. U. S. A* 84, 1502-1506.
- Rea, S. and James, D.E. (1997). Moving GLUT4: the biogenesis and trafficking of GLUT4 storage vesicles. *Diabetes* 46, 1667-1677.
- Risinger, C. and Bennett, M.K. (1999). Differential phosphorylation of syntaxin and synaptosome-associated protein of 25 kDa (SNAP-25) isoforms. *J. Neurochem.* 72, 614-624.
- Ritchie, S.A., Ewart, M.A., Perry, C.G., Connell, J.M., and Salt, I.P. (2004). The role of insulin and the adipocytokines in regulation of vascular endothelial function. *Clin. Sci. (Lond)* 107, 519-532.
- Rizo, J. and Sudhof, T.C. (2002). Snares and Munc18 in synaptic vesicle fusion. *Nat. Rev. Neurosci.* 3, 641-653.
- Robinson, L.J. and James, D.E. (1992). Insulin-regulated sorting of glucose transporters in 3T3-L1 adipocytes. *Am. J. Physiol* 263, E383-E393.
- Robinson, L.J., Pang, S., Harris, D.S., Heuser, J., and James, D.E. (1992). Translocation of the glucose transporter (GLUT4) to the cell surface in permeabilized 3T3-L1 adipocytes: effects of ATP, insulin, and GTP gamma S and localization of GLUT4 to clathrin lattices. *J. Cell Biol.* 117, 1181-1196.
- Rondinone, C.M., Carvalho, E., Rahn, T., Manganiello, V.C., Degerman, E., and Smith, U.P. (2000). Phosphorylation of PDE3B by phosphatidylinositol 3-kinase associated with the insulin receptor. *J. Biol. Chem.* 275, 10093-10098.
- Rothman, J.E. (1994). Intracellular membrane fusion. *Adv. Second Messenger Phosphoprotein Res.* 29, 81-96.
- Roussou, I. and Draetta, G. (1993). Phosphorylation in yeast cell processes. *Cell Signal.* 5, 381-387.
- Roussou, I. and Draetta, G. (1994). The *Schizosaccharomyces pombe* casein kinase II alpha and beta subunits: evolutionary conservation and positive role of the beta subunit. *Mol. Cell Biol.* 14, 576-586.
- ROWE, W.P., HUEBNER, R.J., GILMORE, L.K., PARROTT, R.H., and WARD, T.G. (1953). Isolation of a cytopathogenic agent from human adenoids undergoing spontaneous degeneration in tissue culture. *Proc. Soc. Exp. Biol. Med.* 84, 570-573.
- Russell, W.C. (2000). Update on adenovirus and its vectors. *J. Gen. Virol.* 81, 2573-2604.

Sakaue, H., Ogawa, W., Takata, M., Kuroda, S., Kotani, K., Matsumoto, M., Sakaue, M., Nishio, S., Ueno, H., and Kasuga, M. (1997). Phosphoinositide 3-kinase is required for insulin-induced but not for growth hormone- or hyperosmolarity-induced glucose uptake in 3T3-L1 adipocytes. *Mol. Endocrinol.* 11, 1552-1562.

Salama, N.R. and Schekman, R.W. (1995). The role of coat proteins in the biosynthesis of secretory proteins. *Curr. Opin. Cell Biol.* 7, 536-543.

Saltiel, A.R. and Kahn, C.R. (2001). Insulin signalling and the regulation of glucose and lipid metabolism. *Nature* 414, 799-806.

Sandoval, I.V., Martinez-Arca, S., Valdueza, J., Palacios, S., and Holman, G.D. (2000). Distinct reading of different structural determinants modulates the dileucine-mediated transport steps of the lysosomal membrane protein LIMP2 and the insulin-sensitive glucose transporter GLUT4. *J. Biol. Chem.* 275, 39874-39885.

Scales, S.J., Chen, Y.A., Yoo, B.Y., Patel, S.M., Doung, Y.C., and Scheller, R.H. (2000). SNAREs contribute to the specificity of membrane fusion. *Neuron* 26, 457-464.

Schekman, R. (1992). Genetic and biochemical analysis of vesicular traffic in yeast. *Curr. Opin. Cell Biol.* 4, 587-592.

Scherer, P.E., Williams, S., Fogliano, M., Baldini, G., and Lodish, H.F. (1995). A novel serum protein similar to C1q, produced exclusively in adipocytes. *J. Biol. Chem.* 270, 26746-26749.

Schmid, S.L., McNiven, M.A., and De Camilli, P. (1998). Dynamin and its partners: a progress report. *Curr. Opin. Cell Biol.* 10, 504-512.

Seron, K., Tieaho, V., Precscianotto-Baschong, C., Aust, T., Blondel, M.O., Guillaud, P., Devilliers, G., Rossanese, O.W., Glick, B.S., Riezman, H., Keranen, S., and Haguenaue-Tsapis, R. (1998). A yeast t-SNARE involved in endocytosis. *Mol. Biol. Cell* 9, 2873-2889.

Shepherd, P.R. and Kahn, B.B. (1999). Glucose transporters and insulin action--implications for insulin resistance and diabetes mellitus. *N. Engl. J. Med.* 341, 248-257.

Shewan, A.M., Marsh, B.J., Melvin, D.R., Martin, S., Gould, G.W., and James, D.E. (2000). The cytosolic C-terminus of the glucose transporter GLUT4 contains an acidic cluster endosomal targeting motif distal to the dileucine signal. *Biochem. J.* 350 Pt 1, 99-107.

Shewan, A.M., van Dam, E.M., Martin, S., Luen, T.B., Hong, W., Bryant, N.J., and James, D.E. (2003). GLUT4 recycles via a trans-Golgi network (TGN) subdomain enriched in Syntaxins 6 and 16 but not TGN38: involvement of an acidic targeting motif. *Mol. Biol. Cell* 14, 973-986.

Shimazaki, Y., Nishiki, T., Omori, A., Sekiguchi, M., Kamata, Y., Kozaki, S., and Takahashi, M. (1996). Phosphorylation of 25-kDa synaptosome-associated protein. Possible involvement in protein kinase C-mediated regulation of neurotransmitter release. *J. Biol. Chem.* 271, 14548-14553.

Shuang, R., Zhang, L., Fletcher, A., Groblewski, G.E., Pevsner, J., and Stuenkel, E.L. (1998). Regulation of Munc-18/syntaxin 1A interaction by cyclin-dependent kinase 5 in nerve endings. *J. Biol. Chem.* 273, 4957-4966.

Simonsen, A., Bremnes, B., Ronning, E., Aasland, R., and Stenmark, H. (1998). Syntaxin-16, a putative Golgi t-SNARE. *Eur. J. Cell Biol.* 75, 223-231.

Slot, J.W., Garruti, G., Martin, S., Oorschot, V., Posthuma, G., Kraegen, E.W., Laybutt, R., Thibault, G., and James, D.E. (1997). Glucose transporter (GLUT-4) is targeted to secretory granules in rat atrial cardiomyocytes. *J. Cell Biol.* 137, 1243-1254.

Slot, J.W., Geuze, H.J., Gigengack, S., James, D.E., and Lienhard, G.E. (1991a). Translocation of the glucose transporter GLUT4 in cardiac myocytes of the rat. *Proc. Natl. Acad. Sci. U. S. A* 88, 7815-7819.

Slot, J.W., Geuze, H.J., Gigengack, S., Lienhard, G.E., and James, D.E. (1991b). Immunolocalisation of the insulin regulatable glucose transporter in brown adipose tissue of the rat. *J. Cell Biol.* 113, 123-135.

Sollner, T., Bennett, M.K., Whiteheart, S.W., Scheller, R.H., and Rothman, J.E. (1993). A protein assembly-disassembly pathway in vitro that may correspond to sequential steps of synaptic vesicle docking, activation, and fusion. *Cell* 75, 409-418.

Stegmaier, M., Klumperman, J., Foletti, D.L., Yoo, J.S., and Scheller, R.H. (1999). Vesicle-associated membrane protein 4 is implicated in trans-Golgi network vesicle trafficking. *Mol. Biol. Cell* 10, 1957-1972.

Stegmaier, M., Oorschot, V., Klumperman, J., and Scheller, R.H. (2000). Syntaxin 17 is abundant in steroidogenic cells and implicated in smooth endoplasmic reticulum membrane dynamics. *Mol. Biol. Cell* 11, 2719-2731.

Stegmaier, M., Yang, B., Yoo, J.S., Huang, B., Shen, M., Yu, S., Luo, Y., and Scheller, R.H. (1998). Three novel proteins of the syntaxin/SNAP-25 family. *J. Biol. Chem.* 273, 34171-34179.

Stewart, P.L., Fuller, S.D., and Burnett, R.M. (1993). Difference imaging of adenovirus: bridging the resolution gap between X-ray crystallography and electron microscopy. *EMBO J.* 12, 2589-2599.

Subramaniam, V.N., Loh, E., Horstmann, H., Habermann, A., Xu, Y., Coe, J., Griffiths, G., and Hong, W. (2000). Preferential association of syntaxin 8 with the early endosome. *J. Cell Sci.* 113 (Pt 6), 997-1008.

Sutton, R.B., Fasshauer, D., Jahn, R., and Brunger, A.T. (1998). Crystal structure of a SNARE complex involved in synaptic exocytosis at 2.4 Å resolution. *Nature* 395, 347-353.

Takayama, K., Ueno, H., Pei, X.H., Nakanishi, Y., Yatsunami, J., and Hara, N. (1998). The levels of integrin alpha v beta 5 may predict the susceptibility to adenovirus-mediated gene transfer in human lung cancer cells. *Gene Ther.* 5, 361-368.

Tamori, Y., Hashiramoto, M., Araki, S., Kamata, Y., Takahashi, M., Kozaki, S., and Kasuga, M. (1996). Cleavage of vesicle-associated membrane protein (VAMP)-2 and cellubrevin on GLUT4-containing vesicles inhibits the translocation of GLUT4 in 3T3-L1 adipocytes. *Biochem. Biophys. Res. Commun.* 220, 740-745.

- Tang, B.L., Low, D.Y., Lee, S.S., Tan, A.E., and Hong, W. (1998a). Molecular cloning and localization of human syntaxin 16, a member of the syntaxin family of SNARE proteins. *Biochem. Biophys. Res. Commun.* 242, 673-679.
- Tang, B.L., Low, D.Y., Tan, A.E., and Hong, W. (1998b). Syntaxin 10: a member of the syntaxin family localized to the trans-Golgi network. *Biochem. Biophys. Res. Commun.* 242, 345-350.
- Tang, B.L., Tan, A.E., Lim, L.K., Lee, S.S., Low, D.Y., and Hong, W. (1998c). Syntaxin 12, a member of the syntaxin family localized to the endosome. *J. Biol. Chem.* 273, 6944-6950.
- Tanner, L.I. and Lienhard, G.E. (1987). Insulin elicits a redistribution of transferrin receptors in 3T3-L1 adipocytes through an increase in the rate constant for receptor externalization. *J. Biol. Chem.* 262, 8975-8980.
- Tashiro, F., Niwa, H., and Miyazaki, J. (1999). Constructing adenoviral vectors by using the circular form of the adenoviral genome cloned in a cosmid and the Cre-loxP recombination system. *Hum. Gene Ther.* 10, 1845-1852.
- Tellam, J.T., James, D.E., Stevens, T.H., and Piper, R.C. (1997a). Identification of a mammalian Golgi Sec1p-like protein, mVps45. *J. Biol. Chem.* 272, 6187-6193.
- Tellam, J.T., Macaulay, S.L., McIntosh, S., Hewish, D.R., Ward, C.W., and James, D.E. (1997b). Characterization of Munc-18c and syntaxin-4 in 3T3-L1 adipocytes. Putative role in insulin-dependent movement of GLUT-4. *J. Biol. Chem.* 272, 6179-6186.
- Teng, F.Y., Wang, Y., and Tang, B.L. (2001). The syntaxins. *Genome Biol.* 2, REVIEWS3012.
- Tengholm, A. and Meyer, T. (2002). A PI3-kinase signaling code for insulin-triggered insertion of glucose transporters into the plasma membrane. *Curr. Biol.* 12, 1871-1876.
- Thurmond, D.C., Ceresa, B.P., Okada, S., Elmendorf, J.S., Coker, K., and Pessin, J.E. (1998). Regulation of insulin-stimulated GLUT4 translocation by Munc18c in 3T3L1 adipocytes. *J. Biol. Chem.* 273, 33876-33883.
- Toozc, S.A., Martens, G.J., and Huttner, W.B. (2001). Secretory granule biogenesis: rafting to the SNARE. *Trends Cell Biol.* 11, 116-122.
- Traub, L.M. and Kornfeld, S. (1997). The trans-Golgi network: a late secretory sorting station. *Curr. Opin. Cell Biol.* 9, 527-533.
- Trimble, W.S., Cowan, D.M., and Scheller, R.H. (1988). VAMP-1: a synaptic vesicle-associated integral membrane protein. *Proc. Natl. Acad. Sci. U. S. A* 85, 4538-4542.
- Valdez, A.C., Cabaniols, J.P., Brown, M.J., and Roche, P.A. (1999). Syntaxin 11 is associated with SNAP-23 on late endosomes and the trans-Golgi network. *J. Cell Sci.* 112 (Pt 6), 845-854.
- Verhage, M., Maia, A.S., Plomp, J.J., Brussaard, A.B., Heeroma, J.H., Vermeer, H., Toonen, R.F., Hammer, R.E., van den Berg, T.K., Missler, M., Geuze, H.J., and Sudhof, T.C. (2000). Synaptic assembly of the brain in the absence of neurotransmitter secretion. *Science* 287, 864-869.

- Verhey, K.J., Yeh, J.I., and Birnbaum, M.J. (1995). Distinct signals in the GLUT4 glucose transporter for internalization and for targeting to an insulin-responsive compartment. *J. Cell Biol.* 130, 1071-1079.
- Volchuk, A., Wang, Q., Ewart, H.S., Liu, Z., He, L., Bennett, M.K., and Klip, A. (1996). Syntaxin 4 in 3T3-L1 adipocytes: regulation by insulin and participation in insulin-dependent glucose transport. *Mol. Biol. Cell* 7, 1075-1082.
- Wade, N., Bryant, N.J., Connolly, L.M., Simpson, R.J., Luzio, J.P., Piper, R.C., and James, D.E. (2001). Syntaxin 7 complexes with mouse Vps10p tail interactor 1b, syntaxin 6, vesicle-associated membrane protein (VAMP)8, and VAMP7 in b16 melanoma cells. *J. Biol. Chem.* 276, 19820-19827.
- Wang, W., Hansen, P.A., Marshall, B.A., Holloszy, J.O., and Mueckler, M. (1996). Insulin unmasks a COOH-terminal Glut4 epitope and increases glucose transport across T-tubules in skeletal muscle. *J. Cell Biol.* 135, 415-430.
- Wang, Y., Tai, G., Lu, L., Johannes, L., Hong, W., and Luen, T.B. (2005). Trans-Golgi network syntaxin 10 functions distinctly from syntaxins 6 and 16. *Mol. Membr. Biol.* 22, 313-325.
- Watson, R.T., Kanzaki, M., and Pessin, J.E. (2004). Regulated membrane trafficking of the insulin-responsive glucose transporter 4 in adipocytes. *Endocr. Rev.* 25, 177-204.
- Watson, R.T. and Pessin, J.E. (2000). Functional cooperation of two independent targeting domains in syntaxin 6 is required for its efficient localization in the trans-golgi network of 3T3L1 adipocytes. *J. Biol. Chem.* 275, 1261-1268.
- Weber, T., Zemelmann, B.V., McNew, J.A., Westermann, B., Gmachl, M., Parlati, F., Sollner, T.H., and Rothman, J.E. (1998). SNAREpins: minimal machinery for membrane fusion. *Cell* 92, 759-772.
- Weimbs, T., Low, S.H., Chapin, S.J., Mostov, K.E., Bucher, P., and Hofmann, K. (1997). A conserved domain is present in different families of vesicular fusion proteins: a new superfamily. *Proc. Natl. Acad. Sci. U. S. A* 94, 3046-3051.
- Wendler, F., Page, L., Urbe, S., and Tooze, S.A. (2001). Homotypic fusion of immature secretory granules during maturation requires syntaxin 6. *Mol. Biol. Cell* 12, 1699-1709.
- Wendler, F. and Tooze, S. (2001). Syntaxin 6: the promiscuous behaviour of a SNARE protein. *Traffic*. 2, 606-611.
- Wickham, T.J., Mathias, P., Cheresch, D.A., and Nemerow, G.R. (1993). Integrins alpha v beta 3 and alpha v beta 5 promote adenovirus internalization but not virus attachment. *Cell* 73, 309-319.
- Wijkander, J., Landstrom, T.R., Manganiello, V., Belfrage, P., and Degerman, E. (1998). Insulin-induced phosphorylation and activation of phosphodiesterase 3B in rat adipocytes: possible role for protein kinase B but not mitogen-activated protein kinase or p70 S6 kinase. *Endocrinology* 139, 219-227.
- Wong, S.H., Xu, Y., Zhang, T., and Hong, W. (1998). Syntaxin 7, a novel syntaxin member associated with the early endosomal compartment. *J. Biol. Chem.* 273, 375-380.

- Yamaguchi, T., Dulubova, I., Min, S.W., Chen, X., Rizo, J., and Sudhof, T.C. (2002). Sly1 binds to Golgi and ER syntaxins via a conserved N-terminal peptide motif. *Dev. Cell* 2, 295-305.
- Yang, B., Gonzalez, I., Jr., Prekeris, R., Stegmaier, M., Advani, R.J., and Scheller, R.H. (1999). SNARE interactions are not selective. Implications for membrane fusion specificity. *J. Biol. Chem.* 274, 5649-5653.
- Yang, J. and Holman, G.D. (1993). Comparison of GLUT4 and GLUT1 subcellular trafficking in basal and insulin-stimulated 3T3-L1 cells. *J. Biol. Chem.* 268, 4600-4603.
- Yang, W.S., Lec, W.J., Funahashi, T., Tanaka, S., Matsuzawa, Y., Chao, C.L., Chen, C.L., Tai, T.Y., and Chuang, L.M. (2001). Weight reduction increases plasma levels of an adipose-derived anti-inflammatory protein, adiponectin. *J. Clin. Endocrinol. Metab* 86, 3815-3819.
- Yu, R.C., Hanson, P.I., Jahn, R., and Brunger, A.T. (1998). Structure of the ATP-dependent oligomerization domain of N-ethylmaleimide sensitive factor complexed with ATP. *Nat. Struct. Biol.* 5, 803-811.
- Yu, R.C., Jahn, R., and Brunger, A.T. (1999). NSF N-terminal domain crystal structure: models of NSF function. *Mol. Cell* 4, 97-107.
- Zhang, W.W. (1999). Development and application of adenoviral vectors for gene therapy of cancer. *Cancer Gene Ther.* 6, 113-138.
- Zhang, Y., Su, Z., Zhang, F., Chen, Y., and Shin, Y.K. (2005). A partially zipped SNARE complex stabilized by the membrane. *J. Biol. Chem.* 280, 15595-15600.
- Zhu, J., Grace, M., Casale, J., Chang, A.T., Musco, M.L., Bordens, R., Greenberg, R., Schaefer, E., and Indelicato, S.R. (1999). Characterization of replication-competent adenovirus isolates from large-scale production of a recombinant adenoviral vector. *Hum. Gene Ther.* 10, 113-121.
- Zimmet, P., Alberti, K.G., and Shaw, J. (2001). Global and societal implications of the diabetes epidemic. *Nature* 414, 782-787.

LIBRARY